

Shear strengthening of concrete members with Textile Reinforced Mortar (TRM)

A thesis presented for the degree of

Doctor of Philosophy in Civil Engineering

at The University of Nottingham

by

Zoi Tetta

(4213911)

March 2017

ABSTRACT

The issue of upgrading existing structures is of great importance due to their deterioration (ageing, environmental induced degradation, lack of maintenance, need to meet the current design requirements). Recently, an innovative structural material, the so-called Textile-Reinforced Mortar (TRM), was successfully developed for structural retrofitting of deficient masonry and concrete structures. TRM is an advanced sustainable material which offers well-established advantages (good behaviour at high temperature, compatibility to concrete or masonry substrates material high strength to weight ratio, corrosion resistance, ease and speed of application, minimal change of cross section dimensions) at a low-cost and over the last decade it has been reported in the literature that TRM is a very promising alternative to the FRP (Fibre Reinforced Polymers) retrofitting solution. This study evaluates the use of TRM jacketing for shear strengthening of Reinforced Concrete (RC) beams.

First of all, the materials used for strengthening are described and the tensile and shear behaviour of textiles was characterised through tensile and picture-frame tests, repsectively. Moreover, the tensile properties of TRM composite material are experimentally obtained through bell-shaped TRM coupons. Shear strengthening of RC beams was extensively studied carrying out 55 medium-scale rectangular beams and 14 full-scale T-beam ends.

The key investigated parameters on medium-scale rectangular beams comprise: (a) the strengthening system (TRM versus FRP), the (b) strengthening configuration, (c) the number of layers, (d) the external reinforcement ratio, (e) the textile material mesh characteristics, (f) the shear-span-to depth ratio and (g) the optimisation of the textile geometry. It was concluded that TRM was very effective on increasing the shear resistance of RC beams but its effectiveness was sensitive to parameters such as the strengthening configuration, the number of layers and the textile characteristics.

Experimental work was also conducted on full-scale T-beams focused on the use of a novel end-anchorage system comprising textile-based anchors to delay or prevent the debonding of TRM jacket. In particular, the anchorage percentage of the U-jacket, the number of layers, the textile material, the textile geometry and the strengthening system (TRM versus FRP jackets) were the main investigated parameters. U-shaped TRM jackets significantly increased the shear capacity of full-scale T-beams, whereas

the use of textile-based anchors improved dramatically the effectiveness of the TRM jackets. A simple design model was also proposed to calculate the contribution of anchored TRM jackets to the shear capacity of RC T-beams.

The behaviour of TRM at high temperature used for shear strengthening of both medium-scale and full-scale beams was studied for the first time through demanding tests in which loading and high temperature were simultaneously applied. Based on the experimental results, TRM jacketing remained very effective at high temperature, whereas the effectiveness of side-bonding and U-wrapping FRP jacketing was reduced nearly to zero when subjected at temperatures above the glass transition temperature (T_g). A stress reduction factor for TRM and FRP systems was also introduced to take into account the decrease in the effectiveness of both TRM and FRP jacket due to explosion of specimens to high temperature.

Finally, design models for the prediction of the contribution of the TRM jacket to the total shear resistance were proposed for each failure mode and verified with the available experimental data.

ACKNOWLEDGEMENTS

This thesis was conducted at the University of Nottingham supervised by Dr. Bournas Dionysios. This study has been co-financed by the UK Engineering and Physical Sciences Research Council (EP/L50502X/1) and the University of Nottingham through the Dean of Engineering Prize (a scheme for pump priming support for early career academic staff). The work presented in Chapter 7 (Design models for the calculation of the contribution of the TRM jacketing to the total shear resistance (V_f) of RC beams) was carried out within the framework of the Marie Curie Endure programme (European Network for Durable Reinforcement and Rehabilitation Solutions) at the University of Patras supervised by Prof. Triantafillou Thanasis.

I would like to thank my supervisor, Dr. Bournas Dionysios for giving me the chance to work in this project. His critical thinking, experience and engineering judgement helped me to improve my work. His incessant support all these years helped me to complete my PhD studies. Moreover, I would like also to thank Dr. Triantafyllou Savvas for his help and his support the last year of my PhD. Finally, I would like to thank Prof. Triantafillou Thanasis for giving me the chance to work in Marie Curie Endure program at the University of Patras the last four months.

I would like also to wholeheartedly thank Dr. Lampros Koutas for the perfect collaboration we had all these years that we worked together. His structural knowledge, scientific expertise and lab experience made a big difference to my thesis. His positive thoughts, optimistic character and friendly advice significantly contributed to the completion of this thesis.

I am deeply grateful for the incessant help and support of my friend Saad. His practical and psychological support as well as his jokes at the end of the exhaustive days in the lab was of great importance. We have spent a lot of hours working together in the lab, sharing our scientific thoughts and queries and deal with the difficulties and challenges of our experiments.

I gratefully acknowledge the lab managers Tom Buss and Mike Langford, the chief technician Nigel Rook, and the technicians Balbir Loyla, Gary Davies, Sam Cook, Luke Bedford and Andrea Endruweit for their assistance in the experimental work.

I would like also to thank my past and present collueges in the office, Athina, Vasilis, Kostas, Evgenia, Katerina, Manolis, Florentia, Vaggelis, Andre and Alexis for contributing to the nice working environment.

Furthermore, I wish to thank my parents Zina and Chirstos for their help and advice in each step of my career. Their love and support always motivated me and boosted my self-confidence. Moreover, I would like to thank my brother Kostas for his support and technical help (in some softwares I used) during my PhD period. His positive thoughts, warm feelings and humour made me relax and dissipate the stress of the day. Finally, I wish to deeply thank Miltos for his support and encouragement the last nine years that we are together. His loyalty and warming smile inspire me and give me the motivation to improve myself and fulfil new challenging goals.

Table of contents

1 INTRODUCTION 1

1.1 Background 1

1.2 Aim of the research 2

1.3 Thesis layout 2

2 LITERATURE REVIEW 3

2.1 TRM - Introduction 4

2.2 Use of TRM for strengthening and seismic retrofitting of concrete or masonry members 6

2.2.1 Bond behaviour of TRM 6

2.2.2 Strengthening of Reinforced Concrete (RC) members with TRM 7

2.2.3 Strengthening of masonry members with TRM 9

2.3 Shear strengthening of RC beams with TRM 11

2.4 Performance of TRM at high temperature or fire 16

2.5 Strengthening of existing structures: Selected case studies 18

2.6 Contribution of this study 20

3 MECHANICAL CHARACTERISATION OF MATERIALS USED FOR STRENGTHENING 23

3.1 Mortar 24

3.2 Epoxy Resin 24

3.3 Textile Fibre Materials 24

3.4 Tensile Tests on Textile Fibre Materials 26

3.5 Shear Tests on Textile Fibre Materials 27

3.6 Tensile tests on TRM coupons 30

Use of optical FBG sensors in TRM coupons 35

3.7 Tensile tests on FRP coupons 37

4 SHEAR STRENGTHENING OF MEDIUM-SCALE RECTANGULAR RC BEAMS USING TRM 39

4.1 TRM vs FRP in shear strengthening of RC beams 40

4.1.1 Experimental Programme 40

4.1.1.1 Test specimens and investigated parameters 40

4.1.1.2 Materials and strengthening procedure 42

4.1.1.3 Experimental set-up and procedure 44

4.1.2 Experimental results 44

4.1.3 Discussion 51

4.1.3.1 Strengthening configuration and number of layers 51

4.1.3.2 Deformation aspects of jackets based on DIC 53

4.1.4 Effective Stress and TRM versus FRP Effectiveness Factor: Design Aspects 55
4.1.5 Summary 58
4.2 Effect of amount of external reinforcement ratio, textile material and geometry and shear span-to-depth ratio on RC beams strengthening in shear with TRM 59
4.2.1 Experimental Programme 59
4.2.1.1 Test specimens and investigated parameters 59
4.2.1.1 Materials and strengthening procedure 61
4.2.1.2 Experimental set-up and procedure 62
4.2.2 Experimental results 62
4.2.3 Discussion 67
4.2.3.1 Effect of external reinforcement ratio 67
4.2.3.2 Effect of textile geometry 68
4.2.3.3 Effect of shear span-to-depth ratio 71
4.2.4 Summary 73
4.3 Effect of textile mesh material characteristics (mesh size, amount and material of fibres in the horizontal direction) 74
4.3.1 Experimental Programme 74
4.3.2 Experimental results 76
4.3.3 Discussion 78
4.3.3.1 Effect of fibre rovings characteristics (material and spacing) in the horizontal (non-loading) direction of the textile material 78
4.3.3.1 Effect of textile geometry 80
4.3.3.1 Effect of number of layers 82
4.3.4 Summary 82
5 SHEAR STRENGTHENING OF FULL-SCALE RC T-BEAMS USING TEXTILE-REINFORCED MORTAR AND TEXTILE-BASED-ANCHORS 85
5.1 Experimental Programme 86
5.1.1 Test specimens and investigated parameters 86
5.1.2 Material properties 88
5.1.3 Design and fabrication procedure of textile-based anchors 89
5.1.4 Tensile capacity of anchors 92
5.1.5 Strengthening Procedure 93
5.1.6 Experimental Setup and Procedure 94
5.2 Experimental Results 96
5.2.1 Strengthened specimens without anchors 98
5.2.2 Strengthened specimens with anchors 100
5.3 Discussion 103
5.3.1 Effect of investigated parameters 103

5.3.1.1 Anchorage system of the U-jacket 103
5.3.1.2 Number of Layers 104
5.3.1.3 Textile geometry 105
5.3.1.4 Textile material 106
5.3.1.5 Adhesive Material (TRM vs. FRP Jackets) 106
5.3.2 Deformation Aspects of Jackets based on DIC 107
5.4 Design model 110
5.4.1 Methodology 110
5.4.2 Model calibration to the test results 111
5.5 Summary 112

6 TRM VERSUS FRP JACKETING IN SHEAR STRENGTHENING OF RC MEMBERS SUBJECTED TO HIGH TEMPERATURE 115

6.1 Experimental Programme 116
6.1.1 Test Specimens, Investigated Parameters, Materials and Strengthening Procedure 116
6.1.2 Experimental Setup and Procedure 122
6.2 Experimental Results 124
6.3 Discussion 132
6.3.1 Effect of investigated parameters for medium-scale beams tested at high temperature 132
6.3.1.1 Matrix Material (TRM vs. FRP Jackets) 133
6.3.1.2 Textile properties (geometry, material) 136
6.3.2 Performance of full-scale T-beams strengthened with TRM jackets at 150 ^{o}C 137
6.4 Stress reduction factor for TRM and FRP systems 137
6.5 Summary 139

7 ANALYTICAL MODELS FOR THE CALCULATION OF THE CONTRIBUTION OF THE TRM JACKETING TO THE TOTAL SHEAR RESISTANCE (V_f) OF RC BEAMS 141

7.1 Introduction 142
7.2 Failure of strengthened specimens due to debonding of the TRM (or FRP) jacket 143
7.3 Failure of strengthened specimens due to fracture of the TRM jacket 155
7.4 Failure of strengthened specimens due to local damage of the TRM jacket 157
7.5 Summary of design approach for the calculation of the contribution of TRM jacketing, V_f to the total shear resistance of RC beams 166
7.6 Prediction of shear resistance of un-retrofitted (control) specimens 171
7.7 Summary 172

8 SUMMARY, CONCLUSIONS AND RECOMMENDATIONS FOR FUTURE RESEARCH 175

8.1 Summary 175

8.2 Conclusions 176
8.2.1 Shear strengthening of medium-scale rectangular RC beams using TRM 177
8.2.1.1 TRM vs FRP in shear strengthening of RC beams 177
8.2.1.2 Effect of amount of external reinforcement ratio, textile material and geometry and shear span-to-depth ratio on RC beams strengthening in shear with TRM 177
8.2.1.3 Effect of textile mesh material characteristics (mesh size, amount and material of fibres in the horizontal direction) 178
8.2.2 Shear strengthening of full-scale RC T-beams using TRM and textile-based anchors 179
8.2.3 TRM versus FRP jacketing in shear strengthening of RC members subjected to high temperature 180
8.2.4 Design models for the calculation of the contribution of the TRM jacketing to the total shear resistance (V_f) of RC beams 181
8.2.5 Future Research 182
REFERENCES 183
APPENDIX A – DEFINITION OF λ_s 193
APPENDIX B – DESIGN OF BEAMS 195
APPENDIX C – READINGS OF STRAIN GAUGES IN T-BEAMS 201
APPENDIX D – ADDITIONAL INFORMATION 205
PERSONAL DEVELOPMENT 207

List of abbreviations

DIC – Digital Image Correlation

EB – Externally bonded

FBG – Fibre Bragg Grating

FRCM – Fibre Reinforced Cementitious Matrix

FRP – Fibre Reinforced Polymers

FW – Fully-Wrapped

LVDT – Linear Variable Differential Transducer

PBO – Polyparaphenylene Benzobis Oxazole

RC – Reinforced Concrete

SB – Side-Bonded

SHM – Structural Health Monitoring

TRM – Textile Reinforced Mortar

UW – U-Wrapped

Notations

A_a : Area of anchor fibres

A_{anc} : Area of two anchors (one anchor per beam's side)

A_ℓ : Area of one TRM layer

A_{rov} : Area of one fibre roving

b : Bond width

b_w : Width of the beam

d : Effective depth of the section

d_A : Vertical displacement of the top of the frame at picture-frame shear tests

D_f: : Stress distribution factor

d_{fb} : Bottom end of the effective (TRM or FRP) jacket

d_{ft} : Coordinate of the top end of the effective (TRM or FRP) jacket

E_a : Modulus of elasticity of anchor fibres

E_f : Modulus of elasticity of the fibres

E_{f_FRP} : Modulus of elasticity of the FRP specimen

E_{f_TRM} : Modulus of elasticity of the cracked TRM specimen

$E_{f_textile}$: Modulus of elasticity of bare textile fibre material

f_{bm} : bond strength of mortar

f_c : Compressive strength of concrete

f_{cm} : Mean compressive strength of concrete

f_{ct} : Tensile splitting of concrete

$f_{f,anc}$: Tensile capacity of anchor

$f_{fe,anc}$: Effective strength of anchors

f_{fed} : Design value for the FRP or TRM effective stress

$f_{fed,max}$: Maximum design stress in FRP or TRM

f_{fu} : Ultimate strength of TRM or FRP jacket

F_s : Force applied from the tensile machine in picture-frame tests

f_{tm} : tensile strength of mortar

G : Shear modulus of elasticity of the textile

h_{fe} : Effective height of the bonded reinforcement

h_s : Depth of the slab

h_w : Height of T-beam's web

k_t : Effectiveness factor at high temperature

$k_{TRM/FRP}$: Effectiveness factor

k : Reduction factor

l : Length required to achieve stress value equal to σ

L_e : Effective bond length

L_{frame} : Frame length

L_{max} : Available bond length

L_s : Clear shear span

n_a : Number of anchors

n_ℓ : Number of TRM layers

P_{rov} : Perimeter of a single roving

P_u : Maximum load carried out by the TRM strips on direct shear tests

$P_{u,exp}$: Experimental value of maximum load carried out by the TRM strips on direct shear tests

$P_{u,pre}$: Predicted value of maximum load carried out by the TRM strips on direct shear tests

R : Ratio of effective stress or strain in FRP to its ultimate strength or elongation

s : Anchors spacing

s_f : spacing of FRP or TRM strips measured along longitudinal axis

t_f : Nominal thickness of the textile

T_g : Glass transition temperature

t_{rov} : Thickness of a single fibre roving

V_f : Contribution of strengthening to the shear capacity of the beam

$V_{f,exp}$: Experimental value of the contribution of strengthening to the shear capacity of the beam

$V_{f,pre}$: Predicted value of the contribution of strengthening to the shear capacity of the beam

V_R : Shear force in the critical span at peak load

$V_{R,con}$: Shear resistance of the control specimen

$V_{R,str}$: Shear resistance of the strengthened specimen

γ : Average shear strain at the critical shear span

γ_f : Shear angle in picture-frame tests

γ_{Pmax} : Average shear strain of the critical shear span at peak load

$\gamma_{Pmax,con}$: Average shear strain of the control specimen

$\gamma_{Pmax,str}$: Average shear strain of the strengthened specimen

ε_{eff} : Effective strain

ε_{fu} : Ultimate tensile strain

η_e : Strength reduction factor

θ : Angle between the shear crack and the axis of the beam

θ_f : Angle of the frame in picture-frame tests

ρ_f : Geometrical reinforcement ratio of the composite material which is expressed as $2t_f/b_w$

σ : Stress that the TRM jacket should have when local damage of the jacket is prevented

σ_{eff} : Effective stress

σ_{exp} : Experimental stress value

Table of figures

Figure 2.1. Textile fibre reinforcements: (a) carbon-fibre textile; (b) glass-fibre textile; (c) basalt-fibre textile; (d) PBO-fibre textile (dimensions in mm). 6

Figure 2.2. (a) Surface preparation using hydrojetting; (b) Application of reinforcement mesh at the top portion of tunnel lining (ACI 549.4R-13). 18

Figure 2.3. (a) Detail view of a damaged section (Altmeyer et al., 2012). 19

Figure 3.1. Textiles with equal quantity of fibres in two orthogonal directions used in this study: (a) light carbon-fibre textile (CL); (b) heavy carbon-fibre textile (CH); (c) glass-fibre textile (G); (d) basalt-fibre textile (B) (dimensions in mm). 25

Figure 3.2. FORMAX textiles used in this study: (a) F10x20; (b) F10x40; (c) F20x20; (d) F20x40 (dimensions in mm). 25

Figure 3.3. (a) Test set-up for tensile testing of textile fibre materials; (b) rupture of textile fibre materials. 26

Figure 3.4. Stress versus strain curves for (a) light-weight carbon, heavy-weight carbon, glass and basalt fibre textiles; (b) all FORMAX textiles, namely F10x20, F10x40, F20x20 and F20x40. 27

Figure 3.5. (a) Sample of textile material for shear tests; (b) shear test apparatus; (c) picture-frame: starting position; (d) picture-frame: deformed position. 28

Figure 3.6. (a) Shear force versus shear angle curves for all eight textile materials; (b) shear modulus versus shear angles curves for all eight textile materials; (c) shear modulus versus shear angles curves for FORMAX textile materials. 29

Figure 3.7. (a) Geometry of TRM coupons; (b) test set-up for tensile testing of TRM coupons. 30

Figure 3.8. Typical stress versus strain curve of TRM coupon subjected to tensile testing. 31

Figure 3.9. Stress versus strain curves for (a) light-weight carbon textile (CL); (b) heavy-weight carbon textile (CH); (c) glass textile; (d) basalt textile. 32

Figure 3.10. Stress versus strain curves for (a) F10x20; (b) F10x40; (c) F20x20; (d) F20x40 textile. 32

Figure 3.11. Failure modes of TRM coupons. 33

Figure 3.12. Results of TRM coupons at bar charts format: (a) ultimate tensile strength, f_{fu}; (b) ultimate strain, ε_{fu} (%); (c) modulus of elasticity of cracked specimen, E_{f_TRM}. 35

Figure 3.13. (a) Configuration of FBG sensors; (b) preparation of TRM coupon; (c) stress versus strain curves. 37

Figure 3.14. (a) Geometry of FRP coupons; (b) test set-up for tensile testing of FRP coupons; (c) typical failure mode of FRP coupons; (d) stress versus strain curves for FRP and TRM coupons. 38

Figure 4.1. Test set-up: (a) Overall 3D view; (b) front view (dimensions in mm). 40

Figure 4.2. (a) Beam geometry and reinforcement; (b) cross section (dimensions in mm). 41

Figure 4.3. (a) Groups of specimens. 41

Figure 4.4. (a) Prepared concrete surface before strengthening; (b) impregnation of the textile fibres with epoxy resin; (c) application of an extra layer of mortar on the top of the final textile layer. 43

Figure 4.5. (a) Configuration of the two potentiometers (D1, D2) and the LVDT at the shear-critical span; (b) shear deformation measurement by X configuration. 44
Figure 4.6. Load versus vertical displacement curves for all tested specimens. 45
Figure 4.7. Dominant shear crack in the control beam. 46
Figure 4.8. (a) FRP debonding in SB strengthening configuration; (b),(c) FRP debonding in UW strengthening configuration; (d) flexural failure of specimen with FW FRP jacket. 47
Figure 4.9. (a) Failure modes of TRM-retrofitted specimens: (a)-(c) Specimens SB_M1, UW_M1 and FW_M1 – local damage of the jacket; (d),(e) SB_M2 and UW_M2 – debonding of the jacket over a large area of the shear span: peeling off of the concrete cover; (f) FW_M2 – flexural failure despite the shear cracking of the TRM jacket; (g) SB_M3 – debonding of the jacket over a large area of the shear span: peeling off of the concrete cover; and (h) UW_M3 – abrupt debonding of the TRM jacket over the whole area of the shear span: peeling off of the concrete cover. 48
Figure 4.10. Load versus average shear strain curves. 50
Figure 4.11. (a) Effect of strengthening configuration on the shear capacity enhancement; (b) effect of number of layers on the shear capacity enhancement. 52
Figure 4.12. Overlapping of two textiles with an offset. 53
Figure 4.13. Relative vertical displacements along the beam height at the central cross-section of the critical shear span, at the instant of peak load. 54
Figure 4.14. Field of vertical axis deformations in the critical shear span of TRM-retrofitted specimens at the instant of peak load. 55
Figure 4.15. Experimentally obtained effective strains versus $\rho_f E_f / f_c^{2/3}$ and comparison with the theoretical curve of Triantafillou and Antonopoulos (2000) model. 57
Figure 4.16. (a) Schematic test set-up; (b) cross-section (dimensions in mm). 59
Figure 4.17. Schematic representation of different strengthening configurations. 61
Figure 4.18. (a) Impregnation of the textile fibres with mortar and (b) final layer of mortar on the top of the final textile layer. 62
Figure 4.19. Three-point bending test set-up of beams. 63
Figure 4.20. Load versus vertical displacement curves for all tested specimens of 2.6 shear span-to-depth ratio. 63
Figure 4.21. Shear force versus vertical displacement curves for all tested specimens of shear span-to-depth ratio equal to 1.6, 2.6 and 3.6. 64
Figure 4.22. Failure modes of carbon TRM-retrofitted specimens of 2.6 shear span-to-depth ratio - abrupt debonding of the TRM jacket over the whole area of the shear span: peeling off of the concrete cover for specimens: (a) CL1; (b) CL1_strips; (c) CH1_CL1; (d) CL3; (e) CH2_CL1 and (f) CH3_CL1. 65
Figure 4.23. Failure modes of glass and basalt TRM-retrofitted specimens of 2.6 shear span-to-depth ratio: (a) specimen G1 - fracture of glass TRM jacket; (b)-(c) specimens G3 and G7 - debonding of the glass TRM jacket over the whole area of the shear span: peeling off of the concrete cover; (d)

specimen B1 - fracture of basalt TRM jacket; (e)-(f) specimens B3 and B7 - debonding of the basalt TRM jacket over the whole area of the shear span: peeling off of the concrete cover. _____ *65*

Figure 4.24. Failure modes of specimens of 1.6 and 3.6 shear span-to-depth ratios: (a) specimen CON_3.6 - dominant shear crack; (b) specimen CON_1.6 - multiple shear cracks; (c) specimen CL1_3.6 - debonding of the jacket at area below the shear crack: peeling off of the concrete cover; (d) specimen CL1_1.6 - debonding of the TRM jacket over the whole area of the shear span: peeling off of the concrete cover; (e)–(f) specimens CL3_3.6 and CL3_1.6 - debonding of the TRM jacket over the whole area of the shear span: peeling off of the concrete cover. _____ *66*

Figure 4.25. Experimentally obtained effective strains versus ρ_f values for specimens received: (a) carbon TRM and FRP U-jackets and (b) glass and basalt TRM U-jackets. _____ *67*

Figure 4.26. Textile properties and geometry of roving in: (a) heavy carbon textile (CH); (b) light carbon textile (CL); (c) glass textile (G) and (d) basalt textile (B). _____ *69*

Figure 4.27. Field of vertical axis deformations in the critical shear span of TRM-retrofitted specimens: (a) CH1; (b) CL1_strips; (c) CH2; (d) CL3 at the instant of peak load. _____ *70*

Figure 4.28. Effect of shear-span-to depth ratio, a/d on the shear resistance of the control specimen. _____ *72*

Figure 4.29. Field of vertical axis deformations in the critical shear span of TRM-retrofitted specimens: (a) CL1_1.6; (b) CL3_3.6; (c) CL1; (d) CL3; (e) CL1_1.6; (f) CL3_3.6 at the instant of peak load. _____ *72*

Figure 4.30. Effect of shear-span-to depth ratio on: (a) the contribution of the jacket to the total shear resistance, V_f and (b) the shear capacity enhancement, $V_f/V_{R,con}$ (%). _____ *73*

Figure 4.31. Schematic representation of different strengthening configurations. _____ *74*

Figure 4.32. (a) Prepared concrete surface before strengthening; (b) impregnation of the textile fibres with mortar; (c) final layer of mortar on the top of the final textile layer. _____ *75*

Figure 4.33. Load versus vertical displacement curves for (a) F10x20 and F10x40 textile materials; (b) F20x20 and F20x40 textile materials. _____ *76*

Figure 4.34. (a) Failure modes of specimens received FORMAX textile materials: (a) specimen F10x20_1 – local damage of the jacket; (b),(c) specimen F10x20_3 – debonding of the jacket over a large area of the shear span: peeling off of the concrete cover; (d) specimen F10x40_1 – local damage of the jacket; (e),(f) specimen F10x40_3 – debonding of the jacket over a large area of the shear span: peeling off of the concrete cover; (g) specimen F20x20_1 – local damage of the jacket; (h) specimen F20x20_3 – local damage of the jacket in one side of the beam; (i) specimen F20x20_3 – debonding of the jacket over an area of the shear span; (j) specimen F20x40_1 – local damage of the jacket; (k) specimen F20x40_3 – local damage of the jacket in one side of the beam; (l) specimen F20x40_3 – debonding of the jacket over an area of the shear span. _____ *77*

Figure 4.35. Effect of the fibre rovings characteristics (material and spacing) in the horizontal direction of the textile on the shear capacity enhancement for specimens strengthened with textile

materials with carbon fibre rovings of (a) A_{rov}=0.95 mm^2 and (b) A_{rov}=1.90 mm^2 in the vertical direction. _____ *79*

Figure 4.36. Textile properties and geometry of roving in FORMAX textiles: (a) F10x20; (b) F10x40; (c) F20x20; (d) F20x40. _____ *80*

Figure 4.37. (a) Effect of area of roving, A_{rov} on the shear capacity enhancement; (b) effect of number of layers on the shear capacity enhancement. _____ *81*

Figure 5.1. (a) Schematic test set-up; (b) cross-section (dimensions in mm). _____ *86*

Figure 5.2. Schematic representation of different strengthening configurations. _____ *88*

Figure 5.3. (a) Sketch of textile-based anchor; (b) geometry of the textile-based anchor; (c) partial removal of transverse rovings; (d) separate grid parts of the fanned part of an anchor. _____ *90*

Figure 5.4. (a) Custom-made carbon-fibre rebar to be used for tensile testing; (b) test set-up for tensile testing of the carbon-fibre rebars; (c) strain versus stress curves for the three tested rebars. *92*

Figure 5.5. (a) Impregnation of the textile fibres with mortar; (b) injection of epoxy resin into the slab holes; (c) impregnation of dry fibres at the central part of anchor with epoxy resin; (d) textile-based anchors applied over the TRM layer. _____ *94*

Figure 5.6. (a) Configuration of anchors in (a) specimens CH2_A100 and CL3_A100; (b) specimen CH4_A50, (c) specimen CH4_A100; (d) specimen G7_A100. _____ *95*

Figure 5.7. Three-point bending test set-up of T-beams. _____ *95*

Figure 5.8. Configuration of the two potentiometers (D1, D2) and the LVDT at the shear-critical span. _____ *96*

Figure 5.9. Load versus vertical displacement curves for all tested specimens. _____ *97*

Figure 5.10. (a) Dominant shear crack in the control beam; (b) local damage of the jacket in specimen CH2; (c)-(e) specimens CL3, CH4 and G7 - debonding of the TRM jacket: peeling off of the concrete cover; (f) debonding of the FRP jacket. _____ *98*

Figure 5.11. (a)-(b) Part of U-shaped jacket of specimens CH4 and CH4_R; (c)-(d) shear crack in concrete of specimens CH4 and CH4_R after removal of the jacket. _____ *99*

Figure 5.12. Failure modes of TRM-retrofitted specimens with anchors: (a)-(c) Specimens CH2_A100, CL3_A100 and CH4_A50 – rupture of some anchors and pull-out of the rest; (d) failure of specimen CH4_A100 due to concrete splitting in the slab; (f) fracture of glass TRM jacket in specimen G7_A100. _____ *100*

Figure 5.13. Load versus average shear strain curves. _____ *101*

Figure 5.14. Strain versus load curves using strain gauges readings in specimen CH4_A50. _____ *102*

Figure 5.15. Relative vertical displacements along the T-beam web height at the central cross-section of the critical shear span, at the instant of peak load. _____ *108*

Figure 5.16. Field of vertical axis (in-plane) and out-of-plane (indicating debonding) deformations in the critical shear span of the strengthened specimens at the instant of peak load. _____ *109*

Figure 6.1. Schematic representation of different strengthening configurations adopted in medium-scale rectangular beams. _____ *117*

Figure 6.2. Schematic representation of different strengthening configurations adopted in full-scale T-beams. _____ *119*
Figure 6.3. Effect of temperature on the mortar flexural strength. _____ *121*
Figure 6.4. Photos of the mortar prisms surfaces after the exposure at different temperatures. __ *121*
Figure 6.5. Configuration of all the thermocouples and the LVDT at the shear-critical span in (a) medium-scale rectangular beams and (b) full-scale T-beams. _____ *122*
Figure 6.6. (a) Test set-up and heating system of medium-scale rectangular beams; (b) Test set-up and heating system of full-scale T-beams. _____ *123*
Figure 6.7. Time versus temperature curves for: (a-b) specimen that received three TRM carbon layers for both sides of the beam and (c-d) specimen that received three FRP carbon layers for both sides of the beam. _____ *124*
Figure 6.8. Load versus vertical displacement curves for all medium-scale rectangular beams. ___ *127*
Figure 6.9. Failure modes of medium-scale rectangular beams: (a) CON_150 - dominant shear crack; (b) specimen UW_RCH3_20 - debonding of the jacket: peeling off of the concrete cover; (c)-(f) specimens SB_RCH3_150 and UW_RCH3_150 - adhesive failure at the resin-concrete interface; (g) specimen FW_RCH2_150 - slippage of the vertical fibre rovings through the epoxy resin; (h) specimen FW_RCH2_150 – delamination of textile used for overlapping; (i) specimen UW_RCH3_100 - adhesive failure at the resin-concrete interface; (j)-(k) specimens UW_MCH2_20 and UW_MCH3_20 - debonding of the jacket: peeling off of the concrete cover; (l)-(m) specimens UW_MCH2_150 and FW_MCH2_150 - local damage of the jacket; (n)-(r) specimens. SB_MCH3_150, UW_MCL3_150, UW_MG7_150 and UW_MCH3_250 - debonding of the jacket: peeling off of the concrete cover. *129*
Figure 6.10. (a) Load versus vertical displacement curves for full-scale T-beams. _____ *131*
Figure 6.11. Failure modes of full-scale T-beams: (a) Dominant shear crack in the control beam; (b) specimen CH4 - debonding of the TRM jacket: peeling off of the concrete cover; (c) failure of specimen CH4_A100 due to concrete splitting in the slab; (d) debonding of the TRM jacket in specimen CH4_150: peeling off of the concrete cover; (e) specimen CH4_150 - detached part of TRM jacket including concrete cover; (f) specimen CH4_A100_150 - pull-out of all anchors due to bond adhesive failure. _____ *131*
Figure 6.12. (a) Effect of strengthening configuration on the shear capacity enhancement at high temperature; (b) effect of number of layers on the shear capacity enhancement at high temperature. _____ *133*
Figure 6.13. Effect of temperature on the shear capacity enhancement for both TRM and FRP system. _____ *135*
Figure 7.1. Notation for a general shear strengthening scheme. _____ *144*
Figure 7.2. Experimental versus predicted V_f values for: (a) Chen and Teng – Initial; (b) Chen and Teng – Modified 1 and (c) Chen and Teng – Modified 2. _____ *149*
Figure 7.3. Experimentally obtained effective stress versus (a) $D_f \beta_w \beta_l (E_f f_c^{0.5}/t_f^{0.5})$ and (b) $D_f \beta_w \beta_l (f_c^{0.5}/t_f^{0.5})$. _____ *150*

Figure 7.4. Experimentally obtained effective stress versus (a) $\rho_f E_f / fc^{0.5}$ and (b) $\rho_f / fc^{0.5}$. _____ 150
Figure 7.5. Experimental versus predicted P_u values for: (a) Chen and Teng – Initial; (b) Chen and Teng – Modified 1 and (c) Chen and Teng – Modified 2 models. _____ 155
Figure 7.6. Local bond response between a single roving and the surrounding mortar._____ 159
Figure 7.7. Reduction factor k versus λs values for: (a) all half-scale beams of this study grouped based on their failure mode; (b) all half-scale beams of this study grouped based on the number of layers; (c) for all beams strengthened in shear with TRM presented in Table 9 and (d) for all beams strengthened in shear with TRM tested either at ambient (Table 7.9) or at high temperature (Table 7.10). _____ 162
Figure 7.8. Reduction factor, k versus λ_s values for: (a) all available data obtained from tests on RC beams strengthened in shear with TRM and direct shear tests on concrete prisms received TRM strips; (b) all available data obtained from tests on RC beams strengthened in shear with TRM and direct shear tests on concrete prisms received TRM strips in which the tensile strength of mortar was experimentally obtained. _____ 166
Figure 7.9. Experimental versus predicted stress values for all available data obtained from tests on either RC beams strengthened in shear with TRM jacketing or direct shear tests on TRM strips. _ 171

Table of tables

Table 3.1. Summary of the results of tensile tests on textile fibre materials. _____ 27
Table 3.2. Shear modulus values, G (GPa) for each textile material. _____ 29
Table 3.3. Summary of TRM coupons results._____ 34
Table 4.1. Concrete strength on the day of testing. _____ 42
Table 4.2. Mortar strength on the day of testing. _____ 43
Table 4.3. Summary of test results._____ 46
Table 4.4. Experimental values of effective strains and effectiveness factor for SB and UW TRM jackets._____ 56
Table 4.5. Strengthening configuration and material properties of all specimens._____ 60
Table 4.6. Summary of test results._____ 64
Table 4.7. Summary of FRP-strengthened specimens results. _____ 68
Table 4.8. Strengthening configuration and material properties of all specimens._____ 75
Table 4.9. Summary of tests results._____ 76
Table 5.1. Strengthening configuration and material properties of all specimens._____ 87
Table 5.2. Concrete and mortar strength on the day of testing. _____ 88
Table 5.3. Details of specimens with anchored TRM jackets._____ 91
Table 5.4. Summary of test results _____ 97
Table 5.5. Effective strength of anchors and strength reduction factor for specimens failed due to anchorage loss. _____ 111

Table 6.1. Strengthening configuration and material properties of all specimens. _____ *118*
Table 6.2. Conrete and mortar strength of all specimens. _____ *120*
Table 6.3. Summary of test results of beams tested at ambient temperature and at 150 ^{o}C. _____ *128*
Table 6.4. Summary of tests results of medium-scale beams tested at 20 ^{o}C, 100 ^{o}C, 150 ^{o}C and 250 ^{o}C. _____ *128*
Table 6.5. Experimental values of effective stress and stress reduction factors for TRM and FRP jackets. _____ *138*
Table 7.1. Experimental data on shear strengthening of RC beams with TRM (or equivalent FRP) jacketing that failed due to debonding of the jacket. _____ *146*
Table 7.2. Comparison between experimental and predicted V_f values in case of failure due to debonding of the jacket. _____ *148*
Table 7.3. Experimental data on shear strengthening of RC beams with FRP jackets (consisting of glass continuous sheets) that failed due to debonding of the jacket. _____ *152*
Table 7.4. Comparison between experimental and predicted V_f values for data of Table 7.3. ____ *152*
Table 7.5. Experimental data on double-lap direct shear tests that received TRM strips and failed due to debonding. _____ *152*
Table 7.6. Comparison between experimental and predicted P_u values for failure due to debonding. _____ *154*
Table 7.7. Experimental data on shear strengthening of RC beams with TRM jacketing that failed due to fracture of the jacket. _____ *156*
Table 7.8. Comparison between experimental and predicted V_f values in case of failure due to fracture of the jacket. _____ *157*
Table 7.9. Well reported available experimental data on shear strengthening of RC beams with TRM jacketing consisting of dry textile fibre materials. _____ *161*
Table 7.10. Experimental data on shear strengthening of RC beams with TRM jacketing tested at high temperature. _____ *163*
Table 7.11. Experimental data on direct shear tests that received TRM strips consisting of dry textile fibre materials. _____ *164*
Table 7.12. Comparison between experimental and predicted stress values for all available data obtained from tests on either RC beams strengthened in shear with TRM jacketing or direct shear tests with TRM strips. _____ *168*
Table 7.13. Comparison between experimental and predicted values for the shear resistance of the rectangular medium-scale beams. _____ *172*

Chapter 1

INTRODUCTION

1.1 Background

The issue of upgrading existing structures has been of great importance over the last decades due to their deterioration; ageing, environmental induced degradation, lack of maintenance or need to meet the current design requirements. Replacing the deficient concrete structures in the near future with new is not a viable option as it would be prohibitively expensive. For this reason a shift from new construction towards renovation has been witnessed in the European construction sector, between 2004 and 2013, with practically 50% of the total construction output being renovation and structural rehabilitation.

Fibre reinforced polymers (FRP) have been widely used as externally bonded (EB) reinforcement of existing structurally deficient structures over the last three decades due to their favourable properties (i.e. high strength to weight ratio, corrosion resistance, ease and speed of application, and minimal change of geometry). However, the FRP strengthening technique entails a few drawbacks mainly associated with the use of epoxy resins. In particular, except from their high costs and their inability to apply on wet surfaces, FRP have very poor performance at high temperature as under loading epoxy resins normally lose their tensile capacity. In an attempt to alleviate the problems arising from the use of epoxies, researchers have introduced a novel composite material, namely textile-reinforced mortar (TRM), which combines advanced fibres in form of textiles (with open-mesh configuration) with inorganic matrices, such as cement-based mortars. Over the last decade it has been reported in the literature that TRM is a very promising alternative to the FRP retrofitting solution.

Shear strengthening of RC beams or bridge girders in old RC structures is one of the most common needs when assessing their strength under the current code requirements (i.e. Eurocodes). This is due to insufficient amount of shear reinforcement, corrosion of existing shear reinforcement, low concrete strength and/or

increased design load. Only few researchers have investigated the use of TRM for shear strengthening of RC beams and therefore more research is required in this field.

1.2 Aim of the research

Aim of the research included in this thesis is to evaluate the use of TRM in shear strengthening of RC beams. To achieve this aim, the following objectives were set:

- Studying medium-scale rectangular RC beams strengthened in shear with TRM
- Studying full-scale RC T-beams strengthened in shear with TRM
- Studying the behaviour of TRM at high temperature testing both medium-scale rectangular beams and full-scale T-beams strengthened in shear with TRM
- Proposing design models for the prediction of the contribution of TRM jacket to the total shear resistance of beams

More details about the different parameters investigated in this study are given in section 2.6.

1.3 Thesis layout

This thesis consists of eight chapters with the present chapter to be the introductory. Chapter 2, provides a description of TRM as composite material, whereas a literature review on the use of TRM for strengthening existing RC or masonry members is also included. Description of the components of which TRM (and FRP) are made as well as characterisation of the tensile properties of TRM (and FRP) composite material are included in Chapter 3. Chapter 4 includes all the experimental work conducted on medium-scale rectangular beams, whereas Chapter 5 presents the experimental work on full-scale T-beams. The behaviour of TRM at high temperature is studied in Chapter 6. In chapter 7, the proposed design models for the prediction of the contribution of TRM jacketing to the total shear resistance of the beam are presented and verified with the available experimental data, whereas the main conclusions drawn from this study as well as recommendations for future research are summarised in Chapter 8.

Chapter 2

LITERATURE REVIEW

ABSTRACT

This chapter starts with the description of TRM as composite material, whereas a literature survey on the use of TRM as strengthening material follows. In particular, after a brief description of the studies that investigated the bond of TRM with the concrete substrate, the use of TRM for strengthening RC and masonry members is described. A detailed presentation of the available studies on shear strengthening of RC beams with TRM is also included, whereas the results of the limited studies on the performance of TRM at high temperature are also reported. Case studies of strengthening of existing structures with TRM are also presented and the contribution of this study to the available research on shear strengthening of RC beams with TRM is also presented at the end of Chapter 2.

2.1 TRM - Introduction

The issue of upgrading existing structures has been of great importance over the last decades due to their deterioration; ageing, environmental induced degradation, lack of maintenance or need to meet the current design requirements. Fibre reinforced polymers (FRP) have been widely used as externally bonded (EB) reinforcement of existing structurally deficient structures over the last three decades (i.e. Triantafillou 1998, Khalifa et al. 1998, Bousselham and Chaallal 2006 and Galal and Mofidi 2009) due to their favourable properties (i.e. high strength to weight ratio, corrosion resistance, ease and speed of application, and minimal change of geometry). However, the FRP strengthening technique has a few drawbacks mainly associated with the use of epoxy resins, namely high cost, poor performance in high temperatures, inability to apply on wet surfaces, incompatibility to substrate materials (concrete or masonry). In an attempt to alleviate the problems arising from the use of epoxies, many researchers suggested the replacement of organic (epoxy resins) with inorganic (mortar) matrix. However, the penetration and impregnation of fibre sheets in this case was very difficult due to the size of granules included into the mortar as even a fine mortar cannot impregnate individual fibres as resins do. Improved bond conditions between fibres and matrix in mortar-based composite materials were achieved when continuous fibre sheets were replaced by textiles, introducing a novel composite material, namely textile-reinforced mortar (TRM).

Textile-based composite materials have been experimentally studied the last two decades as they can be used for construction of new prefabricate structural elements made of Textile Reinforced Concrete, TRC (i.e. Curbach and Jesse 1999, Brameshuber et al. 2001) or strengthening of existing structures (Textile Reinforced Mortar, TRM i.e. Triantafillou et al. 2006 and Bournas et al. 2007). TRM combines advanced fibres in form of textiles (with open-mesh configuration) with inorganic matrices, such as cement-based mortars. The same material can also be found in the literature as FRCM. TRM is a low cost, friendly for manual workers, fire resistant, and compatible to concrete and masonry substrates material which can be applied on wet surfaces or at low temperatures. For all these reasons, use of TRM is progressively becoming more attractive for the strengthening of existing concrete and masonry structures than the widely used FRP.

TRM is a composite material that consists of textile mesh materials that constitute the reinforcement of the composite material and inorganic mortar that constitutes the matrix of the composite material.

❖ Textile fibre reinforcement

Textile mesh materials used as reinforcement of the TRM composite material consist of fibre rovings arranged in two or more directions. Fibre rovings are spaced at specific distance to allow for the formation of textile mesh. The perforations between the fibre rovings enable the impregnation of fibres with the matrix material (mortar) and as a result they contribute to the mechanical interlock between the reinforcement and the matrix. Textile mesh material can be fabricated by weaving of warp and wept fibre rovings (woven textiles) or by simply holding the warp with the wept rovings using either stitching or thermo-sealing (non-woven or stitched textiles). Woven textiles are usually quite stable whereas the stability of non-woven textiles depends on the quality of stitching or thermo-sealing used to fasten the warp with the wept fibre rovings. In any case, coating of both woven and non-woven textiles with epoxy resin can improve even more the stability of textile material and the mechanical interlock between the textile and the matrix. However, coated textiles are stiffer and as a result they cannot be easily applied to complex geometries (i.e. U-shaped or fully-wrapped jackets).

The key geometrical characteristics of the textile material are summarized below:

(a) quantity of fibres in each fibre roving which is expressed as the weight in *g* of 1 km of fibre roving (TEX)

(b) spacing between fibre rovings (center to center distance) in each direction

(c) (areal) weight of the textile expressed in g/m^2

(d) distribution of the total quantity of fibres in each direction (i.e. 50%-50% means that equal quantity of fibres are included in both directions)

Another key property of the textile material is the nominal thickness (t_f) in each direction of the textile that is calculated given (c), (d) and the density (that is unique for each material of which the fibres are made).

Figure 2.1 depicts photos of textile materials which are used as reinforcement in TRM.

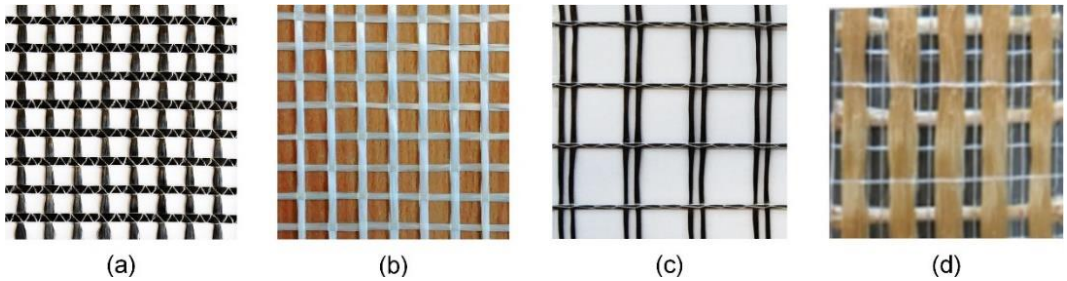


Figure 2.1. Textile fibre reinforcements: (a) carbon-fibre textile; (b) glass-fibre textile; (c) basalt-fibre textile; (d) PBO-fibre textile (dimensions in mm).

❖ Inorganic Matrix

The composition of inorganic matrix significantly affects the response of TRM as a composite material. In specific, impregnation of fibres with inorganic matrix is really important for achieving good bond between the fibres and the matrix. Mortar has to include fine granules and be characterised of plastic consistency, good workability, low viscosity (for easy application in vertical or steep surfaces) and sufficient shear strength (to prevent the debonding of the composite material from the substrate; namely mortar or concrete and masonry). Cement-based mortars are widely used as matrix of TRM composite material. The mechanical properties of mortar, namely the flexural strength and the bond between the matrix and the fibre rovings can be significantly improved by adding polymers.

2.2 Use of TRM for strengthening and seismic retrofitting of concrete or masonry members

2.2.1 Bond behaviour of TRM

The study of bond behaviour between TRM and concrete substrate is of interest as it contributes to the better understanding of forces transferring mechanism in TRM-strengthened members that is necessary for developing design guidelines to be used in TRM-strengthened applications. The main investigated parameters studied on the bond behaviour of TRM comprise: the bond lengths (D'Ambrisi et al. 2013, Ombres 2015, Sneed et al. 2015, Tran et al. 2014 and Raoof et al. 2016), the number of layers (Ombres 2015 and Raoof et al. 2016), the concrete compressive strength (Tran et al. 2014 and Raoof et al. 2016), the surface preparation (D'Antino et al. 2015 and Raoof et al. 2016) and the coating of textiles (Raoof et al. 2016).

In particular, it was concluded that the bond capacity increases in non-proportional way with the bonding length. Specimens strengthened with one TRM layer failed due to slippage of the fibres through the mortar. Increasing the number of layers for a specific bond length results in bond capacity increase and change in the failure mode. Moreover, the concrete compressive strength and the kind of surface preparation marginally affects the bond behaviour of TRM. Finally, coated textiles have much better bond behaviour compared with uncoated textiles, as slippage of fibres through the mortar (that is a very common failure mode in case of one TRM layer) was prevented owing to the improved mechanical interlock conditions between the mortar and the textile achieved by coating the textiles.

2.2.2 Strengthening of Reinforced Concrete (RC) members with TRM

Experimental studies on strengthening of RC members with TRM are grouped as:

- Confinement of concrete members or columns (Triantafillou et al. 2006, Peled 2007 and Ortlepp et al. 2009)
- Confinement of RC columns (Bournas et al. 2007)
- Seismic retrofitting of RC columns (Bournas et al. 2007, Bournas and Triantafillou 2011a, b)
- Flexural strengthening of RC beams or slabs (Jesse et al. 2008, Papanicolaou et al. 2009, D' Ambrisi and Focacci 2011, Schladitz et al. 2012; Elsanadedy et al. 2013, Loreto et al. 2014, and Koutas and Bournas 2016)
- Strengthening of RC beam-column joints (Al-Salloum et al. 2011)
- Shear strengthening of RC beams (Triantafillou et al. 2006, Brückner et al. 2008, Blanksvard et al. 2009, Si Larbi et al. 2010, Contamine et al. 2013, Al-Salloum et al. 2012, Baggio et al. 2014, Azam and Soudki 2014, Tzoura and Triantafillou 2016, Loreto et al. 2015, Ombres 2015, Trapko et al. 2015, Escrig et al. 2015 and Awani et al. 2016)

In this paragraph the most indicative studies on confinement of concrete or RC members are described. Triantafillou et al. (2006) studied the use of TRM jackets for confinement of small-scale concrete specimens. The type of mortar, the comparison of inorganic mortar with resin-based matrix material (TRM versus FRP), the number of textile layers and the effectiveness of bonded versus unbonded confining system were the main investigated parameters. Both cylindrical and rectangular specimens

were tested under compression. Based on the results of tests on cylinders they concluded that TRM constitutes an effective solution on confinement of RC members in terms of compressive strength and deformability but its effectiveness depends on the number of layers. Based on the experimental response of rectangular columns it is concluded that TRM jackets are as effective as FRP jackets in terms of strength and slightly less effective in terms of deformability. Bournas et al. (2009) compared the effectiveness of TRM with FRP jackets on confinement of RC columns. According to the experimental results of short RC prisms (of dimensions 200X200 mm) that were tested under concentric compression, TRM jackets were about 10% less effective comparing with equivalent FRP jackets. TRM jackets increased the compressive strength and deformability of columns by delaying buckling of the longitudinal bars.

Regarding the seismic retrofitting of RC columns, Bournas et al. 2007 tested three full-scale cantilever-type RC columns (shear span of 1.6 m and cross-section of 250X250 mm) under lateral load, indicating that TRM jackets are practically as effective as FRP jackets in terms of deformation capacity and energy dissipation. Furthermore, Bournas et al. (2009) carried out 10 tests on cantilever-type RC columns studying the performance of TRM jackets versus FRP jackets used for seismic retrofitting of RC columns with continuous or lap-sliced bars. They concluded that TRM jackets were 50% more effective than equivalent FRP jackets based on the results of four tests on columns with continuous longitudinal bars. Finally, TRM jackets were slightly less effective than FRP jackets in terms of deformability for columns with short lap length, whereas they are equally effective comparing with FRP jackets for columns with long lap length.

Some important studies on flexural strengthening of RC beams or slabs are summarized in this paragraph. In particular, D' Ambrisi and Focacci (2011) studied the effectiveness of flexural strengthening of RC beams with TRM jackets. A variety of fibre materials, fibre arrangements, types of matrices and strengthening configurations were considered. Based on their experimental results, the performance of PBO-TRM jacket in terms of load capacity was similar with that of FRP materials. In most cases, TRM-strengthened beams failed due to fibre debonding at fibre-matrix interface (slippage of fibres through the mortar) but without involving debonding of the jacket with part of concrete as observed in case of FRP-strengthened beams. Elsanadedy et al. (2013) tested beams strengthened in flexure with TRM, investigating the effect of type of mortar (cementitious and polymer modified cementitious),

number of TRM layers and type of strengthening material (basalt-based TRM and carbon FRP jackets). They concluded that bond characteristics are better in case of polymer-modified cementitious mortar. The flexural strength of RC beams increased from 39% to 91% owing to increase in the number of TRM layers. Basalt-based TRM jackets were more effective than their FRP counterparts in terms of deflection ductility but slightly less effective in terms of flexural strength. Finally, Koutas and Bournas (2016) studied the use of TRM for strengthening of two-way slabs, mainly investigating the number of TRM layers and the material of textile fibres. They concluded that both pre-cracking and post-cracking stiffness as well as the ultimate load capacity increased with the increase in the number of layers. The load capacity increase of glass and carbon TRM jackets was proportional to the axial stiffness of the provided strengthening. Moreover, the effect of the presence of initial damage in the slab (cracked versus uncracked) was also investigated in this study. In specific, a slab was first subjected to a load level where yielding of the steel reinforcement occurred and significant cracking was observed, and then was unloaded. It was finally tested up to failure after strengthening with three carbon TRM layers and curing. The performance of this cracked slab was compared with an uncracked slab that received two carbon TRM layers and tested up to failure. They concluded that the effectiveness of TRM in increasing the flexural capacity two-way slabs is slightly reduced in pre-cracked slabs. However the increase in post-cracking stiffness was found proportional to the number of TRM layers, irrespective of the presence of initial cracking.

The use of TRM for strengthening column-beam joints was only studied from Al-Salloum et al. (2011). They compared the performance of TRM with FRP as strengthening system of seismically deficient RC beam-column joints concluding that TRM constitutes an effective solution in terms of ductility, shear capacity and dissipation of energy, leading to results that are comparable to those of FRP strengthened joints.

Studies on shear strengthening of RC beams which is also the subject of this thesis are separately described in details in section 2.3.

2.2.3 Strengthening of masonry members with TRM

Experimental studies on strengthening of masonry elements with TRM are grouped as:

- Strengthening of masonry elements for enhancement of their in-plane behaviour (Papanicolaou et al. 2007, Papanicolaou et al. 2011)
- Strengthening of masonry elements for enhancement of their out-of-plane behaviour (Papanicolaou et al. 2008, Harajli et al. 2010, Papanicolaou et al. 2011, Babaeidarabad et al. 2014a)
- Confinement of masonry columns (Ombres 2015)
- Strengthening of Masonry-Infilled RC Frames (Koutas et al. 2015)

The first study on in-plane behaviour of masonry elements strengthened with TRM was that of Papanicolaou et al. (2007). The type of matrix (mortar or resin), the number of textile layers and the level of compressive loading were the main studied parameters. They concluded that TRM jackets were 30-35% less effective in terms of strength compared to resin-based textile configurations. In terms of deformability, TRM jackets were more effective than resin-based textile configurations.

Regarding the out-of-plane behaviour of masonry elements, Papanicolaou et al. (2008) studied the effectiveness of TRM jackets versus resin-based textile jackets. The type of matrix (mortar or resin), the number of textile layers and the orientation of the moment with respect to bed joints were the main investigated parameters. It was concluded that when failure occurs due to damage in the masonry walls, TRM jackets are more effective than resin-based textile jackets. When failure is due to tensile fracture of the textile reinforcement, TRM jackets are slightly less effective as compared to resin-based textile jackets. Generally, the use of TRM jackets leaded to increased strength and deformability, whereas their effectiveness increases as the number of textile layers increases. The type of masonry wall, the type of mortar and type of textile were the investigated parameters studied from Harajli et al. (2010) that carried out tests on masonry walls subjected to static and cyclic out-of-plane loading. Based on the experimental results, the use of lime mortar leads to a slightly increased strength but equal displacement capacity as compared to the cement-based mortar. The load-deflection response is not significantly affected by the type of masonry (concrete block, sandstone or brick). The response of masonry walls strengthened with TRM jackets under cyclic loading was really improved in terms of strength and displacement capacity, stiffness and dissipation of energy.

Ombres (2015) studied the effectiveness of carbon TRM (FRCM) as confinement system for masonry columns. Five masonry columns (of 650 mm length and cross-section of 250x250 mm^2) were tested under eccentrically loading;

eccentricity values varies from 0 to 0.2. He concluded that the failure load of the masonry column wrapped with one layer and tested under compression axial load increased by 78.8%, whereas the corresponding values for masonry columns wrapped with one and two layers and subjected to eccentric axial load were 20% and 42.9%, respectively. The failure of all the confined masonry columns was peudo-ductile due to rupture of the carbon textile in contrary to the failure of un-retrofitted columns that was sudden and brittle.

Finally, Koutas et al. (2015) tested a control (un-retrofitted) RC infilled three-storey frame and a second same frame strengthened with TRM jacket combined with custom-made textile-based anchors both subjected to in-plane loading. The main conclusion of this study was that the global response of the retrofitted infilled frame was significantly improved in terms of lateral strength (approximately 56% increase) and deformation capacity (52% increase at the top of the frame at the ultimate strength state).

2.3 Shear strengthening of RC beams with TRM

Shear strengthening of RC beams or bridge girders in old RC structures is one of the most common needs when assessing their strength under the current code requirements. This is due to insufficient amount of shear reinforcement, corrosion of existing shear reinforcement, low concrete strength and/or increase in the applied load. Only few researchers have investigated the use of TRM for shear strengthening of RC beams, the big majority of which were on small or medium-scale rectangular specimens. All studies published so far on shear strengthening of RC beams with TRM are described in the following paragraphs in details, whereas a summary of the main conclusions is presented at the end of this section.

The first study (published in English) on shear strengthening of existing RC beams with TRM is that of Triantafillou et al. (2006) who tested six RC rectangular beams (of 2.60 m length) deficient in shear. The type of matrix (mortar-resin), the number of layers (1 or 2) and the use of ‘conventional wrapping’ versus ‘spirally applied’ textiles were the studied parameters. A high-strength carbon textile was the reinforcement of the applied TRM system. Based on the experimental results of specimens failed in shear, one layer of TRM jacket was at least 55% less effective than the corresponding FRP jacket but still quite effective as compared to the control

specimen, increasing by 40 kN (71.8%) the shear capacity. The effect of each of the aforementioned investigated parameters was not evaluated as four out of six beams failed in flexure.

Brückner et al. (2008) tested twelve T-beams strengthened in shear with multi-axial AR glass fabric. Three T-beams were used as control specimens, while the remaining beams were strengthened with different number of textile layers (2, 4 and 6). Mechanical anchorage system was also applied to six out of nine strengthened beams aiming to delay the debonding of the TRM jacket. They concluded that TRM jacketing can increase the shear capacity of RC T-beams up to 7% in specimens without anchorage system. The application of the anchorage system increased the effectiveness of TRM jacket up to 14%, preventing the debonding of the TRM jacket.

Blanksvärd et al. (2009) tested 23 concrete beams strengthened in shear with SB mineral-based composite jackets, mainly investigating the effect of mortar properties (three commercial cement mortar mixes were used, mainly varied with the amount of polymers and reinforcing polymers), textile mesh properties (three different carbon grids having different mesh size and mechanical properties were used), concrete strength (varied from 48.9 MPa to 73.5 MPa) and shear reinforcement (no stirrups and stirrups spaced at 250 mm and 350 mm, respectively). Only six beams strengthened in shear with mineral-based composites failed in shear after the rupture of strengthening jacket. The authors concluded that the ultimate shear failure load increased when the fibre amount in the carbon grid was increased.

Si Larbi et al. (2010) studied the shear strengthening of RC beams with TRC plate, carrying out eight tests on small scale rectangular RC beams. Three different mortar mixes were studied (hydraulic mortar with glass fibres, inorganic phosphate cement combined with glass fibers and ultra-high mortar performances combined with short metallic fibres). The strengthening plates were bonded to the beam with epoxy resin and therefore the debonding mechanism of the TRC plate from the concrete substrate was not evaluated. They concluded that the TRC plates made of inorganic phosphate cement-glass fibres or ultra-high performances metallic fibres were quite effective in increasing the shear capacity.

Contamine at al. (2012) tested 11 pre-damaged rectangular RC beams. Two different strengthening methods were used; hand lay-up in situ method and gluing prefabricated plates on the substrate of the beam with epoxy resin. Glass textile mesh was used as reinforcement of TRC plates. They concluded that the response of RC

beams strengthened in shear with TRC jackets is quite similar to this of beams strengthened with carbon FRP jackets, whereas the shear capacity increased up to 38% in case of hand lay-up in situ application.

Al Salloum et al. (2012) carried out ten tests on small-scale rectangular RC beams, studying the effectiveness of basalt side-bonded TRM jackets on shear strengthening of RC beams. The type of mortar (cementitious versus polymer-modified cementitious), the number of TRM layers (two and four) and the textile orientation ($0^o/90^o$, $+45^o/-45^o$) were the main studied parameters. Based on the experimental results the TRM jacketing can increase the shear capacity of beams from 36% to 88%. In addition, the gain in shear capacity increases as the number of TRM layers increases. The inclined textile sheets (with angle of $\pm 45^o$) exhibited better shear capacity than these with orientation $0^o/90^o$. As expected the polymer-modified cementitious mortar was more effective than the cementitious mortar. The authors reported that the failure of all specimens included in this study was due to shear compression, thus did not possibly allow for full exploitation of the TRM strengthening effectiveness.

Baggio et al. (2014) studied shear critical RC beams strengthened with various strengthening systems. Only two of their beams that received TRM jacketing, namely one layer of glass U-shaped TRM jacket, without and with (carbon) anchors, respectively. Based on their results the strength of non-anchored and anchored TRM-strengthened beams increased by 32% and 34%, respectively. Both specimens failed in shear due to rupture of TRM jacket and therefore the anchors were not effective.

The textile material (glass-fibre textile and two carbon-fibre textiles of different weight) and the strengthening configuration (side-bonded vs U-wrapped jackets) were the main parameters studied by Azam and Soudki (2014). Based on the experimental results of seven tests conducted on rectangular beams (of 150 mm width and 350 mm height), the shear capacity of beams increased by up to approximately 100%, when the heaviest carbon-fibre textile was applied either on side-bonded or U-shaped configuration; the failure of these two specimens was due to shear-compression in contrary to the failure of the rest beams that was attributed to shear-tension. The authors also found out that the performances of U-wrapped and side-bonded TRM jackets were similar in terms of strength, deformability and failure modes.

Loreto et al. (2015) studied the use of PBO U-wrapped TRM jackets for shear strengthening of RC rectangular beams (of 152 mm width and 306 mm height) mainly

investigating the effect of number of layers (1 and 4) and the concrete compressive strength. All specimens failed due to shear-compression. The effect of number of layers was similar to that reported in the aforementioned studies. The shear capacity increase was slightly lower in specimens with low concrete compressive strength indicating that concrete compressive strength marginally affects the response of strengthened beams, as also reported in Raoof et al. (2016) that investigated the bond behaviour of TRM.

Ombres (2015) tested rectangular beams (of 150 mm width and 250 mm height) strengthened in shear with PBO U-shaped TRM jackets that subjected to monotonic loading. The critical shear span also included internal shear reinforcement. External reinforcement ratio and strengthening configurations including continuous and discontinuous strips were the main investigated parameters. It was concluded that PBO-TRM jacketing increased the shear capacity of RC beams but its effectiveness strongly depends on the width to spacing ratio of the externally applied reinforcement.

Trapko et al. (2015) tested only three RC rectangular beams (of 150 mm width and 250 mm height) strengthened in shear with PBO U-shaped TRM jackets that mainly varied in the angle of inclination of the reinforcement to the longitudinal axis. Actually, the effectiveness of TRM jacket on increasing the shear capacity of beams could not be evaluated as authors did not test an un-retrofitted (control) specimen.

Escrig et al. (2015) tested nine RC beams (two beams were tested for each strengthening configuration) investigating a variety of TRM systems consisting of: (a) bicomponent mortar (designated as PHDM) with high strength cement, glass fibres, selected aggregates and synthetic polymers in aqueous dispersion combined with basalt fibre reinforcement; (b) hydraulic mortar with fibres and special additives combined with carbon fibre reinforcement; (c) hydraulic pozzolanic mortar with additives combined with PBO fibre reinforcement and (d) hydraulic mortar modified with polymeric additions in combination with glass fibres reinforcement. Only three stirrups were placed in the effective span of the beam (of 1500 mm length), one of them was placed at the middle of the beam and the rest two were placed 250 mm from the middle of the beam. TRM jackets were applied only at the part of the shear span without stirrups (the length of strengthening zone was equal to 500 mm). In most strengthened beams, failure was limited at the non-strengthened zone (of 250 mm length) and therefore the effectiveness of TRM jacketing could not be properly evaluated. The shear capacity of the only two beams that failed in shear along the

strengthening zone was increased by 22% when the second of the above described TRM systems was used.

Tzoura and Triantafillou (2016) studied the effect of number of layers (1 and 2), type of textile (a light-weight and a heavy-weight carbon-fibre textile with double the weight of the light-weight textile) and the use of anchorage system, carrying out tests on large-scale T-beams subjected to cycling loading. They also compared both anchored and non-anchored TRM with equivalent FRP jackets. All strengthened specimens received U-shaped jackets. They concluded that increasing the number of layers the effectiveness of TRM jacket also increased in a non-proportional way. The use of mechanical anchors significantly increased the effectiveness of TRM (and FRP) jackets, whereas the spacing of anchors affected only the performance of beams strengthened with the light-weight carbon-fibre textile. Non-anchored TRM jacket was approximately 55% less effective than its counterpart FRP jacket, whereas the effectiveness of anchored TRM jacket was practically the same with the counterpart FRP jacket. Finally, for the same amount of reinforcement, one layer (heavy-weight) textile was found to be more effective than two (light-weight) layers.

Finally, Awani et al. (2016) investigated the effect of the amount of internal shear reinforcement ratio (no stirrups and stirrups with spacing of 0.6d and 0.3d, where d is the effective depth of section), apart from the number layers (1 and 2) and the matrix material (mortar versus resin) that were also examined in previous studies, testing RC rectangular beams (of 150 mm width and 300 mm height) strengthened with side-bonded carbon TRM jackets. All specimens failed in diagonal shear-tension. Shear capacity increased by 110% to 145% for the specimens without stirrups, 64% to 67% for the specimens with a stirrup spacing of 0.6d, and 51 to 58% for the specimens with a stirrup spacing of 0.3d.

To sum up, the key investigated parameters of the above described studies on shear strengthening of RC with TRM jacketing comprise: the number of layers, the matrix material (TRM vs FRP), the strengthening configuration (side-bonded and U-shaped jackets) and the use of mechanical anchors. It was concluded that the increase in the number of layers resulted in significant increase in the shear resistance of beams. Triantafillou et al. (2006) and Tzoura and Triantafillou (2016) concluded that TRM jackets are nearly 50% less effective than their FRP counterparts, whereas Awani et al. (2016) reported that TRM U-jackets can be practically as effective as FRP U-jackets. Azam and Soudki concluded that side-bonded and U-shaped jackets exhibited

similar performance in terms of strength. Bruckner et al. (2008) and Tzoura and Triantafillou (2016) concluded that the use of mechanical end-anchorage system in T-beams strengthened in shear with glass or carbon TRM U-jackets delayed or prevented the early debonding of the jacket from the concrete substrate. Despite the fact that the effectiveness of the TRM jackets was significantly improved, an anchorage system with metallic components is susceptible to corrosion and its use is often associated with tearing failures of the composites due to stress concentrations. Finally, it should be noted that in most studies the description of failure modes of TRM jackets themselves is completely missing, whereas other important information including the properties of both textile reinforcement and mortar are not included in all the aforementioned studies.

2.4 Performance of TRM at high temperature or fire

As mentioned before, the FRP strengthening technique entails a few drawbacks mainly associated with the use of epoxy resins. In particular, except from their high costs and their inability to apply on wet surfaces, FRP have very poor performance at high temperature as under loading epoxy resins normally lose their tensile capacity. Therefore, unless protective (thermal insulation) systems are not provided (Kodur et al. 2006a and Kodur et al. 2006b), the bond capacity at the FRP-concrete interface is extremely low above the glass transition temperature (T_g). A state-of-the-art review on the fire behaviour of reinforced concrete (RC) members strengthened with FRPs was recently conducted by Firmo et al. (2015).

TRM is breathable, non-combustible nor flammable and many researchers have argued that TRM will naturally outperform FRP at elevated temperature or fire. However, research on the performance of TRM at elevated temperature or fire and comparison between TRM and FRP at high temperature or fire is extremely limited. This is attributed to the inherent experimental difficulties in the simultaneous application of loading and high temperature, even for medium or small-scale specimens. For this reason, the studies found are focused on either characterising the tensile stress-strain behaviour of TRM as a composite material at elevated temperatures, or investigating the residual capacity of TRM as a strengthening material of RC members.

In specific, Colombo et al. (2011) studied the behaviour of TRM at high temperature conducting tensile tests on TRM coupons. The specimens were first exposed to high temperature and after a 2 hour stabilization phase, they were cooled down before testing. They concluded that in case of 200 ^{o}C, TRM coupons kept their strength, whereas the stress and strain significantly decreased after the exposure of specimens to 400 ^{o}C and 600 ^{o}C due to deterioration of the textile mesh coating.

Trapko (2013) tested concrete cylinders confined with carbon FRP sheets and PBO TRM jackets after their exposure to a variety of elevated temperatures (40 ^{o}C, 60 ^{o}C and 80 ^{o}C). Based on his results, elevated temperature did not have dramatic effect on PBO TRM-confined specimens in contrary to FRP-confined cylinders in which load-bearing capacity dropped by 10% per each 20 ^{o}C. Recently, Al-Salloum et al. (2016) studied the effect of high temperature on the residual axial capacity of concrete circular columns strengthened with four different strengthening techniques, namely continuous carbon FRP sheets (CF), carbon FRP strips combined with near surface mounted (NSM) steel bars (CFS/NSM), continuous glass FRP sheets combined with NSM steel bars (GF/NSM) and continuous TRM layers combined with NSM steel bars (TRM/NSM). Based on their results, GF/NSM was the most effective technique at high temperature (300 ^{o}C), followed by TRM/NSM, whereas CF and CFS/NSM were the less efficient strengthening techniques in terms of residual axial strength, secant stiffness and peak axial strain.

Ehlig and Hothan (2011) presented the results of seven one-way spanning RC slabs, two of them were ambient temperature control slabs, whereas the remaining five were strengthened with carbon-fibre TRM jackets. The slabs were subjected to sustainable load (varying between 0% and 65% of the ambient temperature ultimate load) and were heated for 30 or 60 min. Most slabs survived the fire tests. During fire, it was not observed concrete spalling, indicating that TRM can also provide fire insulation to pre-existing members apart from structural strengthening.

The only study reported in the literature on TRM versus FRP as strengthening materials at high temperature is that of Bisby et al. (2013), who did flexural strengthening of RC beams. In particular, both un-retrofitted and strengthened beams tested up to failure at ambient temperature, whereas their counterpart specimens were tested under sustained load while being exposed to increasing high temperature. In specimens tested at high temperature, the critical-anchorage zones were kept cool (presuming that debonding of heated anchorage zones is prevented through insulation

or by mechanical means) and therefore the effect of high temperature on the debonding mechanism of the jacket from the concrete substrate was not evaluated.

2.5 Strengthening of existing structures: Selected case studies

In last decade TRM has been used as strengthening material for concrete and masonry structures all over the world (Italy, Greece, The Netherlands, France, Germany, Spain, Turkey, Russia, the United States and Latin America). Some examples of case studies of existing (concrete and masonry) structures strengthened with TRM are briefly presented in this section. All these selected case studies were presented in detail by Bournas (2016).

Egnatia Odos is the Greek part of the European route E90 which extends from the western port of Igoumenitsa to the eastern Greek–Turkish border. Some flexural cracks were observed on a concrete lining of a vehicular tunnel during inspections and therefore TRM was applied as strengthened material to suppress this structural deficiency (Nanni, 2012). A PBO-fibre textile was used as reinforcement of the TRM system, whereas a fine cement-mortar (of 30 MPa compressive strength and 4 MPa tensile strength) was used as matrix. Based on calculations, by applying 1 TRM layer, flexural capacity can be increased by 14% and 4% at top and side and portions respectively, whereas 100% increase in flexural capacity can be achieved in the longitudinal direction at the top of tunnel by applying 2 TRM layers. Figure 2.2 illustrates the surface preparation and the application of TRM strengthening system.

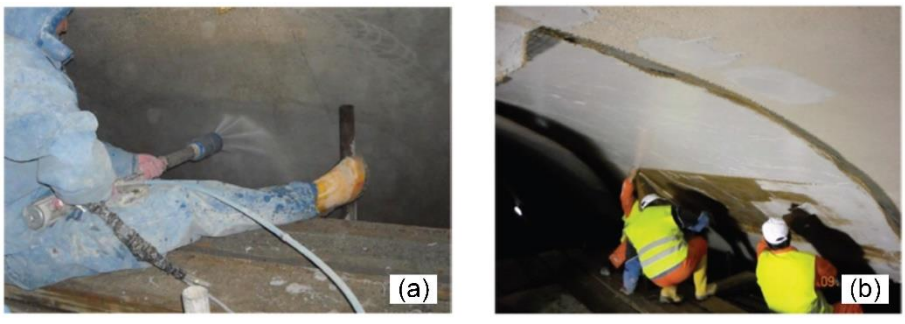


Figure 2.2. (a) Surface preparation using hydrojetting; (b) Application of reinforcement mesh at the top portion of tunnel lining (ACI 549.4R-13).

The cooling towers of Niederaussem Power Station (lignite-fired power station) in the Bergheim, Germany have been deteriorating due to their exposure to weather conditions and multiple loading. In particular, cooling tower E (of 96 m height, 70 m

diameter at the bottom and 0.14 m minimum wall thickness) built in 1968 was damaged due to the operation of the flue gas discharge unit that was built later on and due to high wind pressures and temperatures stresses (Altmeyer et al., 2012). Figure 2.3 illustrates photos of the damaged section. After a detailed assessment of the tower, PBO-TRM jacketing was selected for strengthening of the tower taking into consideration the weather conditions and the high temperatures of the fumes at the concrete surface to which the strengthening will be exposed.

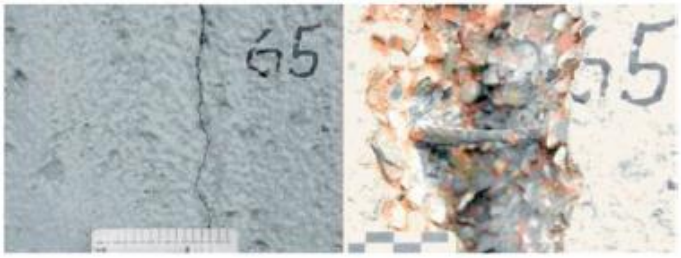


Figure 2.3. (a) Detail view of a damaged section (Altmeyer et al., 2012).

Strengthening of the Maracana Stadium in Rio de Janeiro was required after the addition of a new roof on the stadium, in the framework of the 2013 FIFA Confederations championship test for the 2014 World Cup in Brazil. Therefore, increase in the axial capacity of 60 RC columns was necessary. The choice of steel jacketing was rejected due to the increase of columns sections, time required to apply it and consumption of materials for coverings (for corrosion protection). Therefore, columns were strengthened with two carbon TRM layers. Moreover, 14,000 m^2 of the old stadium tiers were also strengthened with carbon TRM and the strengthening was completed by only two workers in 22 days.

The main (masonry) vault of the San Roque church located in Renedo de la Inera (Italy) was significantly cracked after earthquakes experienced in that area and therefore strengthening was required. Therefore, basalt TRM combined with basalt fibre anchors were applied to the extrados of the vault to prevent the opening of new cracks as well as to limit the development of the existing cracks.

Finally, an unreinforced masonry chimney (of about 38 m height) of a historic sawmill in Gerardmer, France had to be prevented and restored as it comprises a symbol of industrial heritage. Therefore, carbon TRM jacketing was selected for strengthening of chimney (in both the hoop and vertical directions) as it constitutes a reversible and effective technique that is also compatible with the substrate.

2.6 Contribution of this study

From the literature review presented in this chapter, it is clear that TRM can be considered as a promising alternative to FRP in the field of strengthening and seismic retrofitting. Aim of this thesis is to investigate the use of TRM in shear strengthening of RC members. Most studies on shear strengthening of RC beams with TRM (described in section 2.3) have been published the last 2-3 years, indicating that the subject of this study is on the spotlight. In this thesis, shear strengthening of RC beams with TRM is studied in a very systematic way by investigating a great variety of parameters most of which were not studied before. A variety of textile materials (eight in total) were used, both medium-scale and full-scale beams were tested and results and failure modes of all specimens were analysed and discussed in details.

To begin with, this PhD thesis contributed to the understanding of shear strengthening of concrete members with TRM testing firstly 40 medium-scale RC rectangular beams and investigating the following parameters: (a) the strengthening system (TRM or FRP), the (b) strengthening configuration, (c) the number of layers, (d) the external reinforcement ratio, (e) the textile material mesh characteristics, (f) the shear span-to-depth ratio and (g) the optimisation of the textile geometry. Furthermore, in this PhD thesis, shear strengthening of full-scale RC T-beams was studied in a systematic way by investigating for the first time a variety of parameters not studied before on full-scale beams: (a) the use of a novel end-anchorage system comprising textile-based anchors; (b) the anchorage percentage (50% versus 100%) of the U-jacket; (c) the textile material (carbon versus glass); (d) the textile geometry; and (e) the strengthening system (TRM versus FRP jackets). Moreover, this PhD thesis investigates for the first time the behaviour of TRM at high temperature on both medium-scale rectangular beams and full-scale T-beams strengthened in shear with TRM by conducting demanding tests in which loading and high temperature were simultaneously applied. In particular, parameters studied on medium-scale beams include the matrix used to impregnate the fibres (mortar or resin), the level of high temperature, the strengthening configuration, the number of jacketing layers and the textile properties. The performance of both anchored and non-anchored TRM jacketing in shear strengthening of full-scale T-beams at high temperature was additionally investigated. Finally, the development of reliable and accurate design models for shear strengthening of concrete members with TRM is required for

enabling their wide use in real applications. Thus, in this PhD thesis, all the well reported available data were collected and grouped based on the observed failure mode and a design approach to calculate the contribution of the TRM jacket to the total shear resistance of RC beams was suggested.

Chapter 3

MECHANICAL CHARACTERISATION OF MATERIALS USED FOR STRENGTHENING

ABSTRACT

This chapter presents the mechanical properties of the materials used for strengthening, namely the mortar used as binding material for TRM systems, the epoxy resin used as binding material in FRP systems and the textile mesh reinforcements. First, tensile tests were conducted on samples of textile fibre materials, whereas the shear response of the textile materials was experimentally characterised through picture-frame (shear) tests. The tensile properties of the TRM system as composite material, namely the ultimate tensile stress, the ultimate strain and the modulus of elasticity were experimentally obtained through tensile tests on bell-shaped TRM coupons. TRM coupons for each textile material were prepared and tested. Finally, the tensile properties of the FRP system as composite material were experimentally obtained through tensile tests on FRP coupons.

3.1 Mortar

The binding material used for strengthening of beams with TRM system was an inorganic dry binder consisting of cement and polymers at a ratio of 8:1 by weight. The water-binder ratio in the mortar was 0.23:1 by weight, resulting in plastic consistency and good workability. The flexural and compressive strength of the mortar was experimentally obtained on the day of testing using prisms of 40x40x160 mm dimensions, according to the EN 1015-11. The splitting tensile strength of mortar was experimentally obtained by conducting standard tests on cylinders of 100 mm-diameter and 200 mm-height.

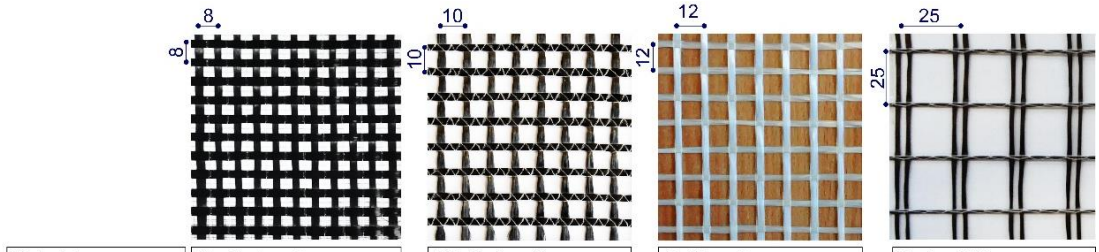
3.2 Epoxy Resin

For the specimens received epoxy adhesive as binding material (FRP system), a commercial adhesive (two-part epoxy resin with a mixing ratio 4:1 by weight, Sikadur® -330) was used with an elastic modulus of 3.8 GPa and a tensile strength of 30 MPa (according to the manufacturer datasheets). The glass transition temperature (T_g) of the epoxy resin was equal to 68 ^{o}C. The low viscosity of the adhesive allowed for the impregnation of the textile meshes by using a plastic roll.

3.3 Textile Fibre Materials

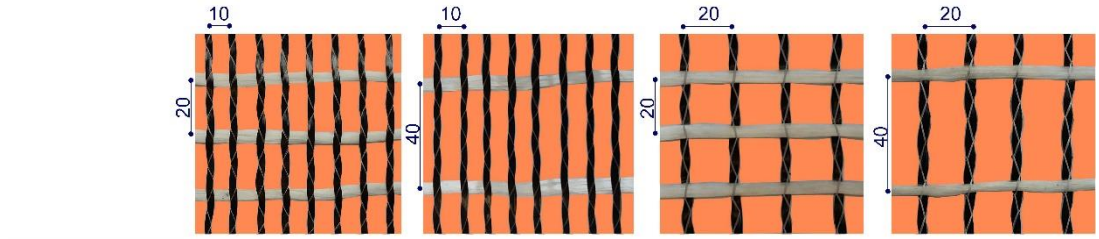
Eight different textile fibre reinforcements were used in this study. In particular, four textile reinforcements (Fig. 3.1) having equal quantity of fibres in two orthogonal directions were used, namely two carbon-fibre textiles [a light-weight (CL) and a heavy-weight (CH) one], a glass-fibre textile (G) and a basalt-fibre textile (B). The areal weight, density, tensile strength and modulus of elasticity of each textile mesh material, according to the manufacturer datasheets, are given in Fig. 3.1. The nominal thickness of a single textile layer was calculated based on the equivalent smeared distribution of fibres and it is actually the ratio of areal weight to density. The nominal thickness, t_f in each direction of a single textile layer is presented in Fig. 3.1. The remaining series were hybrid textile reinforcements (Fig. 3.2) comprising of carbon fibres in the vertical direction (loading direction) and glass fibres in the horizontal direction and were fabricated by a UK company called FORMAX. All four FORMAX textiles had the same quantity of carbon fibres in the vertical direction with the heavy-

weight carbon-fibre textile (CH). Two of FORMAX textiles had the same roving geometry, TEX and mesh size with the heavy-weight carbon textile in the vertical direction, whereas the spacing of glass rovings in the horizontal direction was 20 mm (F10x20) and 40 mm (F10x40), respectively. The remaining two FORMAX textiles had double TEX and mesh size than the heavy carbon textile (CH), whereas the spacing of glass rovings in the horizontal direction was again 20 mm (F20x20) and 40 mm (F20x40), respectively. The weight of carbon fibres, density, nominal thickness (in the vertical direction of a single textile layer) and modulus of elasticity of each textile mesh material according to the manufacturer datasheets are given in Fig. 3.2. All textile mesh materials except from basalt are dry (uncoated); basalt textile is of 220 g/m^2 weight, including 10% coating.



Material	CL: Carbon fibres	CH: Carbon fibres	G: Glass fibres	B: Basalt fibres
Weight	220 g/m^2	348 g/m^2	220 g/m^2	220 g/m^2
Density	1.78 g/cm^3	1.83 g/cm^3	2.50 g/cm^3	2.67 g/cm^3
Nominal thickness	0.062 mm	0.095 mm	0.044 mm	0.037 mm
Tensile strength	3800 MPa	4800 MPa	1400 MPa	-
Modulus of elasticity	225 GPa	225 GPa	74 GPa	89 GPa
	(a)	(b)	(c)	(d)

Figure 3.1. Textiles with equal quantity of fibres in two orthogonal directions used in this study: (a) light carbon-fibre textile (CL); (b) heavy carbon-fibre textile (CH); (c) glass-fibre textile (G); (d) basalt-fibre textile (B) (dimensions in mm).



Material	F10x20: Carbon fibres	F10x40: Carbon fibres	F20x20: Carbon fibres	F20x40: Carbon fibres
Weight	174 g/m^2	174 g/m^2	174 g/m^2	174 g/m^2
Density	1.83 g/cm^3	1.83 g/cm^3	1.83 g/cm^3	1.83 g/cm^3
Nominal thickness	0.095 mm	0.095 mm	0.095 mm	0.095 mm
Modulus of elasticity	225 GPa	225 GPa	225 GPa	225 GPa
	(a)	(b)	(c)	(d)

Figure 3.2. FORMAX textiles used in this study: (a) F10x20; (b) F10x40; (c) F20x20; (d) F20x40 (dimensions in mm).

3.4 Tensile Tests on Textile Fibre Materials

Tensile tests were conducted on the textile fibre materials to characterise their tensile behaviour. In particular, three samples of 50 mm width and 500 mm were tested for each textile. Uniaxial tensile testing was carried out using a universal testing machine with a load-capacity of 50 kN, at a monotonic loading rate of 0.02 mm/sec. The elongation of the gauge length (380 mm) was monitored through an extensometer as shown in Fig. 3.3a. All specimens failed due to rupture of fibres within the gauge length as shown in Fig. 3.3b that includes photos of failed specimens for heavy-carbon, light carbon, glass and basalt fibre textiles, respectively. The tensile properties, namely the ultimate tensile stress (f_{fu}), the ultimate strain (ε_{fu}) and the modulus of elasticity ($E_{f_textile}$) of the textile fibre materials are summarised in Table 3.1. The average stress versus strain curves for light-weight carbon, heavy-weight carbon, glass and basalt fibre textiles are depicted in Fig. 3.4a whereas the corresponding curves for all FORMAX textiles are depicted in Fig. 3.4b.

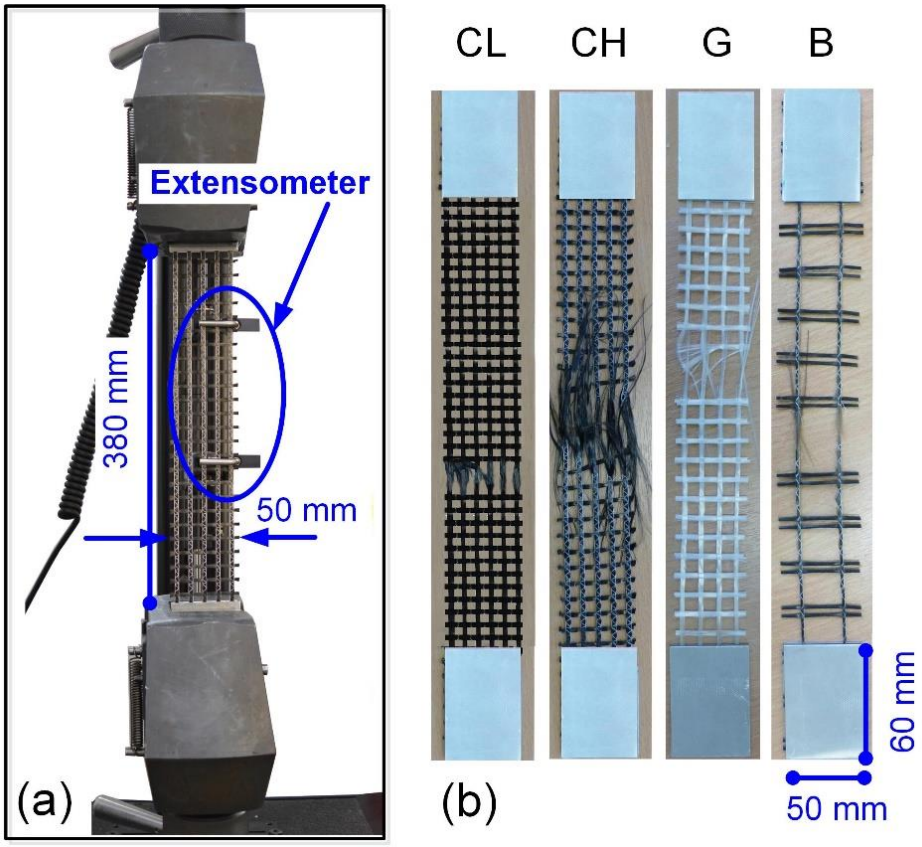


Figure 3.3. (a) Test set-up for tensile testing of textile fibre materials; (b) rupture of textile fibre materials.

Table 3.1. Summary of the results of tensile tests on textile fibre materials.

	CL	CH	G	B	F10x20	F10x40	F20x20	F20x40
f_{fu} (GPa)*	1531.7 (102)	1465.1 (95)	756.3 (45)	1209.9 (53)	1456.0 (111)	1340.1 (95)	1549.3 (120)	1562.1 (123)
ε_{fu} (%)*	0.765 (0.06)	0.792 (0.05)	1.553 (0.08)	1.866 (0.07)	0.700 (0.04)	0.652 (0.06)	0.817 (0.05)	0.934 (0.07)
$E_{f_textile}$ (GPa)*	200.2 (17)	175.7 (21)	48.7 (11)	64.8 (14)	208.0 (18)	205.5 (20)	189.6 (19)	167.2 (13)

*standard deviation in parenthesis

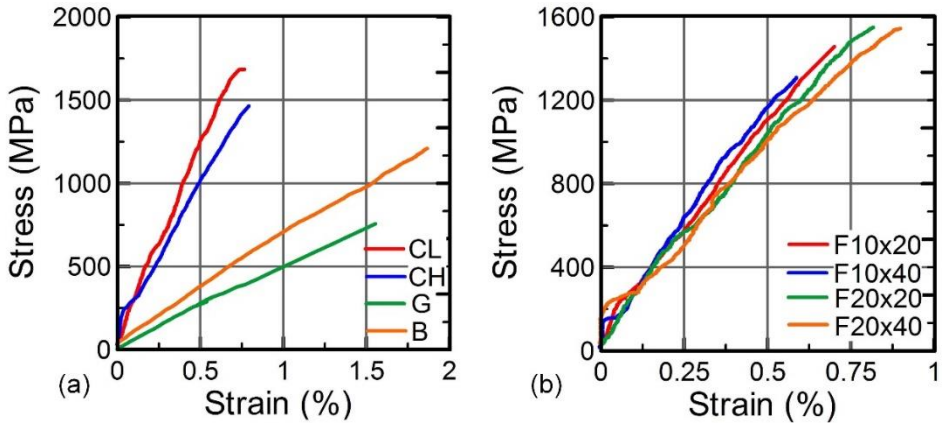


Figure 3.4. Stress versus strain curves for (a) light-weight carbon, heavy-weight carbon, glass and basalt fibre textiles; (b) all FORMAX textiles, namely F10x20, F10x40, F20x20 and F20x40.

3.5 Shear Tests on Textile Fibre Materials

The shear performance of textile materials was characterised through picture-frame tests that were conducted for all eight textile materials described in Section 3.3. Five samples for each textile material with the geometry shown in Fig. 3.5a were prepared. Fig. 3.5b illustrates the picture-frame used for the shear tests. This picture-frame was designed at the University of Nottingham in the framework of a benchmarking project that had started after the '2001 NSF Composite Sheet Forming workshop' to report material testing methods for textile composites (Cao et al. 2008). The corners of the frame are pinned. Slippage of textile material is prevented by clamping it on all edges. Initially, the textile material was properly aligned and tightly clamped into the frame as shown in Fig. 3.5c. During the test, the fibre rovings of textile material start to reorient themselves as they shear and the textile material is adapted to its final geometry mainly by fibre rovings rotation (Fig. 3.5d). Shearing between longitudinal and transverse fibre rovings is called shear angle, γ_f.

Initially, when fibre rovings in two directions are perpendicular to each other, shear angle, γ_f is zero. The angle of the frame, θ_f is calculated by the following equation:

$$\cos\theta_f = \frac{\sqrt{2}L_{frame} + d_A}{2L_{frame}} \tag{3.1}$$

where L_{frame} is the frame length indicated in Fig. 3.5b and d_A is the vertical displacement of point A (Fig. 3.5b). The shear angle, γ_f, is calculated from the geometry of the picture frame:

$$\gamma_f = 90^o - 2\theta_f \tag{3.2}$$

The shear force, Fs, is calculated based on the force applied from the tensile machine by using the following equation:

$$Fs = \frac{F'' - F'}{2\cos\theta_f} \tag{3.3}$$

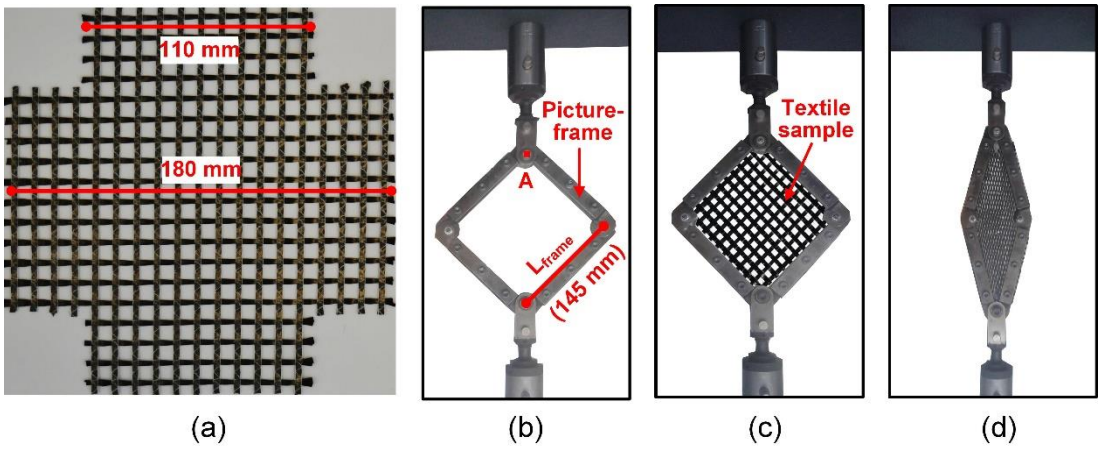


Figure 3.5. (a) Sample of textile material for shear tests; (b) shear test apparatus; (c) picture-frame: starting position; (d) picture-frame: deformed position.

where the term F''-F' corresponds to the net load. In particular, F'' corresponds to the load applied from the machine when the textile material is being deformed in the picture-frame (Fig. 3.5c and d), whereas F' corresponds to the load applied from the machine when the frame itself is being deformed without including a textile sample (Fig. 3.5b).

Figure 3.6a depicts the shear force (Fs) versus shear angle (γ_f) curves; the average response of all five samples (1 layer) tested for each textile material is

illustrated in Fig. 3.6a. The shear modulus of elasticity, G is calculated by the following equation:

$$G = \frac{\frac{Fs}{t_f L_{sample}}}{\tan \gamma_f} \tag{3.4}$$

where L_{sample} (110 mm) is the length of textile sample without the flanges (Fig. 3.5a); this part of textile sample is deformed during the shear test.

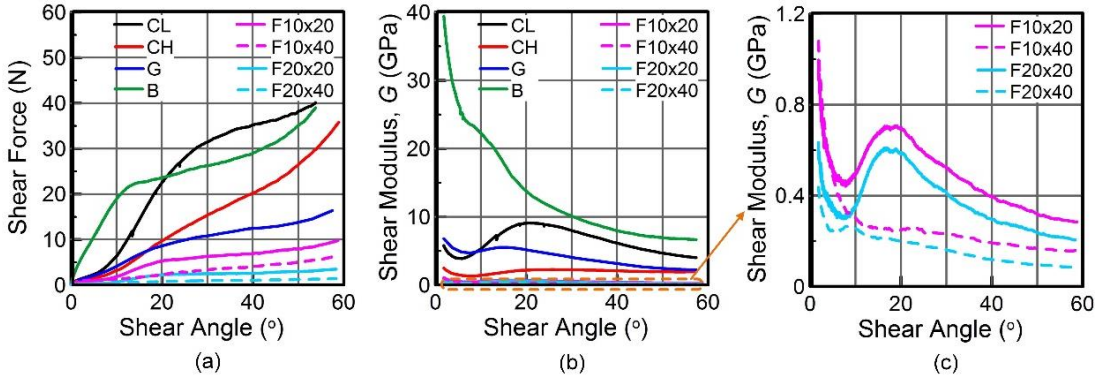


Figure 3.6. (a) Shear force versus shear angle curves for all eight textile materials; (b) shear modulus versus shear angles curves for all eight textile materials; (c) shear modulus versus shear angles curves for FORMAX textile materials.

Table 3.2. Shear modulus values, G (GPa) for each textile material.

	CL	CH	G	B	F10x20	F10x40	F20x20	F20x40
G (GPa)*	5.796 (0.7)	2.492 (0.2)	6.797 (0.5)	39.357 (4.2)	0.997 (0.09)	1.079 (0.11)	0.634 (0.07)	0.437 (0.03)

*standard deviation in parenthesis

The shear modulus versus shear angle curves (average response of five samples) are depicted in Fig. 3.6b and c. As mentioned in Section 3.3, basalt fibres textile is coated and as a result it is more stable and stiffer than the rest textile materials. Therefore, basalt fibre textile has the best shear response compared to the rest textiles, (Fig. 3.6b and c), mainly at low shear angle values. Both light-weight carbon and glass textile materials have the best shear performance among the dry fibre textile materials. All four FORMAX textiles have very low shear modulus value compared to the rest textile materials (Fig. 3.6c). This is maybe due to the very loose connection between the carbon fibre rovings (in the longitudinal direction) with the glass fibre rovings (in

the transverse direction). The values of shear modulus at the beginning of the shear test (γ_f=0^o or θ_f=0^o) are presented at Table 3.2. The shear modulus values and generally the shear response of the textile fibre materials could be quite useful in numerical simulations.

3.6 Tensile tests on TRM coupons

TRM coupons with the geometry shown in Fig. 3.7a were fabricated and tested to characterize the tensile behaviour of composite material with test parameters being the textile mesh material and the number of textile layers. In particular, for all eight textile mesh materials described in section 3.1, three TRM coupons with one and two textile layers, respectively were fabricated. Additionally, only for glass and basalt fibre textiles, three TRM coupons with four textile layers were also fabricated and tested. The mean flexural, splitting tensile and compressive strength (average values from three specimens) of mortar at the day of testing the coupons was 8.6, 3.4 and 28.4 MPa, respectively.

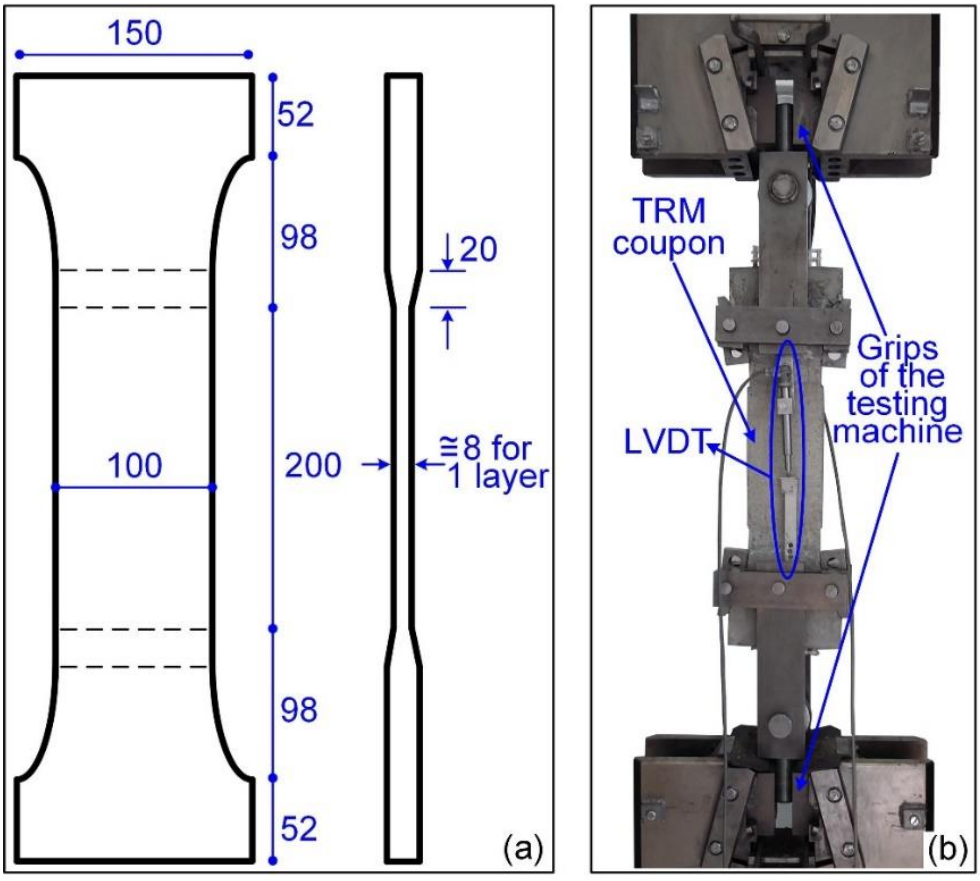


Figure 3.7. (a) Geometry of TRM coupons; (b) test set-up for tensile testing of TRM coupons.

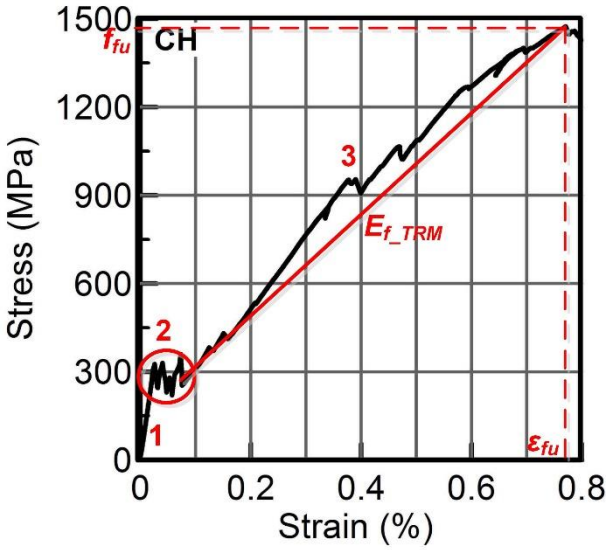


Figure 3.8. Typical stress versus strain curve of TRM coupon subjected to tensile testing.

Uniaxial tensile testing was carried out using a universal testing machine with a load-capacity of 200 kN, at a monotonic loading rate of 0.02 mm/sec. Specially designed steel flanges fitting exactly the curved parts of the specimens were employed for applying tension, whereas the elongation of the gauge length was monitored using two LVDTs (Fig. 3.7b), one on each face of the coupon. The response of all specimens comprised three distinct branches as shown in Fig. 3.8: (1) the specimen remains uncracked; (2) development of multiple cracks after the first cracking occurs and (3) the cracking pattern has fully developed and the increase in resistance is due to the textile itself until rupture of fibres is observed.

Figure 3.9 depicts the stress-strain curves of coupons fabricated with the four textile mesh materials of equal quantity of fibres in two orthogonal directions (CH, CL, G and B), whereas Fig. 3.10 depicts the corresponding results for TRM coupons fabricated with the four FORMAX textile materials. The values of stresses were calculated by dividing the load with the area of the textile material ($n\ t_f$ 100 mm). Each shaded region in Fig. 3.9 and 3.10 encloses all three stress-strain curves of each group of TRM coupons. Figure 3.11 depicts photos of failure of the TRM coupons. The notation of coupon specimens is XN, where X denotes the type of the textile (CL, CH, G, B, F10x20, F10x40, F20x20 and F20x40) and N denotes the number of layers (1, 2 or 4). In all TRM coupons multiple cracks were developed within the gauge length. In general, increase in the number of layers allowed for better tensile stress distribution and thus more cracks to be formed.

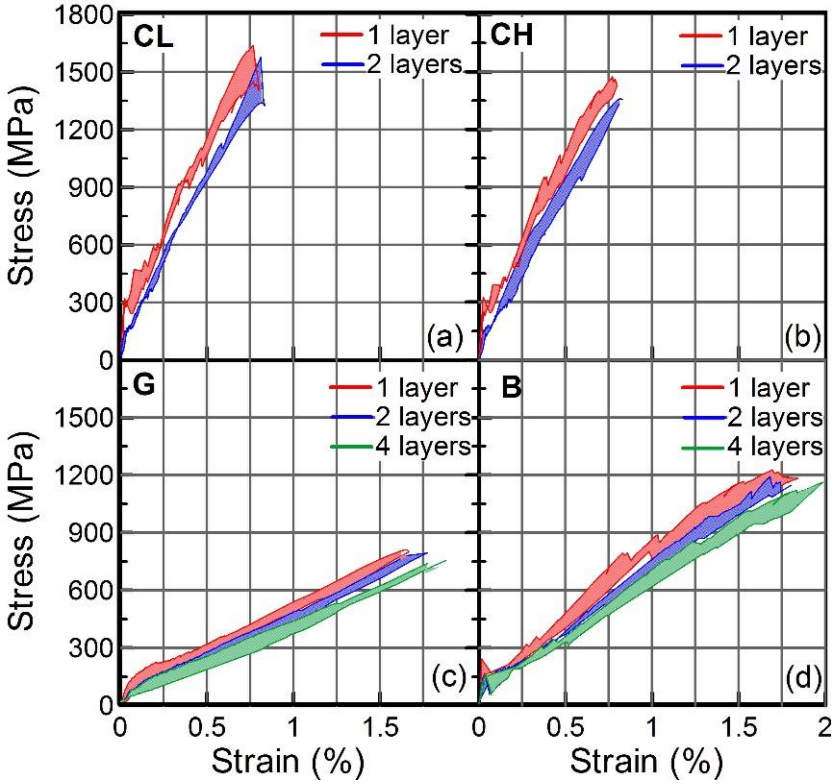


Figure 3.9. Stress versus strain curves for (a) light-weight carbon textile (CL); (b) heavy-weight carbon textile (CH); (c) glass textile; (d) basalt textile.

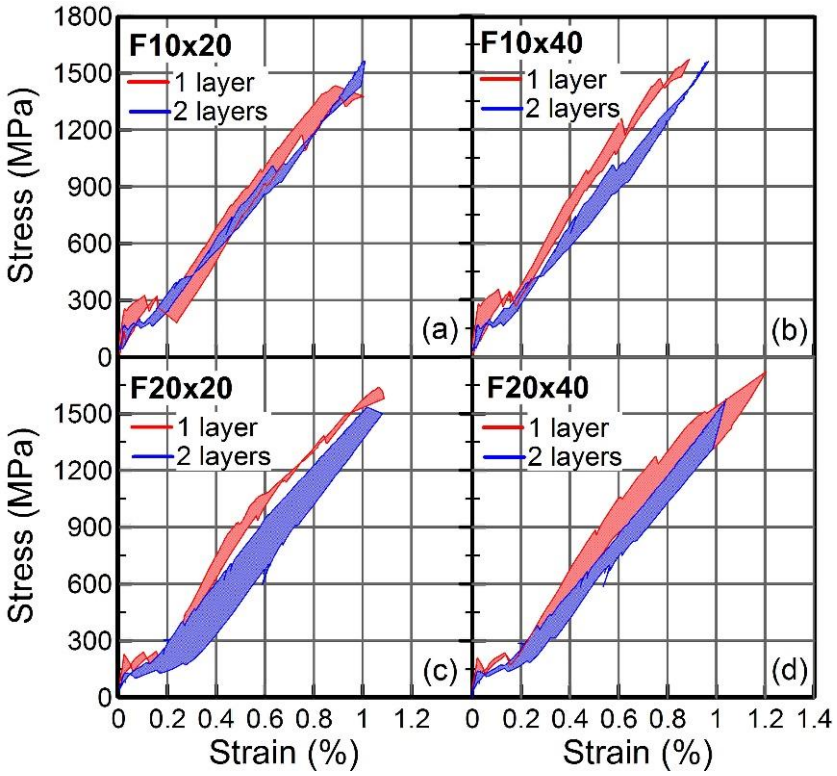


Figure 3.10. Stress versus strain curves for (a) F10x20; (b) F10x40; (c) F20x20; (d) F20x40 textile.

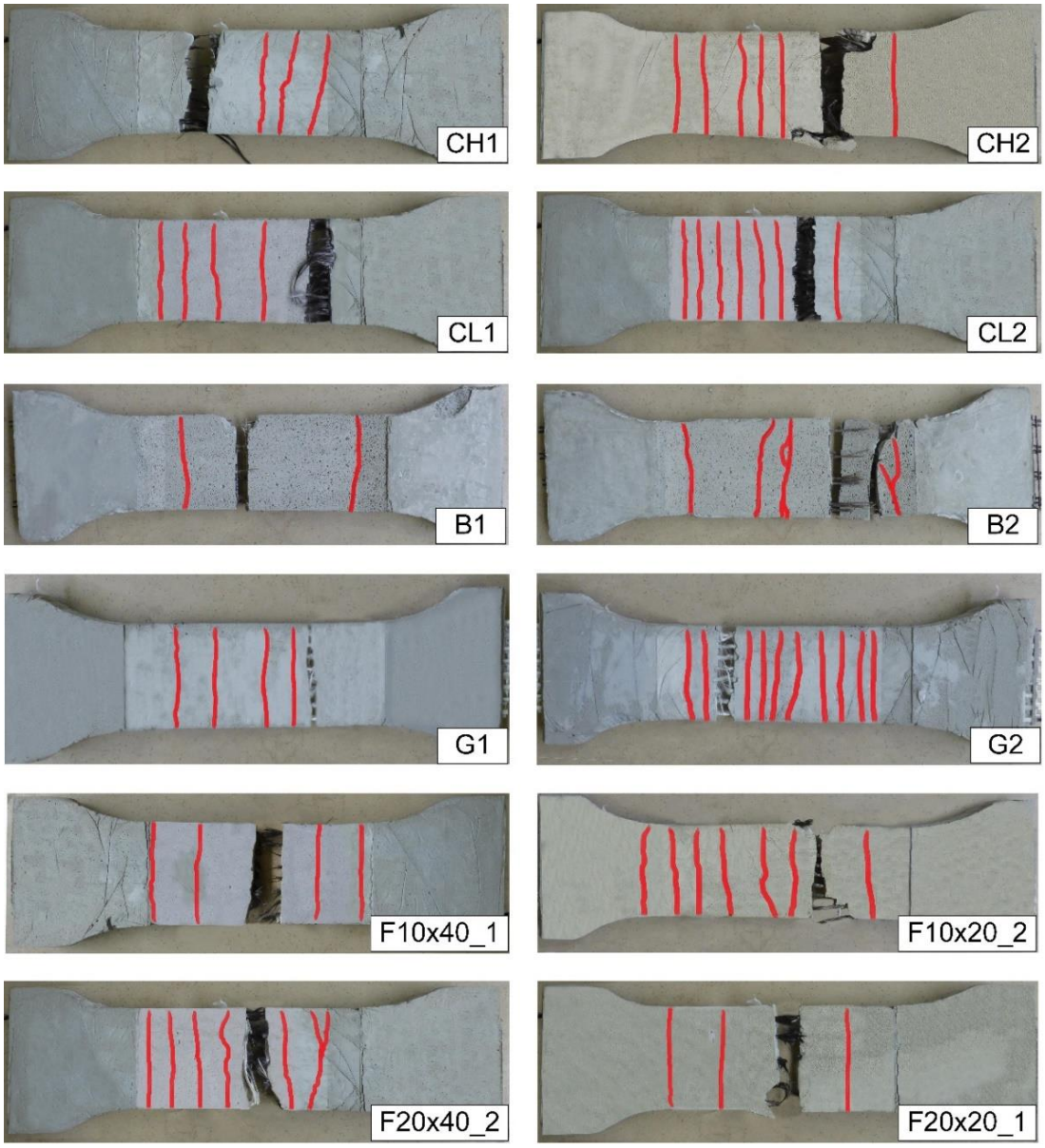


Figure 3.11. Failure modes of TRM coupons.

The ultimate tensile stress (f_{fu}), the ultimate strain (ε_{fu}) and the modulus of elasticity (E_{f_TRM}) derived from the experimental results are summarised in Table 3.3 and are also presented in Fig. 3.12 as bar charts format. The modulus of elasticity, E_{f_TRM} included in Table 3.3, is the secant modulus of elasticity of the third branch of stress-strain curve that represents the cracked behaviour of specimens (Fig. 3.8). Increase in the number of layers resulted in marginal decrease in the ultimate tensile stress (f_{fu}) and the modulus of elasticity of cracked specimen (E_{f_TRM}) and marginal increase in the ultimate strain (ε_{fu}).

Table 3.3. Summary of TRM coupons results.

	Number of layers	Ultimate tensile strength, f_{fu} (MPa)*	Ultimate tensile strain, ε_{fu} (%)*	Modulus of elasticity of cracked specimen, $\boldsymbol{E_{f_TRM}}$ (GPa)*
Light-weight Carbon Textile (CL)	1	1544.6 (132)	0.798 (0.09)	182.6 (21)
	2	1456.3 (115)	0.820 (0.07)	176.6 (16)
Heavy-weight Carbon Textile (CH)	1	1417.9 (86)	0.784 (0.13)	168.7 (5)
	2	1349.9 (127)	0.821 (0.11)	157.9 (8)
Glass Textile (G)	1	794.1 (102)	1.644 (0.09)	41.1 (6)
	2	787.4 (93)	1.710 (0.08)	40.3 (8)
	4	754.1 (110)	1.826 (0.14)	37.7 (10)
Basalt Textile (B)	1	1206.1 (113)	1.800 (0.10)	63.8 (9)
	2	1168.2 (130)	1.876 (0.07)	63.7 (4)
	4	1104.8 (94)	1.916 (0.08)	60.3 (9)
F10x20	1	1404.7 (126)	0.946 (0.12)	161.6 (10)
	2	1496.8 (143)	1.002 (0.11)	150.7 (13)
F10x40	1	1523.7 (149)	0.873 (0.08)	175.7 (10)
	2	1485.4 (151)	0.926 (0.10)	160.61 (8)
F20x20	1	1564.5 (139)	0.996 (0.07)	165.9 (7)
	2	1516.6 (128)	1.048 (0.10)	162.8 (11)
F20x40	1	1610.7 (155)	1.082 (0.13)	159.0 (12)
	2	1444.3 (143)	1.012 (0.09)	153.4 (14)

*standard deviation in parenthesis

In general, all carbon textile meshes (CL, CH, F10x20, F10x40, F20x20 and F20x40) have very similar tensile properties. Both glass and basalt textile meshes have as expected lower ultimate tensile stress and modulus of elasticity compared to carbon textile mesh materials, whereas they have almost double ultimate strain than the carbon textile materials. In general, the tensile properties of the TRM system, namely the ultimate tensile stress, the ultimate strain and the modulus of elasticity of cracked specimen are slightly affected by the number of layers, as shown in Fig. 3.12a-c.

Moreover, as expected, the results of TRM coupons are in very good agreement with the results of tensile tests on bare textile fibre materials presented in Section 3.4. This is because the failure of TRM coupons (Fig. 3.8, 3rd branch) is only governed by the behaviour of the textile materials as the mortar is fully cracked in this stage.

To sum up, tensile tests conducted on TRM coupons with one layer of textile fibres material (or just tensile tests on samples of bare textile fibre materials) can be used to sufficiently characterise the tensile properties of TRM as composite system, even if more than one layer is used in real applications.

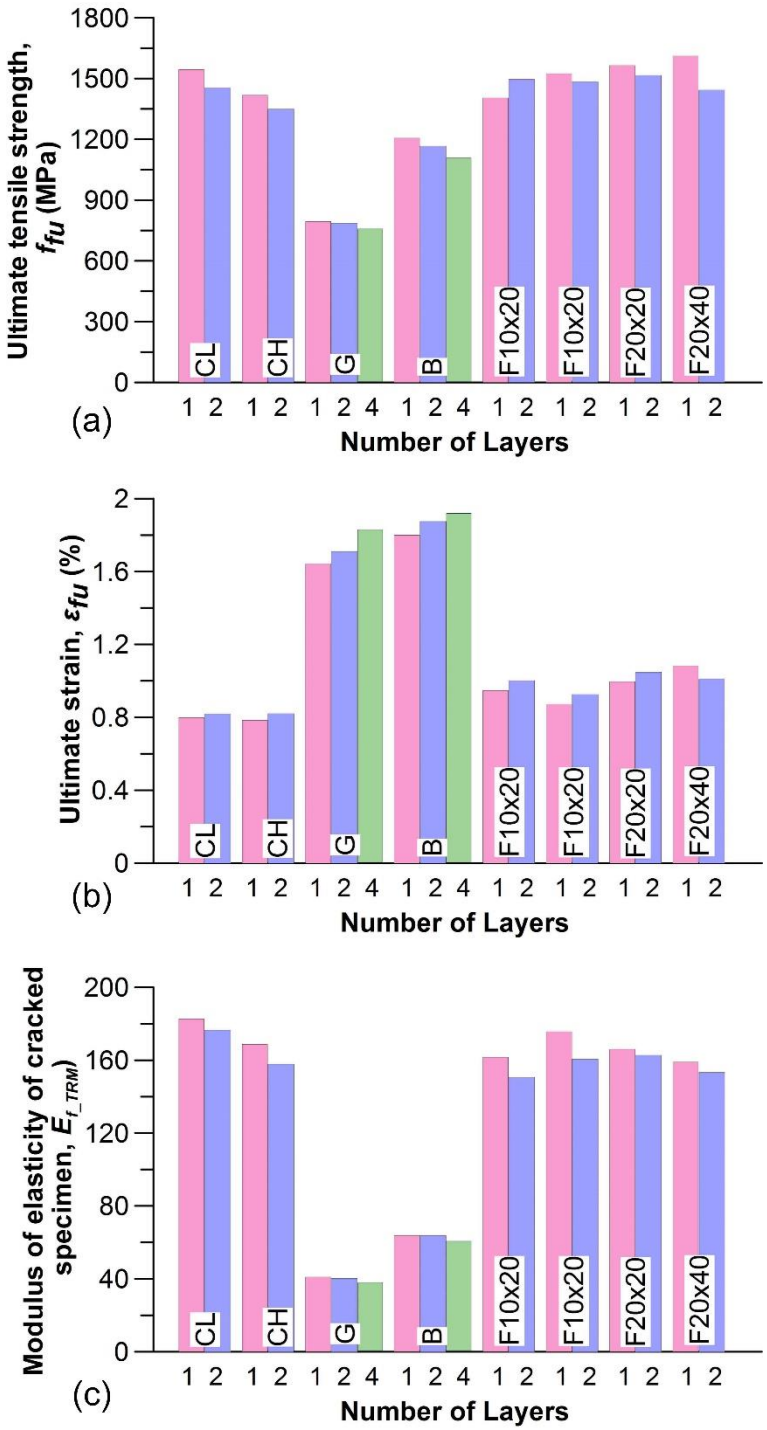


Figure 3.12. Results of TRM coupons at bar charts format: (a) ultimate tensile strength, f_{fu}; (b) ultimate strain, ε_{fu} (%); (c) modulus of elasticity of cracked specimen, E_{f_TRM}.

Use of optical FBG sensors in TRM coupons

Structural Health Monitoring (SHM) constitutes a relative new scientific field that aims to provide reliable data regarding the static and dynamic condition of a structure. A variety of sensors can be used for monitoring, providing data regarding the static or

dynamic response during the application of various loads. SHM offers the possibility of ‘continuous diagnosis’ of a structure and the determination of the potential failure modes. Optical Fibre Bragg Grating (FBG) sensors have been widely used all over the world, including Great Britain for field instrumentation and Structural Health Monitoring. More details about the use of optical FBG sensors can be found in Tsamasphyros et al. 2003 and Majumder et al. 2008.

Structural Health Monitoring of TRM applications constitutes an interesting scientific field. Useful information and reliable data regarding the stress and strain profile of RC structures strengthened with TRM can be gathered by using optical FBG sensors. Therefore, the use of optical FBG sensors in a TRM coupon consisting of a single layer of heavy-weight carbon textile is investigated in this section. In specific, three optical FBG sensors were attached at the central roving of the textile along the gauge length as shown in Fig. 3.13a. TRM coupon was carefully prepared (Fig. 3.13b) as optical fibres are really sensitive and it is easy to accidentally damage them during the casting of TRM coupon. FBG sensors were connecting with a CEM-5000 interrogator system. CEM company took over the application, operation and data recording of FBG sensors. The elongation of the gauge length was also monitored using two LVDTs as in all TRM coupons tested so far and presented in the above paragraphs (see Fig. 3.7b).

In Fig. 3.13c the stress versus strain curves of all three optical FBG sensors are presented and compared with the corresponding average response obtained by the two LVDTs. Based on the results of Fig. 3.13c, the central part of the textile is first deformed (FBG sensor 2), whereas the two ends of the textile (FBG sensors 1 and 3) along the gauge length are not deformed at the very beginning. In general, the two ends of the textile deform symmetrically based on the results of FBG sensors 1 and 3. The response of FBG sensor 2 which was attached at the centre of the textile layer (Fig. 3.13a) was in good agreement with the average response of the two LVDTs and mainly after the development of the cracking pattern of TRM coupon (after 300 kN). Optical fibre ruptured at a strain value equal to 0.3% and therefore the FBG sensors stopped recording after that strain value. The ultimate strain of optical fibres (0.3%) is lower than the ultimate strain of the textile material (0.8%). However, the strain values expected in TRM systems when applied for strengthening of existing buildings at serviceability loading conditions are low. Thus, the use of optical fibres (combined with FBG sensors) for monitoring (SHM) TRM jacketing externally applied to

existing structures seems quite promising and interesting application and could be further investigated in future research.

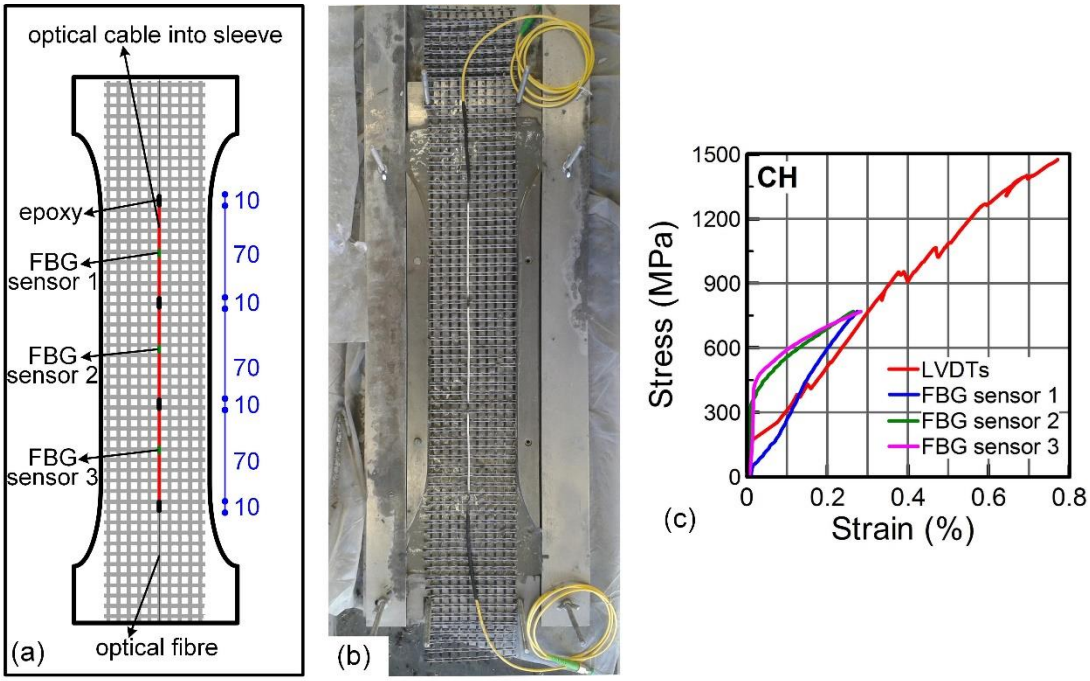


Figure 3.13. (a) Configuration of FBG sensors; (b) preparation of TRM coupon; (c) stress versus strain curves.

3.7 Tensile tests on FRP coupons

The FRP system comprising of the heavy-weight carbon textile and (Sikadur® -330) epoxy resin (see Section 3.2) was used as strengthening material at both medium-scale rectangular beams and full-scale T-beams (Section 4.1, Chapter 5 and Chapter 6, respectively). Therefore, three FRP coupons with the geometry shown in Fig. 3.14a were fabricated and tested to characterize the tensile behaviour of FRP composite material according to ACI 440.3R-04 requirements. Uniaxial tensile testing was carried out using a universal testing machine with a load-capacity of 200 kN, at a monotonic loading rate of 5 kN/min. The elongation of the gauge length (300 mm) was monitored through two LVDTs as shown Fig. 3.14b.

All specimens failed due to rupture of fibres within the gauge length as shown in Fig. 3.14c. The tensile properties, namely the ultimate tensile stress (f_{fu}), the ultimate strain (ε_{fu}) and the modulus of elasticity (E_{f_FRP}) of FRP coupons are 2788.4 MPa, 1.261% and 200.7 GPa, respectively. Stress versus strain curve of FRP coupons is depicted in Fig. 3.14d and is also compared with the corresponding results of the

corresponding TRM coupons with one heavy-carbon layer. Each shaded region in Fig. 3.14d encloses all three stress-strain curves of each group of TRM or FRP coupons. As shown in Fig. 3.14d the mechanical properties of FRP coupons are superior to those of the TRM coupons. This is because a much better impregnation of the fibres is achieved when epoxy resin is used as binding material instead of mortar. Therefore, in FRP coupons, the textile fibres are better utilized in carrying tensile forces and both the stress and strain capacity increase as clearly indicated in Fig. 3.14d.

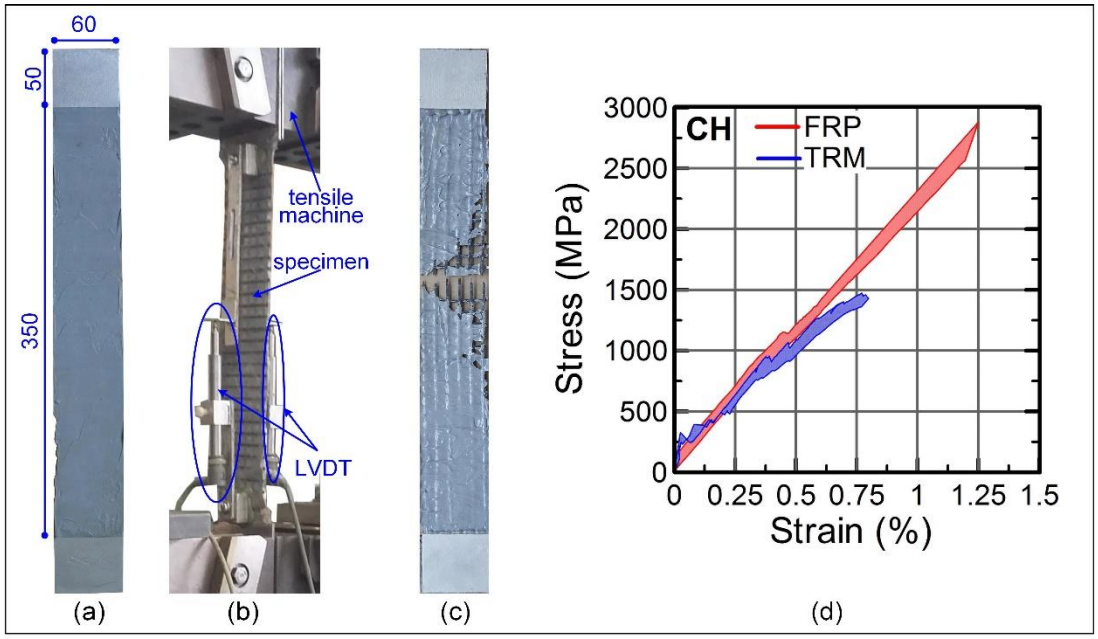


Figure 3.14. (a) Geometry of FRP coupons; (b) test set-up for tensile testing of FRP coupons; (c) typical failure mode of FRP coupons; (d) stress versus strain curves for FRP and TRM coupons.

Chapter 4

SHEAR STRENGTHENING OF MEDIUM-SCALE RECTANGULAR RC BEAMS USING TRM

Abstract

This chapter presents the experimental work carried out on medium-scale rectangular RC beams. Firstly, the effectiveness of TRM is compared with FRP as the strengthening configuration and the number of layers vary. After that, the effect of external reinforcement ratio, textile geometry (textile mesh characteristics) and shear-span-to-depth ratio on beams strengthened in shear with U-shaped TRM jackets was also investigated. Finally, U-shaped TRM jackets consisting of textiles with same amount of fibres in the loading direction but with different fibre roving geometry as well as different material and spacing of fibre rovings in the horizontal (non-loading) direction are compared.

4.1 TRM vs FRP in shear strengthening of RC beams

4.1.1 Experimental Programme

4.1.1.1 Test specimens and investigated parameters

The main objective of this section was to compare the effectiveness between TRM and FRP jacketing in shear strengthening of RC beams. A total of fourteen rectangular half-scale RC beams (cross-section dimensions of 102x203 mm) were constructed and tested as simply supported in (non-symmetric) three-point bending as shown in Fig. 4.1a. The total length of the beams was equal to 1677 mm, whereas the effective flexural span was equal to 1077 mm (Fig. 4.1b), providing adequate anchorage length to the longitudinal reinforcement.

To emulate old detailing practices, the beams were designed to be deficient in shear in one of the two shear spans. To achieve this, the critical shorter shear span of 460 mm length did not include any transverse reinforcement, whereas the larger shear span included 8-mm diameter stirrups at a spacing of 75 mm (Fig. 4.2a).

Strengthening was applied only at the critical shear span aiming to increase its shear resistance. By design, the shear force demand in order to develop the full flexural capacity of the (unretrofitted) beams was targeted to be 3 times their shear capacity. As shown in Fig. 4.2b two 16 mm-diameter and two 10 mm-diameter deformed bars were placed at the tension and compression zone of the rectangular beams, respectively. The geometrical ratio of tensile rebars was 2.2%.

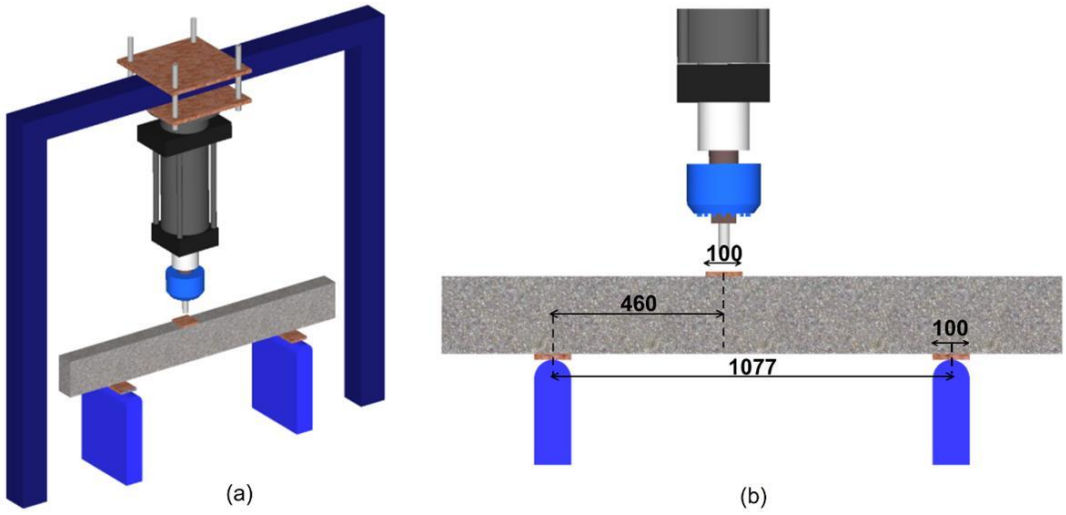


Figure 4.1. Test set-up: (a) Overall 3D view; (b) front view (dimensions in mm).

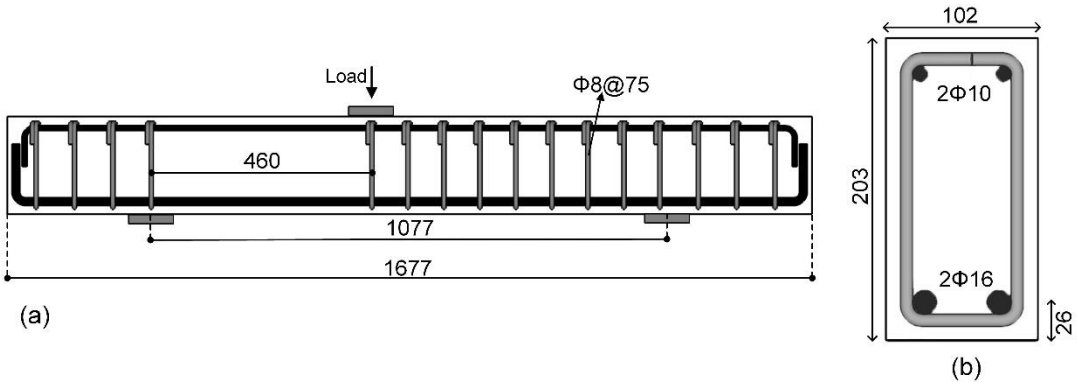


Figure 4.2. (a) Beam geometry and reinforcement; (b) cross section (dimensions in mm).

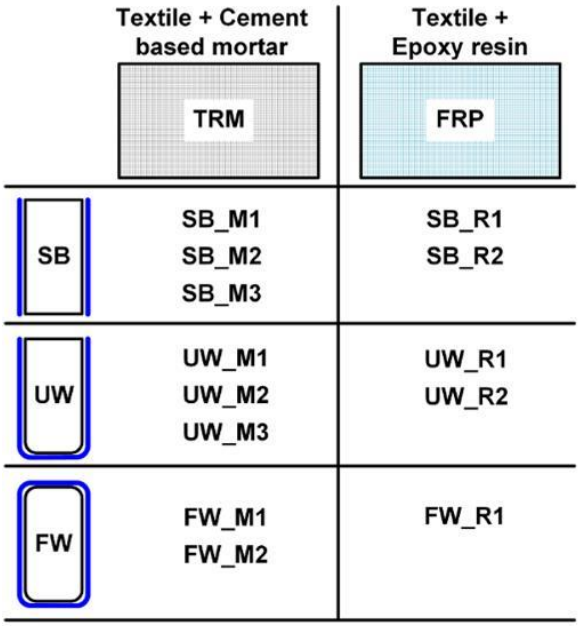


Figure 4.3. (a) Groups of specimens.

The key investigated parameters of this study comprise: (a) the strengthening system (TRM or FRP), (b) the strengthening configuration, and (c) the number of layers. One beam was tested as-built without receiving strengthening and served as control specimen (CON). The remaining 13 beams were divided in two main groups (Fig. 4.3). The first group comprised 8 beams strengthened with TRM jackets, whereas the second group comprised 5 beams strengthened with FRP jackets. Three different strengthening configurations were applied on each group's specimens, namely Side-Bonded jackets (SB), U-Wrapped jackets (UW) and Fully-Wrapped jackets (FW). For the SB and the UW configurations the specimens of the first group received from 1 to 3 TRM layers, whereas the specimens of the second group received 1 and 2 FRP layers. For the FW configuration the first group specimens received 1 and 2 TRM

layers, while only one specimen of the second group received 1 FRP layer. The notation of specimens is X_YN, where X refers to the strengthening configuration (SB, UW and FW), Y denotes the type of the binding material (M for Mortar or R for Resin) and N denotes the number of layers (1, 2 or 3).

4.1.1.2 Materials and strengthening procedure

The specimens were cast in groups of four using the same concrete mix design. The compressive strength and the tensile splitting strength of the concrete were experimentally obtained on the day of testing by conducting standard tests on cylinders of 150 mm-diameter and of 300 mm - height. The results are summarized in Table 4.1 (average values of 3 specimens). The 16 mm-diameter longitudinal bars used as steel reinforcement had a yield stress, ultimate strength and rupture strain of 547 MPa, 602 MPa and 9.96%, respectively (experimentally obtained average values from 3 specimens). The 10 mm-diameter longitudinal bar had a yield stress, ultimate strength and rupture strain equal to 552 MPa, 593 MPa and 8.4%, respectively. The corresponding value for the 8 mm-diameter bars used for stirrups were 568 MPa, 630 MPa and 7.9%.

Table 4.1. Concrete strength on the day of testing.

Group of specimens	Compressive strength (MPa)*	Tensile splitting strength (MPa)*
CON; SB_R1; FW_R1; FW_M2	21.6 (0.60)	2.36 (0.22)
SB_R2; SB_M1; FW_M1	21.6 (0.66)	2.66 (0.16)
UW_R1; UW_R2; UW_M1; UW_M2	23.8 (0.50)	2.73 (0.11)
SB_M2; SB_M3; UW_M3	22.6 (0.53)	2.81 (0.14)

*standard deviation in parenthesis

The heavy-weight carbon reinforcement (CH, Fig. 3.1b) was used in both strengthening systems; the only difference between the two systems was the binding material (epoxy resin in case of FRP and cementitious mortar in case of TRM). The properties of this heavy-weight carbon reinforcement were presented in Section 3.

For the specimens receiving TRM jacketing the mortar described in Section 3.1 was used as binding material. Table 4.2 summarizes the strength properties of the mortar (average values of 3 specimens) obtained experimentally on the day of testing. For the specimens receiving FRP jacket, the epoxy resin described in Section 3.2 was used.

Table 4.2. Mortar strength on the day of testing.

Group of specimens	Flexural strength (MPa)*	Compressive strength (MPa)*	Tensile strength (MPa)*
SB_M1; UW_M1; FW_M1; UW_M2	10.30 (1.03)	31.1 (1.10)	3.40 (0.2)
SB_M2; FW_M2	9.21 (0.82)	28.2 (1.34)	3.40 (0.2)
SB_M3; UW_M3	8.64 (0.52)	26.9 (1.11)	3.40 (0.2)

*standard deviation in parenthesis

Prior to strengthening a thin layer of concrete cover was removed and a grid of grooves (2-3 mm deep) was created as shown in Fig. 4.4a, using a grinding machine. The corners of the specimens receiving UW or FW jackets were rounded to a radius of approximately 15 mm in order to avoid stresses concentration.

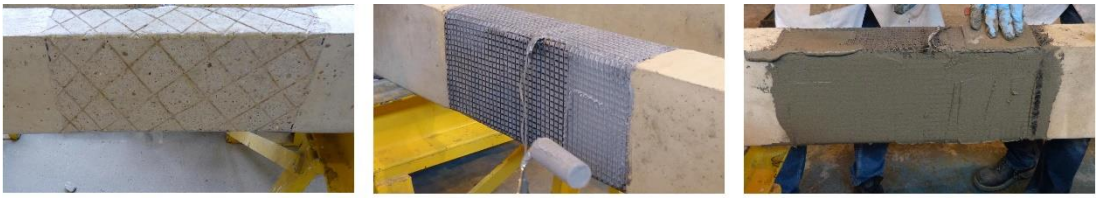


Figure 4.4. (a) Prepared concrete surface before strengthening; (b) impregnation of the textile fibres with epoxy resin; (c) application of an extra layer of mortar on the top of the final textile layer.

For FRP-jacketed specimens the first textile layer was applied on the top of the first resin layer and was then impregnated in-situ with resin using a plastic roll (Fig. 4.4b). Special care was taken to ensure the full impregnation of the textile fibres with resin. If more than one textile layers were to be applied, the process was repeated until the application of all the layers was completed. For TRM-jacketed specimens the mortar was applied in approximately 2 mm-thick layers with a smooth metal trowel. After application of the first mortar layer on the (dampened) concrete surface, the textile was applied and pressed slightly into the mortar, which protruded through all the perforations between the fibre rovings. The next mortar layer covered the textile completely, and the operation was repeated until all textile layers were applied and covered by mortar (Fig. 4.4c). Of crucial importance in this method, as in the case of epoxy resins, was the application of each mortar layer while the previous one was still in a fresh state.

4.1.1.3 Experimental set-up and procedure

The beams were subjected to monotonic loading using a stiff steel reaction frame and a three-point bending set-up configuration as shown in Fig. 4.1a. A vertically positioned 500 kN capacity servo-hydraulic actuator was used for the application of the load at a displacement rate of 0.02 mm/s. As illustrated in Fig. 4.5a the vertical displacement was measured at the position of load application using external Linear Variable Differential Transducer (LVDT); the displacement measured from this sensor was used to plot the load-displacement curve for each specimen. Moreover, measurements from the potentiometers placed at the critical shear span in one side of the beam, were utilized to monitor the average shear strain of the span (Fig. 4.5b).

Additionally, the Digital Image Correlation (DIC) technique was employed to monitor relative displacements within the critical shear span, using two high-resolution cameras (on the side of the beam which was free of sensors). Finally, strain gauges were mounted to the longitudinal bars at the cross-section of maximum moment to monitor possible yielding of the steel reinforcement. It is noted that all data was synchronized and recorded using a fully-computerized data acquisition system.

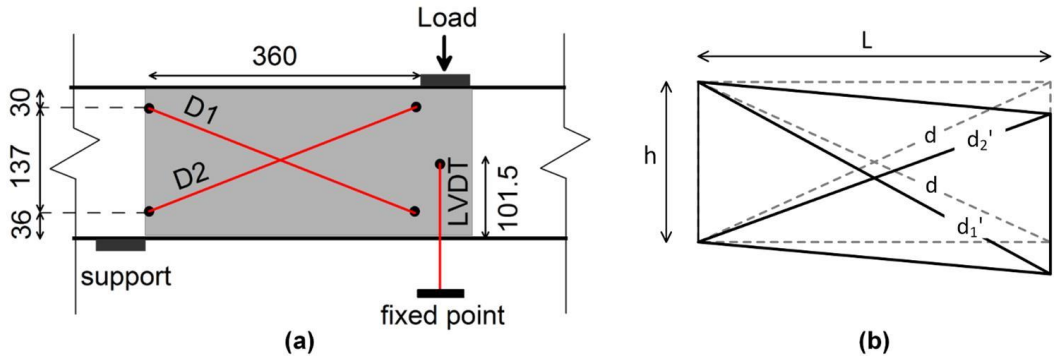


Figure 4.5. (a) Configuration of the two potentiometers (D1, D2) and the LVDT at the shear-critical span; (b) shear deformation measurement by X configuration.

4.1.2 Experimental results

The response of all specimens tested is given in Fig. 4.6 in the form of load - displacement curves. Key results are also presented in Table 4.3.

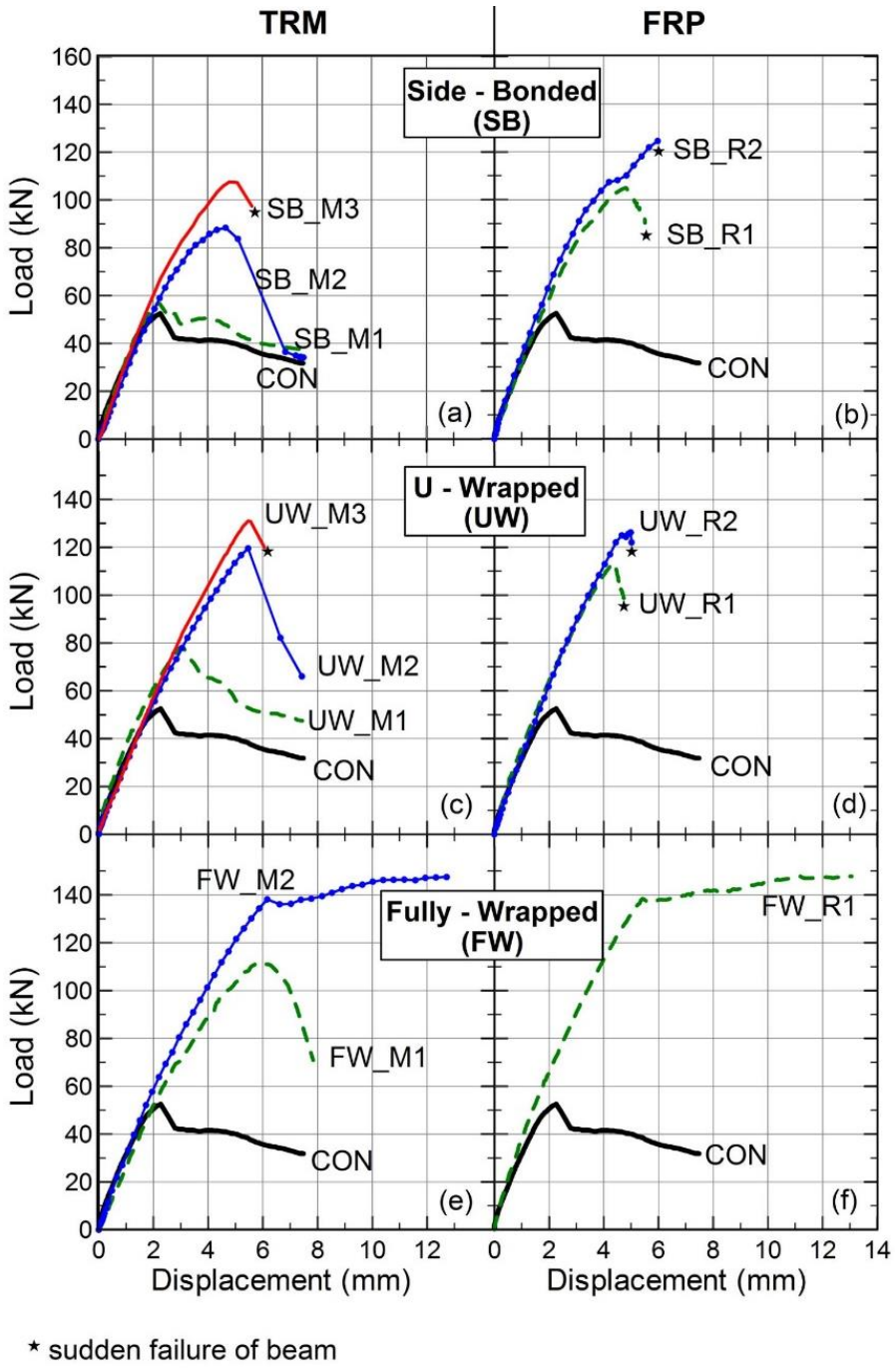


Figure 4.6. Load versus vertical displacement curves for all tested specimens.

They include: (1) The peak load. (2) The observed failure mode. (3) The shear resistance of the critical shear span, V_R, which is the shear force in the critical span at peak load. (4) The contribution of the jacket to the total shear resistance, V_f, which is calculated as the shear resistance of the strengthened specimen minus the shear resistance of the control specimen. (5) The shear strengthening effectiveness which is expressed by the ratio of the shear resistance of a strengthened specimen, $V_{R,str}$, to the shear resistance of the control beam, $V_{R,con}$. (6) The average shear strain of the critical

shear span at peak load, γ_{Pmax}. (7) The shear deformation capacity enhancement of the critical span as expressed by the ratio of the $\gamma_{Pmax,str}$ of the strengthened specimen to the $\gamma_{Pmax,con}$ of the control beam.

The average shear strain at the critical shear span, γ, was obtained from readings of the two potentiometers placed in X configuration (Fig. 4.5b) according to Eq. (4.1).

$$\gamma = \frac{(d_1'-d)d-(d_2'-d)d}{2Lh} \tag{4.1}$$

Table 4.3. Summary of test results.

Specimen	(1) Peak load (kN)	(2) Failure mode	(3) V_R (kN)	(4) V_f (kN)	(5) Shear strengthening effectiveness $V_{R,str}/V_{R,con}$	(6) Shear strain at peak load (‰), γ_{Pmax}	(7) Shear deformation capacity enhancement $\gamma_{Pmax,str}/\gamma_{Pmax,con}$
CON	51.8	shear [a]	29.7	-	-	1.51	-
SB_M1	56.6	shear [b]	32.4	2.7	1.09	2.00	1.32
UW_M1	78.2	shear [b]	44.8	15.1	1.51	4.00	2.65
FW_M1	111.2	shear [b]	63.7	34.0	2.15	3.78	2.50
SB_M2	88.7	shear [c]	50.8	21.1	1.71	3.63	2.40
UW_M2	120.2	shear [c]	68.8	39.2	2.32	4.34	2.87
FW_M2	152.8	flexural	87.5	57.8 [d]	2.95	-	-
SB_M3	108.9	shear [c]	62.4	32.7	2.10	5.10	3.38
UW_M3	131.1	shear [c]	75.1	45.4	2.53	3.07	2.03
SB_R1	105.0	shear [c]	60.2	30.5	2.03	4.82	3.19
UW_R1	113.4	shear [c]	64.9	35.3	2.19	3.33	2.21
FW_R1	150.3	flexural	86.1	56.4 [d]	2.90	-	-
SB_R2	124.5	shear [c]	71.3	41.6	2.40	3.26	2.16
UW_R2	126.2	shear [c]	72.3	42.6	2.43	2.54	1.68

[a] Tensile diagonal cracking, [b] Slippage of the vertical fibre rovings through the mortar and partial fibres rupture, [c] Debonding of the jacket, [d] This value can be considered as a lower limit of V_f due to the flexural failure.

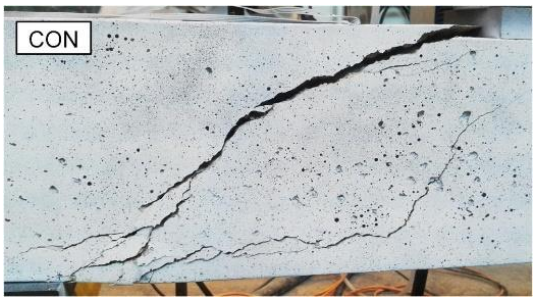


Figure 4.7. Dominant shear crack in the control beam.

The control beam (CON) failed in shear at an ultimate load of 51.8 kN after the formation of a large shear crack in the critical span as shown in Fig. 4.7. The strong dowel action provided by the longitudinal reinforcement prevented the sudden drop of load and contributed to the residual shear resistance of the beam after the peak load.

All beams strengthened with SB or UW FRP jackets failed in shear at an ultimate load substantially higher than that of the control beam; thus confirming the effectiveness of FRP jacketing in shear strengthening of RC members. The peak load attained by specimens SB_R1, UW_R1, SB_R2 and UW_R2 was 105, 113.4, 124.5 and 126.2 kN, respectively, which yields 103%, 119%, 140% and 143% increase in the shear capacity, respectively. In all these specimens failure occurred due to FRP debonding; the excellent bond between the resin and the concrete substrate resulted in peeling off of the FRP jackets with part of the concrete.

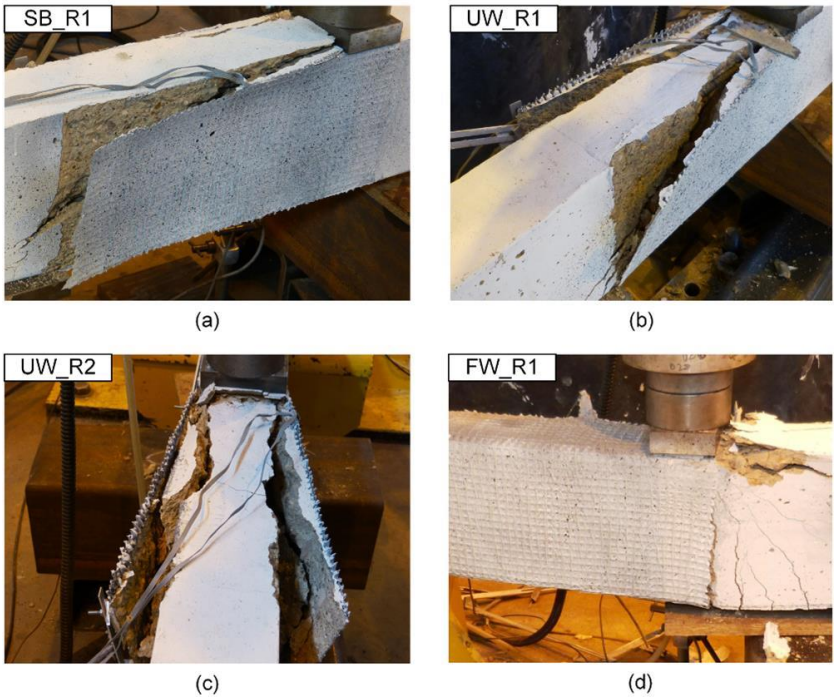


Figure 4.8. (a) FRP debonding in SB strengthening configuration; (b),(c) FRP debonding in UW strengthening configuration; (d) flexural failure of specimen with FW FRP jacket.

It was observed that in specimens with SB jackets the part of concrete that peeled off was thinner with respect to the specimens with UW jackets (Fig. 4.8a and Fig. 4.8b). Debonding of FRP reinforcement was initiated from the point of load application and propagated instantly to the support (Fig. 4.8c). One layer of FW FRP jacket resulted in enhancing at least 2.8 times the shear capacity. Specimen FW_R1

reached its ultimate moment capacity at a load of 150.3 kN and failed due to concrete crushing after yielding of the tensile longitudinal reinforcement (at approximately 140 kN - Fig. 4.8d). This confirmed the high effectiveness of closed FRP jackets. However, the use of closed jackets is not feasible in beams of typical RC buildings or bridge girders due to the presence of concrete slabs or decks, respectively.

With only the exception of specimen FW_M2 which failed in flexure, all the TRM-strengthened specimens failed in shear and displayed considerably higher shear resistance (from approximately 10% up to approximately 150%) compared to the control specimen. The behaviour of TRM-strengthened specimens is described below into groups depending on the number of strengthening layers.

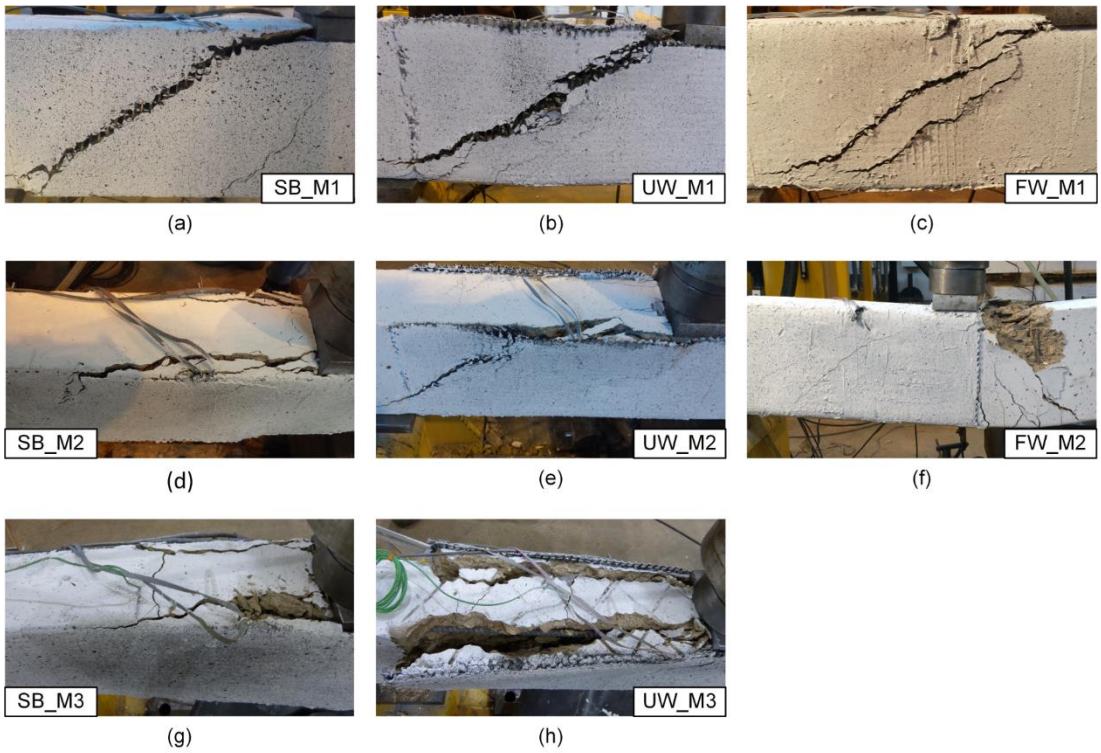


Figure 4.9. (a) Failure modes of TRM-retrofitted specimens: (a)-(c) Specimens SB_M1, UW_M1 and FW_M1 – local damage of the jacket; (d),(e) SB_M2 and UW_M2 – debonding of the jacket over a large area of the shear span: peeling off of the concrete cover; (f) FW_M2 – flexural failure despite the shear cracking of the TRM jacket; (g) SB_M3 – debonding of the jacket over a large area of the shear span: peeling off of the concrete cover; and (h) UW_M3 – abrupt debonding of the TRM jacket over the whole area of the shear span: peeling off of the concrete cover.

Specimens SB_M1, UW_M1 and FW_M1, which received one TRM layer, reached an ultimate load of 56.6, 78.2 and 111.2 kN, respectively. The corresponding increase in their shear capacity was equal to 9%, 51% and 115%. The failure of these

specimens was associated with damage of the TRM jackets (Fig. 4.9a, b, c). The load-drop in these specimens was attributed to the following local phenomena: (a) slippage of the vertical fibre rovings through the mortar and (b) partial rupture of the fibres crossing the shear crack. Going from the SB to the UW and finally to the FW configuration, the second phenomenon is more pronounced, whereas the first one tends to be eliminated. The nature of these local phenomena did not allow for a brittle failure mode. In fact, after the peak load was reached, relatively soft load degradation was recorded. As can be seen in Fig. 4.6 (a, c and e) for specimens strengthened with one layer the descending branch is quite smooth for SB jackets and becomes less smooth in UW and FW jackets, respectively.

Specimens SB_M2 and UW_M2 failed in shear at a load of 88.7 and 120.2 kN, respectively. Compared to the control specimen the increase in the shear resistance was equal to 71% and 132%, respectively. Failure in these specimens was attributed to debonding of the TRM jacket at a large part (approximately 2/3) of the shear span which was accompanied by peeling off of the concrete cover (Fig. 4.9d, e). This type of failure, although it was brittle, it was not as explosive as in the case of FRP-strengthened beams. Finally specimen FW_M2, after the formation of a shear crack at 70 kN, reached its ultimate moment capacity and (identically to FW_R1) failed in flexure due to concrete crushing at the compression zone (Fig. 4.9f).

Specimens SB_M3 and UW_M3 failed in shear at even higher loads (108.9 and 131.1 kN, respectively) when compared to the corresponding specimens strengthened with two TRM layers (SB_M2 and UW_M2). The shear resistance of specimens SB_M3 and UW_M3 was increased by 110% and 153%, respectively, with respect to the control specimen. Specimen SB_M3 (Fig. 4.9g) failed in a similar way with specimen SB_M2 (Fig. 4.9d), whereas the failure mode of specimen UW_M3 was unique among all TRM-strengthened specimens. In the latter case debonding of the U-jacket occurred at the full-length of the shear span (Fig. 4.9h) and was as explosive as in case of all FRP-strengthened specimens.

Figure 4.10 presents the load versus average shear strain curves for all specimens which are plotted up to peak load (specimens FW_M2 and FW_R1 that failed in flexure are plotted up to yielding). The values of shear strain at peak load (γ_{Pmax}) are presented in Table 4.3. Strengthening the beams with TRM or FRP jackets resulted in an increase in the average shear strain over the critical shear span, which at peak load varied from 1.32 to 3.38 times (compared to the control specimen). This increase is

mainly attributed to redistribution of shear stresses in the shear span, which ultimately led to a more dense crack pattern and hence to an increased shear deformation capacity. It is also concluded that, in general, higher average strains were developed in TRM-retrofitted specimens compared to their FRP counterparts.

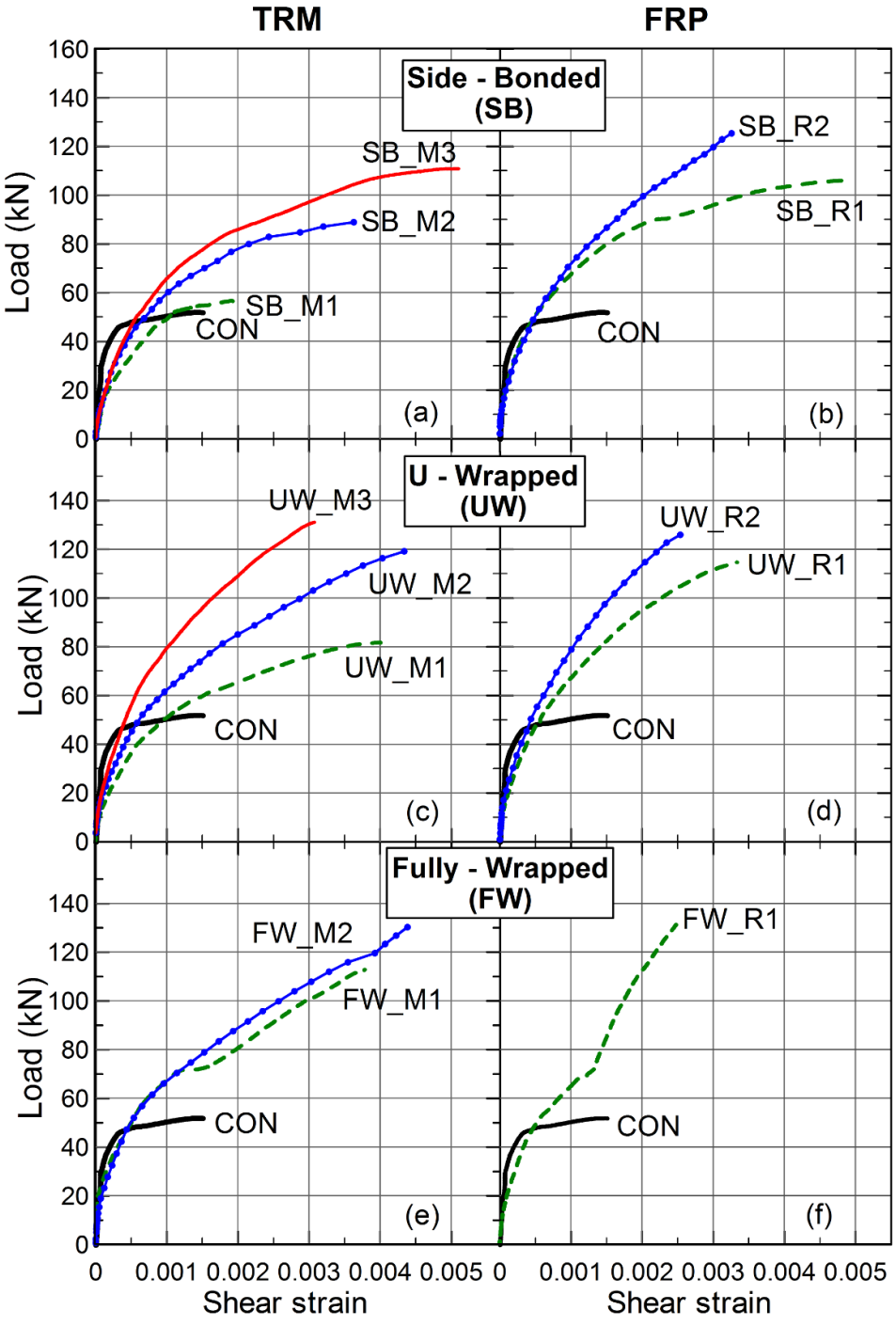


Figure 4.10. Load versus average shear strain curves.

4.1.3 Discussion

4.1.3.1 Strengthening configuration and number of layers

The curves in Fig. 4.11a illustrate the effect of the strengthening configuration (SB, UW or FW) on the shear capacity enhancement (V_f / V_{con} x100%). In FRP-strengthened specimens, the shear capacity was only marginally increased when UW jackets were applied instead of SB ones. On the other hand in TRM-strengthened specimens, the effectiveness of the UW jackets (expressed as the shear capacity enhancement) was 5.5 and 1.85 times the effectiveness of the SB jackets for 1 and 2 layers, respectively. Therefore, the benefit of applying UW instead of SB jackets was more pronounced in TRM than FRP system, especially as the number of layers increased. Finally, FW jacketing was the most effective configuration for both strengthening systems. In particular, the effectiveness of the FW jacket was 2.2 times the UW jacket effectiveness in case of one TRM layer, and at least 1.5 times in case of two TRM layers. For one FRP layer FW jacket was at least 1.6 times more effective than the UW jacket.

The effect of the number of layers on the shear capacity enhancement for SB and UW strengthening configurations is illustrated in Fig. 4.11b. Doubling the amount of TRM reinforcement (two layers instead of one) resulted in dramatic shear capacity increase. In particular, this increase was equal to 7.8 and 2.6 times for the SB and UW jackets, respectively. The corresponding increase when resin was used as binder was 1.35 and 1.2 times. The latter is consistent with the typical behaviour in FRP jackets in which increasing the amount of EB reinforcement results in limiting the effectiveness of FRP strengthening. To further investigate this effect on TRM jackets, beams with three layers were also tested for both SB and UW strengthening configurations. As shown in Fig. 4.11b, applying a third TRM layer resulted in strength increase of 1.55 and 1.15 times for SB and UW jackets, respectively. In the case of UW TRM jackets, increasing the number of layers from two to three had approximately the same effect as in FRP jackets for the increase from one to two layers. This trend is clearly illustrated in Fig. 4.11b from the slope of V_f/V_{con} – no. of layers curves.

A possible explanation for the difference between the two strengthening systems, regarding the effect of increasing the number of layers from one to two, could

be found in the observed failure modes. As described in Section 3, all specimens retrofitted with FRP jackets exhibited the same failure mode which is associated to the failure of the concrete substrate with no damage in the composite jackets. However, in the case of TRM-retrofitted specimens a change in the failure mode was witnessed when the number of layers was increased from one to two or three. In specific, when one layer was applied the failure was attributed to local damage of the TRM jacket; the vertical fibre rovings crossing the developed shear crack at the jacket experienced a combination of partial rupture and slippage through the mortar (Fig. 4.9a, b). The increase in the number of layers in that case prevented these local phenomena and as a result the damage was shifted to the concrete substrate.

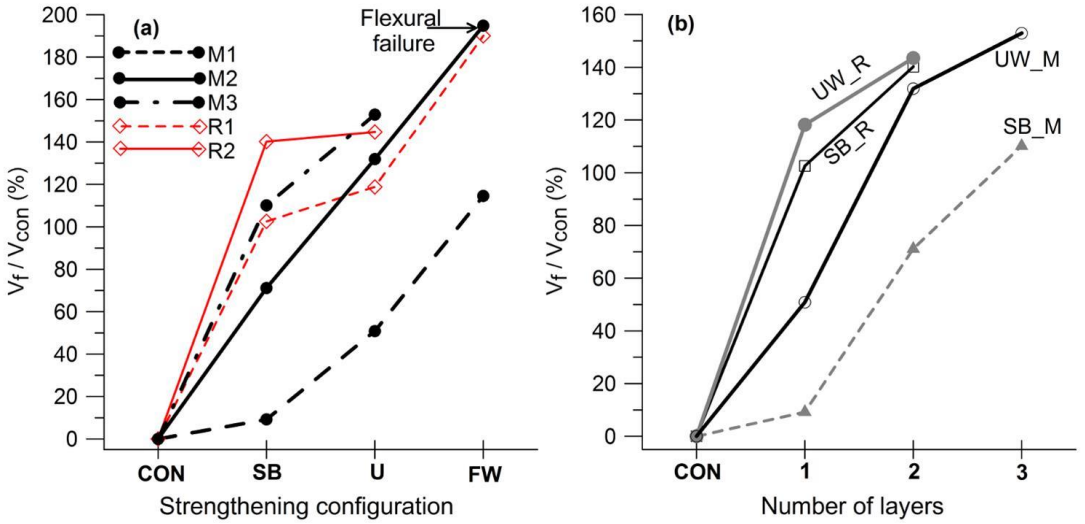


Figure 4.11. (a) Effect of strengthening configuration on the shear capacity enhancement; (b) effect of number of layers on the shear capacity enhancement.

When preventing the local damage of the TRM jacket, due to partial rupture and slippage through the mortar (Fig. 4.9a, b), one of the following failure modes will occur: (a) debonding at the interface between the jacket and the concrete substrate, (b) interlaminar shear failure at the interface between two textile layers, or (c) peeling off of the concrete substrate. The first two, which are premature failure modes, are more likely to happen for low values of mortar tensile strength which could lead to its bond failure. The benefit of using a relatively high-strength mortar (like the one used in this study) is that excellent bond conditions can be achieved, resulting in the development of the third failure mode and therefore yielding the best results in terms of shear capacity enhancement.

The arising question at this point is why the relatively poor behaviour of the TRM jacket at the local level was significantly improved when a second layer of textile was provided. The key answer to this question could be found in the mechanism of transferring forces from the textile reinforcement to the matrix. It seems that by providing just a second layer of textile, the mechanical interlock, which is the main mechanism of transferring forces from the reinforcement to the matrix in TRM systems, is drastically improved. This improvement might be attributed to the fact that two (at least) overlapping textile layers create a denser mesh-pattern than one. This happens due to the possible offset between the two layers (Fig. 4.12). Provided that mortar will not fail in shear; the denser mesh-pattern in turn creates conditions for improved mechanical interlocking characteristics, which ultimately results in altering the failure mode.

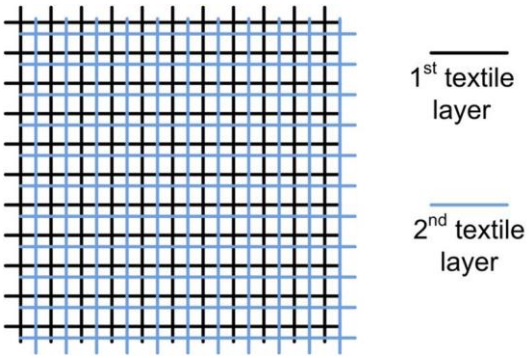


Figure 4.12. Overlapping of two textiles with an offset.

4.1.3.2 Deformation aspects of jackets based on DIC

The response of the TRM and FRP SB and UW jackets, as a means of vertical deformations distribution along the beam height, was captured using the DIC method and is presented in Fig. 4.13. Each curve illustrates the relative displacement of each point along the beam height with respect to the bottom of the beam (at the middle cross-section of the critical shear span) at the instant of peak load. For the sake of comparison, the corresponding curve of the control beam is also plotted in all curves.

As illustrated in Fig. 4.13 the control beam exhibited concentration of the vertical deformations at a specific level, which is related to the development of a single shear crack at that level (at around 130-140 mm from the bottom of the beam). The specimens with one TRM layer exhibited identical behaviour, with concentration of the deformations at a single level. Better distribution of deformations was observed in

the remaining specimens, indicating that the jackets were activated over a broader area due to better redistribution of stresses. Figure 4.13 provides the evidence that in TRM jackets the force transferring mechanism is being modified with additional layers, thus resulting in a performance of the TRM jackets similar to the performance of the FRP jackets. However, the distribution of deformations in FRP jackets is consistently better than the TRM jackets for the same number of layers.

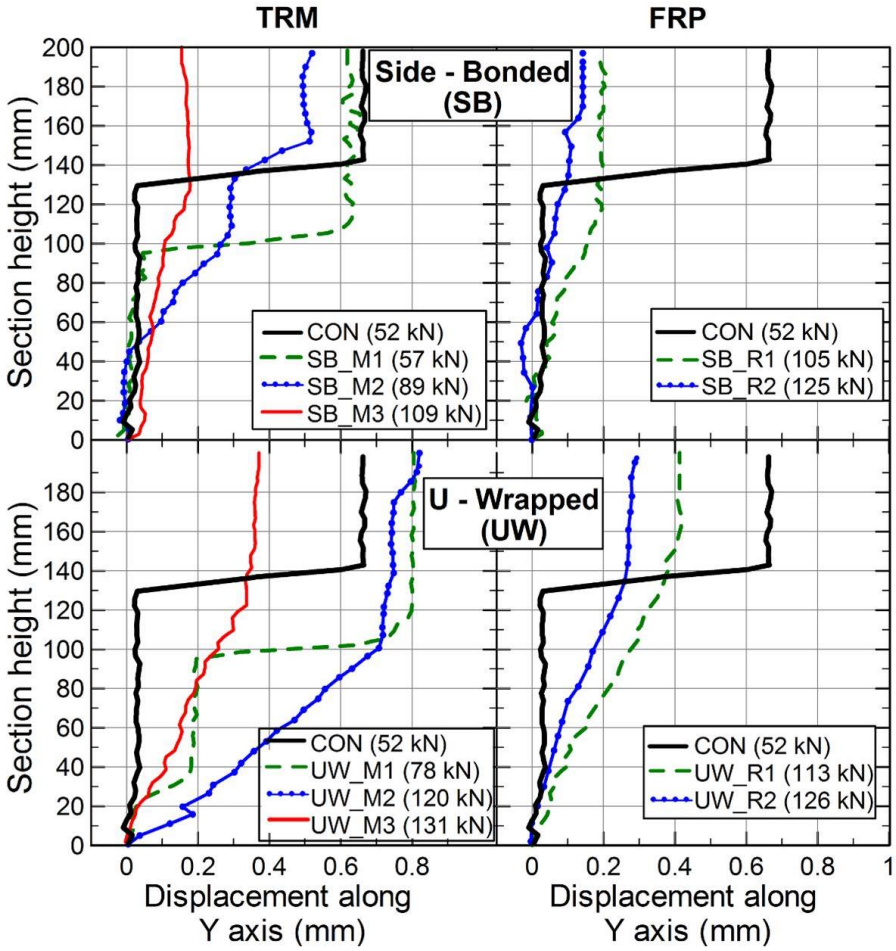


Figure 4.13. Relative vertical displacements along the beam height at the central cross-section of the critical shear span, at the instant of peak load.

Another interesting aspect of the behaviour of the TRM jackets is associated to their strengthening configuration. SB jackets deform at the central region along the beam height (with the two ends being almost inactive), whereas UW jackets deform from the bottom level to a level in the central region, thanks to the anchorage of the jackets at the bottom corner of the beams.

Photos of the vertical deformations field of the TRM jackets, obtained through DIC at peak load are shown in Fig. 4.14. From there it is also evident that in TRM

jackets with two or three layers the vertical deformations are distributed over a broader region of the shear span, when compared to TRM jackets with one layer.

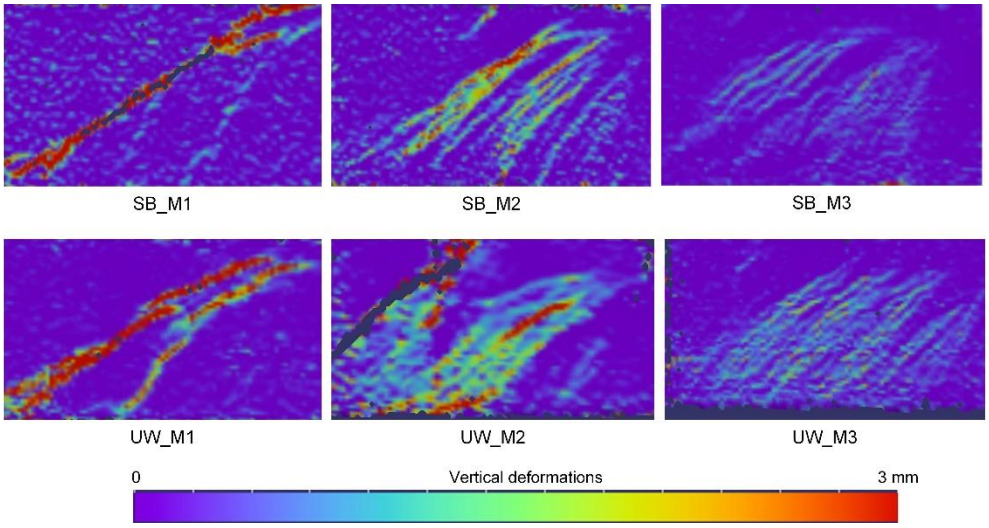


Figure 4.14. Field of vertical axis deformations in the critical shear span of TRM-retrofitted specimens at the instant of peak load.

4.1.4 Effective Stress and TRM versus FRP Effectiveness Factor: Design Aspects

For calculating the FRP contribution to the shear capacity of RC members most of the design models use the effective stress of the FRP (σ_{eff}), which can ideally be described as the average stress of the fibres crossing the shear crack. Given the effective stress, the shear force carried by the FRP, $V_{f,}$ can be calculated using the Eq. (4.2) (Triantafillou 1998) under the assumptions that: (a) the shear crack forms an angle θ=45^o with respect to the member axis, and (b) fibres crossing the crack are perpendicular to the member axis.

$$V_f = \rho_f \sigma_{eff} b_w 0.9d \tag{4.2}$$

where ρ_f is the geometrical reinforcement ratio of the composite material, expressed as $\rho_f = 2t_f / b_w$ (this is valid for continuous FRP sheets and not for FRP strips), b_w is the width of the beam, d is the effective depth of the member section, and t_f is the total thickness of the composite material in the loading direction (usually taken equal to the thickness of the fabric times the number of layers).

According to Triantafillou and Papanicolaou (2006) the format of Eq. (4.2) can also be used for the calculation of the shear force carried by TRM jackets. In particular,

assuming that: (a) the shear crack forms an angle θ=45^o with respect to the member axis, and (b) a two-directional textile is applied with the one direction of fibres being perpendicular to the member axis and the other being parallel to the member axis, then Eq. (4.2) can be used without any modifications.

Application of Eq. (4.2) to the (SB and UW jacketed) beams tested in this study with t_f equal to the nominal thickness of the fibres, results in the values of σ_{eff} and ε_{eff} given in Table 4.4. ε_{eff} is the so-called effective strain and is calculated by dividing σ_{eff} by the modulus of elasticity. The modulus of elasticity of the fibres, E_f according to the manufacturer datasheets was used for defining effective strain, ε_{eff}, as this value is also used in all formulas suggested for calculating ε_{eff} in FRP jackets. In addition, Table 4.4 includes the effectiveness factor $k_{TRM/FRP}$, which is defined as the ratio of the TRM to FRP jackets effective stress.

Table 4.4. Experimental values of effective strains and effectiveness factor for SB and UW TRM jackets.

				Effective stress, σ_{eff} (MPa)	**Effective strain, ε_{eff} (‰)**	**TRM versus FRP effectiveness factor, $k_{TRM/FRP}$ ($\sigma_{eff,TRM}$ /$\sigma_{eff,FRP}$)**
Side-Bonded Jackets	1 layer	TRM	(SB_M1)	89	0.40	0.09
		FRP	(SB_R1)	1008	4.48	
	2 layers	TRM	(SB_M2)	347	1.54	0.50
		FRP	(SB_R2)	694	2.86	
U-Wrapped Jackets	1 layer	TRM	(UW_M1)	499	2.22	0.43
		FRP	(UW_R1)	1166	5.18	
	2 layers	TRM	(UW_M2)	644	3.08	0.91
		FRP	(UW_R2)	710	3.16	

It should be noted that Triantafillou and Papanicolaou (2006) obtained a value of $k_{TRM/FRP}$ = 0.55 from tests on two rectangular RC beams retrofitted with TRM and FRP closed jackets. In the present study the effectiveness factor $k_{TRM/FRP}$ varies significantly not only for different strengthening configuration (SB or UW jacketing), but also for different number of layers. In particular, it varies from 0.09, which corresponds to one layer of SB jacket, to 0.91 which corresponds to two layers of UW jacket. Hence, the results of this study indicate that TRM jackets are less effective than FRP jackets, but the effectiveness is sensitive to parameters such as the strengthening configuration and the number of layers. By increasing the number of layers from one to two the

effectiveness factor increases substantially, whereas the same happens when UW jackets are applied instead of SB jackets.

Figure 4.15 plots the experimentally obtained effective strains versus $\rho_f E_f / f_c^{2/3}$ curves, for different strengthening systems (TRM versus FRP) and configurations (SB versus UW), together with the curve corresponding to the formula suggested in Triantafillou and Antonopoulos (2000) for calculating ε_{eff} in FRP jackets $\{\varepsilon_{eff}=0.65[f_c^{2/3}/(E_f \rho_f)]^{0.56}\}$. The trend of the experimental values for FRP jackets is descending for increasing values of $\rho_f E_f / f_c^{2/3}$ which is in agreement with the analytical curve. On the contrary, TRM jackets do not follow the same trend; there is significant increase of ε_{eff} for low ρ_f values, whereas for higher ρ_f values this effect is eliminated. This is explained by the fact that TRM jackets do not experience a full-composite action for low values of ρ_f.

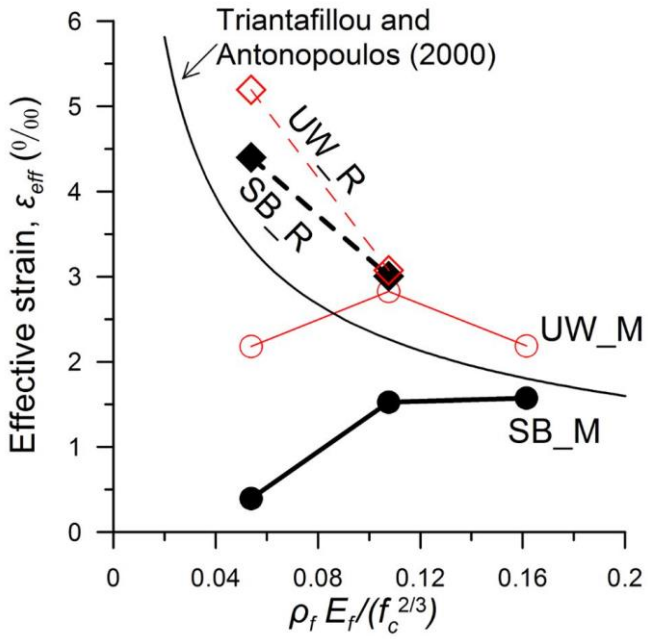


Figure 4.15. Experimentally obtained effective strains versus $\rho_f E_f / f_c^{2/3}$ and comparison with the analytical curve of Triantafillou and Antonopoulos (2000) model.

It seems that after a critical value of ρ_f ($\rho_{f,crit}$), TRM jackets develop full-composite action and behave similar to FRP jackets (e.g. specimen UW_M3). It should be noted that the development of full-composite action of TRM jackets depends on several factors such as the mortar mechanical properties, the strengthening configuration, the number of layers and possibly the textile geometry (see section 4.2).

4.1.5 Summary

Section 4.1 presents an experimental investigation on the effectiveness of TRM and FRP jackets in shear strengthening of rectangular RC beams. Key parameters were: (a) the strengthening system (TRM versus FRP), (b) the strengthening configuration (SB, UW or FW jacketing) and (c) the number of layers. For this purpose, fourteen shear-deficient beams were subjected to three-point bending under monotonic loading: one was tested as-built, whereas the remaining thirteen were strengthened prior to testing. The main conclusions drawn from this study are summarized as follows:

- TRM is generally less effective in increasing the shear capacity of RC beams than FRP jacketing, but the effectiveness depends on both the strengthening configuration and the number of layers. The TRM versus FRP effectiveness factor varies from 0.09, which correspond to one layer of side-bonded jacket, to 0.91, which correspond to two layers of U-wrapped jacket.
- TRM jackets are more effective in increasing the beams deformation capacity (expressed as the average shear strain of the shear-critical span) than FRP jackets.
- U-wrapping (UW) strengthening configuration is much more effective than side-bonding (SB) in case of TRM jackets. On the contrary, in case of FRP jackets the UW configuration was found only slightly more effective than the SB configuration. Full-wrapping (FW) is the most effective strengthening configuration for both strengthening systems.
- A major difference between TRM and FRP strengthening systems is observed by increasing the number of layers from 1 to 2. In particular, the effectiveness of FRP jackets increases by 1.35 and 1.2 times for SB and UW configurations, respectively, whereas the effectiveness of TRM jackets increases by 7.8 and 2.6 times, respectively.
- The considerably higher shear capacity increase achieved by TRM jacketing when two instead of one textile layers are applied is linked to the change in the failure mode. The local damage the TRM jackets experience when one layer is applied (partial fibres rupture and slippage of fibre filaments through the mortar), is being shifted to the concrete substrate when two layers are applied (debonding of the jacket with peeling-off of the concrete). This is attributed to the better mechanical interlock conditions created by the overlapping of at least two textile layers.

4.2 Effect of amount of external reinforcement ratio, textile material and geometry and shear span-to-depth ratio on RC beams strengthening in shear with TRM

4.2.1 Experimental Programme

4.2.1.1 Test specimens and investigated parameters

The results of 22 half-scale RC beams are presented in this section. Three different shear span-to-depth ratios, namely *a/d*=1.6, 2.6 and 3.6 were studied. The geometry and design of beams (in terms of longitudinal reinforcement) were identical to the beams presented in Section 4.1. One shear span did not include any transverse reinforcement as also in beams presented in Section 4.1, whereas the other shear span included 8-mm diameter stirrups at a spacing of 100 mm, 75 mm and 50 mm at the beams of shear span ratio, *a/d* equal to 1.6, 2.6 and 3.6, respectively (Fig. 4.16a).

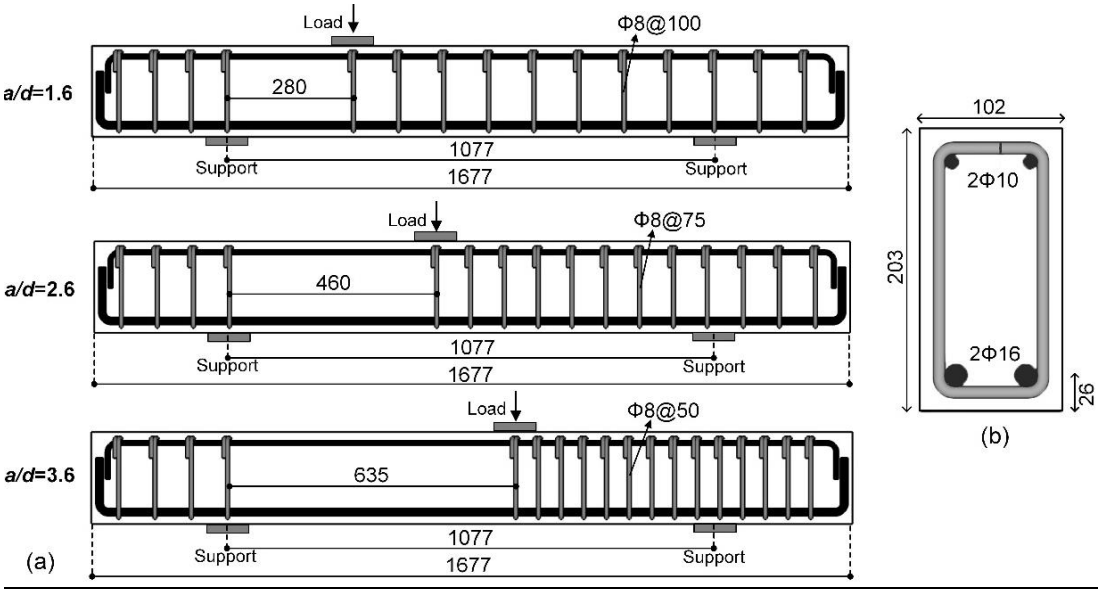


Figure 4.16. (a) Schematic test set-up; (b) cross-section (dimensions in mm).

The key investigated parameters of this section comprised: (a) the effect of the amount of external TRM reinforcement ratio, ρ_f, using different textile materials (carbon, glass and basalt), (b) the textile geometry and (c) the shear span-to-depth-ratio, *a/d*. Three beams with shear span-to-depth ratios equal to 1.6 (CON_1.6), 2.6 (CON, this specimens has been already presented in Section 4.1) and 3.6 (CON_3.6) were tested as-built without receiving strengthening and served as control specimens, whereas the rest of the specimens received U-shaped TRM jackets. All four textile

meshes with equal quantity of fibres in two orthogonal directions (CL, CH, G and B, see Fig. 3.1) were used.

Table 4.5. Strengthening configuration and material properties of all specimens.

Specimen	ρ_f (‰)	E_f (GPa)	E_{f_TRM} (GPa)	Concrete Strength (MPa)		Mortar Strength (MPa)		
				Compressive strength	Tensile splitting strength	Compressive strength	Flexural strength	Tensile splitting strength
***a/d* = 2.6**								
CON	-	-	-	21.6	2.36	-	-	
CL1	1.2	225	167.6	23.0	2.50	38.7	9.10	3.40
CL1_strip	1.9	225	167.6	20.0	1.98	38.7	9.10	3.40
CH1	1.9	225	163.3	23.8	2.73	31.1	10.3	3.40
CH1_CL1	3.1	225	165.5	20.0	1.98	38.7	9.10	3.40
CH2	3.7	225	163.3	23.8	2.73	31.1	10.3	3.40
CL3	3.6	225	167.6	20.8	2.39	35.5	8.10	3.40
CH2_CL1	4.9	225	164.7	20.0	1.98	38.7	9.10	3.40
CH3	5.6	225	163.3	22.6	2.81	26.9	8.64	3.40
CH3_CL1	6.8	225	164.4	20.0	1.98	38.7	9.10	3.40
G1	0.9	74	41.1	20.0	1.98	35.5	8.10	3.40
G3	2.6	74	41.1	20.0	1.98	35.5	8.10	3.40
G7	6.0	74	41.1	20.0	1.98	38.7	9.10	3.40
B1	0.7	89	63.7	23.1	2.48	33.3	11.05	3.40
B3	2.2	89	63.7	23.1	2.48	35.5	8.10	3.40
B7	5.1	89	63.7	23.1	2.48	35.5	8.10	3.40
***a/d* = 1.6**								
CON_1.6	-	-	-	20.5	2.35	-	-	
CL1_1.6	1.2	225	167.6	22.6	1.95	33.3	11.05	3.40
CL3_1.6	3.6	225	167.6	22.6	1.95	33.3	11.05	3.40
***a/d* = 3.6**								
CON_3.6	-	-	-	20.5	2.35	-	-	
CL1_3.6	1.2	225	167.6	22.6	1.95	33.3	11.05	3.40
CL3_3.6	3.6	225	167.6	22.6	1.95	33.3	11.05	3.40

Table 4.5 presents the details of all specimens whereas Fig. 4.17 illustrates all the strengthening configurations adopted. The notation of retrofitted specimens is XN, where X denotes the type of the textile (CL for light carbon, CH for heavy carbon, G for glass and B for basalt) and N denotes the number of layers. For specimens with *a/d* different than 2.6, a suffix with the shear span-to-depth ratio (1.6 or 3.6) was used. The description of the strengthened specimens follows:

- CH1, CH2 and CH3: beams with *a/d* =2.6, strengthened with 1, 2 and 3 heavy carbon TRM layers, respectively. These beams have been already presented in Section 4.1 with the names UW_M1, UW_M2 and UW_M3, respectively.
- CL1 and CL3: beams with *a/d* =2.6, strengthened with 1 and 3 light carbon TRM layers, respectively.

- CH1_CL1, CH2_CL1 and CH3_CL1: beams with *a/d* =2.6, that received 1 light carbon TRM layer combined with 1, 2 and 3 heavy carbon TRM layers, respectively.
- CL1_strips: beam with *a/d* =2.6, that received 1 light carbon TRM layer combined with light carbon strips of 125 mm width, as shown in Fig. 4.17.
- G1, G3 and G7: beams with *a/d* =2.6, strengthened with 1, 3 and 7 glass TRM layers, respectively.
- B1, B3 and B7: beams with *a/d* =2.6, strengthened with 1, 3 and 7 basalt TRM layers, respectively.
- CL1_1.6 and CL3_1.6: beams with *a/d* =1.6, strengthened with 1 and 3 light carbon TRM layers, respectively.
- CL1_3.6 and CL3_3.6: beams with *a/d* =3.6, strengthened with 1 and 3 light carbon TRM layers, respectively.

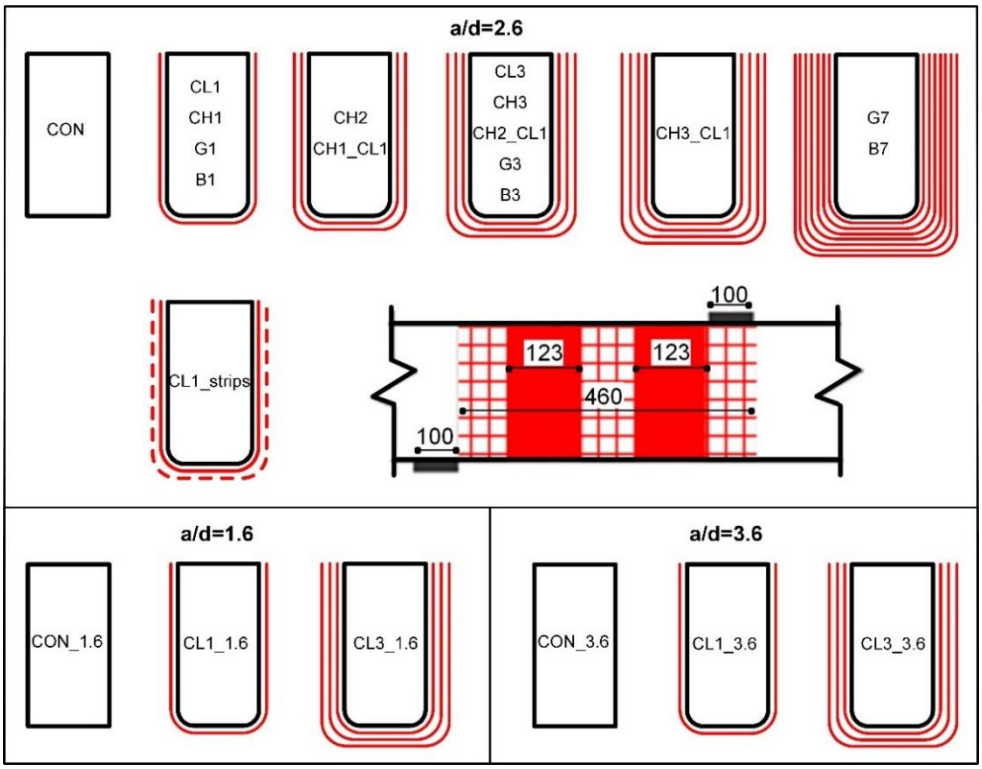


Figure 4.17. Schematic representation of different strengthening configurations.

4.2.1.1 Materials and strengthening procedure

The specimens were cast in groups of four using the same concrete mix design with the beams presented in Section 4.1. The values of compressive strength and

tensile splitting strength of the concrete on the day of testing are summarized in Table 4.5. The mortar described in Section 3.1 was used as matrix of the composite material. The strength properties of the mortar (average values of 3 specimens) on the day of testing are summarised in Table 4.5. The procedure of strengthening was described in detail in Section 4.1.1.2. The main steps are briefly described here as well: (a) surface preparation; (b) applying of a first layer of mortar at the dampened concrete surface; (c) impregnation of the textile fibres with mortar (Fig. 4.18a) and (d) application of a final layer of mortar on the top of the final textile layer (Fig. 4.18b).

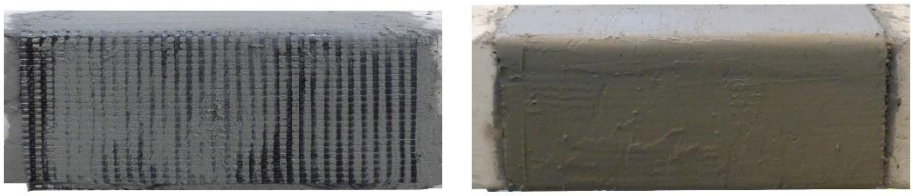


Figure 4.18. (a) Impregnation of the textile fibres with mortar and (b) final layer of mortar on the top of the final textile layer.

4.2.1.2 Experimental set-up and procedure

The beams were subjected to monotonic loading using a three-point bending set-up configuration as shown in Fig. 4.19. The experimental procedure applied was identical to this described in Section 4.1.1.3. The vertical displacement was measured at the position of load application using an external LVDT; the displacement measured from this sensor was used to plot the load-displacement curves presented in Section 4.2.2. Additionally, the Digital Image Correlation (DIC) technique was employed to monitor relative displacements within the critical shear span.

4.2.2 Experimental results

The load versus displacement curves of all beams with *a/d*=2.6 that were strengthened with carbon, glass and basalt TRM jackets are presented in Fig. 4.20a-c, respectively, whereas the shear force versus displacements curves of the beams with different *a/d* ratios are included in Fig. 4.21a-c. Key results are also presented in Table 4.6. The effective strain of the jacket, ε_{eff} (‰) in Table 4.6 was calculated using Eq. (4.3).

$$\varepsilon_{eff} = V_f / \left(\rho_f E_{f_TRM} b_w 0.9d\right) \quad (4.3)$$

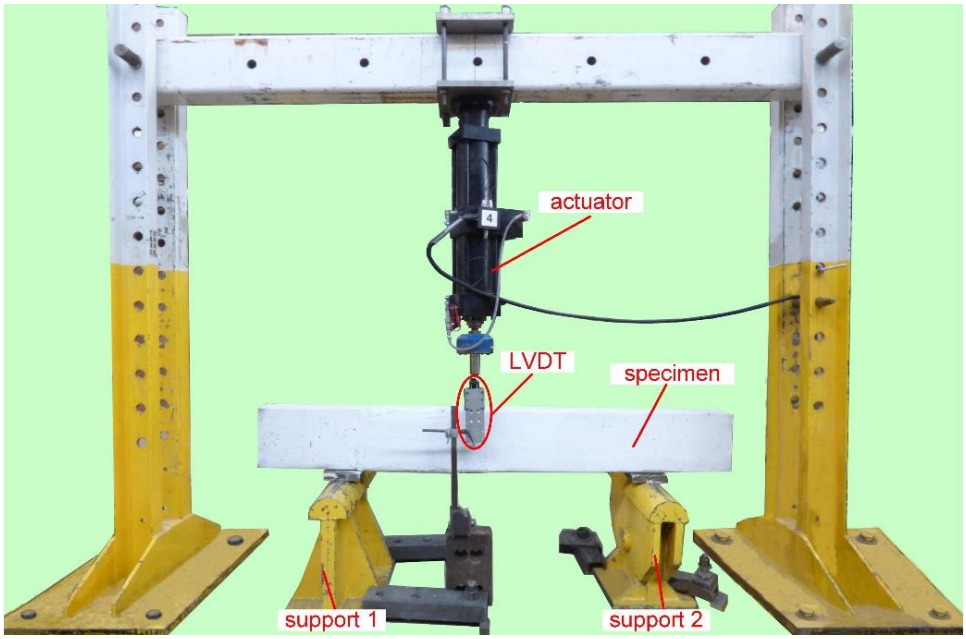


Figure 4.19. Three-point bending test set-up of beams.

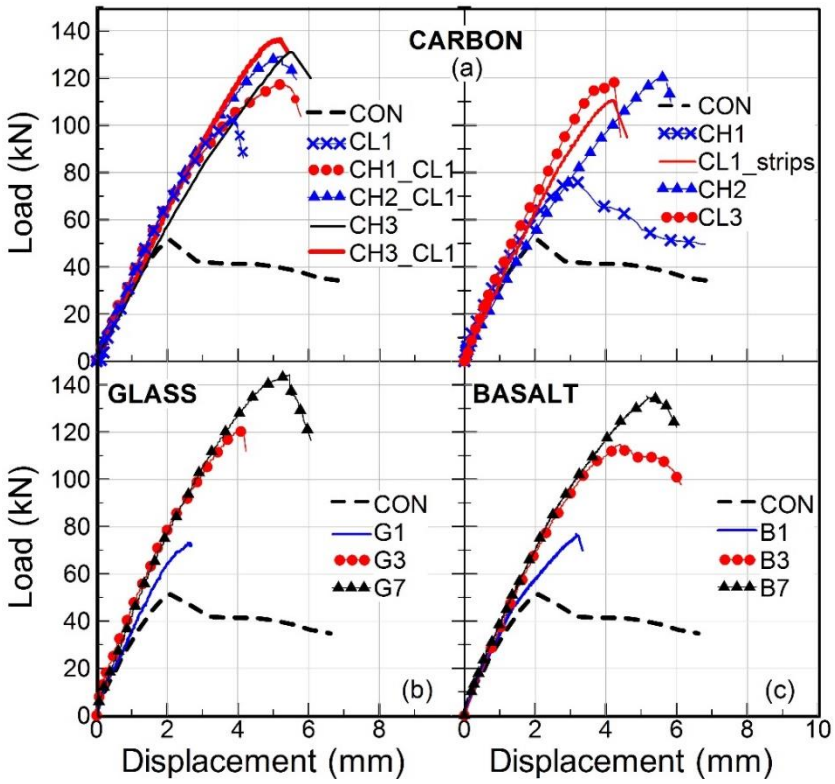


Figure 4.20. Load versus vertical displacement curves for all tested specimens of 2.6 shear span-to-depth ratio.

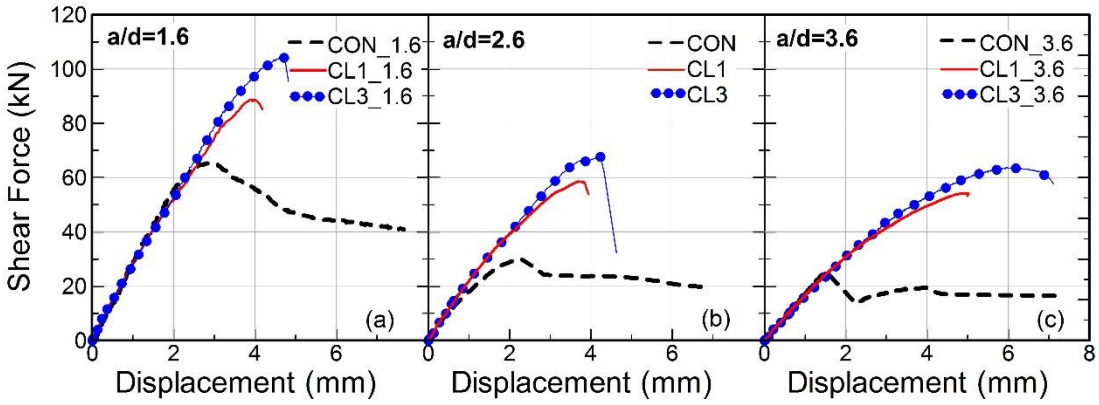


Figure 4.21. Shear force versus vertical displacement curves for all tested specimens of shear span-to-depth ratio equal to 1.6, 2.6 and 3.6.

Table 4.6. Summary of test results.

Specimen	(1) Peak load (kN)	(2) Displacement at peak load (mm)	(3) Failure mode	(4) V_R (kN)	(5) V_f (kN)	(6) Shear capacity increase $V_f/V_{R,con}$ (%)	(7) ε_{eff} (‰)
			***a/d* = 2.6**				
CON	51.8	2.27	shear [a]	29.7	-	-	-
CL1	102.3	3.77	shear [b]	58.6	28.9	97.3	8.73
CL1_strip	110.7	4.22	shear [b]	63.4	33.7	113.5	6.64
CH1	78.2	3.09	shear [c]	44.8	15.1	50.8	3.06
CH1_CL1	117.4	5.19	shear [b]	67.3	37.6	126.6	4.54
CH2	120.2	5.60	shear [b]	68.9	39.2	132.0	3.97
CL3	118	4.38	shear [b]	67.6	37.9	127.6	3.82
CH2_CL1	129.3	5.24	shear [c]	74.1	44.4	149.5	3.36
CH3	131.1	5.47	shear [b]	75.1	45.4	152.9	3.06
CH3_CL1	136.5	5.20	shear [b]	78.2	48.5	163.3	2.67
G1	73.2	2.59	shear [d]	41.9	12.2	41.1	21.1
G3	117.3	4.09	shear [b]	67.2	37.0	124.6	21.4
G7	144.3	5.47	shear [b]	82.7	53	178.5	13.1
B1	76.9	3.16	shear [d]	44.1	14.4	48.5	19.1
B3	114.9	4.38	shear [b]	65.8	36.1	121.5	15.9
B7	135.4	5.15	shear [b]	77.6	47.9	161.3	9.09
			***a/d* = 1.6**				
CON_1.6	88.4	2.93	shear [e]	65.4	-	-	-
CL1_1.6	123.7	3.85	shear [b]	91.5	26.1	39.9	7.88
CL3_1.6	142.7	4.66	shear [b]	105.	40.2	61.5	4.05
			***a/d* = 3.6**				
CON_3.6	62.2	1.51	shear [a]	25.5	-	-	-
CL1_3.6	133.8	4.91	shear [b]	54.9	29.4	115.3	8.88
CL3_3.6	158.7	5.92	shear [b]	65.1	39.6	155.3	3.99

[a] Tensile diagonal cracking; [b] Debonding of the jacket; [c] Slippage of the vertical fibre rovings through the mortar and partial fibres rupture; [d] Fracture of the jacket; [e] shear compression

The control beam with *a/d*=2.6 (CON) failed in shear at an ultimate load of 51.8 kN, as also mentioned in 4.1.2.

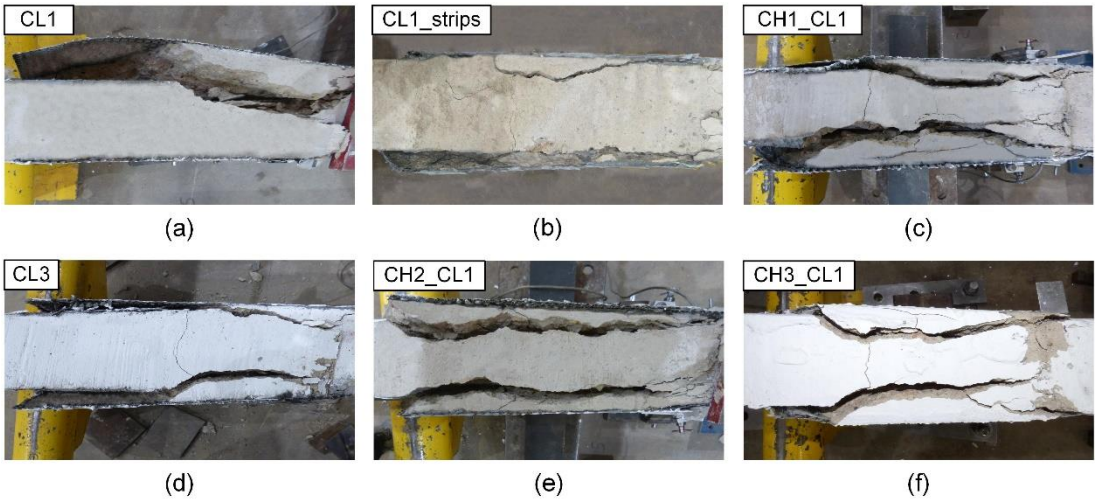


Figure 4.22. Failure modes of carbon TRM-retrofitted specimens of 2.6 shear span-to-depth ratio - abrupt debonding of the TRM jacket over the whole area of the shear span: peeling off of the concrete cover for specimens: (a) CL1; (b) CL1_strips; (c) CH1_CL1; (d) CL3; (e) CH2_CL1 and (f) CH3_CL1.

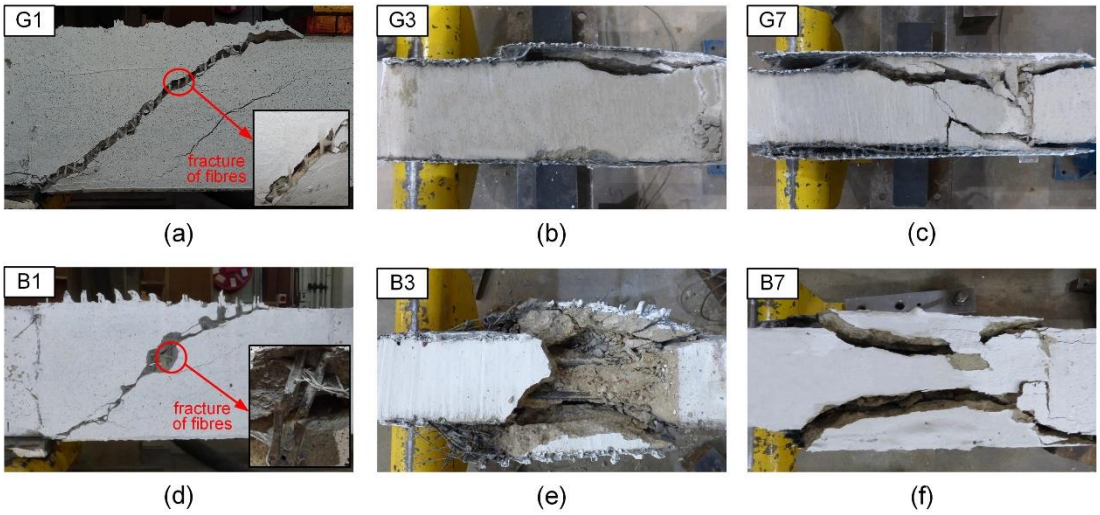


Figure 4.23. Failure modes of glass and basalt TRM-retrofitted specimens of 2.6 shear span-to-depth ratio: (a) specimen G1 - fracture of glass TRM jacket; (b)-(c) specimens G3 and G7 - debonding of the glass TRM jacket over the whole area of the shear span: peeling off of the concrete cover; (d) specimen B1 - fracture of basalt TRM jacket; (e)-(f) specimens B3 and B7 - debonding of the basalt TRM jacket over the whole area of the shear span: peeling off of the concrete cover.

Specimens CH1 and CH2 reached an ultimate load of 78.2 and 120.2 kN, respectively. The failure of specimen CH1 was associated with local damage of the TRM jacket, whereas failure in specimen CH2 was attributed to debonding of the TRM jacket at a large part of the shear span as also mentioned in 4.1.2.

Specimens CL1, CL1_strips, CH1_CL1, CL3, CH2_CL1, CH3 and CH3_CL1 failed in shear at an ultimate load 102.3, 110.7, 117.4, 118, 129.3, 131.1 and 136.5 kN,

respectively, which yields 97.3%, 113.5%, 132%, 127.6%, 149.5%, 152.9% and 163.3% increase in the shear capacity, respectively. Failure of all these specimens was due to debonding of the TRM jacket from the concrete substrate at the full-length of the shear span with peeling off of the concrete cover (Fig. 4.22a-f).

The peak load attained by specimens G1, G3, G7, B1, B3 and B7 was 73.2, 117.3, 144.3, 76.9, 114.9 and 135.4 kN, respectively, which yields 41.1%, 124.6%, 178.5%, 48.5%, 121.5% and 161.3% increase in the shear capacity, respectively. Failure of specimens G1 and B1 was due to fracture of the textile fibres crossing the shear crack (Fig. 4.23a and d), whereas specimens G3, G7, B3 and B7 failed due to debonding of the jacket from the concrete substrate removing part of the concrete cover (Fig. 4.23b-c, e-f).

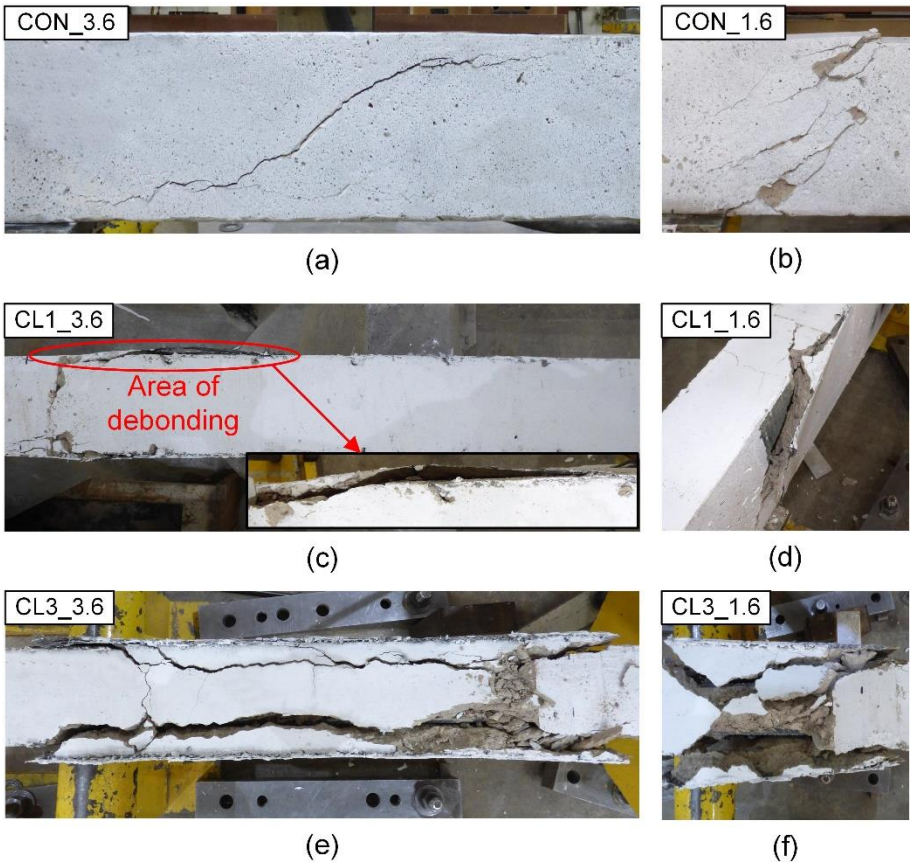


Figure 4.24. Failure modes of specimens of 1.6 and 3.6 shear span-to-depth ratios: (a) specimen CON_3.6 - dominant shear crack; (b) specimen CON_1.6 - multiple shear cracks; (c) specimen CL1_3.6 - debonding of the jacket at area below the shear crack: peeling off of the concrete cover; (d) specimen CL1_1.6 - debonding of the TRM jacket over the whole area of the shear span: peeling off of the concrete cover; (e)–(f) specimens CL3_3.6 and CL3_1.6 - debonding of the TRM jacket over the whole area of the shear span: peeling off of the concrete cover.

The control beams with *a/d*=1.6 and with *a/d*=3.6 failed in shear at an ultimate load of 88.4 and 62.2 kN, respectively. In specimen CON_3.6 a large shear crack was formed at the critical shear span (Fig. 4.24a) similar to the control specimen with *a/d*=2.6. On the contrary, in specimen CON_1.6 multiple shear cracks were developed within the critical shear span (Fig. 4.24b). Finally, specimens CL1_1.6, CL3_1.6, CL1_3.6 and CL3_3.6 reached an ultimate load of 123.7, 142.7, 133.8 and 158.7 kN, respectively, resulting in 39.9%, 61.5%, 115.3% and 155.3% shear capacity increase, respectively. These specimens failed in the same way with their counterpart specimens with *a/d*=2.6, namely debonding of the jacket from the concrete substrate including peeling off of the concrete cover. In specimen CL1_3.6, the debonding was initiated at the load application position and progressed towards the area below the shear crack (Fig. 4.24c), whereas in specimens CL1_1.6, CL3_3.6 and CL3_1.6, the TRM jackets debonded at the full-length of the shear span as shown in Fig. 4.24d-f, respectively.

4.2.3 Discussion

4.2.3.1 Effect of external reinforcement ratio

Figure 4.25a plots the experimentally obtained effective strains, ε_{eff}, against the ρ_f values for the beams retrofitted with carbon-fibre TRM jackets. Results from three FRP-retrofitted beams presented in Section 4.1 (having identical geometry with the beams tested here), are also included in the plot of Fig. 4.25a.

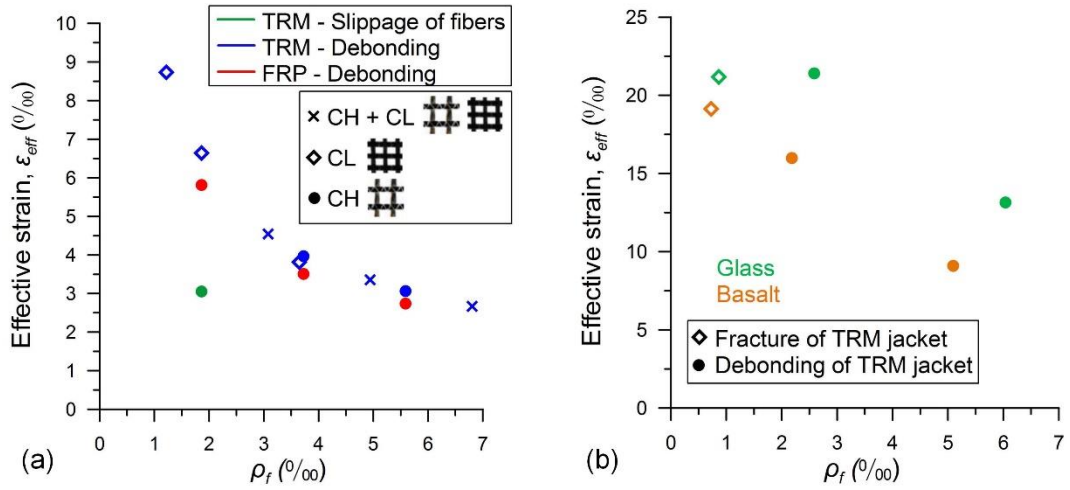


Figure 4.25. Experimentally obtained effective strains versus ρ_f values for specimens received: (a) carbon TRM and FRP U-jackets and (b) glass and basalt TRM U-jackets.

Table 4.7 includes all the important results of the three FRP-strengthened beams. From the comparison in Fig. 4.25a, it becomes evident that TRM is as effective as FRP jacketing in increasing the shear capacity of RC beams, when failure is associated to debonding of the jacket. In specific, for this type of failure the trend of the experimental ε_{eff} values for TRM jackets is descending for increasing ρ_f values, which is in agreement with the typical behaviour of FRP jackets. As also shown in Fwg. 4.25a, TRM consisting of heavy-carbon fibre textile is less effective than equivalent FRP system (in terms of ρ_f) or TRM consisting of light-carbon fiber textile, when premature failure due to slippage of fibres occurs.

Table 4.7. Summary of FRP-strengthened specimens results.

Specimen	ρ_f (‰)	E_f (GPa)	E_{f_FRP} (GPa)	Ultimate tensile strain, ε_{fu} (%)	Ultimate tensile strength, f_{fu} (MPa)	Peak Load (kN)	V_f (kN)	ε_{eff} (‰)
UW_R1	1.9	225	200.7	1.261	2788.4	113.4	35.3	5.81
UW_R2	3.7	225	200.7	1.261	2788.4	126.2	42.6	3.51
UW_R3	5.6	225	200.7	1.261	2788.4	139.0	49.9	2.74

Figure 4.25b plots the experimental effective strains versus, $\varepsilon_{eff,}$ against the ρ_f values for beams strengthened with glass and basalt TRM U-shaped jackets. In case of low ρ_f values (ρ_f <1‰), failure of specimens is associated with the rupture of the fibres (basalt or glass) in the TRM jackets, resulting in full exploitation of the tensile capacity of the textiles. Increasing the ρ_f values, damage is shifted to the concrete substrate (debonding of the jacket with peeling of the concrete cover). As in the case of carbon textiles, the trend of the experimental ε_{eff} values for glass and basalt TRM jackets is also descending for increasing ρ_f values, when failure is due to debonding of the jacket from the concrete substrate.

4.2.3.2 Effect of textile geometry

In this section the effect of the textile geometry on the failure mode and performance of TRM jackets is studied. The effect of the textile geometry on the behaviour of specimens that received equivalent (in terms of ρ_f) carbon TRM jackets is first discussed, whereas the effect on the failure mode of beams that received one TRM layer of different textile material (carbon, glass and basalt) follows next.

Specimens CL1_strips and CH1 had the same reinforcement ratio (equal to 1.9‰), comprising TRM jackets with carbon textiles of different geometry (see Fig.

3.1). Following the same concept, specimens CL3 and CH2 received correspondingly 3 and 2 layers of light and heavy carbon textile, having the same reinforcement ratio ($\rho_f \approx 3.6‰$). Fig. 4.26a and b depicts the mesh pattern of both heavy and light carbon fibre textiles. It can be observed that the combination of wider rovings (4 mm) with smaller mesh size (8 mm) in the light carbon textile (Fig. 4.26b), allows for a denser mesh-pattern when compared to the heavy carbon textile with 3 mm-wide rovings and 10 mm-mesh.

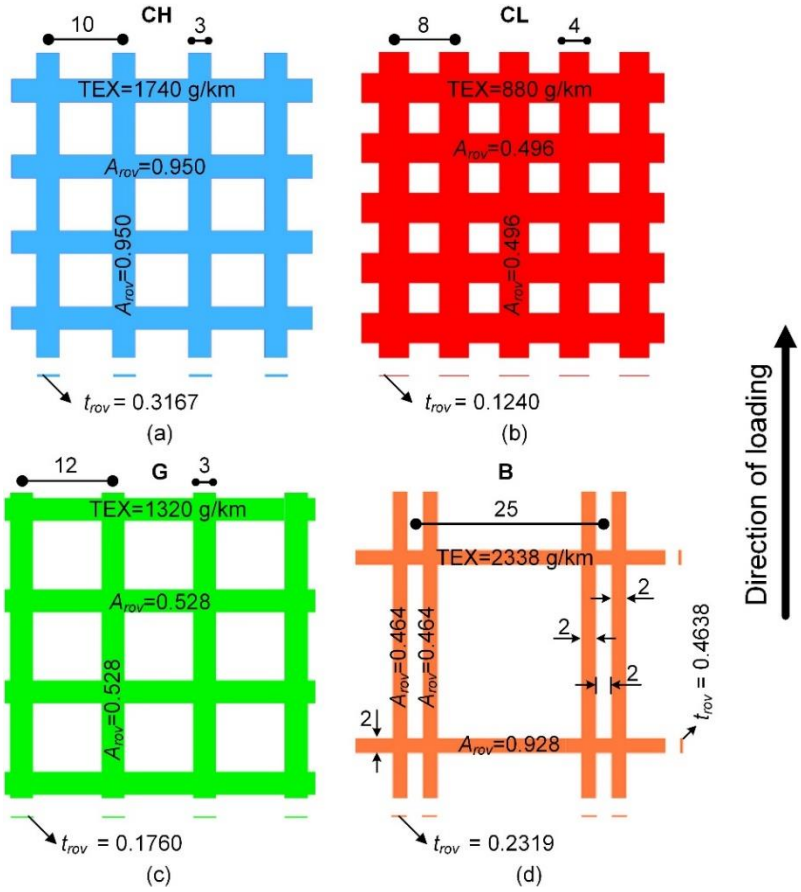


Figure 4.26. Textile properties and geometry of roving in: (a) heavy carbon textile (CH); (b) light carbon textile (CL); (c) glass textile (G) and (d) basalt textile (B).

A comparison of the results between specimens CH1 and CL1_strips, shows that the textile geometry has a strong effect on the failure mode and as a result on the shear capacity of beams in case of low external reinforcement ratio ($\rho_f \approx 1.9‰$). As mentioned before in Section 4.1, specimen CH1 failed due to local damage of the TRM jacket (slippage of fibres through the mortar and partial rupture of fibres crossing the shear crack) contrary to specimen CL1_strips that failed due to debonding of the TRM jacket from the concrete substrate. The shear capacity increase of specimens CH1 and

CL1_strips, was 50.8% and 113.5%, respectively, whereas the effective strains for specimens CH1 and CL1_strips were 3.06‰ and 6.64‰, respectively. Photos of the vertical deformations field of the TRM jackets, obtained through DIC system at the instant of peak load are shown in Fig. 4.27a-d. From Fig. 4.27a, it is evident that in specimen CH1, the TRM jacket deformed only along the main and secondary shear cracks, whereas the remaining part of the jacket was not activated. On the contrary, in specimen CL1_strips (Fig. 4.27b), the distribution of deformations was better, indicating that the jacket was activated over a broader area due to favourable redistribution of stresses. The superior performance of the light carbon textile is possibly associated with the better fibres distribution along the shear span (denser mesh-pattern of the textile), which in turn improves the mechanical interlock between the textile reinforcement and the matrix.

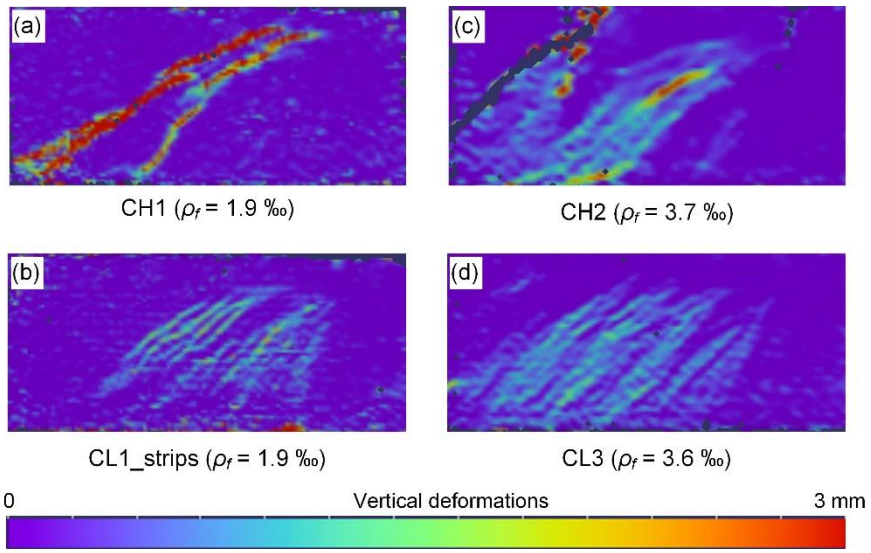


Figure 4.27. Field of vertical axis deformations in the critical shear span of TRM-retrofitted specimens: (a) CH1; (b) CL1_strips; (c) CH2; (d) CL3 at the instant of peak load.

Specimens CH2 and CL3 both failed due to debonding of the TRM jacket from the concrete substrate, with similar shear capacity increase (132% and 127.6%, respectively). As shown in Fig. 4.27c – d, in both specimens the vertical deformations were distributed over a broad region of the shear span. Thus, the increase of external reinforcement ratio, ρ_f (through the increase of the number of layers), eliminated the effect of the textile geometry.

A comparison of the results for specimens CL1, CH1, G1 and B1 shows that the performance of the heavy-carbon fibre textile was poor as its failure was associated

with local damage of the jacket (slippage of the fibers through the mortar) contrary to the remaining textiles (light-carbon, glass and basalt) in which slippage of the fibres through the mortar was not observed at the load level that CH1 specimen failed. This could be attributed to the characteristics of the roving in each textile. As shown in Fig. 4.26a-d, the area of one roving in the direction of loading of the light-carbon, glass and basalt textile is approximately 0.5 mm^2, whereas the roving area in the heavy-carbon textile is almost double (0.95 mm^2). As a result, in textiles with small roving area (A_{rov}), the degree of impregnation of fibres with cement paste is higher, resulting in improved bond characteristics. On the other hand, textiles with bigger roving size are more prone to slippage of the fibre rovings through the mortar, unless they are coated, as in the case of the basalt textile used in this study.

4.2.3.3 Effect of shear span-to-depth ratio

Figure 4.28 illustrates the effect of the shear span-to-depth ratio (*a/d*) on the shear resistance of the unretrofitted specimens, $V_{R,con}$. It is well-known that increasing the *a/d* ratio the shear resistance decreases; this is verified in this study, as shown in Fig. 4.28. This behaviour is explained through the different load-carrying mechanisms in each case. In specific, the arch action is the dominant mechanism of shear resistance in unretrofitted beams with low *a/d* ratio (i.e. *a/d*=1.6, deep beams), whereas beam action (truss analogy mechanism) is developed in beams of high shear span-to-depth ratios (*a/d*=2.6 and 3.6). A comparison between specimens CL1_1.6, CL3_1.6, CL1, CL3, CL1_3.6 and CL3_3.6 shows that the *a/d* ratio had no effect on the failure mode of specimens strengthened with the same TRM jackets. All specimens failed due to debonding of the TRM jacket with peeling off of the concrete cover. In specific, when 3 TRM layers were applied in specimens of any *a/d* ratio, the part of concrete that peeled off from the substrate was thicker with respect to the specimens received 1 TRM layer (Fig. 4.24c-f). Figure 4.29a-f presents images of the in-plane vertical deformations of the TRM jackets in beams of different shear spans, obtained using DIC measurements at the instant of maximum load. In general, vertical deformations of TRM jackets with both 1 and 3 light-carbon TRM layers were distributed over a broad region of the shear span for all beams of different shear span to-depth-ratios, *a/d* as a result of the good mechanical interlocking characteristics and the small roving size of the light carbon textile.

Figure 4.30a illustrates the effect of the *a/d* ratio on the contribution of the jacket to the total shear resistance, V_f, for two different external reinforcement ratios (ρ_f =1.2‰ and ρ_f =3.6‰). The *a/d* ratio has practically no effect on the V_f values for TRM jackets regardless the external reinforcement ratio. Figure 4.30b illustrates the effect of the *a/d* ratio on the shear capacity enhancement (V_f / $V_{R,con}$ x100%) for two different external reinforcement ratios (ρ_f =1.2‰ and ρ_f =3.6‰). The shear capacity enhancement considerably increases with *a/d*. This is attributed to the reduced shear resistance of the unretrofitted specimens when increasing the *a/d* ratio (Fig. 4.28).

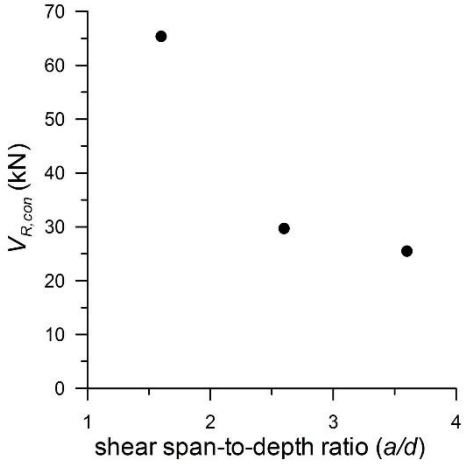


Figure 4.28. Effect of shear-span-to depth ratio, a/d on the shear resistance of the control specimen.

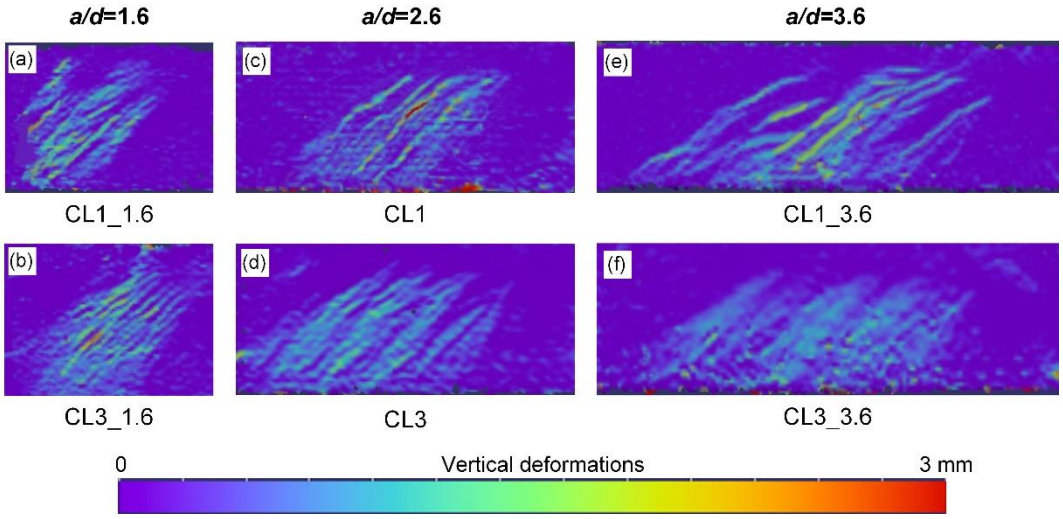


Figure 4.29. Field of vertical axis deformations in the critical shear span of TRM-retrofitted specimens: (a) CL1_1.6; (b) CL3_3.6; (c) CL1; (d) CL3; (e) CL1_1.6; (f) CL3_3.6 at the instant of peak load.

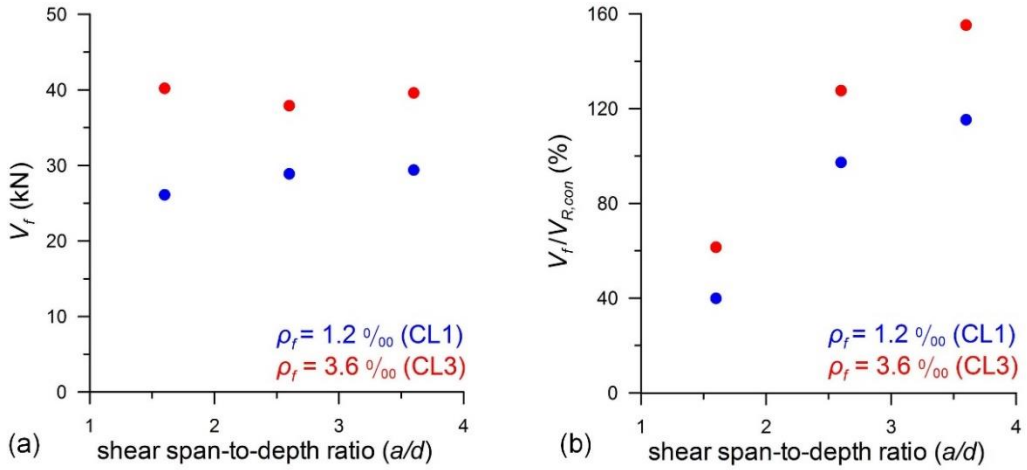


Figure 4.30. Effect of shear-span-to depth ratio on: (a) the contribution of the jacket to the total shear resistance, V_f and (b) the shear capacity enhancement, $V_f/V_{R,con}$ (%).

4.2.4 Summary

This Section presents an experimental investigation on the effectiveness of TRM jackets in shear strengthening of rectangular RC beams. Key parameters of this study were: the amount of external TRM reinforcement ratio (ρ_f) using three different textile materials (carbon, glass and basalt), the textile geometry and the shear span-to-depth ratio (a/d) in RC rectangular beams strengthened in shear with U-shaped TRM jackets. The main conclusions drawn are summarized as follows:

- Carbon TRM U-jackets are as effective as carbon FRP U-jackets in increasing the shear capacity of RC beams, when failure is due to debonding of the jacket from the concrete substrate including peeling off of the concrete cover.
- The trend of the experimental effective strain values, ε_{eff}, for carbon, glass or basalt TRM jackets is descending for increasing ρ_f values, when failure is associated with debonding of the jacket, which is in agreement with the typical behaviour of FRP jackets.
- In case of low external reinforcement ratio, different carbon fibre textile geometries with the same reinforcement ratio result in different load increase and failure mode. The effect of the different textile geometry is drastically mitigated by increasing the external reinforcement ratio.
- The textile roving geometry affects the performance of TRM jackets in case of low external reinforcement ratio. In particular, textiles with smaller roving area

arranged in a denser pattern result in better bond characteristics between the textile and the mortar, and hence improved efficiency.

- The shear span-to-depth ratio has no effect on both the failure mode and the contribution of the jacket to the total shear resistance of the beams.

4.3 Effect of textile mesh material characteristics (mesh size, amount and material of fibres in the horizontal direction)

4.3.1 Experimental Programme

The main objective of this section was to investigate the effect of textile geometry on the performance of U-shaped TRM jackets on shear strengthening of RC rectangular beams. For this scope, eleven (three out of eleven specimens have been already presented in Section 4.1) half-scale RC beams were constructed and tested. The design, geometry and set-up of these beams is identical to the beams presented already in Section 4.1 (see Fig. 4.1 and 4.2). The key investigated parameters comprise: (a) the textile geometry, namely the fibre roving size in the vertical direction and the material and spacing of fibre rovings in the horizontal direction and (b) the number of layers. The four FORMAX textile mesh materials (F10x20, F10x40, F20x20 and F20x40, Fig. 3.2) and the heavy-weight carbon textile (Fig. 3.1b, CH) were used as external reinforcement. Figure 4.31 illustrates all the strengthening configurations adopted, whereas Table 4.8 presents the details of all specimens. The notation of retrofitted specimens is X_N, where X denotes the type of the textile (F10x20, F10x40, F20x20, F20x40 and CH) and N denotes the number of layers (1 and 3). It should be mentioned that the control specimen as well as CH_1 and CH_3 specimens have been already presented in Section 4.1 with names CON, UW_M1 and UW_M3, respectively but they are also presented in this section for an easy comparison among the results.

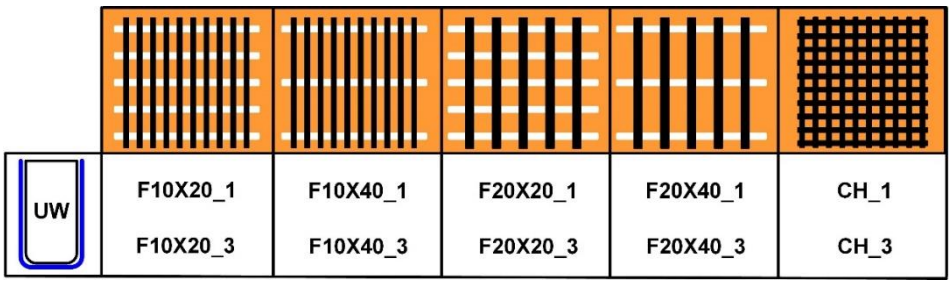


Figure 4.31. Schematic representation of different strengthening configurations.

The specimens were cast in groups of four using the same concrete mix design. The compressive strength and the tensile splitting strength of the concrete were experimentally obtained on the day of testing by conducting standard tests on cylinders of 150 mm-diameter and of 300 mm - height. The results are summarized in Table 4.8 (average values of 3 specimens). The properties of steel bars used as flexural and shear reinforcement were presented in section 4.1. The mortar described in Section 3.1 was used as binding material. The strength properties of the mortar (average values of 3 specimens) obtained experimentally on the day of testing are summarised in Table 4.8.

Table 4.8. Strengthening configuration and material properties of all specimens.

Specimen	ρ_f (‰)	E_{f_TRM} (GPa)	Concrete Strength (MPa)		Mortar Strength (MPa)		
			Compressive strength	Tensile splitting strength	Compressive strength	Flexural strength	Tensile splitting strength
CON	-	-	21.6	2.36	-	-	-
CH_1	1.9	168.7	23.8	2.73	31.1	10.3	3.40
CH_3	5.6	168.7	22.6	2.81	26.9	8.64	3.40
F10x20_1	1.9	161.6	21.4	2.35	46.6	9.46	3.40
F10x20_3	5.6	161.6	21.4	2.35	46.6	9.46	3.40
F10x40_1	1.9	175.7	21.4	2.35	46.6	9.46	3.40
F10x40_3	5.6	175.7	21.4	2.35	46.6	9.46	3.40
F20x20_1	1.9	165.9	20.1	2.28	32.8	7.80	3.40
F20x20_3	5.6	165.9	20.1	2.28	32.8	7.80	3.40
F20x40_1	1.9	159.0	20.1	2.28	32.8	7.80	3.40
F20x40_3	5.6	159.0	20.1	2.28	32.8	7.80	3.40



Figure 4.32. (a) Prepared concrete surface before strengthening; (b) impregnation of the textile fibres with mortar; (c) final layer of mortar on the top of the final textile layer.

The procedure of strengthening of the beams with TRM was already described in details in Section 4.1.1.2. It includes the following steps: (a) surface preparation (Fig. 4.32a); (b) applying of a first layer of mortar at the dampened concrete surface; (c) impregnation of the textile fibres with mortar (Fig. 4.32b) and (d) application of a final layer of mortar on the top of the final textile layer (Fig. 4.32c).

The beams were subjected to monotonic loading using a stiff steel reaction frame and a three-point bending set-up configuration as shown in Fig. 4.1 and 4.19. As

illustrated in Fig. 4.5 the vertical displacement was measured at the position of load application using external Linear Variable Differential Transducer (LVDT); the displacement measured from this sensor was used to plot the load-displacement curve for each specimen.

4.3.2 Experimental results

The response of all specimens is given in Fig. 4.33, whereas key results are also presented in Table 4.9.

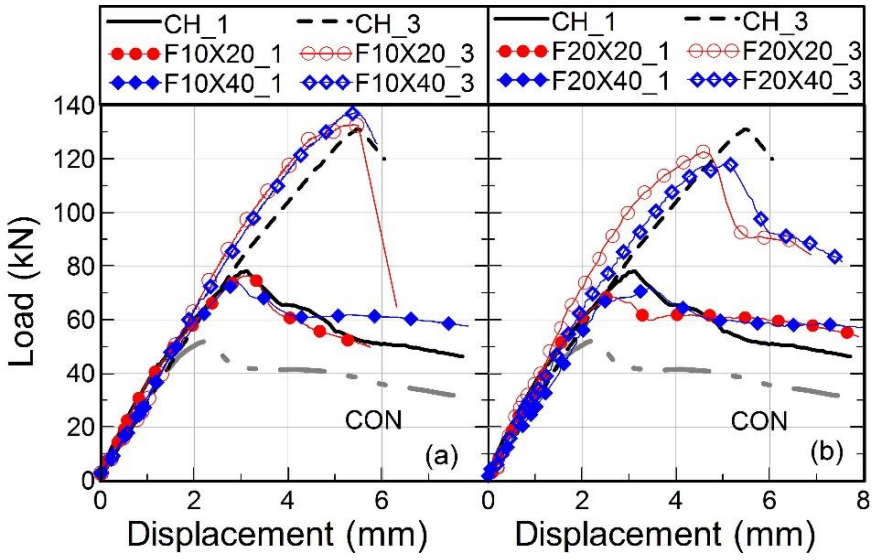


Figure 4.33. Load versus vertical displacement curves for (a) F10x20 and F10x40 textile materials; (b) F20x20 and F20x40 textile materials.

Table 4.9. Summary of tests results.

Specimen	(1) Peak Load (kN)	(2) Failure mode	(3) V_R (kN)	(4) V_f (kN)	(5) Shear capacity increase $V_f/V_{R,con}$ (%)	(6) ε_{eff} (‰)
CON	51.8	shear [a]	29.7	-	-	-
CH_1	78.2	shear [b]	44.8	15.1	50.8	3.06
CH_3	131.1	shear [b]	75.1	45.4	152.9	3.06
F10x20_1	76.4	shear [b]	43.8	14.1	47.5	2.88
F10x20_3	132.9	shear [c]	76.1	46.4	156.2	3.16
F10x40_1	74.1	shear [b]	42.5	12.8	43.1	2.41
F10x40_3	137.4	shear [c]	78.7	49	165.0	3.07
F20x20_1	69.1	shear [b]	39.6	9.9	33.3	1.97
F20x20_3	123.1	shear [b, c]	70.5	40.8	137.4	2.71
F20x40_1	72.0	shear [b]	41.2	11.5	38.7	2.39
F20x40_3	118.4	shear [b, c]	67.8	38.1	128.3	2.64

[a] Tensile diagonal cracking, [b] Slippage of the vertical fibre rovings through the mortar and partial fibres rupture, [c] Debonding of the jacket.

As also mentioned in 4.1, the control beam failed in shear at an ultimate load of 51.8 kN, after the formation of a large shear crack in the critical shear span.

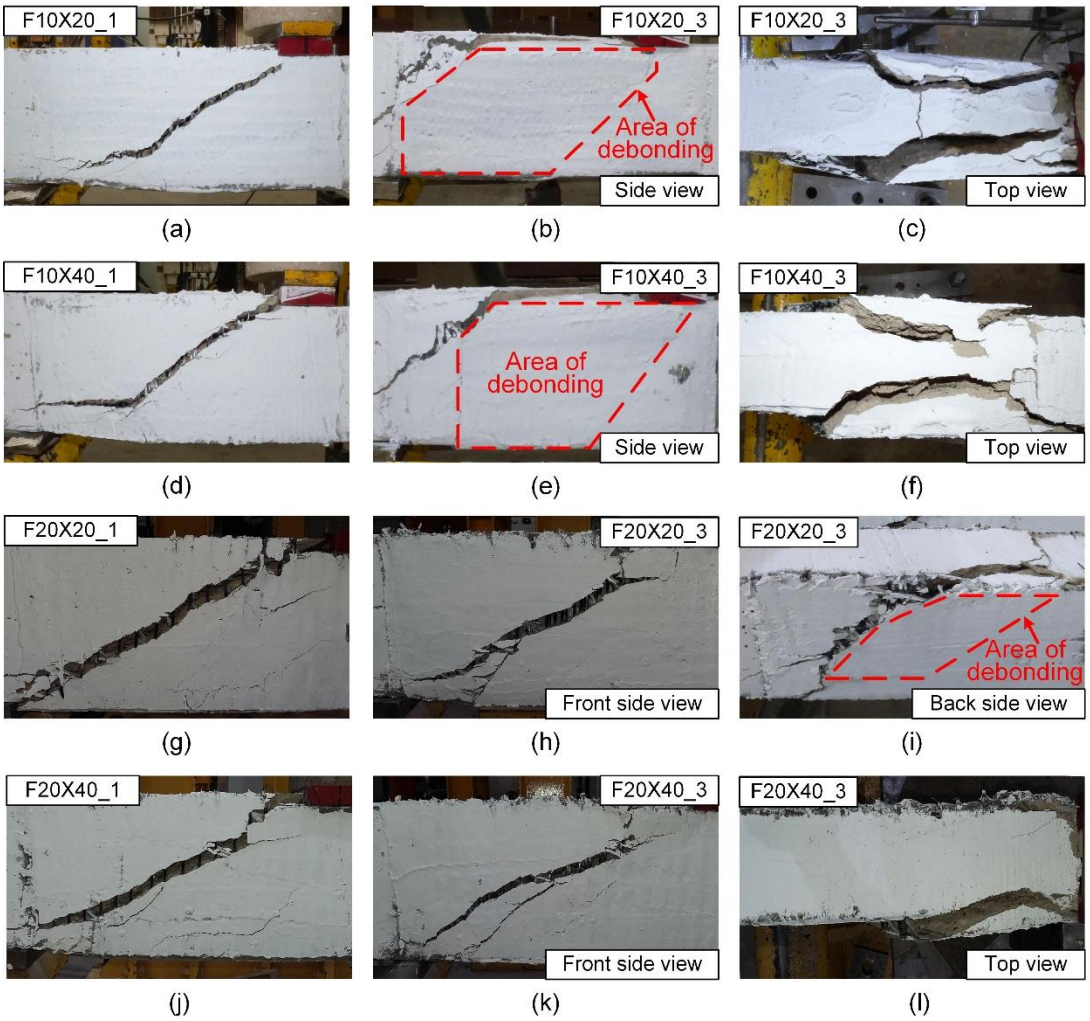


Figure 4.34. (a) Failure modes of specimens received FORMAX textile materials: (a) specimen F10x20_1 – local damage of the jacket; (b),(c) specimen F10x20_3 – debonding of the jacket over a large area of the shear span: peeling off of the concrete cover; (d) specimen F10x40_1 – local damage of the jacket; (e),(f) specimen F10x40_3 – debonding of the jacket over a large area of the shear span: peeling off of the concrete cover; (g) specimen F20x20_1 – local damage of the jacket; (h) specimen F20x20_3 – local damage of the jacket in one side of the beam; (i) specimen F20x20_3 – debonding of the jacket over an area of the shear span; (j) specimen F20x40_1 – local damage of the jacket; (k) specimen F20x40_3 – local damage of the jacket in one side of the beam; (l) specimen F20x40_3 – debonding of the jacket over an area of the shear span.

Specimens CH_1 (UW_M1 in 4.1 and CH1 in 4.2) and CH_3 (UW_M3 in 4.1 and CH3 in 4.2) reached an ultimate load 78.2 and 131.1 kN, respectively, resulting in 50.8% and 152.8% increase of the shear capacity (more details can be found in 4.1.2),

whereas specimens F10x20_1, F10x20_3, F10x40_1 and F10x40_3 reached an ultimate load 76.4, 132.9, 74.1 and 137.4 kN, respectively, resulting in 47.5%, 156.2%, 43.1% and 165% increase of the shear capacity. The failure of specimens CH_1 (specimen UW_M1 in 4.1), F10x20_1 (Fig. 4.34 a) and F10x40_1 (Fig. 4.34 d) was associated with damage of the TRM jackets including (a) slippage of the vertical fibre rovings through the mortar and (b) partial rupture of the fibres crossing the shear crack. The failure of F10x20_3 and F10x40_3 specimens was due to debonding of the TRM jacket at a large part of the shear span which was accompanied by peeling off of a thick part of the concrete cover (Fig. 4.34 b-c and e-f) similar to the failure of CH_3 specimen that was due to debonding of the TRM jacket at the full length of the shear span.

Finally, specimens F20x20_1, F20x20_3, F20x40_1 and F20x40_3 failed in shear at a load of 69.1, 123.1, 72 and 118.4 kN, respectively. Compared to the control specimen the increase in the shear resistance was equal to 33.3%, 137.4%, 38.7% and 128.3%, respectively. The failure of specimens F20x20_1 and F20x40_1 was associated with damage of the jacket (slippage of the vertical fibre rovings through the mortar and partial rupture of the fibres) identical to specimens CH_1, F10x20_1 and F10x40_1. In both specimens F20x20_3 and F20x40_3, TRM jacket was debonded at a part of the shear span (approximately 1/3) in one side of the beam (Fig. 4.34 i and l), whereas damage of the jacket (slippage of the vertical fibre rovings through the mortar and partial rupture of the fibres) was observed at the other side of the beam (Fig. 4.34 h and k).

4.3.3 Discussion

All specimens responded as designed and failed in shear. This response allowed for the evaluation of the capacity of all strengthening systems in increasing the shear resistance of the beams. An examination of the results in terms of shear capacity increase and failure modes, revealed the following information.

4.3.3.1 Effect of fibre rovings characteristics (material and spacing) in the horizontal (non-loading) direction of the textile material

In this section, specimens strengthened with textiles of the same amount of carbon fibres and same geometry of fibre rovings in the pricinpal (loading, vertical) direction

but different material or spacing of fibre rovings in the horizontal direction are compared. In particular, heavy-weight carbon textile (CH) has the same amount of carbon fibres, fibre roving area (A_{rov}=0.95 mm^2) and mesh size (10 mm) with F10x20 and F10x40 (FORMAX) textiles in vertical direction, whereas the amount and material of fibres in the horizontal direction significantly vary (CH: carbon fibres of 10 mm spacing in the horizontal direction, F10x20: glass fibres of 20 mm spacing in the horizontal direction and F10x40: glass fibres of 40 mm spacing in the horizontal direction). Similarly, F20x20 and F20x40 textiles have the same amount of fibres, fibre roving area (A_{rov}=1.90 mm^2) and mesh size (20 mm) in the vertical direction whereas they have glass fibres of different spacing in the horizontal direction (F20x20: glass fibres of 20 mm spacing in the horizontal direction and F20x40: glass fibres of 40 mm spacing in the horizontal direction).

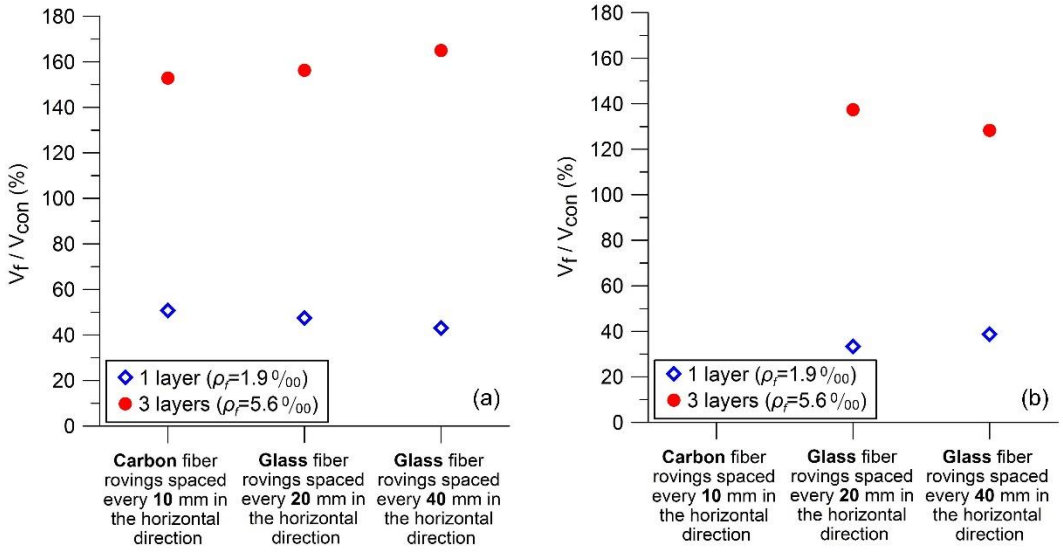


Figure 4.35. Effect of the fibre rovings characteristics (material and spacing) in the horizontal direction of the textile on the shear capacity enhancement for specimens strengthened with textile materials with carbon fibre rovings of (a) A_{rov}=0.95 mm^2 and (b) A_{rov}=1.90 mm^2 in the vertical direction.

The effect of the material and spacing of fibre rovings in the horizontal direction of the textile on the shear capacity enhancement is illustrated in Fig. 4.35. A comparison of the results for specimens received one or three carbon fibre textile layers of 0.95 mm^2 roving area at the longitudinal direction (Fig. 4.35a) shows that the material (carbon or glass) or spacing (10, 20 or 40 mm) of fibre rovings in the horizontal direction of the textile has practically no effect on the performance nor the failure mode of specimens and just the fibres in the vertical direction contribute to

carrying forces. The same conclusion is also drawn by comparing specimens strengthened with one or three carbon fibre textile layers of 1.90 mm^2 roving area at the longitudinal direction (Fig. 4.35b). This can lead to significant cost benefits in real applications due to the considerable material savings in the horizontal direction of the textile.

4.3.3.1 Effect of textile geometry

In this paragraph, the effect of textile geometry is studied. Figure 4.36 depicts the mesh pattern and textile geometry of all four FORMAX textile materials, whereas the mesh pattern of heavy-weight carbon textile material is depicted in Fig. 4.26.

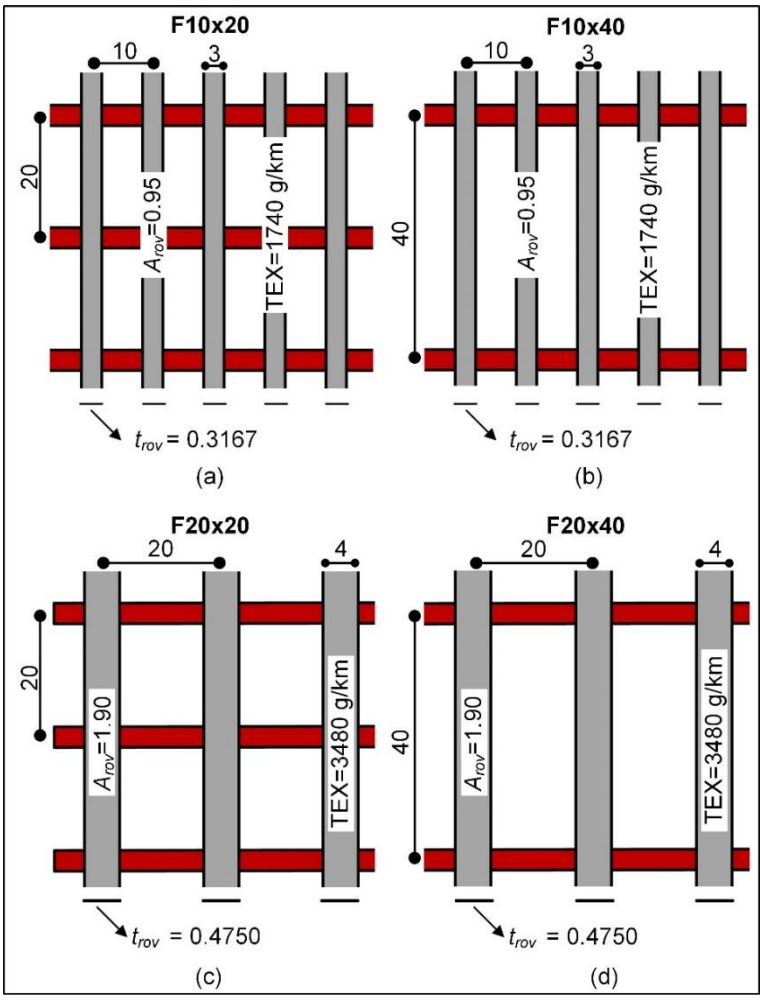


Figure 4.36. Textile properties and geometry of roving in FORMAX textiles: (a) F10x20; (b) F10x40; (c) F20x20; (d) F20x40.

As shown in Fig. 4.36 the roving area in F20x20 and F20x40 textile materials are double than that of F10x20 and F10x40 textile materials but they have equal

amount of reinforcement in the direction of loading. Figure 4.37a illustrates the effect of the roving area, A_{rov} on the shear capacity enhancement (V_f / V_{con} x100%). As shown in Fig. 4.37a, doubling the area of roving, resulted in decrease of the TRM jacket effectiveness for low (1 TRM layer or ρ_f=1.9‰) and mainly for high external reinforcement ratio (3 TRM layers or ρ_f=5.6‰).

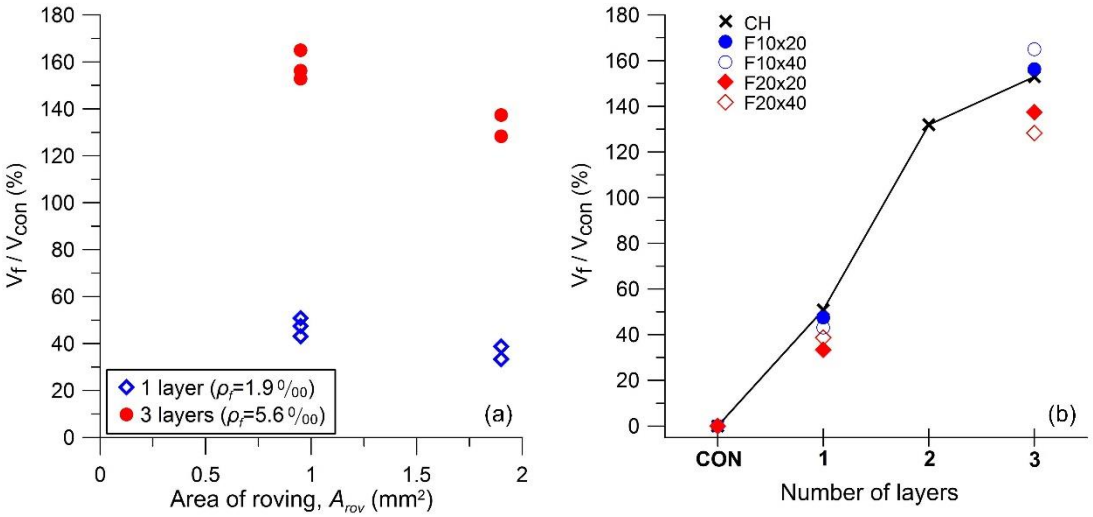


Figure 4.37. (a) Effect of area of roving, A_{rov} on the shear capacity enhancement; (b) effect of number of layers on the shear capacity enhancement.

The textile geometry has no effect on the failure mode of specimens that received one TRM layer; the failure of these specimens was associated with local damage of the jacket (slippage of fibres through the mortar and partial rupture of fibres crossing the shear crack). On the other hand, the increase in the area of roving adversely affected the failure mode of specimens that received three TRM layers. In specific, F10x20_3 and F10x40_3 specimens (A_{rov}=0.95 mm^2) failed due to debonding of the TRM jacket at a large part of the shear span (approximately 2/3), whereas in specimens F20x20_3 and F20x40_3 (A_{rov}=1.90 mm^2), local damage of the jacket (slippage of fibres through the mortar and partial rupture of fibres crossing the shear crack) was observed in one side of the beam apart from debonding of the jacket (at a part of the shear span) which was developed in the other side of the beam. Thus, it seems that in textiles with small roving area (A_{rov}), the degree of impregnation of fibres with mortar is higher, resulting in improved bond characteristics and mechanical interlock and therefore improved composite action. This conclusion is in very good agreement with the results presented in 4.2.

4.3.3.1 Effect of number of layers

The effect of the number of layers on the shear capacity enhancement for specimens strengthened with textile materials of different textile geometry is illustrated in Fig. 4.37b. Tripling the amount of reinforcement (three layers instead of one) resulted in dramatic increase of the TRM jackets effectiveness. The increase in the number of layers can totally (CH_1 - CH_3, F10x20_1 - F10x20_3, F10x40_1 - F10x40_3) or partially (F20x20_1 - F20x20_3, F20x40_1 vs F20x40_3) prevent the local damage of the TRM jacket, shifting the damage to the concrete substrate. As also described in section 4.1.3.1, this is possibly attributed to better mechanical interlock conditions created by the overlapping of multiple textile layers.

4.3.4 Summary

This section studies the geometry of textile materials used in TRM jackets for shear strengthening of RC beams. Key parameters are: the effect of fibres in the transverse direction, the textile geometry and the number of TRM layers. For this purpose, eleven shear-deficient beams were tested under monotonic load. Five different textile materials were used and compared, namely the heavy-weight carbon textile and all four FORMAX textile materials. The main conclusions drawn in this section are summarized as follows:

- Shear capacity increase and failure mode of U-wrapped TRM jackets having the same amount of carbon fibres and roving geometry in the vertical direction (direction of loading) are not affected by the material or spacing (amount) of fibre rovings in the horizontal direction.
- The effectiveness of the TRM jacket is improved as the fibre roving area of the textile in the vertical direction (loading direction) decreases (for both low and high external reinforcement ratios).
- The number of layers affects the failure mode of TRM U-wrapped jackets. When number of layers increases, local damage of the TRM jacket is limited (in case of large roving area) or totally prevented (in case of small roving area).

Taking into account the aforementioned conclusions, textile mesh materials having the following characteristics can be both performance and cost effective when used for shear strengthening of RC members: (a) distribution of fibres mainly in the vertical direction (principal direction of loading) and not in the horizontal direction of

textile material and (b) as much as possible small area of rovings in the vertical direction resulted in a dense-mesh pattern of fibres provided that the perforations between the fibre rovings enable the impregnation of fibres with mortar (this is also proved by the performance of light versus heavy carbon fibre textile presented in 4.2).

Chapter 5

SHEAR STRENGTHENING OF FULL-SCALE RC T-BEAMS USING TEXTILE-REINFORCED MORTAR AND TEXTILE-BASED-ANCHORS

Abstract

This chapter presents a study on the effectiveness of TRM jacketing in shear strengthening of full-scale reinforced concrete (RC) T-beams focusing on the behaviour of a novel end-anchorage system comprising textile-based anchors. The parameters examined in this study include: (a) the use of textile–based anchors as end-anchorage system of TRM U-jackets; (b) the number of TRM layers; (c) the textile properties (material, geometry); and (d) the strengthening system, namely textile-reinforced mortar (TRM) jacketing and fibre-reinforced polymer (FRP) jacketing for the case without anchors. In total, 11 full-scale RC T-beam ends were tested as simply supported in three-point bending. The results showed that: (a) The use of textile–based anchors increases dramatically the effectiveness of TRM U-jackets; (b) increasing the number of layers in non-anchored jackets results in an almost proportional increase of the shear capacity, whereas the failure mode is altered; (c) the use of different textile geometries with the same reinforcement ratio in non-anchored jackets result in practically equal capacity increase; (d) TRM jackets can be as effective as FRP jackets in increasing the shear capacity of full-scale RC T-beams. Finally, a simple design model is proposed to calculate the contribution of anchored TRM jackets to the shear capacity of RC T-beams.

5.1 Experimental Programme

5.1.1 Test specimens and investigated parameters

The experimental programme included 11 tests performed on full-scale T-beams, simply-supported in asymmetric three-point bending. The total length of the T-beams was equal to 6000 mm, whereas the effective flexural span was equal to 3700 mm (Fig. 5.1a), providing adequate anchorage length to the longitudinal reinforcement. To emulate old detailing practices, the beams were designed to be deficient in shear in one of the two shear spans. To achieve this, the critical shorter shear span of 880 mm length did not include any transverse reinforcement, whereas the larger shear span was over-reinforced including 10-mm diameter stirrups at a spacing of 100 mm.

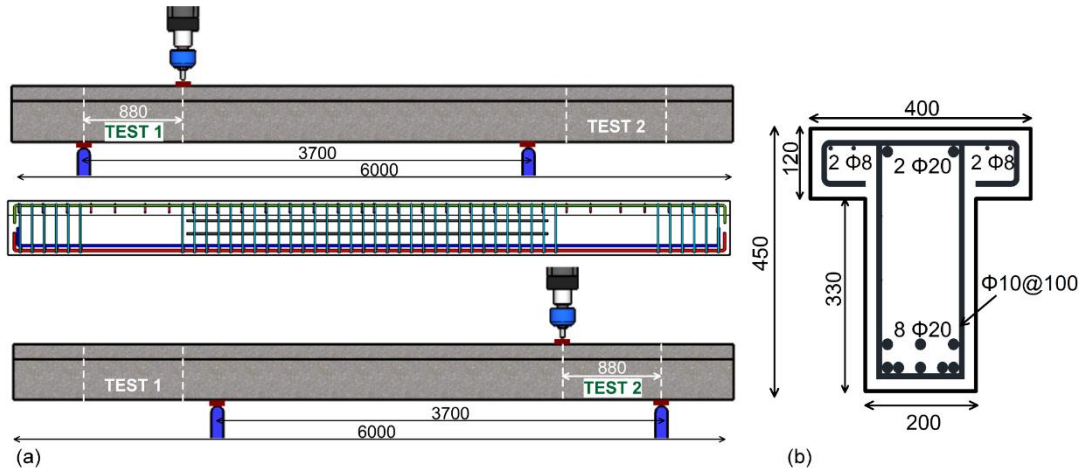


Figure 5.1. (a) Schematic test set-up; (b) cross-section (dimensions in mm).

Strengthening was applied only at the critical shear span aiming to increase its shear resistance. By design, the shear force demand in order to develop the full flexural capacity of the (unretrofitted) beams was targeted to be 3.5 times their shear capacity. To achieve that eight 20 mm-diameter and two 20 mm-diameter deformed bars were placed at the tension and compression zone of the T-beams web, respectively (Fig. 5.1b). Four 8 mm-diameter deformed bars were additionally placed at the T-beam flanges. The geometrical ratio of tensile steel reinforcement was 3.2%, whereas the effective depth was 385 mm.

The key investigated parameters of this study comprised: (a) the use of textile–based anchors as end-anchorage system of the U-jacket, (b) the number of TRM layers,

(c) the textile geometry, (d) the textile material and (e) the comparison between equivalent TRM and FRP jackets. One beam-end was tested as-built and served as the control specimen (CON), whereas the remaining ten beams received strengthening. Three different textile meshes were used, namely two carbon textiles (the light-weight, CL and the heavy-weight carbon textile, CH) and the glass textile (G).

Table 5.1 presents the details of all tested specimens whereas Fig. 5.2 illustrates all the strengthening configurations adopted.

Table 5.1. Strengthening configuration and material properties of all specimens.

Specimen	**Textile used**	**t_f* (mm)**	**No. of layers**	**ρ_f (‰)**	**Anchorage percentage (%)**
CON	-	-	-	-	-
CH2	CH	0.095	2	1.9	-
CL3	CL	0.062	3	1.9	-
CH4	CH	0.095	4	3.8	-
G7	G	0.044	7	3.1	-
CH2_A100	CH	0.095	2	1.9	100
CL3_A100	CL	0.062	3	1.9	100
CH4_A50	CH	0.095	4	3.8	50
CH4_A100	CH	0.095	4	3.8	100
G7_A100	G	0.044	7	3.1	100
CH4_R	CH	0.095	4	3.8	-

* Nominal thickness of textile in one direction based on the equivalent smeared distribution of fibres

The notation of retrofitted specimens is XN_AP, where X denotes the type of the textile (CL for light carbon, CH for heavy carbon and G for glass) and N denotes the number of layers (2, 3, 4 or 7). AP refers to specimens with anchors with A indicating anchors and P denoting the anchorage percentage of the TRM jackets (50% or 100%). Finally, the suffix R was only used for one specimen that received FRP jacketing. The description of the strengthened specimens follows:

- CH2 and CH4: strengthened with 2 and 4 heavy carbon TRM layers, respectively.
- CL3: strengthened with 3 light carbon TRM layers.
- G7: strengthened with 7 glass TRM layers.
- CH2_A100: Strengthened with 2 heavy carbon TRM layers anchored by 100% (with seven textile-based anchors on each side of the beam's web).
- CL3_A100: Strengthened with 3 light carbon TRM layers anchored by 100% (with seven textile-based anchors per side)

- CH4_A50 and CH4_A100: strengthened with 4 heavy carbon TRM layers anchored by 50% and 100%, respectively (with seven and fifteen anchors per side, respectively).
- G7_A100: strengthened with 7 glass TRM layers anchored by 100% (with four textile-based anchors per side)
- CH4_R: strengthened with 4 carbon FRP layers equivalent to 4 carbon TRM layers

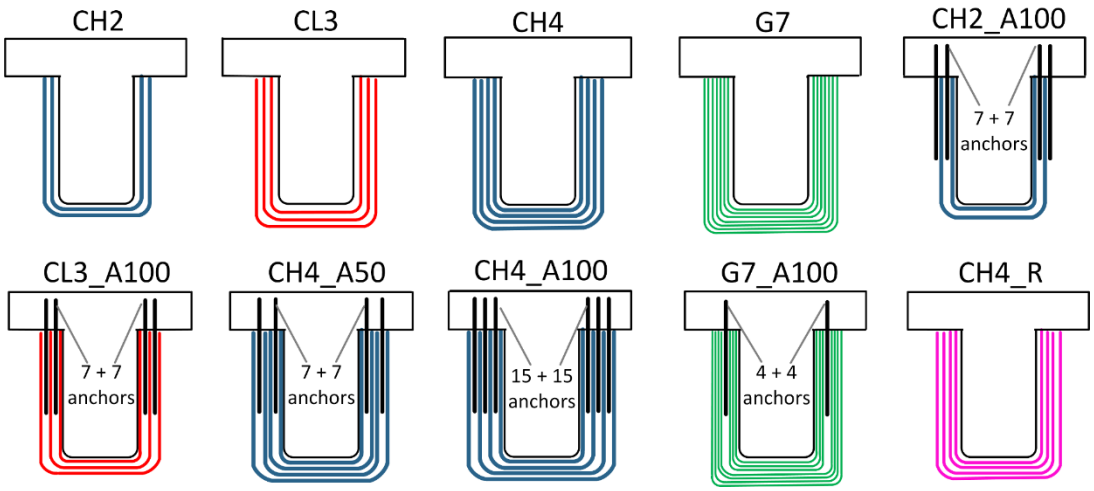


Figure 5.2. Schematic representation of different strengthening configurations.

5.1.2 Material properties

Table 5.2. Concrete and mortar strength on the day of testing.

Concrete Strength (MPa)		Mortar Strength (MPa)		
Compressive strength	**Tensile splitting strength**	**Compressive strength**	**Flexural strength**	**Tensile splitting strength**
14.0	1.39	-	-	-
15.2	1.67	37.4	8.79	3.40
13.8	1.37	35.8	8.05	3.40
14.0	1.39	36.1	8.12	3.40
13.8	1.37	33.7	8.25	3.40
15.2	1.67	34.5	8.11	3.40
14.9	1.60	37.9	8.74	3.40
14.9	1.60	36.6	8.75	3.40
14.5	1.44	33.4	8.41	3.40
14.5	1.44	37.4	8.67	3.40
14.7	1.48	-	-	-

The specimens were cast in two batches of ready-mix concrete. The compressive and the tensile splitting strength of concrete were obtained experimentally on the day of

testing by conducting standard tests on cylinders of 150 mm-diameters and of 300 mm-height. The results are summarized in Table 5.2 (average values of 3 cylinders) for each specimen. The 20 mm-diameter longitudinal bars used as steel reinforcement had a yield stress, ultimate strength and rupture strain of 571 MPa, 628 MPa and 12%, respectively (experimentally obtained average values from 3 specimens). The 8 mm-diameter longitudinal bar had a yield stress, ultimate strength and rupture strain equal to 568 MPa, 630 MPa and 7.9%, respectively. The corresponding value for the 10 mm-diameter bars used for stirrups were 552 MPa, 593 MPa and 8.4%.

Seven layers of glass fibre textile are equivalent to one layer of carbon fibre textile in terms of axial stiffness, which is expressed by the product $n_\ell \ t_f \ E_f$ [(7*0.044*74)/(1*0.095*225)=1.07], where n_ℓ is the number of TRM layers, t_f is the nominal thickness of the textile and E_f is the elastic modulus of the fibres (according to manufacture datasheets, see 3.3). In accordance, two heavy-weight carbon layers are equivalent to three light-weight carbon layers [(2*0.095*225) / (3*0.062*225) = 1.02].

For the nine specimens retrofitted with TRM jackets, the binding material used for strengthening was the inorganic dry binder described in section 3.1. Table 5.2 summarizes the strength properties of the mortar (average values of 3 specimens) which were obtained experimentally on the day of testing. For the FRP retrofitted specimen, the binding material was the commercial epoxy adhesive described in section 3.2.

5.1.3 Design and fabrication procedure of textile-based anchors

Unlike metallic anchors, textile-based anchors are versatile, non-corrosive, lightweight and compatible with the materials used for TRM jackets. These are the main advantages of the anchorage system proposed in this study, over systems using metallic components. The concept of the textile-based anchors, which were developed and used in Koutas et al. (2014) and Koutas et al. (2015) for strengthening masonry-infilled RC frames, is the same with that of the spike anchors which are combined with FRP strengthening systems (Koutas et al. 2013, Bournas et al 2015 and Ozbakkaloglu et al. 2009). The fan-shaped part of the anchors (see Fig. 5.3a) serves for the distribution of stresses between the textile reinforcement to be anchored and the anchor itself. The dowel part of the anchor (see Fig. 5.3a) serves for its installation

into holes and anchorage into the concrete mass. All anchors used in this study were identical, and their geometry was based on the following:

1. The length of the anchor's dowel part was selected to be 80 mm (see Fig. 5.3b). This was the maximum value based on the restrictions imposed by the flange thickness and the position of the compressive steel reinforcement.

2. The length of the anchor's fan was selected to be equal to 200 mm (see Fig. 5.3b).

3. The fan angle was selected to be 45° (see Fig. 5.3b) as in the study of Koutas et al. (2014). Given the fan angle and length, the resulted fan width was 155 mm.

4. Once the fan geometry had been finalized, the amount of anchor fibres in the direction of loading was calculated based on: (a) the maximum number of anchors that could be installed per beam's side, and (b) the maximum area of fibres to be anchored in a U-jacket comprising 4 heavy-carbon TRM layers (nearly 300 mm^2). By considering that anchors would be installed in 3 sets of 5 in-between the 1^{st} - 2^{nd}, the 2^{nd} - 3^{rd}, and the 3^{rd} – 4^{th} (see 5.1.5) layers, the total amount of anchors is equal to 15, which means that the fibres area for each anchor should be 20 mm^2 (300 mm^2 /15).

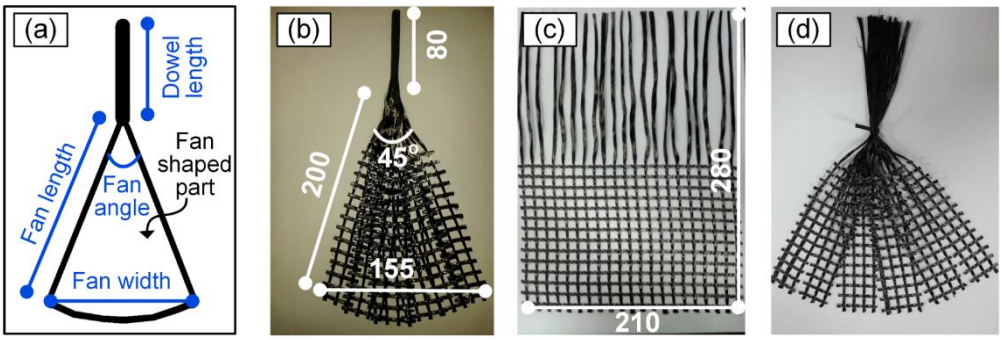


Figure 5.3. (a) Sketch of textile-based anchor; (b) geometry of the textile-based anchor; (c) partial removal of transverse rovings; (d) separate grid parts of the fanned part of an anchor.

The last row of Table 5.3 presents the exact percentage of anchorage of the TRM jackets in all specimens with anchors. This is calculated as the ratio of the jacket's axial stiffness (based on the fibres properties) to the axial stiffness of all the anchors in one beam's side (based on the volume of fibres in the dowel part of the anchors).

The procedure followed to form the anchors follows: Initially, a piece of textile was cut in the desired dimensions. The length of the textile was equal to 280 mm while the width was equal to 210 mm (which gives a total fibres area of 20 mm^2 in the

loading direction). A tow of fibers at one end of the anchor was formed, by removing half of fibre rovings in the direction parallel to the width of the textile (Fig. 5.3c). For the fanned part of the anchor it was important to be easily applied over a TRM layer and have good bonding conditions. It was therefore necessary to retain the grid of the textile at the fan shaped part and ensure the alignment of the fibre rovings that would be activated in tension. A way to achieve that was by cutting the fibre rovings in the direction parallel to the width of the textile at certain distances (every two or three vertical rovings), thus creating separate grid parts (Fig. 5.3d).

Table 5.3. Details of specimens with anchored TRM jackets.

	CH2_A100	**CL3_A100**	**CH4_A50**	**CH4_A100**	**G7_A100**
Area of anchor fibres, A_a (mm^2)	20	20	20	20	20
Number of anchors, n_a	7	7	7	15	4
Modulus of elasticity of anchor fibres, E_a (GPa)	225	225	225	225	225
Area of one TRM layer, A_ℓ (mm^2)	74.1	48.4	74.1	74.1	34.3
Number of TRM layers, n_ℓ	2	3	4	4	7
Modulus of elasticity of TRM layer, E_f (GPa)	225	225	225	225	74
Anchorage Percentage (%) [($E_a n_a A_a$ / $E_f n_\ell A_\ell$) x 100]	94.5	96.4	47.2	101.2	101.3

Finally, both the fibres of the fanned part and the tow were impregnated with epoxy resin followed by a period of 2 days for curing. Impregnation of the fanned part of anchors provides a stable and easy-to-apply material, creating in addition better mechanical interlock conditions between the textile and the mortar. Impregnation of the tow fibres facilitates the insertion of that part of the anchor into the predrilled hole into the slab. A commercial, low viscosity, two-part epoxy resin with tensile strength, modulus of elasticity and T_g equal to 72.4 MPa, 3.2 GPa and 82 ^{o}C was used to impregnate the fibres of the anchors (the same was used to fill the holes in which the anchors were installed). In order to allow for some flexibility of the anchor during the application process, a small area at the central part was left with dry fibres; these were

impregnated locally with epoxy resin during the strengthening application (see Section 5.1.5).

5.1.4 Tensile capacity of anchors

The tensile capacity of the anchors was experimentally obtained through tensile tests on custom-made bars. The aim was to determine the upper limit of force that the anchors could transfer from the jacket to the concrete mass. For this reason, three bars having the same amount of fibres as the anchors (20 mm^2 taken from the same carbon textile material used in the anchors), were fabricated and tested according to ACI 440.3R-04 requirements. The tow of fibres used to form the bars had a length of 800 mm and was fully-impregnated with the same epoxy resin used for the impregnation of the anchors tow (see Section 5.1.3). After curing of the adhesive, the two ends of the bars were inserted into two steel tubes (of 300 mm length each – Fig. 5.4a) which were filled with the same epoxy resin used to impregnate the anchors fibres. This served for the mounting of the bar-type specimens to testing machine (Fig. 5.4b).

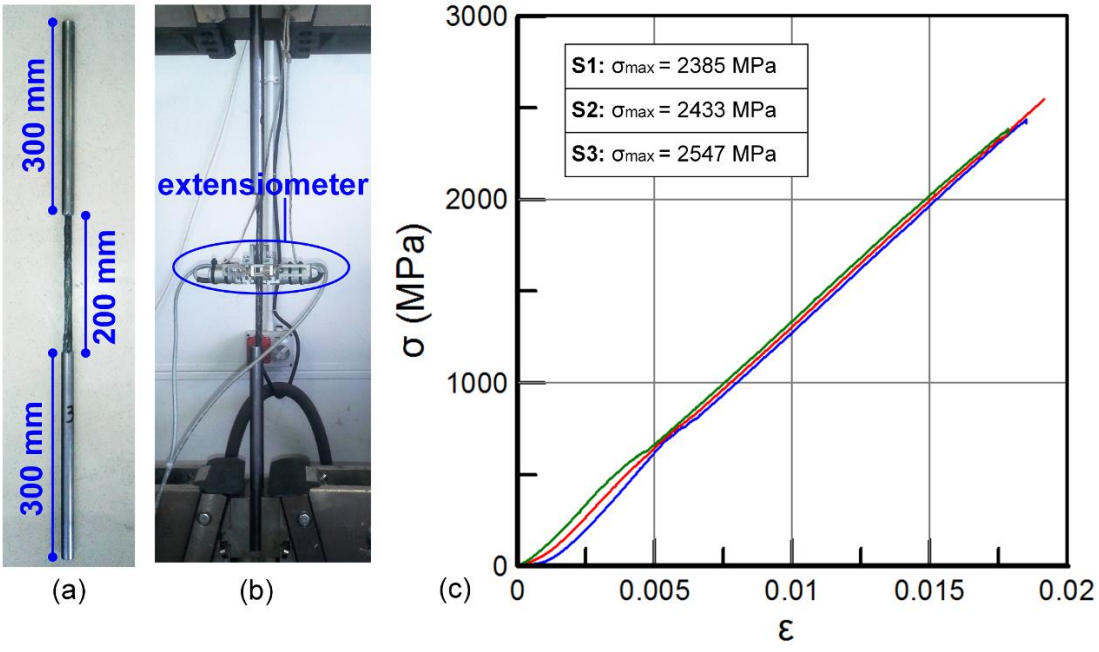


Figure 5.4. (a) Custom-made carbon-fibre rebar to be used for tensile testing; (b) test set-up for tensile testing of the carbon-fibre rebars; (c) strain versus stress curves for the three tested rebars.

Uniaxial tensile testing was carried out using a universal testing machine with a load-capacity of 200 kN, at a monotonic loading rate of 5 kN/min. An extensometer

was attached on the bar to record its axial deformation during testing (Fig. 5.4b). The response of the three bars tested is given in Fig. 5.4c in the form of axial stress–strain curves. The average tensile strength and ultimate strain of the three bars were 2455 MPa (or 49.1 kN) and 1.85%, respectively.

5.1.5 Strengthening Procedure

Prior to strengthening a thin layer of concrete cover was removed and a grid of grooves (2-3 mm deep) was created using a grinding machine. The strengthening application in specimens with anchors included the following steps: (1) drilling holes into the T-beam flanges with a diameter of 12 mm and a depth of 80 mm; (2) removing the dust from the holes with compressed air; (3) dampening of the surfaces receiving mortar; (4) application of a mortar layer; (5) bonding the textile by hand pressure (Fig. 5.5a); (6) application of mortar at the regions that the fanned part of the anchors would cover; (7) filling of the holes with low viscosity epoxy resin (Fig. 5.5b); (8) local impregnation of the dry fibres of the anchors (those who were not impregnated during anchor preparation) using a two-part epoxy resin with tensile strength and modulus of elasticity equal to 20 MPa and 3 GPa, respectively (Fig. 5.5c); (9) installation of the anchors, including placement of the anchors into the holes and bonding of the fan over the first textile layer by hand pressure (Fig. 5.5d); and (10) application of mortar in between the layers while the previous layer was in a fresh state. In case of specimens strengthened with TRM jackets without anchors, steps (1)-(2) and (7)-(9) were omitted. For the FRP-jacketed specimen the first textile layer was applied on the top of the first resin layer and was then impregnated in-situ with resin using a plastic roll. For additional textile layers the same process was repeated. To avoid stress concentrations in the jacket, the two bottom edges of each beam were rounded to a radius equal to 25 mm.

In both CH2_A100 and CL3_A100 specimens, 4 anchors were placed in-between the 1st and the 2nd TRM layer whereas the remaining 3 were placed over the 2nd TRM layer (on each side, Fig. 5.6a). In CH4_A50 specimen, 4 anchors were placed between the 1st and the 2nd TRM layer; whereas the rest 3 were placed in-between the 3rd and the 4th TRM layer (Fig. 5.6b). In CH4_A100 specimen, 5 anchors were placed in each of the three interfaces between two consecutive TRM layers (3x5=15, Fig

5.6c). Finally, in G7_A100 specimen, the 4 anchors were placed between the 3rd and the 4th TRM layer (Fig. 5.6d).

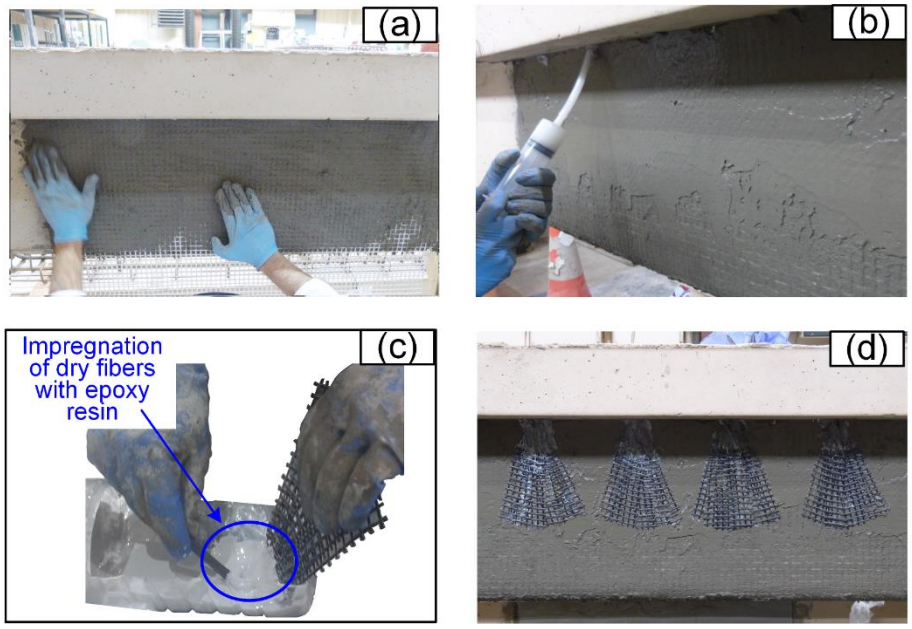


Figure 5.5. (a) Impregnation of the textile fibres with mortar; (b) injection of epoxy resin into the slab holes; (c) impregnation of dry fibres at the central part of anchor with epoxy resin; (d) textile-based anchors applied over the TRM layer.

5.1.6 Experimental Setup and Procedure

The beams were subjected to monotonic loading using a stiff steel reaction frame and an asymmetric three-point bending set-up configuration (Fig. 5.7). A vertically positioned, 1000 kN-capacity servo-hydraulic actuator was used for the application of the load at a displacement rate of 0.01 mm/s. As illustrated in Fig. 5.7, the vertical displacement of the beam was measured at the position of load application using an external LVDT (Linear Variable Differential Transducer); the displacement measured from this sensor was used to plot the load-displacement response curves of the specimens. Moreover, measurements from LVDTs diagonally at the critical shear span in one side of the beam, were utilized to monitor the average shear strain of the span (Fig. 5.8). The diagonal LVDTs were placed at 110 mm from the bottom of the beam to facilitate the installation of the bolts holding the LVDTs to the beam as the top end of longitudinal steel reinforcement was at 90 mm from the bottom of the beam.

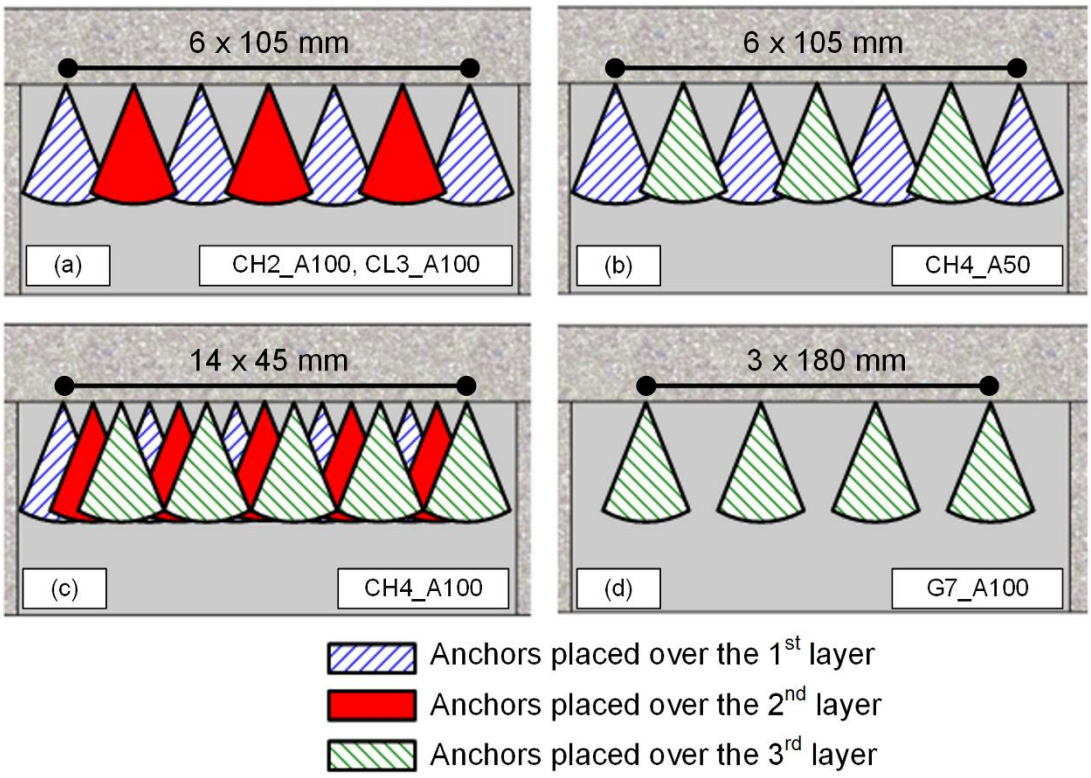


Figure 5.6. (a) Configuration of anchors in (a) specimens CH2_A100 and CL3_A100; (b) specimen CH4_A50, (c) specimen CH4_A100; (d) specimen G7_A100.

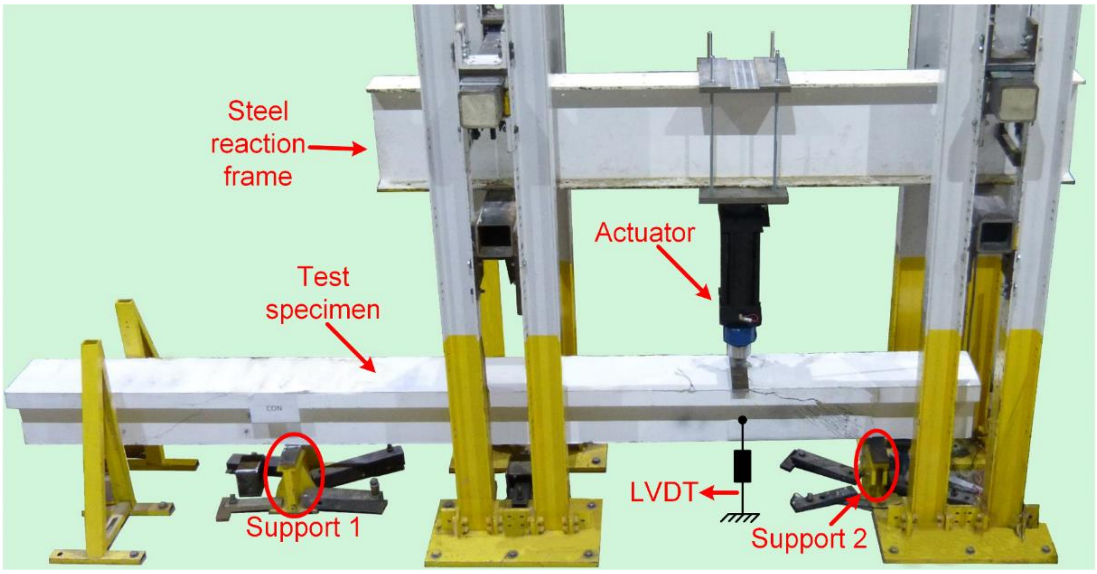


Figure 5.7. Three-point bending test set-up of T-beams.

Additionally, the digital image correlation (DIC) technique was employed to monitor relative displacements within the critical shear span, using two high-resolution cameras (on the side of the beam which was free of sensors). In specimens

with anchors, strain gauges were attached very close to the end of the TRM jacket (10 mm from the flange) in one side of the beam. The strain gauges were bonded to the face of the TRM jacket at the position of anchors. Finally, strain gauges were mounted to the longitudinal bars at the cross-section of maximum moment to monitor possible yielding of the steel reinforcement. It is noted that all data was synchronized and recorded using a fully-computerized data acquisition system.

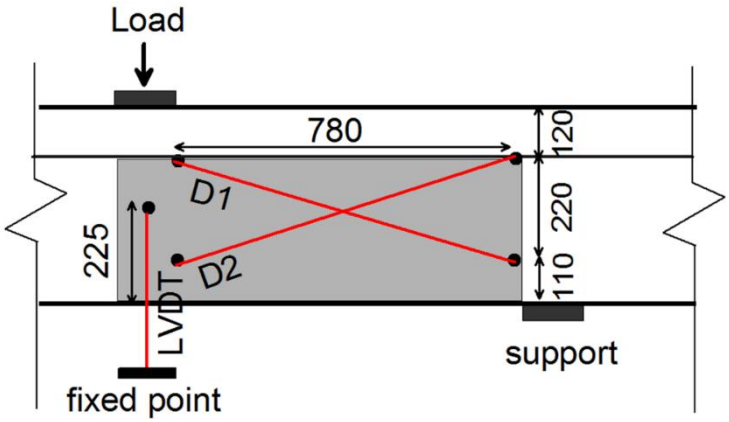


Figure 5.8. Configuration of the two potentiometers (D1, D2) and the LVDT at the shear-critical span.

5.2 Experimental Results

The response of all specimens tested is presented in Fig. 5.9 in the form of load - displacement curves. Key results are also presented in Table 5.4. They include: (1) The peak load. (2) The displacement at peak load. (3) The observed failure mode. (4) The shear resistance of the critical shear span, V_R, which is the shear force in the critical span at peak load. (5) The contribution of the jacket to the total shear resistance, V_f, which is calculated as the shear resistance of the strengthened specimen, $V_{R,str}$, minus the shear resistance of the control specimen, $V_{R,con}$. (6) The shear capacity increase due to strengthening, which is expressed by the ratio, V_f /$V_{R,con}$. (7) The effectiveness of the anchorage system, which is calculated as the ratio of the contribution to shear capacity (V_f) of the strengthened specimen with anchors to the contribution of the corresponding specimen without anchors (i.e. CH2_A100 versus CH2 specimen: 112/46=2.43). (8) The effective strain of the jacket, ε_{eff}, which is calculated using Eq. (5.1).

$$\varepsilon_{eff} = V_f/(\rho_f E_f b_w(d\text{-}h_s)) \quad (5.1)$$

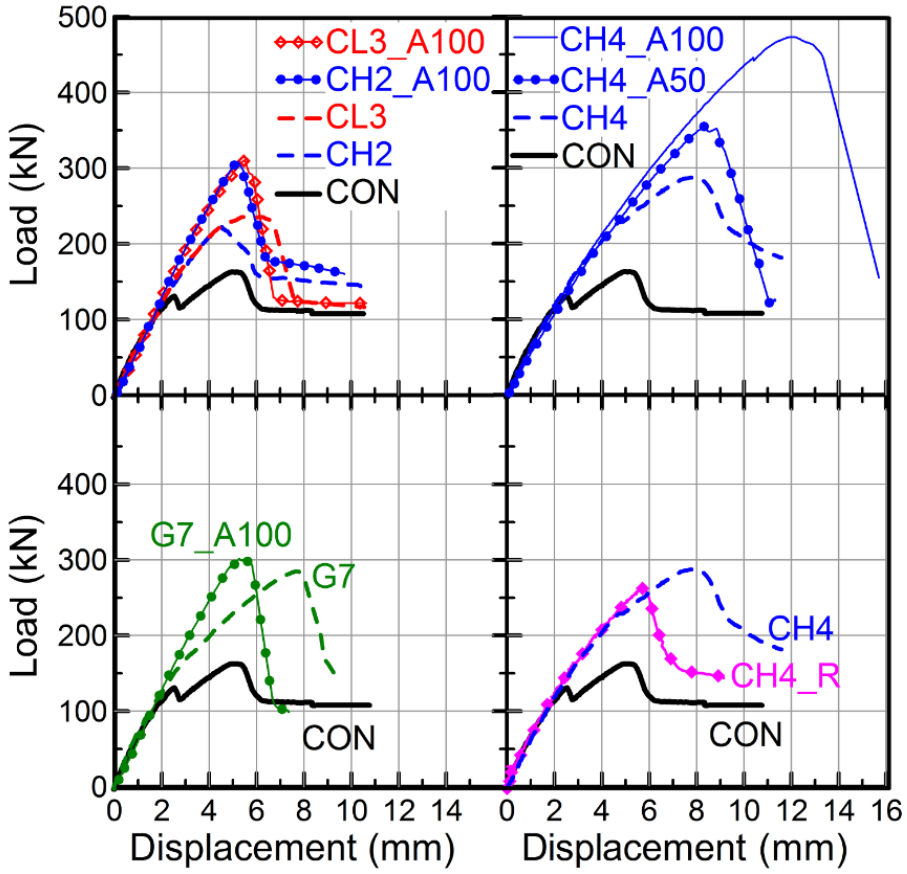


Figure 5.9. Load versus vertical displacement curves for all tested specimens.

Table 5.4. Summary of test results

Specimen	(1) Peak load (kN)	(2) Displacement at peak load (mm)	(3) Failure mode	(4) V_R (kN)	(5) V_f (kN)	(6) Shear capacity increase $V_f/V_{R,con}$ (%)	(7) Effectiveness of anchorage system	(8) ε_{eff} (‰)
CON	163	5.1	shear [a]	124	-	-	-	-
CH2	223	4.5	shear [b]	170	46	37.1	-	2.03
CL3	237	5.7	shear [c]	181	57	46.0	-	2.58
CH4	288	7.9	shear [c]	220	95	77.4	-	2.10
G7	285	7.7	shear [c]	217	93	75.0	-	7.70
CH2_A100	309	5.3	shear [d]	236	112	90.3	2.43	4.94
CL3_A100	311	5.5	shear [d]	237	113	91.1	1.98	5.11
CH4_A50	355	8.4	shear [d]	271	147	118.5	1.53	3.24
CH4_A100	473	12.0	shear [e]	361	236	191.1	2.47	5.21
G7_A100	302	5.3	shear [f]	230	106	85.5	1.14	8.78
CH4_R	264	5.8	shear [c]	201	77	62.1	-	1.70

[a] Tensile diagonal cracking; [b] Slippage of the vertical fibre rovings through the mortar and partial fibres rupture; [c] Debonding of the jacket; [d] Rupture of some anchors and pull-out of some other anchors, [e] pull-out of anchors due to concrete splitting in the slab, [f] Fracture of the jacket

It is worth mentioning that calculation of V_f values and therefore ε_{eff} values have been based on the simplified hypothesis that the two mechanisms of carrying forces

(concrete contribution and jacket contribution) are superimposed without considering any interaction between them. The interaction between mechanisms of carrying forces is more pronounced when stirrups are used.

The control beam (CON) failed in shear at an ultimate load of 163 kN. A large shear crack was firstly formed in the web of the critical shear span (Fig. 5.10a), which was then propagated into the flange of the T-beam and resulted in significant load drop. All strengthened specimens failed in shear and displayed substantially higher shear resistance (from 37% up to 191%) compared to the control specimen.

5.2.1 Strengthened specimens without anchors

All the strengthened specimens without anchors failed in shear and displayed considerably higher shear resistance (from 37.1 up to 77.4%) compared to the control specimen. In particular, specimen CH2 failed at an ultimate load of 223 kN, resulting in 37.1% increase of the shear capacity. The failure of specimen CH2 (with two layers of heavy carbon textile) was associated with damage of the TRM jacket (Fig. 5.10b), that included the following local phenomena: (a) slippage of the vertical fibre rovings through the mortar and (b) partial rupture of the fibres crossing the shear crack. The nature of these local phenomena did not result in very brittle failure mode. In fact, after the peak load was reached, relatively smooth load degradation was recorded.

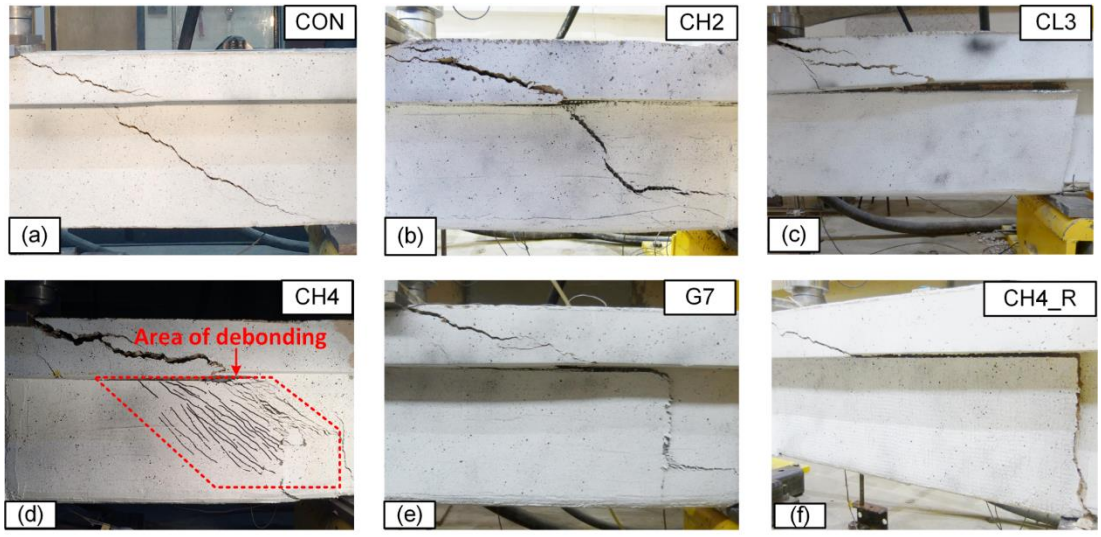


Figure 5.10. (a) Dominant shear crack in the control beam; (b) local damage of the jacket in specimen CH2; (c)-(e) specimens CL3, CH4 and G7 - debonding of the TRM jacket: peeling off of the concrete cover; (f) debonding of the FRP jacket.

The peak load attained by specimen CL3 (with three layers of light carbon textile) was 237 kN, which yields 46% increase in the shear capacity. Failure in this specimen was due to debonding of the TRM jacket without including any local damage of the TRM jacket (Fig. 5.9c). The good bond between the mortar and the concrete substrate resulted in debonding of the TRM jackets from the concrete substrate accompanied with peeling off of the concrete cover.

Specimen CH4 (with four layers of heavy carbon textile) reached a higher load (288 kN) with respect to specimen CH2 (223 kN), owing to the contribution of two extra TRM layers. Its failure was due to debonding of the TRM jacket at a large part (approximately 2/3) of the shear span (Fig. 5.10d), which was also accompanied with peeling off of the concrete cover. Compared to the control specimen the increase in the shear resistance of specimen CH4 was 77.4%.

Specimen G7 (with seven layers of glass textile) failed in the same way with specimen CH4 (Fig. 10e), reaching an ultimate load of 285 kN that corresponds to 75% increase in the shear capacity.

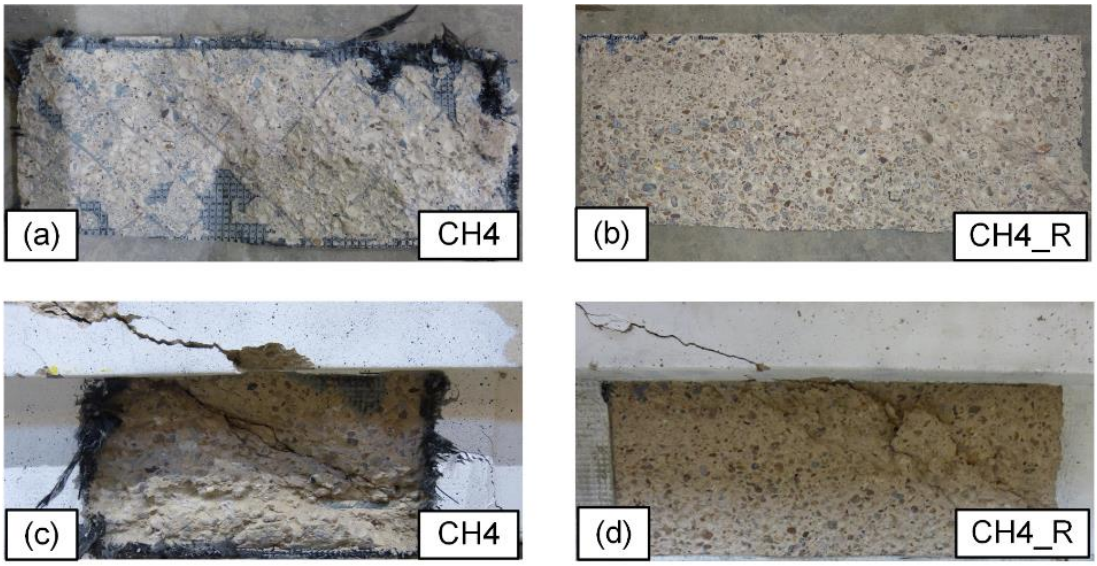


Figure 5.11. (a)-(b) Part of U-shaped jacket of specimens CH4 and CH4_R; (c)-(d) shear crack in concrete of specimens CH4 and CH4_R after removal of the jacket.

Finally, specimen CH4_R (with four layers of heavy carbon textile bonded with resin) failed due to debonding of the jacket from the concrete substrate with peeling off of the concrete cover, at an ultimate load equal of 264 kN (62.1% shear capacity increase). Debonding of the FRP jacket was initiated from the point of load application

and propagated instantly to the support (Fig. 5.10f). Figure 5.11 illustrates the part of concrete cover that was bonded to the jacket of CH4 (Fig. 5.11a) and CH4_R (Fig. 5.11b) specimen, respectively indicating the very good bond between both adhesives (mortar and resin) with the concrete substrate. The type of failure of specimens CL3, CH4, CH4_R and G7 was rather brittle and always occurred after the shear failure of concrete as shown in Fig. 5.11c and Fig. 5.11d taken after removal of the jacket.

5.2.2 Strengthened specimens with anchors

The debonding of TRM jackets was delayed considerably using textile-based anchors. Specimens CH2_A100 (with two layers of fully anchored heavy carbon textile), CL3_A100 (with three layers of fully anchored light carbon fibre textile), CH4_A50 (with four layers of heavy carbon fibre textile anchored by 50%), CH4_A100 (with four layers of fully anchored heavy carbon fibre textile) and G7_A100 (with seven layers of fully anchored glass fibre textile) failed in shear at even higher loads; 309 kN, 311 kN, 355, 473 and 302 kN, respectively, when compared to the corresponding specimens without anchors; namely CH2, CL3, CH4 and G7.

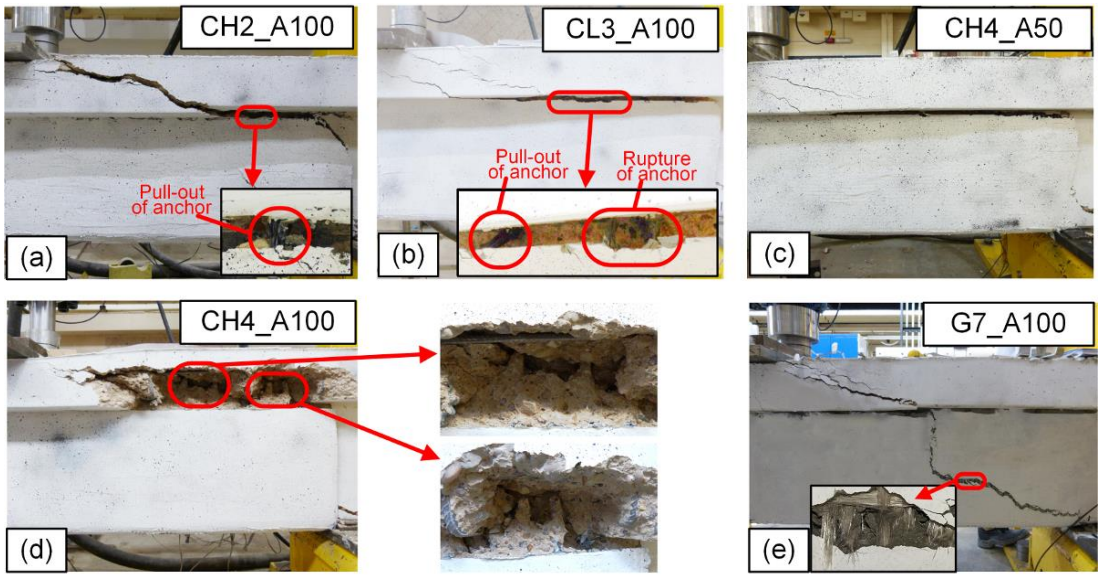


Figure 5.12. Failure modes of TRM-retrofitted specimens with anchors: (a)-(c) Specimens CH2_A100, CL3_A100 and CH4_A50 – rupture of some anchors and pull-out of the rest; (d) failure of specimen CH4_A100 due to concrete splitting in the slab; (f) fracture of glass TRM jacket in specimen G7_A100.

The shear capacity of specimens CH2_A100, CL3_A100, CH4_A50, CH4_A100 and G7_A100 was increased by 90.3%, 91.1%, 118.5%, 191.1% and

85.5% respectively, with respect to the control specimen. In specimens CH2_A100, CL3_A100 and CH4_A50, debonding of the TRM jacket was initiated at the region where the shear crack on the web intersects with the slab and was expanded to a broader area of the beam when the anchors failed due to fibres rupture or pull-out from the slab (Fig. 5.12a, b and c). In particular, in specimen CH2_A100, 5 (out of 14) anchors were pulled out from the slab, while 3 anchors (out of 14) were ruptured. In specimens CL3_A100 and CH4_A50, 4 anchors (out of 14) were ruptured, whereas 4 anchors (out of 14) were pulled out from the slab. Failure of specimen CH4_A100 was attributed to anchors pull-out (8 on each side) due to concrete splitting at the two flanges (Fig. 5.12d). Finally, failure of specimen G7_A100 was attributed to fracture of the glass TRM jacket (Fig. 5.12e) without including any failure of the anchors.

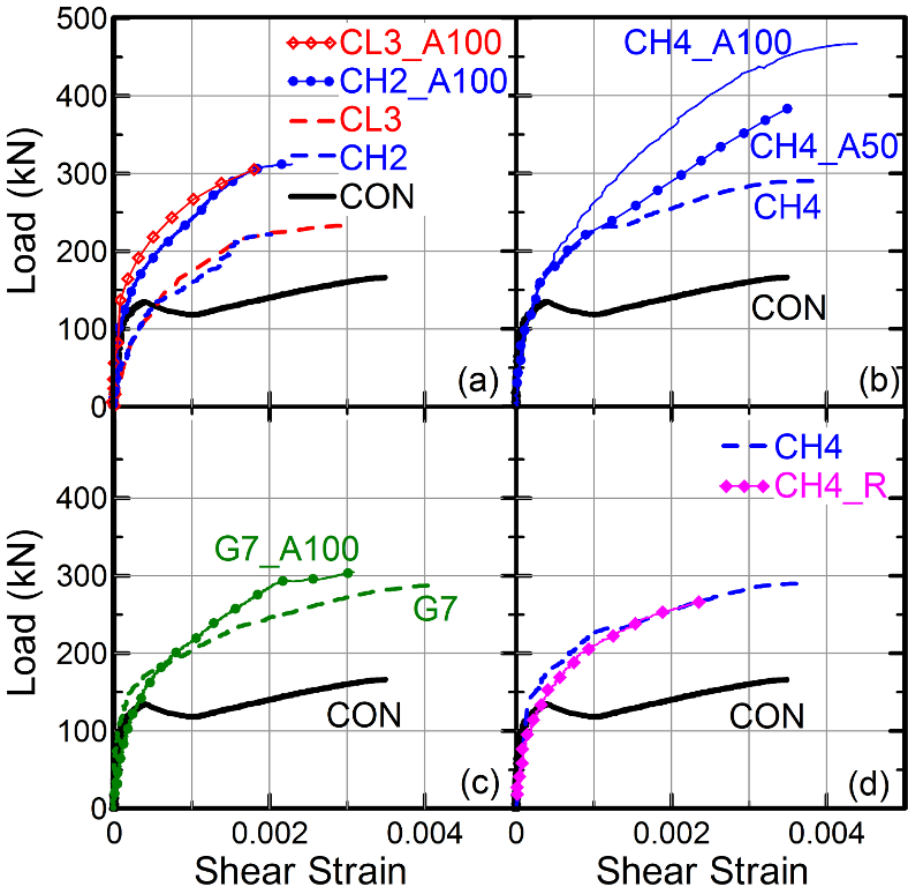


Figure 5.13. Load versus average shear strain curves.

Figure 5.13 presents the load versus average shear strain curves for all specimens which are plotted up to peak load. The average shear strain at the critical shear span, γ, was obtained from readings of the two LVDTs placed in X configuration (Fig. 4.5b)

according to Eq. (4.1). The results show that strengthening the beams with TRM or FRP jackets resulted in decrease in the average shear strain over the critical shear span, for the same load level (compared to the control specimen), after cracking. In other words, retrofitted beams are much stiffer in shear after cracking of the beam than the unretrofitted one. Moreover, the shear stiffness of specimens with anchored jackets is higher than their counterpart specimens without anchors. Finally, higher average shear strains at the ultimate load level were developed in CH4 specimen compared to its FRP counterpart (CH4_R) which was also reported in 4.1.2.

Strain gauges were affixed at the positions of anchors in order to better understand the response of the specimens with anchors. Figure 5.14 illustrates the load versus TRM jacket strains in specimen CH4_A50, at the positions of anchors (see also Section 5.1.6). As shown in Fig. 5.14, the anchors activation started with a phase difference from the load-application position towards the support. The TRM jacket at the vicinity of anchor '3', debonded before the peak load, namely at around 265 kN. Strain gauge '4' started recording strains with higher rate between 300 kN and 335 kN when debonding of TRM jacket propagated progressively to the vicinity of anchor '4'. At that point (335 kN), strains of anchors '2' and '5' are increasing in higher rate. This rate change in development of strains is probably related to the redistribution of stresses from one anchor to another one. The behavior observed to all strengthened specimens with anchors was identical (the load versus TRM jacket strains in the rest anchored TRM specimens are presented in Fig. C.3-C.6 of Appendix C).

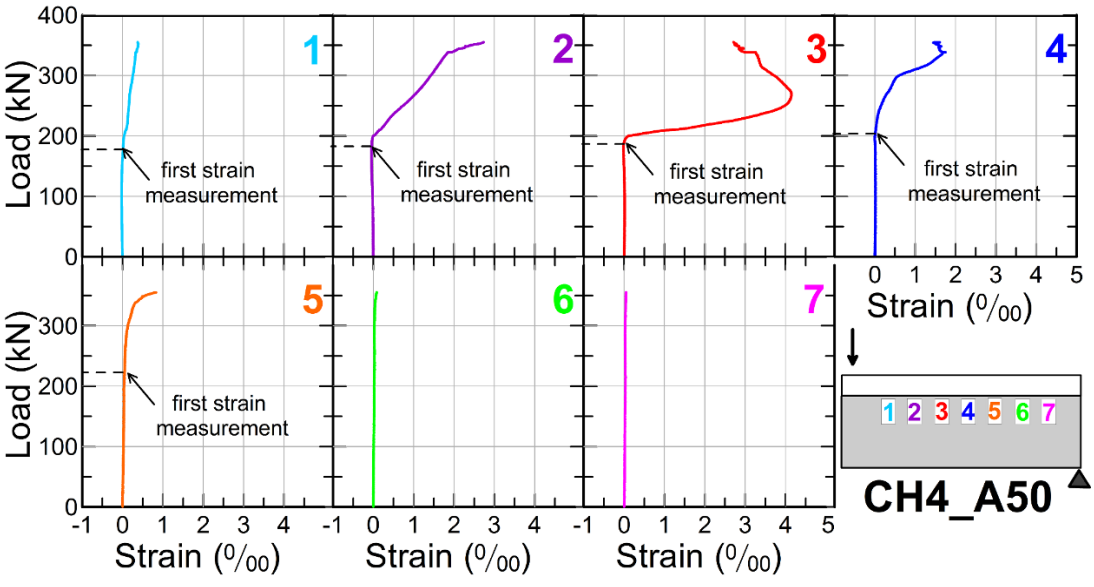


Figure 5.14. Strain versus load curves using strain gauges readings in specimen CH4_A50.

5.3 Discussion

5.3.1 Effect of investigated parameters

All specimens responded as designed and failed in shear prior to yielding of the longitudinal steel reinforcement. This response allowed for the evaluation of the capacity of all strengthening systems in increasing the shear resistance of the full-scale T-beams. In terms of the various parameters investigated in this experimental programme, an examination of the results (Table 5.4) in terms of shear capacity, failure modes and effective strains, revealed the following information.

5.3.1.1 Anchorage system of the U-jacket

The effectiveness of the anchored U-jackets in increasing the shear capacity of the T-beam (specimens CH2_A100; CL3_A100; CH4_A50; CH4_A100; G7_A100) was from 1.14 to 2.47 times the effectiveness of the non-anchored jackets (see Table 5.4). The increase was depending on the number of the TRM layers, the percentage of jacket's anchorage, and the material of the fibres in the jacket.

Particularly, in specimen CH2_A100, the use of 7 anchors per side of the beam (that provided full anchorage of the applied layers) increased the shear resistance of the beam by 90.3% compared to the control specimen, whereas the effectiveness of the TRM jacket was increased by 143% compared to the corresponding specimen without anchors (CH2). The full anchorage of three light carbon layers provided by 7 anchors per beam's side (CL3_A100) improved the effectiveness of the TRM jacket by 98% compared with its counterpart specimen without anchors (CL3) resulting in 91.1% increase in the shear resistance compared with the control specimen. The 50% (CH4_A50) and 100% (CH4_A100) anchorage of four heavy carbon layers increased the shear resistance of the control specimen dramatically, namely by 118.5% and 191.1%, respectively, improving at the same time the effectiveness of the TRM jacket by 53% and 147%, respectively, when compared to specimen CH4. In specimen G7_A100, the effectiveness of glass TRM jacket was improved by only 14% using 4 anchors on each side of the beam, whereas its shear resistance increased by 85.5% as compared to the control specimen. In this case the limited effectiveness of the anchorage system is attributed to the fact that the non-anchored jacket had already

developed an effective strain (7.70‰) that was just 12% lower than the effective strain developed at fibres rupture in the anchored jacket (8.78‰).

In specimens CH2_A100, CL3_A100 and CH4_A50, the TRM jacket debonded following the failure of the anchorage system. The local damage of the TRM jacket which occurred in specimen CH2 without anchors (including slippage of the vertical fibre rovings through the mortar and partial fibres rupture) was limited when the jacket was anchored in specimen CH2_A100, thanks to the additional fibres provided by the fan-part of the anchors (Fig. 5.5d and Fig. 5.6). It is important to note that specimen CH2_A100, strengthened with two carbon TRM layers and anchors, was 17% more effective (in terms of V_f, see in Table 5.4) than specimen CH4 which was strengthened with four carbon and had approximately 28% more material. This can lead to significant cost benefits in real applications due to the considerable material savings. In specimen CH4_A100, the anchors were pulled out suddenly from the slab due to concrete splitting before reaching their tensile capacity. Finally, failure of specimen G7_A100 was due to fracture of the glass TRM jacket without any failure of the anchorage system.

The beam strengthened with two and four heavy carbon (CH2 and CH4) TRM layers and three light carbon (CL3) TRM layers without anchors had effective strain, ε_{eff}, equal to 2.03‰, 2.10‰ and 2.58‰, respectively (see Table 5.4). The effectiveness of carbon TRM jacket was considerably improved by providing full anchorage to the TRM jackets with textile-based anchors. In particular, the TRM jacket effective strain, ε_{eff} of specimens CH2_A100, CH4_A100 and CL3_A100 was equal to 4.94‰, 5.21‰, and 5.11‰, respectively. The corresponding value for CH4_A50 specimen was 3.24‰.

Unexpectedly, specimen CH4_A100 failed in shear due to concrete splitting in the flange of the T-beams (Fig. 5.12d). Such a failure mode, which is related to the tensile strength of the concrete, sets an upper limit on the shear capacity increase of the U-TRM jackets anchored in the slab.

5.3.1.2 Number of Layers

The contribution of TRM jackets to the beam shear capacity was increased in an almost proportional way with the number of TRM layers (for the same type of textile). Doubling the amount of reinforcement of the non-anchored jackets (4 layers instead

of 2) resulted in 2.09 times increase of the contribution to the shear resistance (CH4 versus CH2). The corresponding increase was 2.12 when anchors were used to provide full anchorage of the TRM jacket (CH4_A100 versus CH2_A100).

As described in Section 5.2, a change in the failure mode was witnessed when the number of layers was increased from two to four in case of specimens without anchors. In particular, the failure of specimen that received two layers (CH2) was dominated by local damage of the TRM jacket (the vertical fibre rovings crossing the developed shear crack at the jacket experienced a combination of slippage through the mortar and partial rupture). Contrary, the failure mode of specimen that received four layers (CH4) is associated to the failure of the concrete substrate with no damage in the composite jacket. Thus, the increase in the number of layers prevented these local phenomena and as a result the damage was shifted to the concrete substrate. This is attributed to the better mechanical interlock conditions created by the overlapping of multiple textile layers as also reported in 4.1.3.1 (or Tetta et al. 2015).

The effective strains of specimens received 2 and 4 non-anchored TRM layers (CH2, CH4) were 2.03‰ and 2.10‰, respectively. The corresponding values for specimens received 2 and 4 fully-anchored TRM layers (CH2_A100 and CH4_A100) were 4.94‰ and 5.21‰, respectively.

5.3.1.3 Textile geometry

Specimens CH2 and CL3 received correspondingly 2 and 3 layers carbon textile of different geometry, having although the same external reinforcement ratio (ρ_f=1.9‰). The light carbon textile used in specimen CL3 has denser mesh-pattern and TEX (which is the weight of each roving in g/km) equal to 880; whereas the TEX of the heavy carbon textile is equal to 1740. The shear capacity increase of CH2 and CL3 specimens was 37.1% and 46.0%, respectively (compared to the control specimen), whereas the effective strains at ultimate load were 2.03‰ and 2.58‰, respectively.

A comparison of the results for specimens CH2 and CL3 shows that the textile geometry has an effect on the failure mode. As mentioned before, CH2 specimen failed due to local damage of the TRM jacket (slippage of fibres through the mortar and partial rupture of fibres crossing the shear crack) in contrary to specimen CL3 that failed due to debonding of the TRM jacket from the concrete substrate. The difference in failure mode observed in these specimens is possibly associated with the dense

mesh-pattern of the textile (thanks to the smaller mesh size of the light-weight carbon fibre textile) in specimen CL3, which resulted in better fibres distribution along the shear span and therefore the mechanical interlock between the textile and the mortar was improved. Similar results were reported in the corresponding medium-scale rectangular beams presented in Section 4.2.

The shear capacity increase of the corresponding specimens with full anchored TRM jacket (CH2_A100, CL3_A100) was 90.3% and 91.1%, respectively (compared to the control specimen), whereas the effective strains were 4.94‰ and 5.11‰, respectively. Thus, the presence of anchors mitigated the effect of textile geometry in specimens CH2_A100 and CL3_A100, as the failure of these specimens was governed by the behaviour of anchors (rupture of some anchors and pull-out of some other anchors) and not from the behaviour of TRM jacket as in case of the non-anchored specimens (CH2, CL3).

5.3.1.4 Textile material

Specimen G7 strengthened with seven glass textile layers had approximately the same shear capacity with specimen CH4 that received four heavy carbon textile layers, despite the fact that seven glass textile layers are equivalent to just one heavy-carbon textile layer (in terms of axial stiffness as explained in Section 5.1.2). In specific, the shear capacity increase of specimens G7 and CH4 was 77.4% and 75.0%, respectively. As a result, the effective strain of the TRM jacket, ε_{eff}, was much higher in specimen G7 (7.70‰) when compared with that of CH4 (2.10‰). The latter indicates that glass fibres are more effective than carbon fibres in shear strengthening of concrete beams with U-shaped TRM jackets. Both specimens exhibited similar failure mode, namely debonding of the TRM jacket from the concrete substrate.

The evaluation of the effect of textile material in case of anchored TRM jacketing is not feasible, as the failure of specimen CH4_A100 was due to concrete splitting in a part of the slab, whereas the failure of specimen G7_A100 was due to fracture of the glass TRM jacket.

5.3.1.5 Adhesive Material (TRM vs. FRP Jackets)

The effect of the adhesive material on the shear capacity increase of non-anchored U-jackets was negligible. When resin was used as bonding agent (specimen CH4_R with

four heavy carbon textile layers) the shear capacity of the beam was increased by 62.1%. This is marginally less than the capacity increase observed in its mortar impregnated counterpart specimen CH4 (77.4%). The effective strains of specimens CH4 and CH4_R were 2.10‰ and 1.70‰, respectively. The failure mode in both specimens was associated with debonding of the jacket; the strong bond between the adhesive material (mortar or resin) with the substrate concrete resulted in peeling off of the concrete substrate. It is noted, that the corner radius at the bottom edges of the beam's web (equal to 25 mm for both TRM and FRP systems) did not have any effect on the failure mode of the beams.

5.3.2 Deformation Aspects of Jackets based on DIC

The response of the strengthened specimens, as a means of vertical deformations distribution along the beam height, was captured using the DIC method and is presented in Fig. 5.15. Each curve illustrates the relative displacement of each point along the T-beam web height with respect to the bottom of the beam (at the middle cross-section of the critical shear span) at the instant of peak load. For the sake of comparison, the corresponding curve of the control beam is also plotted in all curves.

As illustrated in Fig. 5.15 the control specimen exhibited concentration of the vertical deformations at a specific level, which is related to the development of a single shear crack at that level (at around 190-210 mm from the bottom of the beam). Specimen that received two heavy TRM layers (CH2) exhibited similar behaviour with concentration of stresses in specific levels (at around 100 mm and 190 mm from the bottom of the beam). Deformations were better distributed in the rest specimens, indicating that the jackets were activated over a broader area due to better redistribution of stresses. Specimens that received TRM or FRP jacketing without anchors deform from the bottom level of the beam (thanks to the anchorage of the jackets at the bottom corner of the beams) to a level in the central region, with the top end being almost inactive. The anchorage system improves the deformation capacity of the TRM jacket at the top end of the beam. Another interesting point of the behaviour of the strengthened specimens with anchors is associated with the inclination change of the curve at the end of the anchors fanned part (at around 130mm from the bottom of the beam). Thus, the area covered by the anchors is stiffer thanks to the extra amount of fibers in anchors.

Images of the in-plane and out-of-plane deformations of the TRM jackets, obtained using DIC measurements at the instant of maximum load, are presented in Fig. 5.16 for each retrofitted specimen (one side of the jacket was monitored). In specimens with anchored jackets, white and black dots are used at the top of TRM jacket to indicate which anchors were (white dots) and which were not (black dots) activated based on the strain gauges readings.

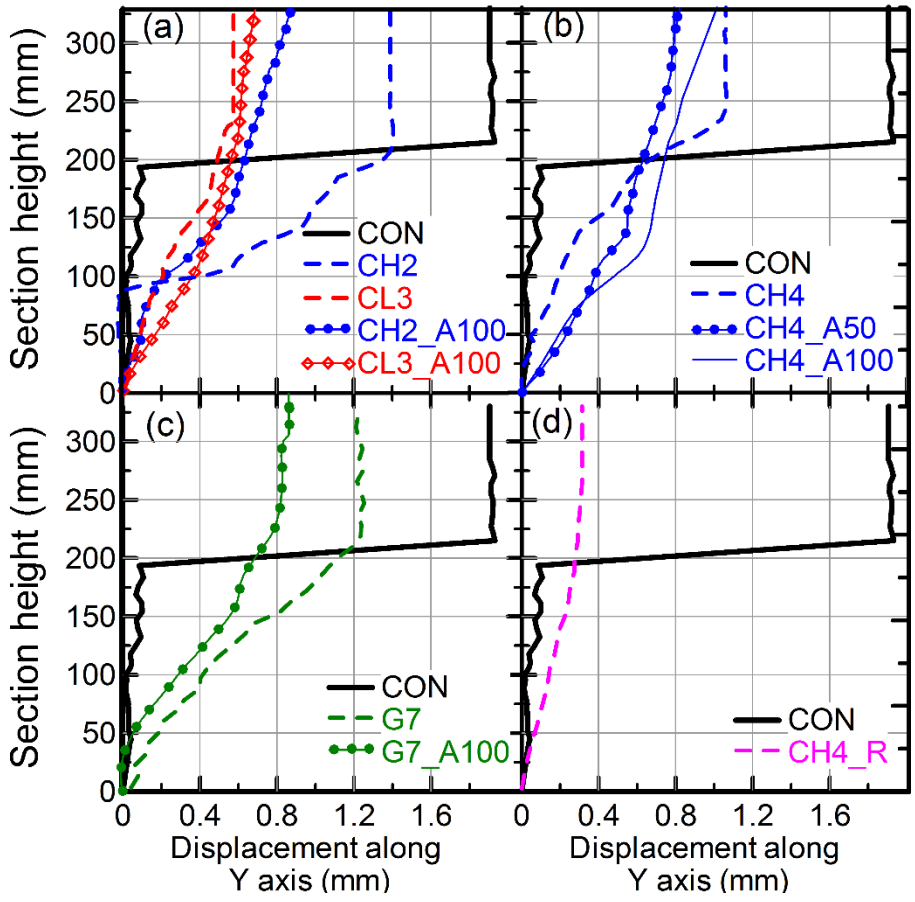


Figure 5.15. Relative vertical displacements along the T-beam web height at the central cross-section of the critical shear span, at the instant of peak load.

Application of anchors reduced the evolution of the jacket debonding (out-of-plane deformations) at the shear span of the beam. The TRM jacket of specimen CH2 started debonding but local damage of the jacket finally dominated the failure. In specimen CH2_A100, although these local phenomena were limited compared to CH2, signs of local damage of the jacket (two cracks were formed) were evident in-between the anchors.

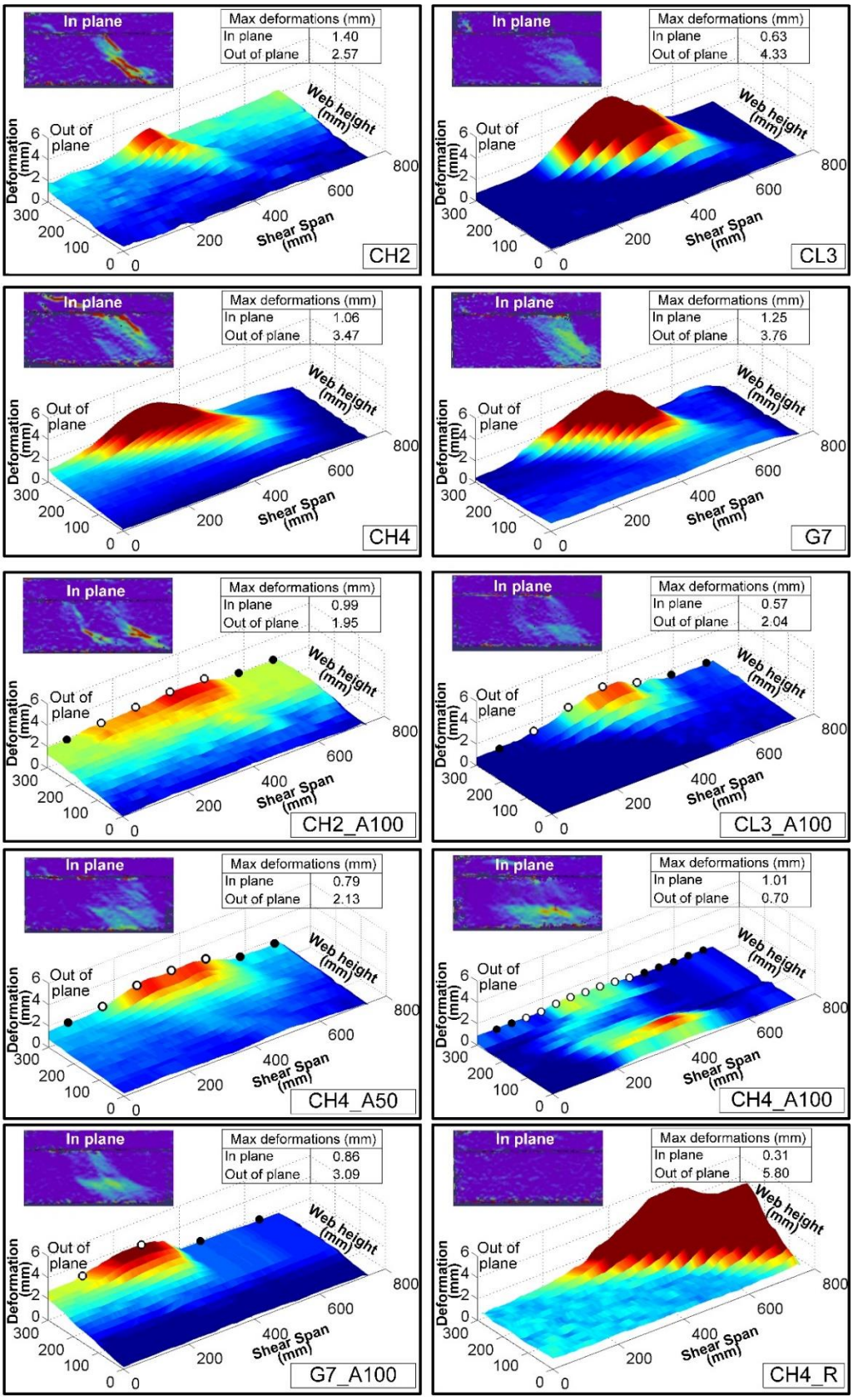


Figure 5.16. Field of vertical axis (in-plane) and out-of-plane (indicating debonding) deformations in the critical shear span of the strengthened specimens at the instant of peak load.

Debonding of the TRM jacket in specimen CL3_A100 was significantly reduced (in both amplitude and width) than the corresponding specimen without anchors (CL3). In specimen CH4_A50, the use of anchors that provided 50% anchorage of the applied TRM layers substantially limited the extent of TRM jacket debonding as compared to its counterpart specimen without anchors (CH4).

The performance of specimen CH4_A100 was quite impressive as the TRM jacket debonding was prevented up to a load of 473 kN that the anchors failed. The presence of anchors in specimen G7_A100 slightly reduced the TRM debonding as compared to specimen G7, as the glass TRM jacket fractured before the full activation of the applied anchors.

5.4 Design model

5.4.1 Methodology

In this paragraph, a simplifying methodology for calculating the contribution of anchored TRM U-jackets to the shear resistance of RC beams is proposed. It is based on the following assumptions:

- The number of anchors provided is sufficient to increase the effectiveness of the non-anchored jacket. In lack of data, this could be translated as a minimum number of anchors which corresponds to anchorage of 50% of the jacket fibres.
- The anchored TRM jacket is idealized as discrete vertical shear links at a distance *s* (distance between the anchors) which connect the compression zone with the tensile (longitudinal) reinforcement of the beam. The shear links have the properties of the anchors. By this idealization the behavior of the jacket is governed by the behavior of the anchors, and the contribution of each (U-jacket and anchors) is not considered separately.

By applying the Morsch truss analogy, the following equation can be used to calculate the contribution of anchored TRM U-jackets to the total shear resistance of a T-beam:

$$V_f = A_{anc} f_{fe,anc} \frac{h_w}{s} \cot\theta \tag{5.2}$$

Similarly to the case of internal steel stirrups, the term (h_w/s) cotθ in Eq. (5.2) determines the number of anchors that are activated in tension.

The effective strength of the anchors, $f_{fe,anc}$, is a reduced value of their tensile capacity, $f_{f,anc}$, to account for: (a) local concentration of stresses at the point where the anchor enters the concrete slab, and (b) the non-uniform distribution of stresses between activated anchors. It is expressed by the following equation:

$$f_{fe,anc} = \eta_e f_{f,anc} \tag{5.3}$$

where η_e is the strength reduction factor with values less than 1.0.

It is important to note that there are two upper limits for the value of V_f calculated according to Eq. (2): (a) the shear force corresponding to rupture of the fibres in the TRM jacket (as in the case of specimen G7_A100), and (b) the force at which the concrete of the slab fails due to tensile splitting (as in the case of specimen CH4_A100).

5.4.2 Model calibration to the test results

Using the experimental values of V_f (calculated according to the approach that the concrete and jacket contribution are superimposed without considering any interaction between; see Table 5.4), the effective strength of the anchors, $f_{fe,anc}$, was calculated using Eq. (5.2) for specimens CH2_A100, CL3_A100 and CH4_A50, in which the ultimate load was governed by the anchors failure (rupture or pull-out from the slab). The results are presented in Table 5.5 (using $\theta = 45^o$).

Table 5.5. Effective strength of anchors and strength reduction factor for specimens failed due to anchorage loss.

Specimen	$V_{f,exp}$ (kN)	A_{anc} (mm^2)	h_w/s	$f_{fe,anc}$ (MPa)	η_e
CH2_A100	112	40*	3.1	903	0.37
CL3_A100	113	40	3.1	911	0.37
CH4_A50	147	40	3.1	1185	0.48

* Fibres area of two anchors (one per each beam's side).

The effective strength of the anchors was almost the same for the two cases with 100% anchorage of the fibres of the jacket, and approximately equal to 900 MPa. This value gives a strength reduction factor of 0.37 when divided by the tensile capacity reported in Section 5.1.4 (2455 MPa). In the case of 50% anchorage of the jacket's fibres, the resulting value was higher and equal to 1185 MPa, which yields a strength reduction factor of 0.48.

Although it seems that anchoring 50% of the jacket fibres results in higher effective strength of the anchors, it is not safe to conclude due to the limited available data. For this reason, and before more experimental data will be available, a value of η_e= 0.3 is suggested for design purposes.

5.5 Summary

This chapter presents a large experimental investigation on the effectiveness of TRM U-jackets in shear strengthening of full-scale RC T-beams. Key parameters of this study were: (a) the use of textile–based anchors as end-anchorage system of the U-jacket, (b) the number of TRM layers, (c) the textile geometry, (d) the textile material (two carbon-fibre textiles and a glass-fibre textile) and (e) the performance of equivalent FRP jackets for the case without anchors. For this purpose, eleven shear-deficient T-beams were subjected to three-point bending under monotonic loading: one was tested as-built, whereas the rest ten were strengthened prior to testing. The main conclusions drawn from this study are summarized as follows:

- The use of textile–based anchors dramatically increases the effectiveness of carbon TRM U-jackets. Full anchorage of the carbon TRM layers improved the effectiveness of the jackets by 98% to 148%, depending on the number of TRM layers and the textile geometry.
- High effective strains, ε_{eff} can be achieved when the TRM jacket is anchored. Values ranging from 3.24‰ to 5.21‰ (depending on the number of TRM layers and the amount of anchors) were achieved in this study. Contrary, the effective strain in the TRM jackets without anchors ranged between 2.03‰ and 2.58‰.
- Anchoring the 2 (heavy) carbon layers TRM jacket is almost equivalent to the application of 4 (heavy) carbon TRM layers without anchorage, yielding significant cost benefits.
- The number of layers affects the failure mode of non-anchored TRM U-jackets. When number of layers increases, local damage of the TRM jacket (partial fibres rupture and slippage of fibre filaments through the mortar) is prevented and damage is shifted to the concrete substrate.
- In non-anchored jackets, different textile geometries with the same reinforcement ratio result in practically the same load increase but different failure

modes develop. In anchored jackets the effect of the different textile geometry is eliminated as the failure is governed by the anchors behaviour.

- The effect of different textile material (glass versus carbon) is more pronounced in non-anchored jackets, where seven glass textile layers had approximately the same shear capacity with four heavy carbon textile layers, despite the fact that seven glass textile layers were equivalent to just one heavy-carbon textile layer (in terms of axial stiffness).
- TRM U-jackets are as effective as FRP U-jackets in increasing the shear capacity of full-scale RC T-beams.
- A simple analytical model which calculates the contribution of anchored TRM jackets to the shear capacity of RC T-beams can be used for design purposes.

Chapter 6

TRM VERSUS FRP JACKETING IN SHEAR STRENGTHENING OF RC MEMBERS SUBJECTED TO HIGH TEMPERATURE

Abstract

This chapter presents the first study on the performance of TRM and FRP jacketing in shear strengthening of reinforced concrete (RC) members subjected to ambient and high temperatures, including both medium-scale rectangular beams and full-scale T-beams. Key parameters investigated on the medium-scale rectangular RC beams include: (a) the matrix used to impregnate the fibres, namely resin or mortar, resulting in two strengthening systems (TRM or FRP), (b) the level of high temperature to which the specimens are exposed (20 ºC, 100 ºC, 150 ºC, 250 ºC), (c) the strengthening configuration (side-bonding, U-wrapping and full-wrapping), (d) the number of jacketing layers (2 and 3) and (e) the textile properties (geometry, material). The effectiveness of both non-anchored and anchored TRM jackets in shear strengthening of full-scale T-beams at high temperature was also studied. It is concluded that TRM possess excellent performance as strengthening material at high temperature. TRM jacketing remained very effective in shear strengthening of concrete at high temperature; on the contrary the effectiveness of side-bonding and U-wrapping FRP jacketing was reduced nearly to zero when subjected at temperatures above the glass transition temperature.

6.1 Experimental Programme

6.1.1 Test Specimens, Investigated Parameters, Materials and Strengthening Procedure

The main objective of this study was to evaluate the effectiveness of TRM versus FRP jacketing in shear strengthening of RC beams subjected to high temperature. The experimental program consists of two Series of tests; Series A and Series B. Series A comprises 28 tests carried out on medium-scale rectangular RC beams, and investigated the following parameters: (a) the matrix used to impregnate the fibres, namely resin or mortar, resulting in two strengthening systems (TRM or FRP), (b) the temperature to which the specimens were exposed (20 ^{o}C, 100 ^{o}C, 150 ^{o}C, 250 ^{o}C), (c) the strengthening configuration (side-bonding, U-wrapping and full-wrapping), (d) the number of jacketing layers (2 and 3) and (e) the textile properties (geometry, material). Since the performance of the medium-scale specimens that received TRM jacketing at high temperature was very promising, it was decided to assess the TRM system in the shear strengthening of real-scale specimens. Thus, Series B comprises 5 tests performed on full-scale T-beams, investigating: (a) the performance of TRM jacketing in shear strengthening of full-scale T-beams and (b) the use of textile–based anchors as end-anchorage system of the U-jacket, at high temperatures.

The experimental programme of Series A included 28 tests performed on medium-scale rectangular RC beams simply-supported in asymmetric three-point bending. Sixteen specimens tested at high temperatures (100 ^{o}C, 150 ^{o}C and 250 ^{o}C), whereas the rest twelve specimens tested at ambient temperature at Chapter 4. The design, geometry and set-up of the beams has been already presented in Section 4.1 (see Fig. 4.1 and Fig. 4.2). Figure 6.1 illustrates the strengthening configurations of all specimens of Series A, whereas Table 6.1 presents theirs details. Two beams were tested as-built without receiving strengthening and served as control specimens at ambient (CON_20) and at 150 ^{o}C (CON_150). The notation of strengthened specimens is X_YMN_T, where X refers to the strengthening configuration, namely SB for side-bonding, UW for U-wrapping and FW for full-wrapping, Y denotes the matrix material [M for Mortar (TRM system) or R for Resin (FRP system)], M denotes the type of the textile (CL, CH and G; see Fig. 3.1), N denotes the number of layers

(2, 3 or 7) and T denotes the temperature in which the specimens were exposed during the test (20 ºC, 100 ºC, 150 ºC or 250 ºC).

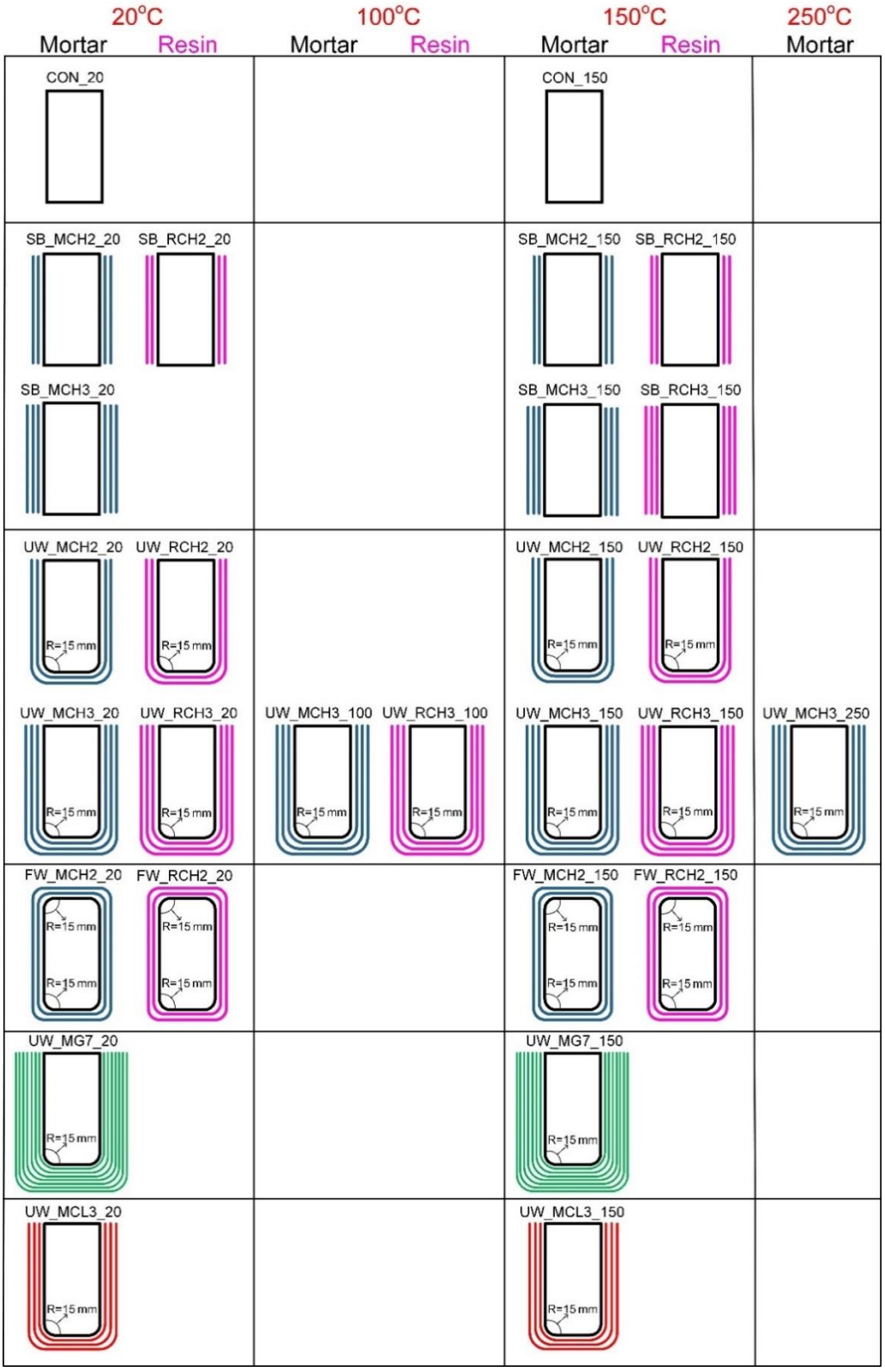


Figure 6.1. Schematic representation of different strengthening configurations adopted in medium-scale rectangular beams.

Five full-scale T-beams were tested in three-point bending. The design, geometry and set-up of these beams have been already described in Section 5.1 (see Fig. 5.1 and 5.7), whereas the design, fabrication procedure and tensile capacity of textile-based anchors used in specimens CH4_A100_20 and CH4_A100_150 are described in Sections 5.1.3 and 5.1.4.

Table 6.1. Strengthening configuration and material properties of all specimens.

Specimen	Textile used	t_f [a] (mm)	No. of layers	ρ_f (‰)	Anchorage percentage (%)	Temperature (ºC)
CON_20	-	-	-	-	-	20
CON_150	-	-	-	-	-	150
SB_MCH2_20	CH	0.095	2	3.7	-	20
SB_MCH2_150	CH	0.095	2	3.7	-	150
SB_MCH3_20	CH	0.095	3	5.6	-	20
SB_MCH3_150	CH	0.095	3	5.6	-	150
UW_MCH2_20	CH	0.095	2	3.7	-	20
UW_MCH2_15	CH	0.095	2	3.7	-	150
UW_MCH3_20	CH	0.095	3	5.6	-	20
UW_MCH3_15	CH	0.095	3	5.6	-	150
UW_MCH3_10	CH	0.095	3	5.6	-	100
UW_MCH3_25	CH	0.095	3	5.6	-	250
UW_MCL3_20	CL	0.062	3	3.6	-	20
UW_MCL3_15	CL	0.062	3	3.6	-	150
UW_MG7_20	G	0.044	7	6.0	-	20
UW_MG7_150	G	0.044	7	6.0	-	150
FW_MCH2_20	CH	0.095	2	3.7	-	20
FW_MCH2_15	CH	0.095	2	3.7	-	150
SB_RCH2_20	CH	0.095	2	3.7	-	20
SB_RCH2_150	CH	0.095	2	3.7	-	150
SB_RCH3_150	CH	0.095	3	5.6	-	150
UW_RCH2_20	CH	0.095	2	3.7	-	20
UW_RCH2_15	CH	0.095	3	3.7	-	150
UW_RCH3_20	CH	0.095	3	5.6	-	20
UW_RCH3_15	CH	0.095	3	5.6	-	150
UW_RCH3_10	CH	0.095	3	5.6	-	100
FW_RCH2_20	CH	0.095	1	1.9	-	20
FW_RCH2_150	CH	0.095	2	3.7	-	150
CON[T]	-	-	-	-	-	20
CH4_20[T]	CH		4	3.8	-	20
CH4_150[T]	CH	0.095	4	3.8	-	150
CH4_A100_20[T]	CH	0.095	4	3.8	100	20
CH4_A100_150	CH	0.095	4	3.8	100	150

[a] Nominal thickness of textile in one direction based on the equivalent smeared distribution of fibres
[T] Full-scale T-beams

Table 6.1 presents the details of all specimens of Series B, whereas Fig. 6.2 illustrates the strengthening configurations adopted. One beam was tested as control specimen at

ambient temperature (CON), whereas four specimens were strengthened with TRM jackets. The notation of retrofitted specimens is XN_AP_T, where X denotes the type of the textile (CH for heavy carbon), N denotes the number of layers which was 4 for all retrofitted specimens and T denotes the temperature in which the specimens were exposed during the test (20 ^{o}C, 150 ^{o}C). 'AP' refers to specimens with anchors if any, with 'A' indicating anchors and 'P' denoting the anchorage percentage of the TRM jackets (100%). In specific, specimens CH4_20 and CH4_150 strengthened with 4 U-Wrapped heavy carbon TRM layers and tested at both ambient temperature (20 ^{o}C) and at 150 ^{o}C, respectively, whereas specimens CH4_A100_20 and CH4_A100_150 strengthened with 4 U-Wrapped heavy carbon TRM layers anchored by 100% (with fifteen anchors per side) and tested at both ambient temperature (20 ^{o}C) and at 150 ^{o}C, respectively.

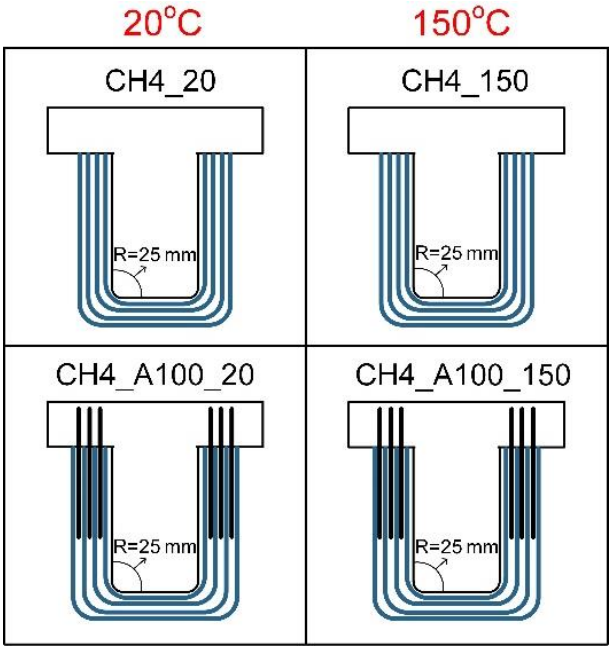


Figure 6.2. Schematic representation of different strengthening configurations adopted in full-scale T-beams.

The medium-scale beams were cast in groups of four using the same concrete mix design. The full-scale T-beam specimens were cast in one batch of ready-mix concrete. The compressive and the tensile splitting strength of concrete were obtained experimentally on the day of testing by conducting standard tests on cylinders of 150 mm-diameters and of 300 mm-height. The results are summarized in Table 6.2 (average values of 3 cylinders). Three different textile reinforcements, namely the

light-weight (CL), the heavy-weight (CH) and the glass fibre (G) textile (see Fig. 3.1) were used. As also mentioned in 5.1.2, seven layers of glass fibre textile are equivalent to one layer of carbon fibre textile in terms of axial stiffness. For the TRM jacketed specimens, the mortar described in Section 3.1 was used.

Table 6.2. Conrete and mortar strength of all specimens.

Specimen	Concrete Strength (MPa)		Mortar Strength (MPa)		
	Compressive strength	Tensile splitting strength	Compressive strength	Flexural strength	Tensile splitting strength
CON_20	21.6	2.36	-	-	-
CON_150	21.8	2.33	-	-	-
SB_MCH2_20	22.6	2.81	28.2	9.21	3.40
SB_MCH2_150	22.2	1.63	16.2	2.12	-
SB_MCH3_20	22.6	2.81	26.9	8.64	3.40
SB_MCH3_150	22.2	1.63	16.2	2.12	-
UW_MCH2_20	23.8	2.73	31.1	10.3	3.40
UW_MCH2_150	22.2	1.63	16.2	2.12	-
UW_MCH3_20	22.6	2.81	26.9	8.64	3.40
UW_MCH3_150	22.6	1.63	16.2	2.12	-
UW_MCH3_100	20.7	1.64	17.3	2.70	-
UW_MCH3_250	20.7	1.64	17.0	2.55	-
UW_MCL3_20	20.8	2.39	38.7	9.10	3.40
UW_MCL3_150	20.7	1.64	16.2	2.12	-
UW_MG7_20	20.0	1.80	35.5	8.10	3.40
UW_MG7_150	20.7	1.64	16.2	2.12	-
FW_MCH2_20	21.6	2.36	28.2	9.21	3.40
FW_MCH2_150	21.8	2.33	16.2	2.12	-
SB_RCH2_20	21.6	2.66	-	-	-
SB_RCH2_150	21.8	2.33	-	-	-
SB_RCH3_150	21.8	2.33	-	-	-
UW_RCH2_20	23.8	2.73	-	-	-
UW_RCH2_150	21.8	2.33	-	-	-
UW_RCH3_20	20.8	2.16	-	-	-
UW_RCH3_150	20.8	2.16	-	-	-
UW_RCH3_100	24.6	2.47	-	-	-
FW_RCH2_20	21.6	2.36	-	-	-
FW_RCH2_150	21.8	2.33	-	-	-
CON[T]	14.0	1.39	-	-	-
CH4_20[T]	14.0	1.39	36.1	8.12	3.40
CH4_150[T]	14.5	1.44	22.9	2.83	-
CH4_A100_20[T]	13.1	1.23	33.4	8.41	3.40
CH4_A100_150[T]	13.8	1.25	19.3	2.91	-

[T] Full-scale T-beams

Table 6.2 summarizes the compressive and flexural strength of the mortar (average values of 3 specimens), which were obtained experimentally on the day of

testing at various temperature levels (20 ºC, 100 ºC, 150 ºC or 250 ºC), whereas Fig. 6.3 illustrates the mortar flexural and compressive strength versus temperature curve (the tensile strength of mortar was not experimentally defined at high temperatures). Based on Fig. 6.3 both compressive and flexural strength of mortar decreased up to 150 ºC, whereas the strength of mortar at 250 ºC was improved compared to 150 ºC. Photos of the surface of the mortar prisms after their exposure to ambient and high temperature and before testing are depicted in Fig. 6.4. The cracking pattern at the surface of the mortar prism at each temperature is in agreement with the strength values. In other words, the surface of mortar prism exposed to 150 ºC had multiple cracks, whereas as expected the surface of mortar at ambient temperature (20 ºC) was uncracked.

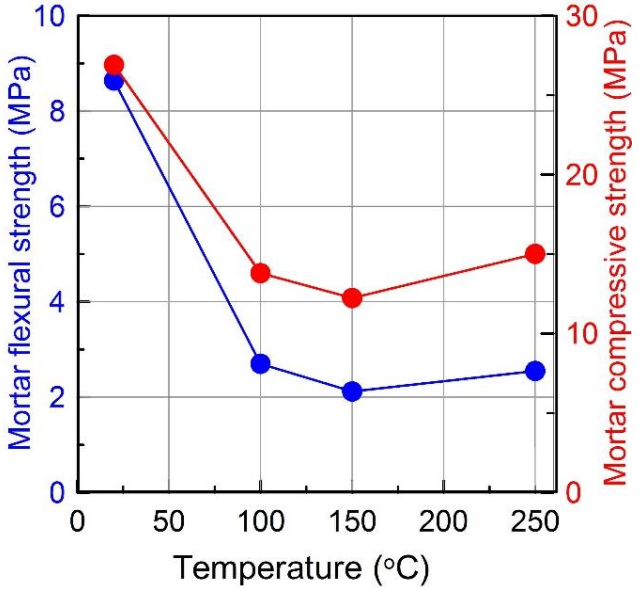


Figure 6.3. Effect of temperature on the mortar flexural strength.

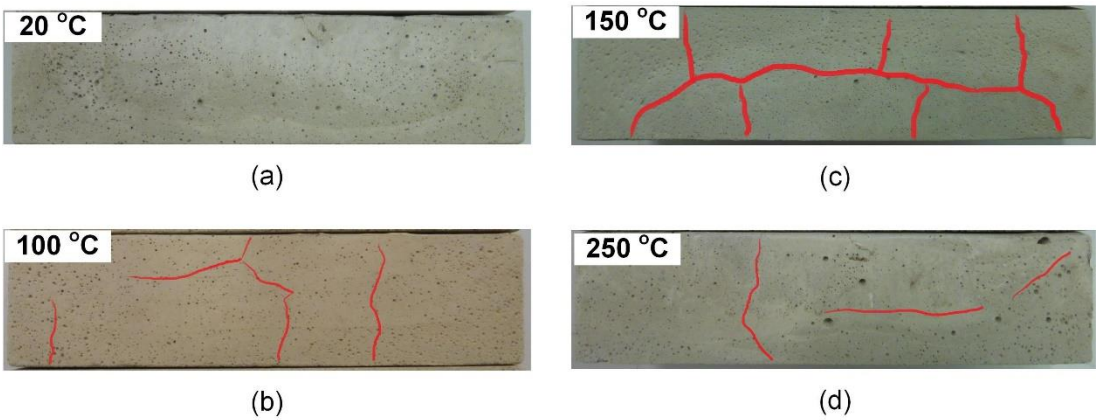


Figure 6.4. Photos of the mortar prisms surfaces after the exposure at different temperatures.

For the FRP retrofitted specimen, the epoxy resin mentioned in Section 3.2 was used. Finally, the strengthening procedure of medium-scale and full-scale T-beams was in details described in Section 4.1.1.2 and 5.1.5, respectively.

6.1.2 Experimental Setup and Procedure

All beams were subjected to monotonic three-point loading using a stiff steel reaction frame. Vertically positioned, 500 kN-capacity and 1000 kN-capacity servo-hydraulic actuators were used for the application of the load on the medium-scale rectangular beams and full-scale T-beams, respectively. The beams tested under high temperature were heated until the target high temperature was reached. After the target high temperature was reached the application of the monotonic loading started. The temperature was kept constant during loading.

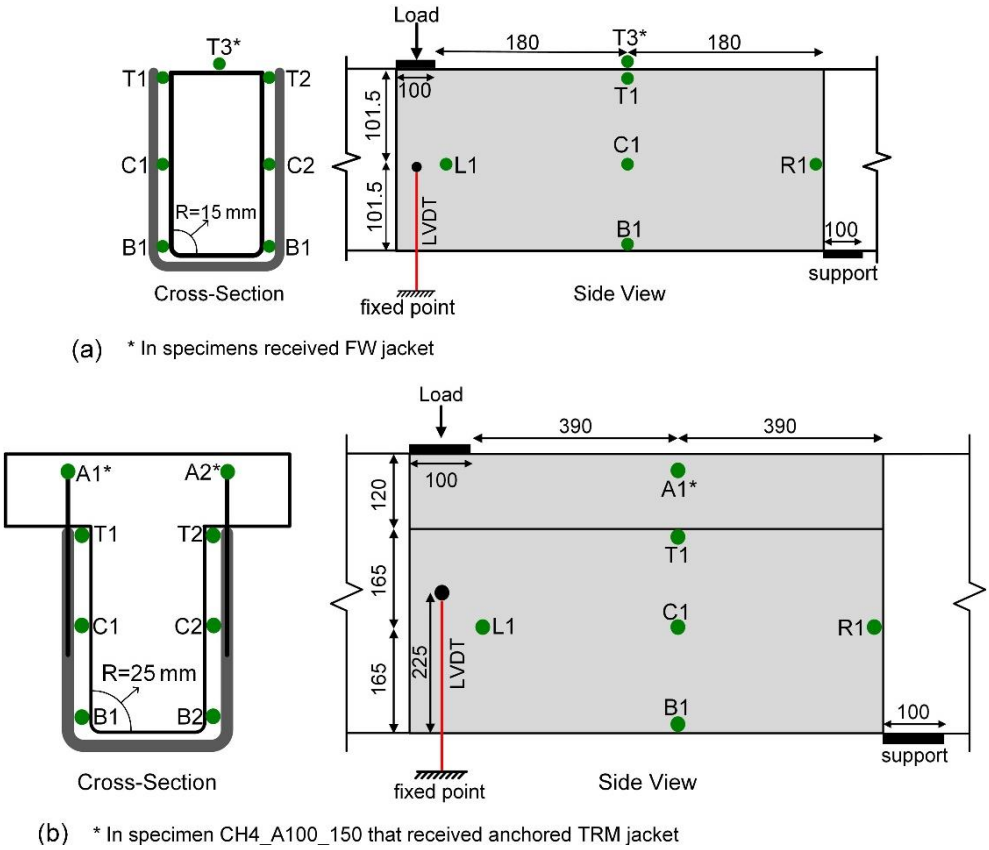


Figure 6.5. Configuration of all the thermocouples and the LVDT at the shear-critical span in (a) medium-scale rectangular beams and (b) full-scale T-beams.

The specimens of Series A and B were loaded at displacement rates of 0.02 mm/s and 0.01 mm/s, respectively. As illustrated in Fig. 6.5, for the specimens of Series A

and B respectively, the vertical displacement of the beam was measured at the position of load application using an external LVDT (Linear Variable Differential Transducer); the displacement measured from this sensor was used to plot the load-displacement response curves of the specimens.

The heating system used to provide heating in the critical shear span of medium-scale rectangular beams and full-scale T-beams is depicted in Fig. 6.6a and Fig. 6.6b, respectively. The heating system consists of eight 1000 W ceramic heaters of 60 mm height, 245 mm width and 30 mm thickness. The maximum surface temperature of each single heater is 700 ^{o}C and has 5000-10000 hours working life. Ceramic heaters were placed into steel cases that were fixed at a stainless steel frame, as shown in Fig. 6.6a and Fig. 6.6b. Four heaters were placed on each side of the beam at 100 mm distance from the beam surface. As shown in Fig. 6.6b, a protection steel cage was covering the area subjected to heating in order to prevent a possible touch of the jacket with the heaters after the failure of the specimen.

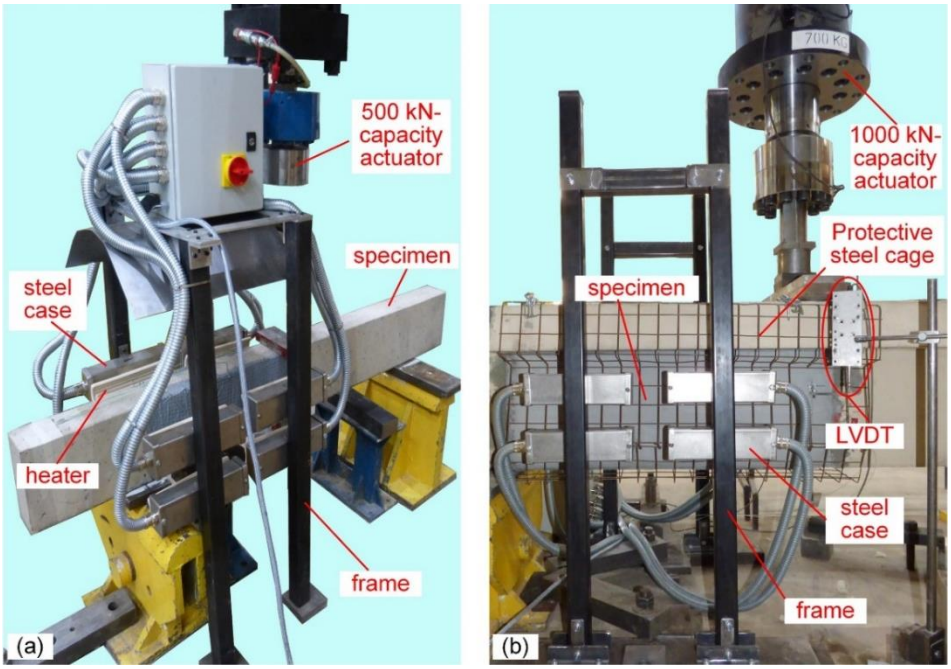


Figure 6.6. (a) Test set-up and heating system of medium-scale rectangular beams; (b) Test set-up and heating system of full-scale T-beams.

For specimens tested at high temperatures, ten (type K) thermocouples were affixed to the concrete surface (5 on each side) of the beam before the application of the strengthening system (Fig. 6.5a and b). Their distribution ensured that the desired temperature was reached along the critical shear span. In specimen CH4_A100_150,

two (one on each side) additional thermocouples (A1 and A2) were applied at the end of the dowel part of the central anchor (Fig. 6.5b); whereas in specimens FW_MCH2_150 and FW_RCH2_150 one additional thermocouple (T3) was applied at the top of the beam (Fig. 6.5a). The temperature of the beams was controlled by the central thermocouples (C1 and C2, Fig. 6.5a and b). All data was synchronized and recorded using a fully-computerized data acquisition system. It is noted that the maximum variation from the target temperature recorded on the beams sides was 4-5 ^{o}C, indicating the effectiveness of the heating system in developing even heating over the selected zone.

Time versus temperature curves for specimens that received three TRM (a-b) and FRP layers (c-d), respectively are presented in Fig. 6.7 a-d, based on the readings of thermocouples applied in both sides of the beams.

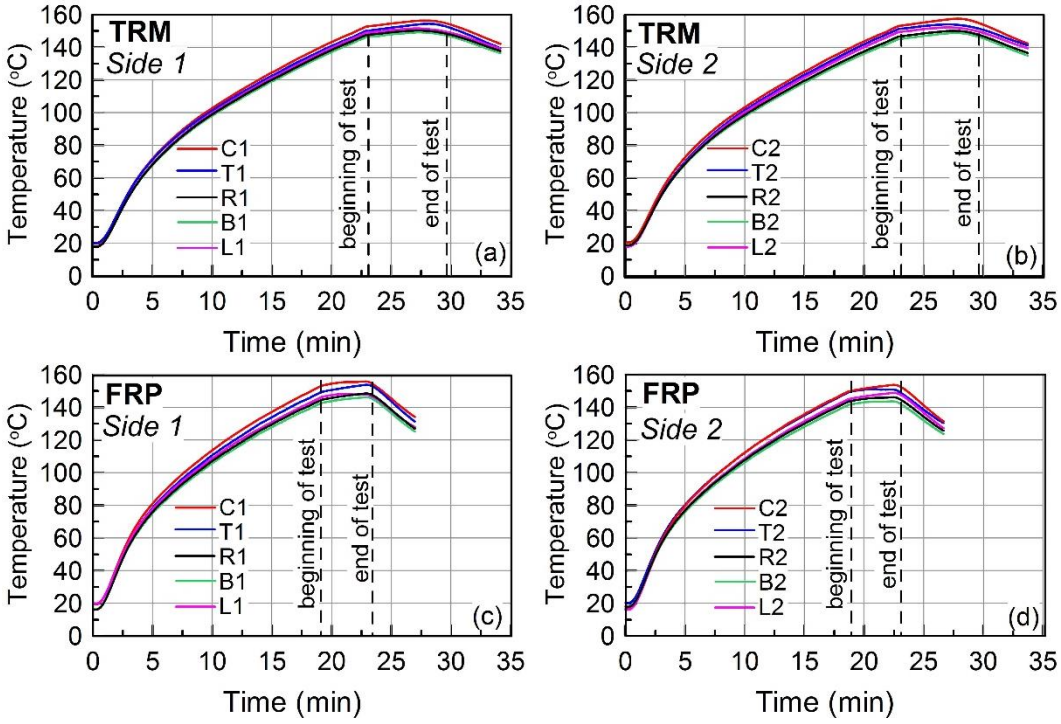


Figure 6.7. Time versus temperature curves for: (a-b) specimen that received three TRM carbon layers and (c-d) specimen that received three FRP carbon layers.

6.2 Experimental Results

A: Medium-scale rectangular beams

The response of all medium-scale beams strengthened with heavy carbon textile tested at 150 ^{o}C, as well as their counterparts tested at ambient temperature (that have been

already presented in Chapter 4) are presented in Fig. 6.8a-e in the form of load - displacement curves. Figures 6.8f and 6.8g present the load – displacement curves for specimens strengthened with light carbon and glass TRM jacketing, respectively. Key results of these specimens are presented in Table 6.3. They include for both ambient temperature and 150 ^{o}C: The peak load; the observed failure mode; the contribution of the jacket to the total shear resistance, V_f, which is calculated as the shear resistance of the strengthened specimen minus the shear resistance of the control specimen, $V_{R,con}$; the shear capacity increase due to strengthening, which is expressed by the ratio, V_f /$V_{R,con}$. The last column presents the reduction of the contribution of the jacket to the total shear resistance due to the effect of high temperature, which is expressed by the ratio, ($V_{f\,A.T.}$- $V_{f\,H.T.}$)/ $V_{fA.T.}$.

Figures 6.8 h and 6.8i present the load – displacement curves of specimens strengthened with three heavy carbon TRM and FRP layers, respectively and tested at different temperatures. In particular, both FRP and TRM-strengthened specimens tested at 100 ^{o}C and 150 ^{o}C, whereas a TRM specimen was additionally tested at 250 ^{o}C. Key results of the aforementioned specimens are also presented in Table 6.4. A detailed description of the results for control, FRP and TRM specimens at both ambient and high temperature follows.

The control beam at ambient temperature (CON_20) failed in shear at an ultimate load of 52 kN ($V_{R,con}$= 29.7kN) after the formation of a large shear crack in the critical span. The control beam tested at 150 ^{o}C (CON_150) failed in shear in identical manner with specimen CON_20, namely at the same ultimate load and by forming a large shear crack in the critical shear span (Fig. 6.9a). Thus, the response and failure mode of the un-retrofitted RC beam was not affected by its exposure to 150 ^{o}C.

All beams strengthened with SB or UW FRP jackets and tested at ambient temperature failed in shear at an ultimate load substantially higher than that of the control beam. The peak load attained by specimens SB_RCH2_20, UW_RCH2_20 and UW_RCH3_20 was 125, 126 and 139 kN, respectively, yielding 141%, 145% and 168% increase in the shear capacity. In all these specimens failure occurred due to FRP debonding, including peeling off of the concrete cover (i.e. Fig 6.9b). Specimen FW_RCH2_20 reached its ultimate moment capacity at a load of 152 kN and failed due to concrete crushing after yielding of the tensile longitudinal reinforcement.

All beams strengthened with SB or UW FRP jacketing and tested at 150 ºC failed in shear at ultimate loads dramatically lower than their counterparts tested at 20 ºC. The peak load attained by specimens SB_RCH2_150, SB_RCH3_150, UW_RCH2_150 and UW_RCH3_150 was 51, 51, 62 and 62 kN (Fig. 6.8a-d), respectively, resulting in 0%, 0%, 20% and 20% increase in the shear capacity. Thus, the contribution of the FRP jacket to the total shear resistance of the beam at 150 ºC decreased by 100%, 100%, 86% and 88%, respectively. In all these specimens, adhesive failures at the concrete-resin interface were observed (Fig. 6.9c-f). In specific, FRP jackets delaminated at the concrete-resin interface without peeling off of the concrete cover due to the poor bond behaviour of epoxy resin at temperature above the T_g. Finally, the fully wrapped specimen FW_RCH2_150 reached an ultimate load of 129 kN, which yields at least 22.8% decrease in the effectiveness of the FRP jacket. Failure of this specimen was due to slippage of the vertical fibre rovings (Fig. 6.9g) through the resin (which was completely decomposed due to high temperature) combined with delamination of the last textile layer used for overlapping at the top of the beam (Fig. 6.9h). The temperature recorded from the thermocouple placed at the top of the beam (T3, see Fig. 6.5a) at the instant of failure was 138 ºC.

Specimen UW_RCH3_100 reached a higher load (86 kN) with respect to specimen UW_RCH3_150 (62 kN) resulting in 67% increase in the shear capacity compared to the control specimen. The effectiveness of the FRP jacket decreased by 60% due to its exposure at 100 ºC. Adhesion failure at the resin-concrete interface was also observed in specimen UW_RCH3_100 (Fig. 6.9i) as was the case for specimen UW_RCH3_150 (Fig. 6.9e-f).

TRM jacketed specimens SB_MCH2_20, SB_MCH3_20, UW_MCH2_20, UW_MCH3_20, UW_MCL3_20 and UW_MG7_20, tested at ambient temperature, failed in shear at an ultimate load of 89, 109, 120, 131, 118 and 144 kN, respectively, resulting in 71%, 111%, 131%, 152%, 128% and 178% increase in the shear capacity. Failure in specimens SB_MCH2_20, SB_MCH3_20 and UW_MCH2_20 was attributed to debonding of the TRM jacket at a large part (approximately 2/3) of the shear span which was accompanied by peeling off of the concrete cover (Fig. 6.9j). Specimens UW_MCH3_20, UW_MCL3_20 and UW_MG7_20 failed in shear due to debonding of the U-jacket at the full-length of the shear span (Fig. 6.9k). Finally, specimen FW_MCH2_20 reached its ultimate moment capacity and (identically to FW_RCH2_20) failed in flexure due to concrete crushing at the compression zone.

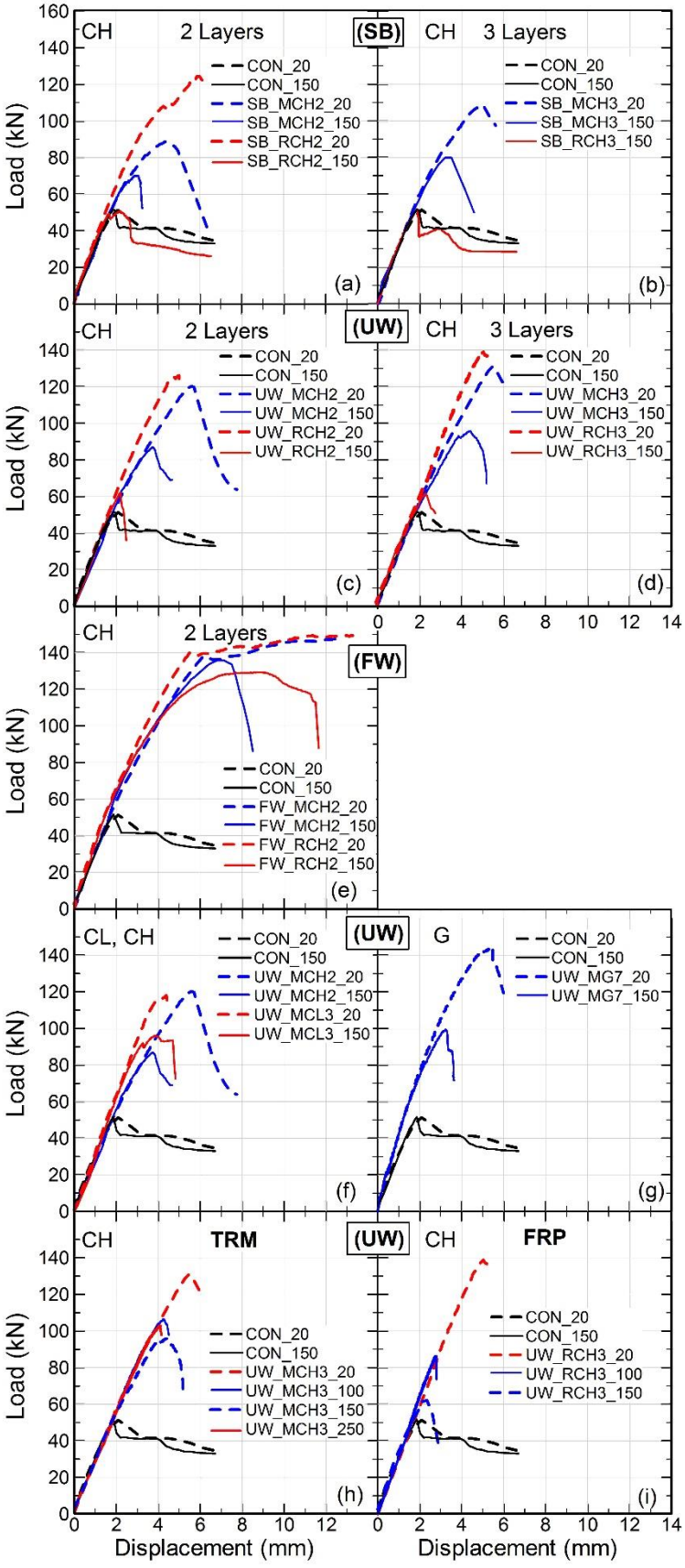


Figure 6.8. Load versus vertical displacement curves for all medium-scale rectangular beams.

Table 6.3. Summary of test results of beams tested at ambient temperature and at 150 ºC.

	Ambient Temperature (20ºC)				High Temperature (150ºC)				
Specimen	**Peak Load (kN)**	**Failure mode**	**V_f (kN)**	**V_f / $V_{R,con}$ (%)**	**Peak load (kN)**	**Failure mode**	**V_f (kN)**	**V_f / $V_{R,con}$ (%)**	**($V_f^{A.T.}$-$V_f^{H.T}$)/ $V_f^{H.T}$ (%)**
CON	52	shear [a]	-	-	52	shear [a]	-	-	-
SB_MCH2	89	shear [c]	21	71	70	shear [b]	11	37	47.6
SB_MCH3	109	shear [c]	33	111	81	shear [c]	17	57	48.5
UW_MCH2	120	shear [c]	39	131	87	shear [b]	20	67	48.7
UW_MCH3	131	shear [c]	45	152	96	shear [c]	25	84	44.4
UW_MCL3	118	shear [c]	38	128	96	shear [c]	25	84	34.2
UW_MG7	144	shear [c]	53	178	99	shear [c]	27	91	49.1
FW_MCH2	153	flexural	58[h]	195	136	shear [b]	48	162	17.2
SB_RCH2	125	shear [c]	42	141	51	shear [d]	0	0	100.0
SB_RCH3	-	shear [c]	-	-	51	shear [d]	0	0	100.0
UW_RCH2	126	shear [c]	43	145	62	shear [d]	6	20	86.0
UW_RCH3	139	shear [c]	50	168	62	shear [d]	6	20	88.0
FW_RCH2	152	flexural	57[h]	192	129	shear [e]	44	148	22.8
CON[T]	163	shear [a]	-	-	-	-	-	-	-
CH4[T]	288	shear [c]	95	77	249	shear [c]	66	53	30.5
CH4_A100[T]	473	shear [f]	236	190	319	shear [g]	119	96	49.6

[a] Tensile diagonal cracking; [b] Slippage of the vertical fibre rovings through the mortar; [c] Debonding of the jacket with peeling off of the concrete cover; [d] Adhesive failure at the resin-concrete interface; [e] Slippage of the vertical fibre rovings through the epoxy resin and delamination of the textile used for overlapping; [f] Pull-out of anchors due to concrete splitting in the slab; [g] Pull-out of all anchors due to adhesive bond failure; [h] Lower limit of V_f due to the flexural failure; [T] Full-scale T-beams.

Table 6.4. Summary of tests results of medium-scale beams tested at 20 ºC, 100 ºC, 150 ºC and 250 ºC.

	Specimen	**UW_MCH3**	**UW_RCH3**
Ambient temperature (20ºC)	**Peak Load (kN)**	131	139
	Failure mode	shear [a]	shear [a]
	V_f (kN)	45	50
	$V_f/V_{R,con}$ (%)	152	168
Elevated temperature 1 (100ºC)	**Peak Load (kN)**	107	86
	Failure mode	shear [a]	shear [b]
	V_f (kN)	31	20
	$V_f/V_{R,con}$ (%)	104	67
	($V_f^{A.T.}$-$V_f^{H.T.}$)/$V_f^{A.T.}$ (%)	31	60
Elevated temperature 2 (150ºC)	**Peak Load (kN)**	96	62
	Failure mode	shear [a]	shear [b]
	V_f (kN)	25	6
	$V_f/V_{R,con}$ (%)	84	20
	($V_f^{A.T.}$-$V_f^{H.T.}$)/$V_f^{A.T.}$ (%)	44	88
Elevated temperature 3 (250ºC)	**Peak Load (kN)**	103	-
	Failure mode	shear [a]	-
	V_f (kN)	29	-
	$V_f/V_{R,con}$ (%)	98	-
	($V_f^{A.T.}$-$V_f^{H.T.}$)/$V_f^{A.T.}$ (%)	36	-

[a] Debonding of the jacket with peeling off of the concrete cover; [b] adhesive failure at the resin-concrete interface.

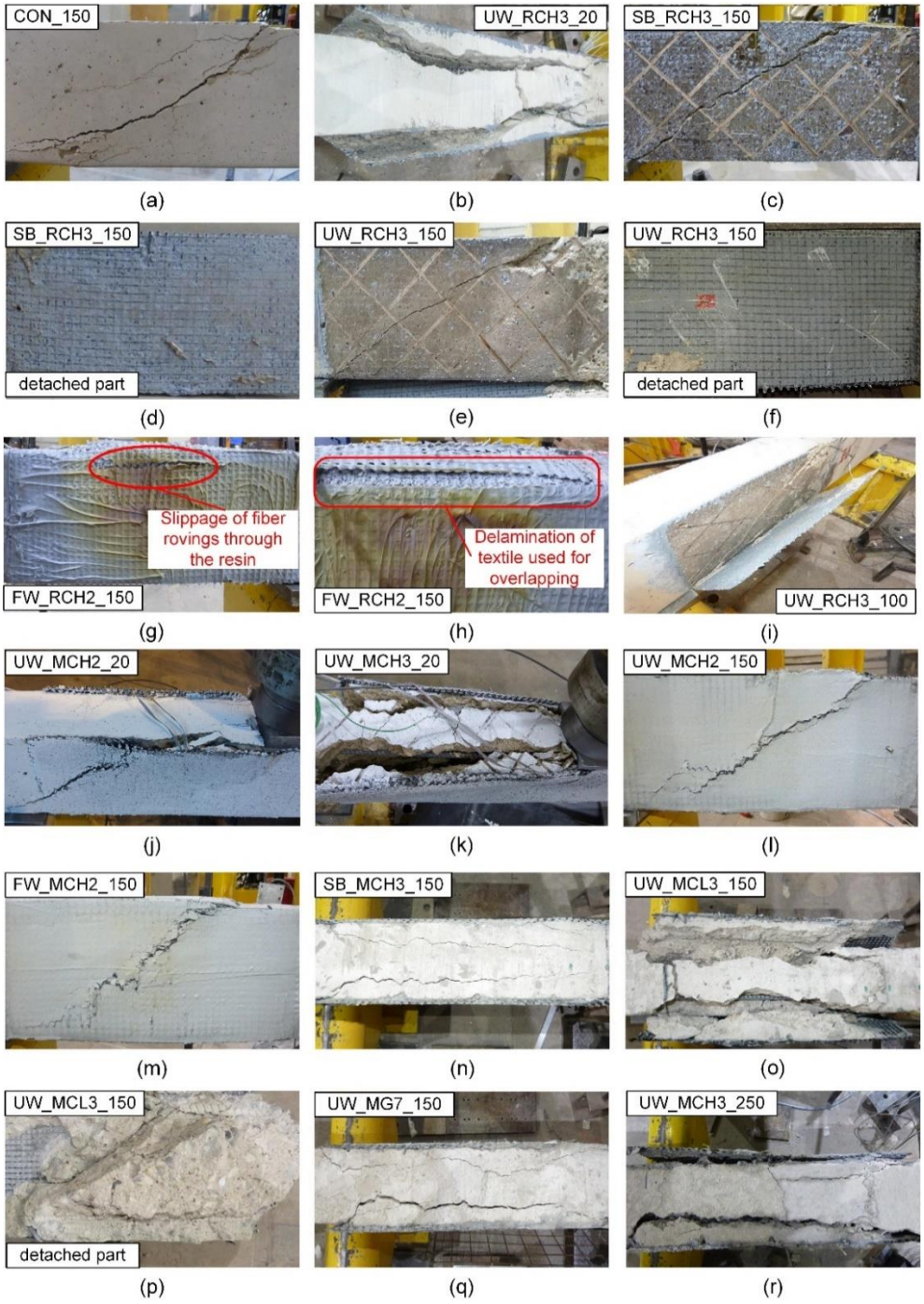


Figure 6.9. Failure modes of medium-scale rectangular beams: (a) CON_150 - dominant shear crack; (b) specimen UW_RCH3_20 - debonding of the jacket: peeling off of the concrete cover; (c)-(f) specimens SB_RCH3_150 and UW_RCH3_150 - adhesive failure at the resin-concrete interface; (g) specimen FW_RCH2_150 - slippage of the vertical fibre rovings through the epoxy resin; (h) specimen FW_RCH2_150 – delamination of textile used for overlapping; (i) specimen UW_RCH3_100 - adhesive failure at the resin-concrete interface; (j)-(k) specimens UW_MCH2_20 and UW_MCH3_20 - debonding of the jacket: peeling off of the concrete cover; (l)-(m) specimens UW_MCH2_150 and FW_MCH2_150 - local damage of the jacket; (n)-(r) specimens. SB_MCH3_150, UW_MCL3_150, UW_MG7_150 and UW_MCH3_250 - debonding of the jacket: peeling off of the concrete cover.

The behaviour of the TRM jacketed specimens at 150 ^{o}C was far better compared with their FRP counterparts. Specimens SB_MCH2_150, UW_MCH2_150, FW_MCH2_150, SB_MCH3_150, UW_MCH3_150, UW_MCL3_150 and UW_MG7_150, reached an ultimate load of 70, 87, 136, 81, 96, 96 and 99 kN, respectively, resulting in 37%, 67%, 162%, 57%, 84%, 84%, 91% increase of the shear capacity. The effectiveness of the TRM jacketing at 150 ^{o}C was decreased by 47.6%, 48.7%, 17.2%, 48.5%, 44.4%, 34.2% and 49.1%, respectively. The failure of specimens SB_MCH2_150, UW_MCH2_150 and FW_MCH2_150 strengthened with two layers of TRM jackets was associated with damage of the TRM jackets that included the following local phenomena: (a) slippage of the vertical fibre rovings through the mortar, and (b) partial rupture of the fibres crossing the shear crack (Fig. 6.9l-m). Finally, specimens SB_MCH3_150, UW_MCH3_150, UW_MCL3_150 and UW_MG7_150, which strengthened with 3 layers of carbon fibre or 7 of glass fibre textile, failed due to debonding of the TRM jacket from the concrete substrate with peeling off of the concrete cover (Fig. 6.9n-q), demonstrating good bond between the concrete substrate and the TRM jacket at high temperature.

The peak load attained by specimens UW_MCH3_100 and UW_MCH3_250, at 100 ^{o}C and 250 ^{o}C, respectively, was 107 kN and 103 kN, yielding 104% and 98% increase in the shear capacity. The contribution of the jacket to the total shear resistance of the beam decreased by 31% and 36%, respectively compared to the corresponding specimen tested at ambient temperature. Failure of these specimens was due to debonding of the jacket from the concrete substrate with peeling off of the concrete cover (i.e. Fig. 6.9r) identically to specimen UW_MCH3_150 (Fig. 6.9o).

Series B: Full-scale T-beams

The load-displacement curves of the full-scale specimens are presented in Fig. 6.10. Key results are also presented in Table 6.3. The control beam (CON) tested at ambient temperature failed in shear at an ultimate load of 163 kN ($V_{R,con}$=124kN). A large shear crack was firstly formed in the web of the critical shear span (Fig. 6.11a), which was then propagated into the flange of the T-beam and resulted in significant load drop. It was decided to not test a control beam at 150 ^{o}C, as based on the test results of Series A, the response of the un-retrofitted RC beam was not affected at this temperature.

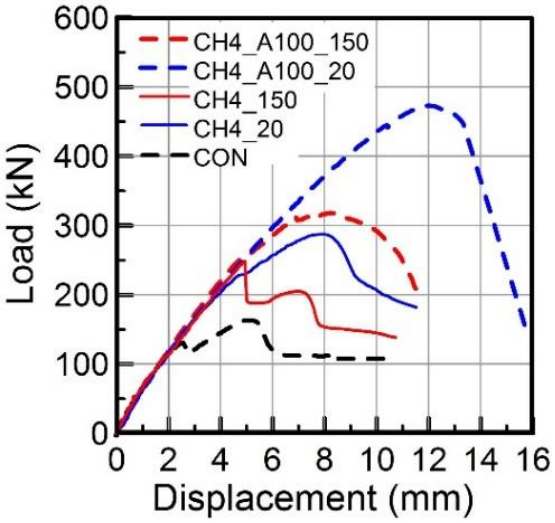


Figure 6.10. (a) Load versus vertical displacement curves for full-scale T-beams.

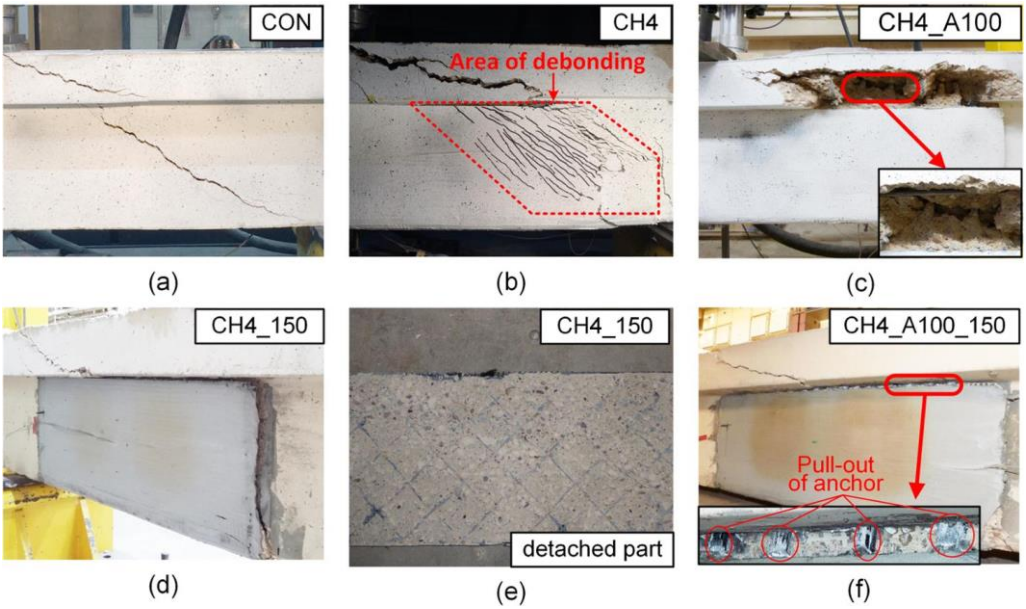


Figure 6.11. Failure modes of full-scale T-beams: (a) Dominant shear crack in the control beam; (b) specimen CH4 - debonding of the TRM jacket: peeling off of the concrete cover; (c) failure of specimen CH4_A100 due to concrete splitting in the slab; (d) debonding of the TRM jacket in specimen CH4_150: peeling off of the concrete cover; (e) specimen CH4_150 - detached part of TRM jacket including concrete cover; (f) specimen CH4_A100_150 - pull-out of all anchors due to bond adhesive failure.

The two TRM strengthened specimens tested at ambient temperature failed in shear and displayed considerably higher shear resistance compared to the control specimen. In particular, specimen CH4_20 reached an ultimate load of 288 kN, resulting in 77% increase in the shear capacity compared to the control specimen. Its failure was due to debonding of the TRM jacket at a large part (approximately 2/3) of

the shear span (Fig. 6.11b), which was also accompanied by peeling off of the concrete cover. Specimen CH4_A100_20 that had anchors failed in shear at an ultimate load of 473 kN, yielding 190% increase in the shear capacity, with respect to the control specimen. Failure of specimen CH4_A100_20 was attributed to anchors pull-out (8 on each side) due to concrete splitting at the two flanges (Fig. 6.11c).

The two TRM jacketed specimens tested at 150 ^{o}C failed in shear displaying considerably higher shear resistance compared to the control specimen but lower shear resistance with respect to the corresponding specimens tested at ambient temperature. Specimens CH4_150 and CH4_A100_150 reached an ultimate load of 249 kN and 319 kN, resulting in 53% and 96%, respectively increase in the shear capacity. The effectiveness of the TRM jacketing decreased by 30.5% and 49.6%, respectively, compared to the corresponding specimens tested at ambient temperature. The failure of specimen CH4_150 was due to debonding of the TRM jacket from the concrete substrate (Fig. 6.11d) including peeling off of the concrete cover (Fig. 6.11e). Finally, the failure of specimen CH4_A100_150 was attributed to debonding of the jacket including peeling off of the concrete cover due to failure of anchors (Fig. 6.11f). In particular, all anchors were pulled-out due to the softening and decomposition of the epoxy resin used to fill the holes into which the dowel part of anchors was anchored, as the mean temperature at the top of central anchors (as this was recorded from the thermocouples A1 and A2, Fig. 6.5b) was 128 ^{o}C, namely well above from the T_g (82 ^{o}C) of the epoxy resin.

6.3 Discussion

6.3.1 Effect of investigated parameters for medium-scale beams tested at high temperature

All specimens tested at high temperature failed in shear, allowing for the evaluation of the effectiveness of all strengthening systems. In terms of the various parameters investigated in this experimental programme, an examination of the results in terms of shear capacity and failure modes, revealed the following information.

6.3.1.1 *Matrix Material (TRM vs. FRP Jackets)*

The matrix material (mortar vs epoxy resin) significantly affects the response of the strengthened beams at high temperature. In the following paragraphs, the effect of the adhesive material on the performance of jacketed specimens exposed to high temperature is studied, as (a) the strengthening configuration, (b) the number of layers and (c) the temperature to which the specimens are exposed vary.

(a) Strengthening Configuration

The curves in Fig. 6.12a illustrate the effect of the strengthening configuration (SB, UW or FW) on the shear capacity enhancement (V_f / V_{con} x100%) at 150 ºC. In FRP-strengthened specimens, the shear capacity was only increased by 6kN (20%) when UW jackets were applied instead of SB ones for both 2 and 3 layers. On the other hand in TRM-strengthened specimens, the effectiveness of the UW jackets (expressed as the shear capacity enhancement) was 1.81 and 1.47 times the effectiveness of the SB jackets for 2 and 3 layers, respectively. FW jacketing was the most effective configuration for both strengthening systems. In particular, the effectiveness of the FW jacket was 2.4 and 7.3 times the UW jacket effectiveness in case of two TRM and FRP layers, respectively. The effect of SB and UW configurations on the shear capacity enhancement at high temperature was quite similar to this observed at ambient temperature for both TRM and FRP systems, whereas the benefit of applying FW was more pronounced at high temperature than ambient temperature for both strengthening systems (TRM, FRP).

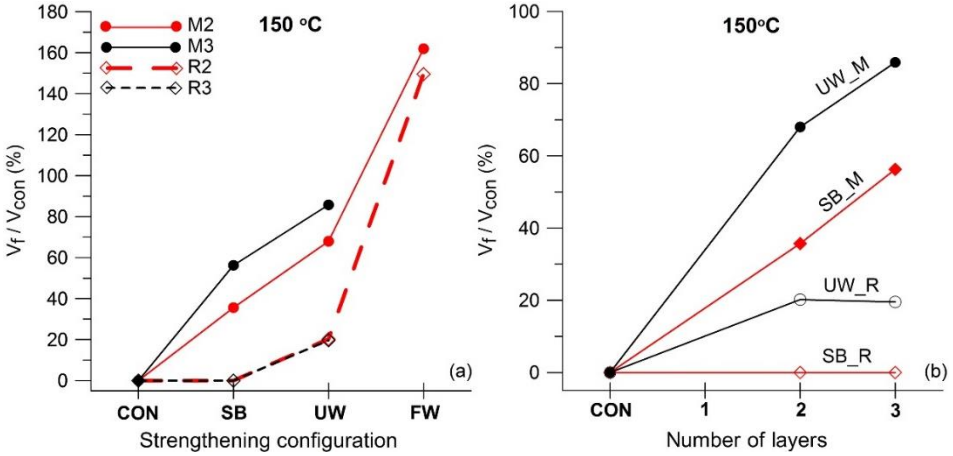


Figure 6.12. (a) Effect of strengthening configuration on the shear capacity enhancement at high temperature; (b) effect of number of layers on the shear capacity enhancement at high temperature.

(b) Number of layers

The effect of the number of layers on the shear capacity enhancement for SB and UW strengthening configurations under high temperature conditions is illustrated in Fig. 6.12b. Increasing the amount of reinforcement from 2 to 3 layers, resulted in 1.55 and 1.25 higher V_f for the beams received SB and UW TRM jackets, respectively. Zero increase in the shear capacity was observed when resin was used as binder for both SB and UW jackets.

When the number of layers was increased from two to three, a change in the failure mode was witnessed in TRM-strengthened specimens tested at high temperature. In particular, the beams received 2 layers of SB and UW TRM jackets failed due to local damage (the vertical fibre rovings crossing the developed shear crack at the jacket experienced a combination of slippage through the mortar and partial rupture Fig. 6.9l-m). Contrary, the failure mode of specimens received three SB and UW layers is associated to debonding of the jacket from the concrete substrate. Thus, the increase in the number of layers prevented these local phenomena and as a result the damage was shifted to the concrete substrate. This is attributed to the better mechanical interlock conditions created by the overlapping of multiple textile layers as also reported in [Raoof and al. 2016, Tetta et al. 2015 (Section 4.1) and Tetta et al. 2016 (Chapter 5)]. The failure mode of SB and UW FRP-strengthened specimens tested at high temperature was not affected from the increase in the number of layers.

It worth's mentioning that in case of the TRM system, this change in failure mode (from local damage of the TRM jacket to its debonding), witnessed here in specimens with 2 and 3 layers tested at high temperature, was also observed for an increase from 1 to 2 layers in specimens tested at ambient temperature, as reported by Tetta et al. (2015). Local damage of the jacket is observed in case of poor mechanical interlock which is affected from the textile geometry [see Tetta et al. (2016) and Section 4.2), the number of layers (Raoof et al. 2016 and Tetta et al. 2015) and the mortar strength. In specimens received 1 TRM layer and tested at ambient temperature, the textile geometry, namely the sparse-mesh pattern of the heavy-carbon textile, mainly caused the slippage of the vertical rovings through the mortar which was although prevented when at least two TRM layers were applied (Tetta et al. 2015).

For specimens received two SB or UW TRM layers and tested at high temperature, the decrease of the mortar strength at high temperature caused damage in

the TRM jacket and impaired the mechanical interlock effect activated in Tetta et al. (2015) for two TRM layers. At high temperature, the mechanical interlock beneficial effect reappeared when specimens received three SB or UW TRM layers.

(c) Temperature

The effect of high temperature on the shear capacity enhancement for specimens received 3 UW layers is depicted in Fig. 6.13. The effectiveness of the FRP strengthening system was dramatically reduced from the temperature increase. In specific, the contribution of the FRP jacket to the shear resistance decreased by 60% and 88% when the temperature increased from 20 ^{o}C to 100 ^{o}C and 150 ^{o}C, respectively. The failure mode of both specimens tested at high temperature (UW_RCH3_100 and UW_RCH3_150) was attributed to adhesive failure at the interface between the FRP jacket and the concrete substrate. Thus, the bond between the FRP jacket and the concrete substrate at 100 ^{o}C was better than this experienced at 150 ^{o}C (as this reflected at the shear capacity increase) but not good enough to shift the failure from the interface (between the jacket and the concrete) to the concrete substrate, as occurred at the corresponding specimen tested at ambient temperature.

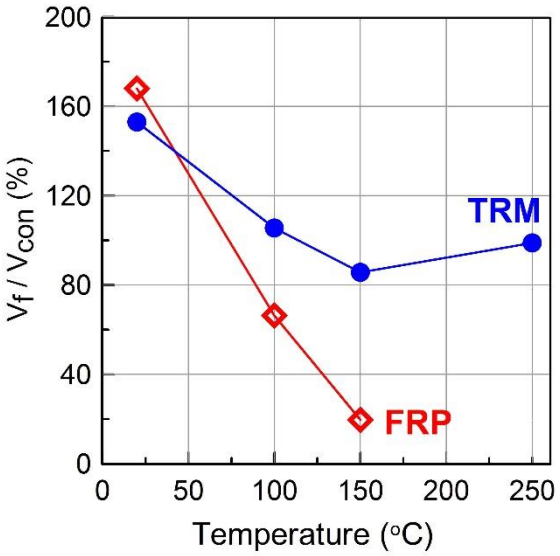


Figure 6.13. Effect of temperature on the shear capacity enhancement for both TRM and FRP system.

The effectiveness of specimens strengthened with 3 TRM layers and tested at 100 ^{o}C, 150 ^{o}C and 250 ^{o}C decreased by 31%, 44% and 36%, respectively. It is striking to note that by increasing the temperature from 150 ^{o}C to 250 ^{o}C, the contribution of

TRM jacket to the shear resistance increased by 16% (Fig. 6.13). This could be attributed to flexural and compressive strength of mortar, which as shown in Fig. 6.3, at this temperature range, follows a quite similar trend with this of shear capacity enhancement (V_f/V_{con}). Finally, the exposure of TRM-strengthened specimens at different high temperature levels (100 ºC, 150 ºC and 250 ºC) had no effect on the failure mode that was debonding of the jacket from the concrete substrate.

6.3.1.2 Textile properties (geometry, material)

Specimens UW_MCH2_150 and UW_MCL3_150 received correspondingly 2 and 3 layers carbon textile of different geometry, having although the same amount of external reinforcement (ρ_f =1.9‰). The light carbon textile used in specimen UW_MCL3 has denser mesh-pattern than the heavy carbon textile (Fig. 3.1a and b). The shear capacity increase of both specimens tested at ambient temperature was almost the same and their failure was due to debonding of the TRM jacket from the concrete substrate.

A comparison of the results for specimens UW_MCH2_150 and UW_MCL3_150 shows that the textile geometry can affect the failure mode of specimens exposed to high temperature. In specific, UW_MCH2_150 specimen failed due to local damage of the TRM jacket (Fig. 6.9l) in contrary to specimen UW_MCL3_150 that failed due to debonding of the TRM jacket from the concrete substrate (Fig. 6.9o). The difference in failure mode is possibly associated with the dense mesh-pattern of the light-carbon textile used in specimen UW_MCL3_150, which resulted in better fibres distribution along the shear span and therefore the mechanical interlock between the textile and the mortar was improved. Thus, the local damage of the jacket was prevented in specimen UW_MCL3_150 thanks to the better mechanical interlock conditions despite the decreased (due to the high temperature) mortar strength. The shear capacity increase of specimens UW_MCH2_150 and UW_MCL3_150 was 67% and 84%, respectively compared to the control specimen.

Specimen UW_MG7 strengthened with seven glass textile layers had higher shear capacity than specimen UW_MCH3 that received three heavy carbon textile layers, at both ambient and high temperature, despite the fact that seven glass textile layers are equivalent to just one heavy-carbon textile layer (in terms of axial stiffness). In specific, the shear capacity increase of specimens UW_MG7_20 and

UW_MCH3_20 tested at ambient temperature was 178% and 152%, respectively. The corresponding values for specimens tested at 150 ºC was 91% and 84%, respectively. All specimens exhibited similar failure mode at both ambient and high temperature, namely debonding of the TRM jacket from the concrete substrate.

6.3.2 Performance of full-scale T-beams strengthened with TRM jackets at 150 ºC

The effectiveness of TRM jacketing in shear strengthening of full-scale beams remained high at 150 ºC. In particular, in specimen CH4_150 tested at 150 ºC, four heavy carbon TRM layers increased the shear capacity of the beam by 53% compared to the control specimen. The contribution of the TRM jacket to the shear resistance decreased by 30.5% compared to the corresponding specimen tested at ambient temperature. In specimen CH4_A100_150 tested at 150 ºC, the full anchorage of four heavy carbon layers provided by 15 anchors per beam's side improved the effectiveness of the TRM jacket by 80.3% compared with its counterpart specimen without anchors (CH4_150), resulting in 119% increase in the shear resistance compared to the control specimen. The exposure of specimen at 150 ºC (CH4_A100_150) resulted in 49.6% decrease in the effectiveness of the anchored TRM jacket.

The T-beam ends received non-anchored jackets (CH4_20, CH4_150) exhibited identical failure mode, namely debonding of the TRM jacket from the concrete substrate, at both ambient temperature and 150 ºC. In specimens received anchored TRM jacket, anchors were pulled-out from the slab at both ambient temperature and at 150 ºC due to concrete splitting in the slab (CH4_A100_20) and melting of the resin in the anchorage holes (CH4_A100_150), respectively.

6.4 Stress reduction factor for TRM and FRP systems

For calculating the FRP contribution to the shear capacity of RC members most of the design models use the effective stress of the FRP (σ_{eff}), which can ideally be described as the average stress of the fibres crossing the shear crack. The effective stress of the jacket, σ_{eff} is calculated using Eq. (6.1). The experimental values of V_f were calculated according to the approach that the concrete and jacket contribution are superimposed.

$$\sigma_{eff} = V_f / \left(\rho_f b_w 0.9d\right) \tag{6.1}$$

For T-beam specimens, the term 0.9*d* in Eq. (6.1) is replaced from the term d-h_s, where d is the effective depth of the section and h_s the depth of the slab.

The effective stress of FRP or TRM jackets at high temperature, σ_{eff}, high, is a reduced value of their effective stress, σ_{eff}, at ambient temperature. It is expressed by the following equation:

$$\sigma_{eff,high} = k_t \sigma_{eff} \tag{6.2}$$

where k_t is the stress reduction factor with values less than 1.0.

Table 6.5. Experimental values of effective stress and stress reduction factors for TRM and FRP jackets.

		σ_{eff} (MPa)	$\sigma_{eff,high}$ (MPa)	
		Ambient Temperature	**150 ºC**	k_t
TRM	**SB_MCH2**	347	182	0.52
	SB_MCH3	363	187	0.52
	UW_MCH2	644	330	0.51
	UW_MCH3	496	275	0.56
	UW_MCL3	641	422	0.66
	UW_MG7	489	540	0.51
	CH4	477	328	0.69
	CH4_A100	1177	591	0.50
		Ambient Temperature	**100 ºC**	
	UW_MCH3	496	341	0.69
		Ambient Temperature	**250 ºC**	
	UW_MCH3	496	319	0.64
		Ambient Temperature	**150 ºC**	
	FW_MCH2*	958	793	0.83
FRP	**SB_RCH2**	694	0	0.00
	SB_RCH3	-	0	0.00
	UW_RCH2	710	99	0.14
	UW_RCH3	551	66	0.12
		Ambient Temperature	**100 ºC**	
	UW_RCH3	551	220	0.40
		Ambient Temperature	**150 ºC**	
	FW_RCH2**	942	727	0.77

* the temperature at the top of the beam was 136 ºC at the instant of the peak load.
** the temperature at the top of the beam was 138 ºC at the instant of the peak load.

The values of the effective stress of TRM and FRP jackets at both ambient and high temperature, σ_{eff} and $\sigma_{eff,\,high}$, respectively are given in Table 6.5. In addition, Table 6.5 includes the stress reduction factor, k_t.

In this study, k_t value varies with the strengthening system (TRM, FRP), the strengthening configuration (SB, UW and FW) and the level of high temperature (100 ^{o}C, 150 ^{o}C or 250 ^{o}C). In particular, for TRM jackets, k_t varies from 0.50, which corresponds to four fully anchored TRM layers (applied to full-scale T-beam) exposed to 150 ^{o}C to 0.83 which corresponds to two layers of FW jacket exposed at 150 ^{o}C. In case of FRP jackets, k_t significantly varies from 0 and 0.14 for both two and three layers of SB and UW jackets, respectively tested at 150 ^{o}C to 0.77 which corresponds to two FW layers tested at 150 ^{o}C. Hence, TRM jackets are more effective than FRP jackets at high temperature, but the effectiveness is sensitive to parameters such as the strengthening configuration and the level of high temperature.

Based on the results of this study, the use of SB or UW FRP jackets is not recommended for shear strengthening of RC beams when fire or high temperature is a critical issue in the design, unless protective (thermal insulation) systems are provided. The fully-wrapped FRP jacket remained quite effective at high temperature. However, the use of closed jackets is not feasible in beams of typical RC buildings or bridge girders due to the presence of concrete slabs or decks, respectively.

SB and UW (both non-anchored and anchored) TRM jackets are applicable for shear strengthening of RC beams exposed to high temperature. Based on the limited experimental data of the present study and before more experimental data will be available, a value of k_t equal to 0.4 could be used for design beams strengthened in shear with TRM jacketing in case of their exposure to high temperature (up to 250 ^{o}C).

6.5 Summary

This chapter presents a large experimental investigation on the effectiveness of TRM jackets in shear strengthening of both medium-scale rectangular RC beams and full-scale RC T-beams at high temperature. The main investigated parameters studied on medium-scale rectangular beams include: (a) the strengthening system (TRM or FRP), (b) the level of high temperature to which the specimens are exposed (20 ^{o}C, 100 ^{o}C, 150 ^{o}C, 250 ^{o}C), (c) the strengthening configuration (side-bonding, U-wrapping and full-wrapping), (d) the number of jacketing layers (2 and 3) and (e) the textile

properties (geometry, material), whereas the effectiveness of both non-anchored and anchored TRM jackets in shear strengthening of full-scale T-beams at high temperature was also studied. The main conclusions drawn from this chapter are summarized as follows:

- TRM is much more effective in increasing the shear capacity of RC beams subjected to high temperature than FRP jacketing.
- The strengthening configuration affects considerably the shear capacity increase for both TRM and FRP jackets at high temperature. In specific, fully-wrapping (FW) is the most effective strengthening configuration, following by U-wrapping (UW), whereas side-bonding (SB) is the less effective strengthening configuration, for both TRM and FRP jackets.
- The failure mode of SB and UW TRM jacketed specimens tested at high temperature is altered for different number of layers. Increasing them from 2 to 3, prevented the local damage of the TRM jacket and shifted it to the concrete surface. On the other hand, the increase in number of layers has no effect on the shear capacity increase nor the failure mode of SB and UW FRP jackets.
- The exposure of specimens strengthened with 3 layers of TRM or FRP to high temperatures (100 ^{o}C, 150 ^{o}C, 250 ^{o}C) had no effect on their failure mode. The effectiveness of FRP jackets dropped dramatically by increasing the temperature from 100 ^{o}C to 150 ^{o}C. On the other hand, the effectiveness of TRM jackets is marginally affected from their exposure to high temperatures, namely from 100 ^{o}C to 150 ^{o}C and 250 ^{o}C, respectively.
- For TRM strengthened members tested at high temperature, the denser geometry in the carbon textile is more effective in shear strengthening of concrete members.
- Both non-anchored and anchored U-wrapped TRM jackets applied at full-scale T-beams remained very effective at high temperature. The shear capacity increase of non-anchored TRM jacket decreased by 30.5% due to its exposure at 150 ^{o}C, whereas the failure mode was not affected. The use of anchors increased the effectiveness of the TRM jacket by 80% despite the pull-out of anchors due to adhesive bond failure caused from the high temperature.

Chapter 7

ANALYTICAL MODELS FOR THE CALCULATION OF THE CONTRIBUTION OF THE TRM JACKETING TO THE TOTAL SHEAR RESISTANCE (V_f) OF RC BEAMS

Abstract

TRM is a very promising alternative to the FRP retrofitting solution for shear strengthening of RC beams, based on the experimental results presented in this study. Thus, development of reliable and accurate design models for shear strengthening of concrete members with TRM is required for enabling their wide use in real applications. The available experimental data in the literature are limited and, in most cases, a detailed description of the failure modes observed at the TRM jackets and information related to the characteristics of the textile material and the mortar strength are missing, complicating the development of design guidelines. In this chapter, design models to calculate the contribution of the TRM jacket to the total shear resistance were developed using all the well reported available data that were grouped based on the observed failure mode. Specifically, local damage of the jacket including slippage of the vertical fibres through the mortar constitutes a recurring failure mode in concrete beams strengthened in shear with TRM jackets, apart from debonding or fracture of TRM jacketing that are also observed in case of FRP jacketing. The key parameters affecting each failure mode were defined and design formulations to calculate the contribution of the TRM jacket to the total shear resistance of RC beams for each failure mode were suggested, whereas a criterion indicating when each failure mode is possible to be observed was also set for using the proper formulation for each TRM system.

7.1 Introduction

The use of TRM for strengthening existing RC members has been widely studied the last decade. This study investigates the use of TRM for shear strengthening of RC beams, examining a variety of parameters. TRM is a very promising alternative to the FRP retrofitting solution, based on the experimental results presented in the previous chapters of this study and the experimental data that are available from other published studies on shear strengthening of RC beams with TRM. However, developing reliable and accurate design models for shear strengthening of RC beams with TRM is required for enabling the wide use of TRM in real applications. The available experimental data in the literature are extremely limited and in most cases, a detailed description of the failure modes observed at the TRM jackets and information related with the characteristics of the textile material (i.e. thickness, mesh size, roving geometry and ultimate stress) and the mortar strength are missing, complicating even more the development of design models.

It is well known that the most common failure modes of RC beams strengthened in shear with FRP jackets (tested at ambient temperature) are: (a) debonding of the FRP jackets with peeling off of the concrete cover, in case of SB or UW FRP jackets and (b) fracture of FRP jacketing mainly observed in FW jackets or glass, basalt and aramid SB or UW jackets. Sometimes, delamination of SB or UW FRP jackets in the concrete – resin interface (adhesion failure) is also experienced. The aforementioned failure modes of RC beams received FRP jackets were also observed in RC beams strengthened in shear with TRM jackets. However, in case of TRM jacketing, local damage of the jacket including slippage of the vertical fibres through the mortar constitutes a recurring failure mode. As also mentioned in previous chapters, TRM is as effective as FRP jacketing in increasing the shear capacity of RC beams when failure is associated with debonding of the jacket, whereas TRM is less effective than equivalent in terms of ρ_f FRP system when failure is attributed to local damage of the jacket instead of debonding. Therefore, it is really important to illuminate the failure mode associated with the local damage of the TRM jacket and specify TRM systems that are prone to slippage of the fibre rovings through the mortar. Thus, in this chapter, the parameters affected local damage of the TRM jacket are defined and design models for the calculation of the contribution of TRM jacketing to the total shear resistance

of RC members are developed taking into account the TRM characteristics (textile geometry and mortar strength). Details are provided in the following sections.

7.2 Failure of strengthened specimens due to debonding of the TRM (or FRP) jacket

Based on the results presented in this study (see Chapter 4 and 5), TRM jackets are as effective as FRP jackets when local damage of the TRM jackets (slippage of fibres through the mortar and partial rupture of fibres crossing the shear crack) is prevented and the failure is attributed to debonding of the TRM jacketing from the concrete substrate. Therefore, the formulas that have been developed so far for the prediction of the contribution of the FRP jacketing to the total shear resistance, V_f could be also used for TRM jackets in case of failure due to debonding. A variety of models have been suggested so far for the calculation of the contribution of the FRP jacket to the total shear resistance, V_f. In particular, initially some regression-based models were suggested, expressing the effective strain of the FRP jacketing (or the ratio of the effective strain to the ultimate strain of fibres, R) as a function of its axial rigidity, $\rho_f E_f$ (i.e. Khalifa et al. 1998, Triantafillou 1998 and Adhikary et al. 2004), usually combined with the concrete compressive strength (i.e. Triantafillou and Antonopoulos 2000). Following the regression-based models, mechanics-based models were also developed (i.e. Chen and Teng 2003, Carolin and Taljsten 2005 and Monti and Liotta 2007) in an attempt to predict in more accuracy the contribution of the FRP jacket to the total shear resistance.

Chen and Teng 2003 model is one of the most accurate models for the prediction of the contribution of the FRP jacket to the total shear resistance. Chen and Teng model can be applied for both SB and UW jackets, both strips and continuous sheets and it takes into account the axial rigidity of the FRP jacket ($\rho_f E_f$). Furthermore, the available bond length is considered in this model (as also in all the mechanism-based models), resulting in more accurate results for both rectangular beams and T-beams contrary to the regression-based models. Finally, Chen and Teng model has been derived from (single or double-lap) direct shear tests and therefore it had been already verified with bond test results. Based on Lima and Barros 2007, the Australian guidelines provisions CIDAR (CT) Design Proposal (2006) that is based on Chen and Teng model had very good performance from a statistical point of view compared with

other design guidelines [*fib* 2001, the Italian guidelines provisions, CNR Design Proposal (2004) and ACI design proposal] as it combines an appropriate global safety factor with the one of most least scattered behaviors. For all the aforementioned reasons, Chen Teng model was selected to be used in this Chapter for the prediction of the contribution of both TRM and FRP jackets to the total shear resistance, V_f as TRM jackets are as effective as FRP jackets when failure is attributed to debonding of the jacket with peeling off of the concrete cover, as also mentioned before. A short description of the Chen Teng model follows:

The general equation of Chen and Teng model, Eq. (7.1) is based on the truss model theory:

$$V_f = 2 f_{fed} t_f h_{f_e} b_w \left(\cot\theta \sin\beta + \cos\beta\right) \frac{w_f}{s_f} \tag{7.1}$$

where $f_{fed} = D_f \ f_{fed,max}$, $h_{fe}=z_b-z_t$, $z_b=0.9d-(h-d_{fb})$; $z_t=d_{ft}$ and d_{fb} and d_{ft} is the coordinate of the bottom and top end, respectively of the effective jacket, as shown in Fig. 7.1.

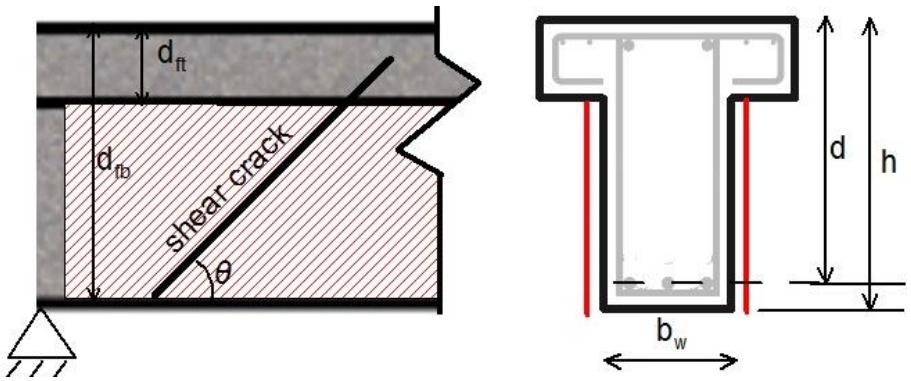


Figure 7.1. Notation for a general shear strengthening scheme.

The average stress of the jacket, f_{fed}, is based on the assumption that stress distribution in the jacket along the shear crack is not uniform at the ultimate limit state. The maximum stress in the strengthening jacket intersected by the shear crack, $f_{fed,max}$ and the stress distribution factor, D_f are the key factors of this model. The maximum stress, $f_{fed,max}$ is given by the following equation:

$$f_{fed,\max} = 0.427 \beta_w \beta_l \sqrt{\frac{E_f \sqrt{f_c}}{t_f}} \text{ (units of MPa and mm should be used)} \tag{7.2}$$

The two coefficients β_l and β_w that reflect the effective bond length and the effect of jacket to concrete width ratio, respectively are given by the following equations:

$$\beta_l = \begin{cases} 1, \lambda \geq 1 \\ \sin\left(\frac{\pi\lambda}{2}\right), \lambda < 1 \end{cases} \tag{7.3}$$

$$\beta_w = \sqrt{\frac{2 - w_f/(s_f \sin\beta)}{1 + w_f/(s_f \sin\beta)}} \tag{7.4}$$

The stress distribution factor, D_f is given by the following equation:

$$D_f = \begin{cases} \frac{2}{\pi\lambda}\left(\frac{1-\cos\left(\frac{\pi\lambda}{2}\right)}{\sin\left(\frac{\pi\lambda}{2}\right)}\right), \lambda \leq 1 \\ 1 - \frac{\pi - 2}{\pi\lambda}, \lambda > 1 \end{cases} \tag{7.5}$$

The normalized maximum bond length parameter λ, the available bond length L_{max} and the effective bond length L_e are given by the following equations:

$$\lambda = L_{max}/L_e \tag{7.6}$$

where $L_{max}=h_{fe}/\sin\beta$ for UW jackets and $L_{max}=h_{fe}/(2\sin\beta)$ for SB jackets (7.7)

and $L_e = \sqrt{\frac{E_f t_f}{\sqrt{f_c}}}$ (units of MPa and mm should be used) (7.8)

Figure D.1 of Appendix D illustrates the λ versus D_f values.

In particular, all the data available in literature from tests on RC beams that received TRM jackets or counterpart FRP jackets (consisting of the same textile fibre materials used in TRM combined with epoxy resin instead of mortar) included in the same studies and failed in shear-tension due to debonding of the jacket with peeling off of the concrete cover at a large part or at the full-length of the shear span are included in Table 7.1. In total, data from 41 tests are included in Table 7.1, among which 31 tests were conducted within the framework of this study whereas the remaining 10 are available in the literature.

Table 7.1. Experimental data on shear strengthening of RC beams with TRM (or equivalent FRP) jacketing that failed due to debonding of the jacket.

Specimen	(1) b_w (mm)	(2) h_{fe} (mm)	(3) f_c (MPa)	(4) ρ_w (%)	(5) Jacketing properties[2]	(6) f_{fu} (MPa)	(7) t_f (mm)	(8) ρ_f (‰)	(9) E_f (GPa)	(10) $V_{f,exp}$ (kN)
Data of this study										
CH2_SB	102	79.65	22.6	0	C, SB	1417.9	0.190	3.73	225	21.1
CH3_SB	102	79.65	22.6	0	C, SB	1417.9	0.285	5.59	225	32.7
CH2	102	159.3	23.8	0	C, UW	1417.9	0.190	3.73	225	39.2
CH3	102	159.3	22.6	0	C, UW	1417.9	0.285	5.59	225	45.4
CL1	102	159.3	23.0	0	C, UW	1544.6	0.062	1.22	225	28.9
CH1_CL1	102	159.3	20.0	0	C, UW	1481.3	0.157	3.08	225	37.6
CH2_CL1	102	159.3	20.0	0	C, UW	1460.1	0.252	4.94	225	44.4
CH3_CL1	102	159.3	20.0	0	C, UW	1449.6	0.347	6.80	225	48.5
CL1_strips	102	159.3	20.0	0	C, UW	1544.6	0.098	1.92	225	33.7
G3	102	159.3	20.0	0	G, UW	794.1	0.132	2.59	74	37.0
G7	102	159.3	20.0	0	G, UW	794.1	0.308	6.04	74	53.0
B3	102	159.3	23.1	0	B, UW	1206.1	0.111	2.18	89	36.1
B7	102	159.3	23.1	0	B, UW	1206.1	0.260	5.09	89	47.9
CL3	102	159.3	20.8	0	C, UW	1544.6	0.186	3.65	225	37.9
F10x20_3	102	159.3	22.0	0	C, UW	1404.7	0.291	5.71	225	46.5
F10x40_3	102	159.3	22.0	0	C, UW	1523.7	0.291	5.71	225	49.0
F20x20_3	102	159.3	22.0	0	C, UW	1564.5	0.291	5.71	225	40.9
F20x40_3	102	159.3	22.0	0	C, UW	1610.7	0.291	5.71	225	38.2
CL1_3.6	102	159.3	20.2	0	C, UW	1544.6	0.062	1.22	225	29.4
CL3_3.6	102	159.3	20.2	0	C, UW	1544.6	0.186	3.65	225	39.6
CL1_1.6	102	159.3	20.2	0	C, UW	1544.6	0.062	1.22	225	26.1
CL3_1.6	102	159.3	20.2	0	C, UW	1544.6	0.186	3.65	225	40.2
CH1_R_SB[1]	102	79.65	21.6	0	C, SB	2788.4	0.095	1.86	225	30.5
CH2_R_SB[1]	102	79.65	21.6	0	C, SB	2788.4	0.190	3.73	225	41.6
CH1_R[1]	102	159.3	23.8	0	C, UW	2788.4	0.095	1.86	225	35.3
CH2_R[1]	102	159.3	23.8	0	C, UW	2788.4	0.190	3.73	225	42.6
CH3_R[1]	102	159.3	20.8	0	C, UW	2788.4	0.285	5.59	225	50.0
CH4[3]	200	238.5	14.1	0	C, UW	1417.9	0.380	3.80	225	95.0
CL3[3]	200	238.5	14.0	0	C, UW	1544.6	0.186	1.86	225	57.0
G7[3]	200	238.5	13.8	0	G, UW	794.1	0.308	3.08	74	93.0
CH4_R[1, 3]	200	238.5	14.7	0	C, UW	2788.4	0.380	3.80	225	77.0
Awani et al. 2016										
S0-FRCM-1	150	112.5	36.0	0	C, SB	-	0.144	1.92	230	66.5
S0-FRCM-2	150	112.5	36.0	0	C, SB	-	0.288	3.84	230	87.2
S0-FRP-1[1]	150	112.5	36.0	0	C, SB	-	0.144	1.92	230	77.8
S1-FRCM-1	150	112.5	36.0	0.3	C, SB	-	0.144	1.92	230	68.4
S1-FRCM-2	150	112.5	36.0	0.3	C, SB	-	0.288	3.84	230	72.1
S1-FRP-1[1]	150	112.5	36.0	0.3	C, SB	-	0.144	1.92	230	72.2
S2-FRCM-1	150	112.5	36.0	0.5	C, SB	-	0.144	1.92	230	67.6
S2-FRCM-2	150	112.5	36.0	0.5	C, SB	-	0.288	3.84	230	73.6
S2-FRP-1[1]	150	112.5	36.0	0.5	C, SB	-	0.144	1.92	230	77.8
Tzoura and Triantafillou 2014										
RL2[1 3]	150	144.5	20.7	0	C, UW	-	0.096	1.28	225	25.8

[11] FRP jackets, [2] C for carbon fibre textile, G for glass fibre textile, B for basalt fibre textile, SB for side-bonded jackets and UW for U-wrapped jackets, [3] T-beam section.

Table 7.1 includes: (1) The width of the beam, b_w. (2) The effective height of the bonded reinforcement, h_{fe}. (3) The concrete compressive strength, f_c. (4) The internal shear reinforcement ratio, ρ_w. (5) The jacketing properties, namely the material of textile fibres and the strengthening configuration. (6) The ultimate tensile

stress, f_{fu} of TRM or FRP system defined from coupon tests (see Chapter 3). (7) The nominal thickness of the textile, t_f. (8) The geometrical reinforcement ratio of the composite material, ρ_f. (9) The modulus of elasticity of the fibres, E_f. (10) The experimental value of the contribution of strengthening to the shear capacity of the beam, $V_{f,exp}$. The values of all terms of Chen and Teng model, namely Le, λ, D_f and β_l values for all data of Table 7.1 are included in Table D.1 of Appendix D, whereas the λ values versus f_{fed} values are plotted in Fig. D.2.

The comparison between the experimental and predicted V_f values (using θ = 45^o and β = 90^o) is presented in Table 7.2 (Chen and Teng *Initial*) and is also supported by Fig. 7.2a. It should be noted that the modulus of elasticity of fibres, E_f was used in this model, as the modulus of elasticity of the textile material was not known for all the specimens included in Table 7.1 [tensile tests on the composite systems (TRM or FRP) were not carried out in all studies of Table 7.1].

In general, V_f values predicted from Chen and Teng model are in good agreement with the experimental V_f values ($V_{f,exp}$), taking into account that beams of different geometry (rectangular, T-beams), scale (medium-scale, full-scale), shear span-to-depth ratio (a/d varies from 1.6 to 3.6), with or without stirrups that received jackets of different textile fibre material (carbon, glass, basalt and PBO) and matrix (mortar, resin) are compared. In specific, Chen and Teng (*Initial*) model underestimates the V_f values, whereas it gives quite conservative results for both glass and basalt TRM jackets. In particular, the average ratio of predicted to experimental peak load $V_{f,pre}$ /$V_{f,exp}$ is equal to 0.754 and the coefficient of variation, CoV value is equal to 21.92%. The average ratio of predicted to experimental peak load ($V_{f,pre}$ /$V_{f,exp}$) for all five specimens received either glass or basalt TRM jackets is 0.49, indicating that this model considerably underestimates the contribution of both glass and basalt TRM jackets to the total shear resistance.

To improve the prediction of V_f values for data presented in Table 7.1, a modification of the Chen and Teng model is attempted. This modification involves the replacement of '0.427' factor used for calculating the maximum stress, $f_{fed,max}$ (see Eq. 7.6) with a new factor derived after calibration of data included in Table 7.1. Figure 7.3a illustrates the term $D_f \beta_w \beta_l (E_f f_c^{0.5}/t_f)^{0.5}$ at the horizontal axis for all data of Table 7.1 and the experimental stress values, σ_{exp} (calculated using Eq. 4.2) at the vertical axis. By applying a linear-type expression that best fits at the data included in Fig. 7.3a a new factor equal to 0.579 (instead of 0.427) is derived.

Table 7.2. Comparison between experimental and predicted V_f values in case of failure due to debonding of the jacket.

		Chen and Teng *Initial*		Chen and Teng *Modified-1*		Chen and Teng *Modified-2*	
Specimen	$V_{f,exp}$ **(kN)**	$V_{f,pre}$ **(kN)**	$V_{f,pre}/V_{f,exp}$	$V_{f,pre}$ **(kN)**	$V_{f,pre}/V_{f,exp}$	$V_{f,pre}$ **(kN)**	$V_{f,pre}/V_{f,exp}$
Data of this study							
CH2_SB	21.1	24.7	1.170	33.5	1.587	33.40	1.583
CH3_SB	32.7	25.9	0.793	35.2	1.076	35.10	1.073
CH2	39.2	34.5	0.881	46.8	1.195	46.73	1.192
CH3	45.4	39.0	0.860	52.9	1.166	52.81	1.163
CL1	28.9	21.8	0.755	29.6	1.024	29.52	1.021
CH1_CL1	37.6	30.5	0.810	41.3	1.098	41.23	1.096
CH2_CL1	44.4	36.0	0.811	48.8	1.099	48.69	1.097
CH3_CL1	48.5	39.7	0.819	53.8	1.110	53.71	1.107
CL1_strips	33.7	25.4	0.752	34.4	1.020	34.31	1.017
G3	37.0	18.0	0.485	24.4	0.658	33.40	0.903
G7	53.0	25.7	0.485	34.9	0.658	51.87	0.979
B3	36.1	18.8	0.521	25.5	0.707	37.71	1.045
B7	47.9	27.0	0.563	36.6	0.764	51.61	1.078
CL3	37.9	32.8	0.866	44.5	1.175	44.43	1.172
F10x20_3	46.5	38.9	0.838	52.8	1.137	52.67	1.134
F10x40_3	49.0	38.9	0.794	52.8	1.077	52.67	1.075
F20x20_3	40.9	38.9	0.952	52.8	1.291	52.67	1.288
F20x40_3	38.2	38.9	1.019	52.8	1.382	52.67	1.379
CL1_3.6	29.4	21.0	0.715	28.5	0.970	28.44	0.967
CL3_3.6	39.6	32.5	0.822	44.1	1.114	44.01	1.111
CL1_1.6	26.1	21.0	0.805	28.5	1.092	28.44	1.090
CL3_1.6	40.2	32.5	0.809	44.1	1.097	44.01	1.095
CH1_R_SB	30.5	20.9	0.686	28.4	0.931	28.32	0.929
CH2_R_SB	41.6	24.2	0.582	32.8	0.789	32.76	0.788
CH1_R	35.3	26.4	0.747	35.8	1.013	35.67	1.011
CH2_R	42.6	34.5	0.811	46.8	1.100	46.73	1.097
CH3_R	50.0	37.9	0.759	51.5	1.029	51.33	1.027
CH4	95.0	62.8	0.661	85.1	0.896	84.93	0.894
CL3	57.0	47.8	0.839	64.8	1.137	64.67	1.135
G7	93.0	36.9	0.397	50.0	0.538	78.27	0.842
CH4_R	77.0	63.7	0.827	86.4	1.122	86.16	1.119
Awani et al. 2016							
S0-FRCM-1	66.5	46.0	0.692	62.4	0.938	61.80	0.929
S0-FRCM-2	87.2	56.6	0.649	76.7	0.880	76.13	0.873
S0-FRP-1	77.8	46.0	0.592	62.4	0.802	61.80	0.795
S1-FRCM-1	68.4	46.0	0.673	62.4	0.912	61.80	0.903
S1-FRCM-2	72.1	56.6	0.785	76.7	1.064	76.13	1.056
S1-FRP-1	72.2	46.0	0.637	62.4	0.864	61.80	0.856
S2-FRCM-1	67.6	46.0	0.680	62.4	0.923	61.80	0.914
S2-FRCM-2	73.6	56.6	0.769	76.7	1.043	76.13	1.035
S2-FRP-1	77.8	46.0	0.592	62.4	0.802	61.80	0.795
Tzoura and Triantafillou 2014							
RL2	25.8	31.7	1.227	42.9	1.663	42.85	1.659
Average			0.754		1.023		1.049
Standard Deviation			0.165		0.224		0.188
CoV (%)			21.92		21.92		17.91

Thus, the maximum stress, $f_{fed,max}$ in the Chen and Teng – *modified 1* is calculated by the following equation:

$$f_{fed,\max} = 0.579\beta_w\beta_l\sqrt{\frac{E_f\sqrt{f_c}}{t_f}} \text{ (units of MPa and mm should be used)} \quad (7.9)$$

The comparison between the experimental and predicted V_f values of the modified Chen and Teng model is presented in Table 7.2 (Chen and Teng *modified 1*) and is also supported by Fig. 7.2b. The average ratio of predicted to experimental peak load is $V_{f,pre}$ /$V_{f,exp}$ = 1.023, the standard deviation is 0.224 and the coefficient of variation, *CoV* (%) value is equal to 21.92%. Thus, the modified Chen and Teng model (Chan and Teng – *Modified 1*) is improved in terms of $V_{f,pre}$ /$V_{f,exp}$ ratio, whereas the coefficient of variation value, *CoV*(%) is the same for both versions (*Initial* and *Modified 1*) of Chen and Teng model.

It is clear from Fig. 7.3a that specimens that received non-carbon fibre jackets, namely glass or basalt fibre textiles demonstrate large divergence from the linear-type expression. In other words, the average ratio of predicted to experimental peak load, $V_{f,pre}/V_{f,exp}$ is significantly lower than 1 for all five specimens that received glass or basalt TRM jackets. This discrepancy is maybe associated with the modulus of elasticity of fibres, as both glass and basalt fibres have lower modulus of elasticity values (74 GPa and 89 GPa, respectively) than the carbon fibres (225-230 GPa).

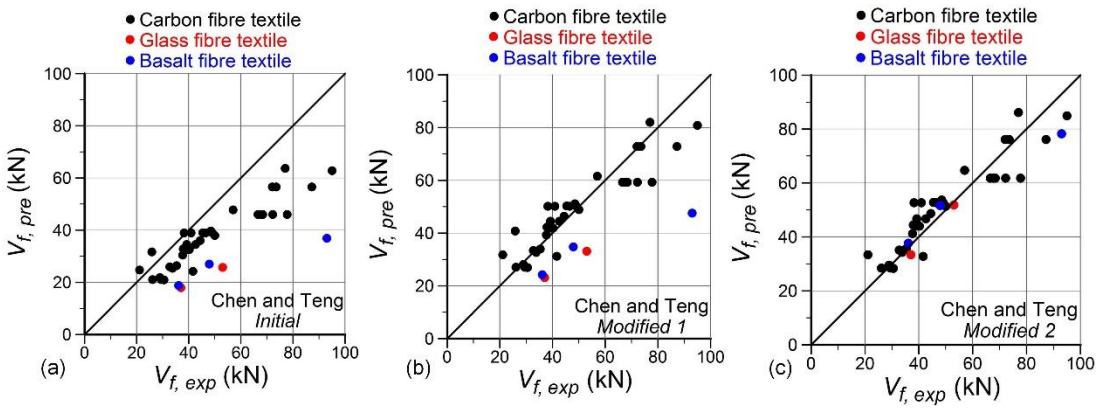


Figure 7.2. Experimental versus predicted V_f values for: (a) Chen and Teng – Initial; (b) Chen and Teng – Modified 1 and (c) Chen and Teng – Modified 2.

In attempt to clarify the effect of the textile material on the debonding of the jacket, Fig. 7.4a plots the experimentally obtained effective stress, σ_{eff}, against the $\rho_f E_f / f_c^{0.5}$ values for all medium-scale beams of a/d=2.6 of this study that received UW TRM or equivalent FRP (use of epoxy resin instead of mortar at the same textile reinforcement) jackets and failed due to debonding of the jacket. It becomes evident

from Fig. 7.4a that both glass and basalt data do not fit with the carbon data in this graph. By plotting the effective stress, σ_{eff} values against $\rho_f / f_c^{0.5}$ instead of $\rho_f E_f / f_c^{0.5}$ values (Fig. 7.4b), the results are significantly improved as the carbon fibre data perfectly fit with both glass and basalt fibre data.

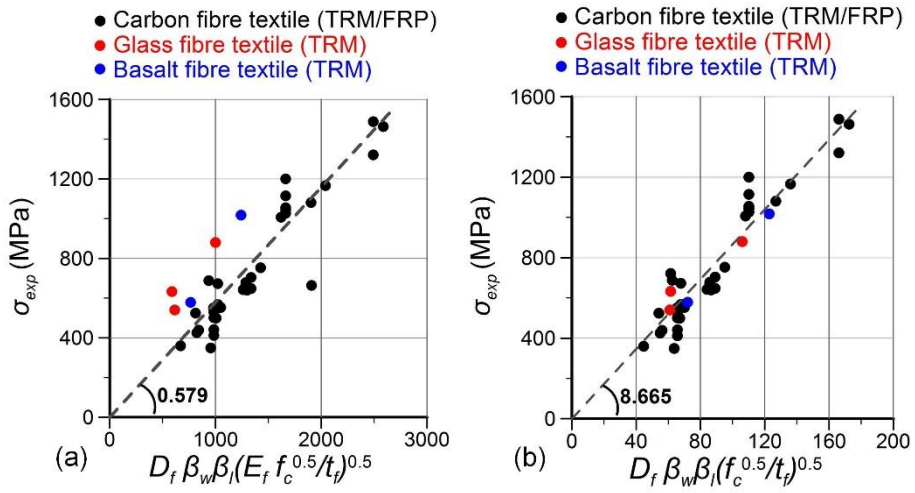


Figure 7.3. Experimentally obtained effective stress versus (a) $D_f \beta_w \beta_l (E_f f_c^{0.5}/t_f^{0.5})$ and (b) $D_f \beta_w \beta_l (f_c^{0.5}/t_f^{0.5})$.

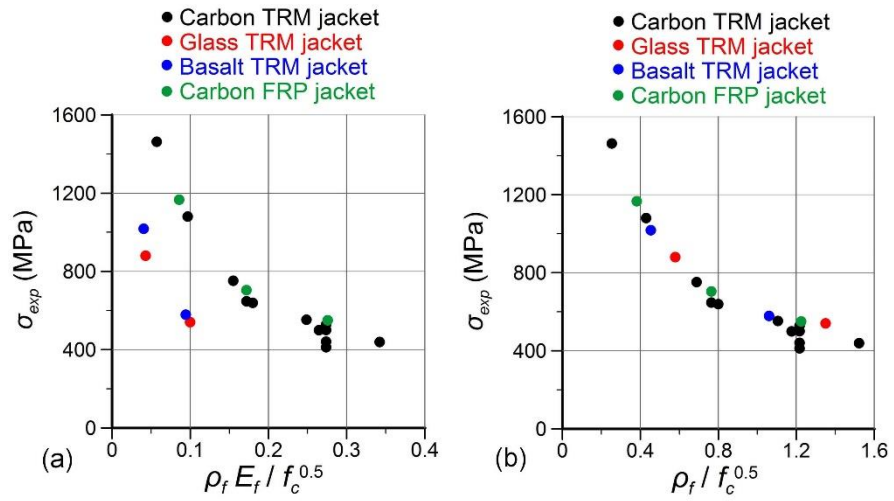


Figure 7.4. Experimentally obtained effective stress versus (a) $\rho_f E_f / fc^{0.5}$ and (b) $\rho_f / fc^{0.5}$.

Therefore, a second modification of Chen and Teng model is attempted to further improve the prediction of V_f values. Specifically, the modulus of elasticity, E_f was removed from Eq. (7.8) and (7.9) and a new calibration was applied (Fig. 7.3b) ending up with the following equations [instead of Eq. (7.6) and (7.13)]:

$$f_{fed,\max} = 274\beta_w\beta_l\sqrt{\frac{\sqrt{f_c}}{t_f}} \text{ (units of MPa and mm should be used)} \quad (7.10)$$

and $$L_e = 474\sqrt{\frac{t_f}{\sqrt{f_c}}} \text{ (units of MPa and mm should be used)} \quad (7.11)$$

Equation (7.11) was derived on the basis that L_e values should not be changed for the carbon data. Therefore, a factor equal to √225=15 was introduced in Eq. (7.11), as the modulus of elasticity, E_f of carbon fibres is around 225 GPa. By using the second modified version of Chen and Teng 2003 model, the average ratio of predicted to experimental peak load is $V_{f,pre}$ /$V_{f,exp}$ = 1.049, the standard deviation is 0.188 and the coefficient of variation, CoV (%) value is equal to 17.91% (Table 2, *modified 2*). Thus, the second modified version of Chen and Teng 2003 model has the best performance from a statistical point of view compared to both *Initial* and *Modified 1* Chen and Teng 2003 models. Moreover, the $V_{f,pre}$ /$V_{f,exp}$ value is significantly improved ($V_{f,pre}$ /$V_{f,exp}$ =0.97) for all specimens received non-carbon fibre TRM jackets (G3, G7, B3, B7 and G7[3]).

This is a quite interesting outcome that indicates that the contribution of the TRM (or FRP) jacket can be satisfactory predicted without using at all the modulus of elasticity value. This approach is really simple and overcomes the difficulty to select the proper modulus of elasticity value, namely using the modulus of elasticity of fibres, E_f or the modulus of elasticity of the composite material ($E_{f,TRM}$ or $E_{f,FRP}$). However, the data of specimens that received glass or basalt jackets included in Table 7.1 are extremely limited (just five) and they are all related with TRM jacketing. Moreover, the available data in the literature with beams strengthened in shear with non-carbon FRPs (FRP systems consisting of either continuous sheets or textile fibre materials) and their failure are attributed to debonding of the jacket are also extremely limited. In specific, based on the first studies on shear strengthening of RC beams with FRPs, only five data found in the literature [Berset 1992: specimens B(3) and B(4) and Al-Sulaimani et al. 1994: specimens SO, SP and WO] that received SB FRP jackets consisting of glass continuous sheets and failed due to debonding of the jacket. However, in these five specimens the thickness of the cured FRP plate or sheet is only reported and as a result these data cannot be compared with the data of Table 7.1 in which the nominal thickness of the textile material (before the impregnation of the textile with mortar or resin) is used.

Table 7.3. Experimental data on shear strengthening of RC beams with FRP jackets (consisting of glass continuous sheets) that failed due to debonding of the jacket.

Specimen	(1) b_w (mm)	(2) h_{fe} (mm)	(3) f_c (MPa)	(4) ρ_w (%)	(5) Jacketing properties[3]	(6) f_{fu} [2] (MPa)	(7) t_f [2] (mm)	(8) ρ_f (‰)	(9) E_f [2] (GPa)	(10) $V_{f,exp}$ (kN)
Baggio et al. 2014										
Beam 6	150	265.5	50	0.21	G, UW	2300	0.174	1.16	76	55.5
Beam 7	150	220.5	50	0.21	G, UW	2300	0.174	1.16	76	41.0

[1] G for glass fibre textile and UW for U-wrapped jackets, [2] based on manufacturer datasheet

Table 7.4. Comparison between experimental and predicted V_f values for data of Table 7.3.

Specimen	$V_{f,exp}$ (kN)	Chen and Teng *Initial* $V_{f,pre}$ (kN)	Chen and Teng *Initial* $V_{f,pre}/V_{f,exp}$	Chen and Teng *Modified-1* $V_{f,pre}$ (kN)	Chen and Teng *Modified-1* $V_{f,pre}/V_{f,exp}$	Chen and Teng *Modified-2* $V_{f,pre}$ (kN)	Chen and Teng *Modified-2* $V_{f,pre}/V_{f,exp}$
Baggio et al. 2014							
Beam 6	55.5	23.07	0.416	31.28	0.564	51.27	0.924
Beam 7	41.0	18.91	0.461	25.65	0.626	41.60	1.015

Table 7.5. Experimental data on double-lap direct shear tests that received TRM strips and failed due to debonding.

Specimen	(1) b (mm)	(2) L (mm)	(3) f_c (MPa)	(4) Jacketing properties[1]	(5) f_{fu} (MPa)	(6) t_f (mm)	(7) E_f (GPa)	(8) $P_{,exp}$ (kN)
Raoof et al. 2016								
L50_3	80	50	31.2	C	1417.9	0.285	225	22.6
L50_4	80	50	31.2	C	1417.9	0.380	225	27.9
L100_3	80	100	30.4	C	1417.9	0.285	225	31.2
L100_4	80	100	30.4	C	1417.9	0.380	225	35.0
L150_3	80	150	31.2	C	1417.9	0.285	225	35.1
L150_4	80	150	31.2	C	1417.9	0.380	225	37.9
L200_3	80	200	32.8	C	1417.9	0.285	225	36.0
L200_4	80	200	32.8	C	1417.9	0.380	225	41.5
L250_3	80	250	32.5	C	1417.9	0.285	225	38.0
L250_4	80	250	32.5	C	1417.9	0.380	225	41.8
L100_3	80	100	14.7	C	1417.9	0.285	225	29.9
L100_4	80	100	14.7	C	1417.9	0.380	225	32.2
L150_3	80	150	14.7	C	1417.9	0.285	225	30.7
L150_4	80	150	14.7	C	1417.9	0.380	225	35.1
L200_3	80	200	14.7	C	1417.9	0.285	225	34.9
L200_4	80	200	14.7	C	1417.9	0.380	225	37.7
L100_3	80	100	29.3	C	1417.9	0.285	225	31.2
L100_4	80	100	29.3	C	1417.9	0.380	225	36.1
L150_3	80	150	29.3	C	1417.9	0.285	225	33.9
L150_4	80	150	29.3	C	1417.9	0.380	225	37.2
L200_3	80	200	29.3	C	1417.9	0.285	225	40.4
L200_4	80	200	29.3	C	1417.9	0.380	225	41.9
L150_1_C	80	150	30.4	C	1417.9	0.095	225	21.9
L200_1_C	80	200	30.4	C	1417.9	0.095	225	23.9
L150_2_C	80	150	30.4	C	1417.9	0.190	225	29.5
L200_2_C	80	200	30.4	C	1417.9	0.190	225	31.9

[1] C for carbon fibre textile

Recently, Baggio et al. (2014) investigated the shear strengthening of RC beams with glass TRM (or FRCM) jackets, carbon and glass FRP jackets. Based on their

results the two specimens received glass U-shaped FRP jackets failed in shear due to debonding. Table 7.3 summarizes the characteristics of these two beams and the properties of the applied external reinforcement, whereas the comparison between the experimental and predicted V_f values using all three versions of Chen and Teng model (*Initial, Modified 1 and Modified 2*) is presented in Table 7.4. Both Chen and Teng – *Initial* and Chen and Teng – *Modified 1* models considerably underestimate the contribution of glass FRP jackets (similar to the non-carbon data of Table 7.2), whereas the V_f values predicted from Chen and Teng – *Modified 2* model are in very good agreement with the experimental V_f values. Thus, the accuracy of Chen and Teng – *Modified 2* model in predicting the contribution of non-carbon TRM or FRP jackets to the total shear resistance of the beam is again verified. The above models (Chen Teng - *Initial*, Chen Teng – *Modified 1* and Chen and Teng – *Modified 2*) can be also used to calculate the peak load of both single-lap and double-lap direct shear tests carried out to investigate the bond between TRM and concrete substrates by using the following equations:

$P_u = f_{fed,max}\, t_f\, b$ for single-lap direct shear tests (7.12)

$P_u = 2\, f_{fed,max}\, t_f\, b$ for double-lap direct shear tests (7.13)

where P_u is the maximum load carried out by the TRM strips and b is the bond width. The maximum stress, $f_{fed,max}$ is calculated from Eq. (7.2), (7.9) and (7.10) for Chen Teng - *Initial*, Chen Teng – *Modified 1* and Chen and Teng – *Modified 2* models, respectively.

Table 7.5 includes all the data of direct shear tests on TRM-strengthened prisms found in literature and failed due to debonding of the TRM jacket; all of them were carried from Raoof et al. 2016. Raoof et al. 2016 conducted double-lap direct shear tests using high tensile strength carbon fibre textile as reinforcement of the strengthening system. In particular, Table 7.5 includes: (1) The bond width, b. (2) The bond length, L. (3) The concrete compressive, f_c. (4) The jacketing properties, namely the material of textile fibres. (5) The ultimate tensile stress, f_{fu} of TRM or FRP system defined from coupon tests (see Chapter 3). (6) The nominal thickness of the textile, t_f. (7) The modulus of elasticity of the fibres, E_f. (8) The experimental value of the peak load, $P_{,exp}$. The comparison between the experimental and predicted P_u values using the three aforementioned versions of Chen and Teng model (*initial, modified 1* and *modified 2*) are presented in Table 7.6 and are also supported by Fig. 7.5. Based on the results of Table 7.6, Chen and Teng – *Initial* model underestimates the peak load, P_u

of direct shear tests (P_{pre} /P_{exp} = 0.797) similarly to specimens strengthened in shear with TRM (Table 7.2, $V_{f,pre}$ /$V_{f,exp}$ = 0.754 when Chen and Teng – *Initial* model was used). Both Chen and Teng *Modified 1* and *Modified 2* models can perfectly predict the peak load of the double-lap direct shear tests presented in Table 7.6. In practice, both modified versions of Chen and Teng model give almost same results as all specimens presented in Table 7.6 received carbon TRM jacketing (quite different predictions are obtained from the two modified versions of Chen and Teng model when non-carbon fibre jackets are applied). In particular, using Chen and Teng *modified 1* model, the average ratio of predicted to experimental peak load is P_{pre} /P_{exp} = 1.081, the standard deviation is 0.093 and the coefficient of variation, *CoV* (%) value is equal to 8.57%, whereas the corresponding values for Chen and Teng *modified 2* model are 1.079, 0.092 and 8.57%.

Table 7.6. Comparison between experimental and predicted P_u values for failure due to debonding.

		Chen and Teng *Initial*		**Chen and Teng *Modified-1***		**Chen and Teng *Modified-2***	
Specimen	$P_{u\ exp}$ **(kN)**	$P_{u,\ pre}$ **(kN)**	$P_{u,pre}$ /$P_{u,exp}$	$P_{u,pre}$ **(kN)**	$P_{u,pre}$ /$P_{u,exp}$	$P_{u,pre}$ **(kN)**	$P_{u,pre}$ /$P_{u,exp}$
Raoof et al. 2016							
L50_3	22.6	19.34	0.856	26.23	1.161	26.17	1.158
L50_4	27.9	19.80	0.710	26.84	0.962	26.78	0.960
L100_3	31.2	28.53	0.915	38.69	1.240	38.60	1.237
L100_4	35.0	31.59	0.903	42.83	1.224	42.74	1.221
L150_3	35.1	28.91	0.824	39.20	1.117	39.11	1.114
L150_4	37.9	33.38	0.881	45.26	1.194	45.16	1.192
L200_3	36.0	29.27	0.813	39.69	1.103	39.60	1.100
L200_4	41.5	33.80	0.814	45.83	1.104	45.73	1.102
L250_3	38.0	29.20	0.768	39.60	1.041	39.51	1.039
L250_4	41.8	33.72	0.807	45.73	1.094	45.62	1.091
L100_3	29.9	22.45	0.751	30.44	1.018	30.37	1.016
L100_4	32.2	24.01	0.746	32.56	1.011	32.49	1.009
L150_3	30.7	23.95	0.780	32.48	1.058	32.40	1.055
L150_4	35.1	27.66	0.788	37.50	1.068	37.41	1.066
L200_3	34.9	23.95	0.686	32.48	0.931	32.40	0.928
L200_4	37.7	27.66	0.734	37.50	0.995	37.41	0.992
L100_3	31.2	28.23	0.905	38.27	1.227	38.19	1.224
L100_4	36.1	31.18	0.864	42.28	1.171	42.18	1.169
L150_3	33.9	28.46	0.839	38.59	1.138	38.50	1.136
L150_4	37.2	32.86	0.883	44.56	1.198	44.45	1.195
L200_3	40.4	28.46	0.704	38.59	0.955	38.50	0.953
L200_4	41.9	32.86	0.784	44.56	1.063	44.45	1.061
L150_1_C	21.9	16.58	0.757	22.48	1.027	22.43	1.024
L200_1_C	23.9	16.58	0.694	22.48	0.941	22.43	0.939
L150_2_C	29.5	23.45	0.795	31.80	1.078	31.73	1.075
L200_2_C	31.9	23.45	0.735	31.80	0.997	31.73	0.995
Average			0.797		1.081		1.079
Standard Deviation			0.068		0.093		0.092
CoV (%)			8.57		8.57		8.57

To sum up, Chen and Teng 2003 – *Initial* model underestimates both the contribution of the TRM (or FRP) jacket to the total shear resistance (V_f) and the peak load of direct shear tests on specimens received TRM strips (P_u). Chen and Teng – *Modified 1* model accurately predicts the V_f and P_u values when carbon fibre TRM jacketing is applied, whereas it considerably underestimates the contribution of the TRM jacket to the total shear resistance when glass or basalt fibre TRM jackets were used. Finally, the predicted V_f and P_u values obtained using Chen and Teng – *Modified 2* model are in very good agreement with the corresponding experimental values when failure is attributed to debonding of the jacket based on 67 data that are available in the literature [41 tests on concrete beams strengthened in shear with TRM (26 data with carbon fibre TRM, 3 data with glass fibre TRM and 2 data with basalt fibre TRM) or FRP (10 data with carbon fibre FRP) jackets and 26 double-lap direct shear tests on concrete prisms received carbon TRM strips].

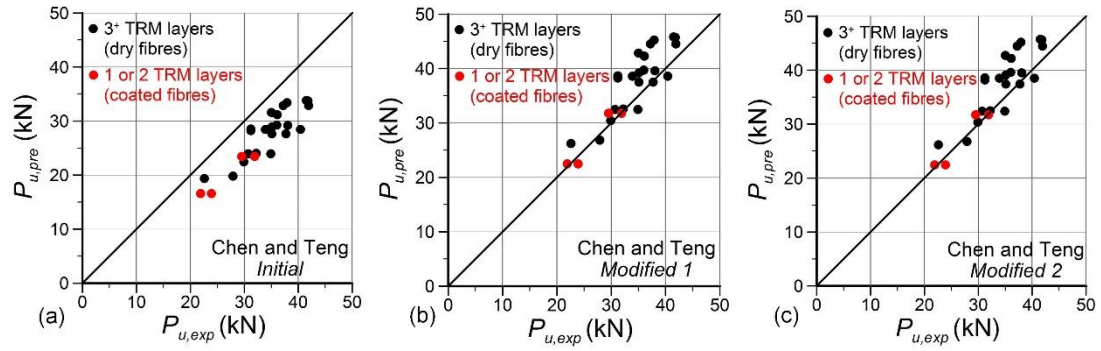


Figure 7.5. Experimental versus predicted P_u values for: (a) Chen and Teng – Initial; (b) Chen and Teng – Modified 1 and (c) Chen and Teng – Modified 2 models.

7.3 Failure of strengthened specimens due to fracture of the TRM jacket

Beams strengthened in shear with TRM jacketing that failed due to fracture of the jacket are extremely limited. In particular, Table 7.7 presents the specimens that failed due to fracture of the TRM jacket; three of these specimens received glass U-shaped TRM jacket, whereas one specimen strengthened with basalt U-shaped TRM jacket. When the failure of the TRM-strengthened beams is attributed to fracture of the jacket, the ultimate stress, f_{fu} defined from tensile tests on TRM coupons can be used for the calculation of the contribution of the TRM jacketing to the total shear resistance of the RC beam (V_f) as follows:

$$V_f = 2 f_{fu} t_f h_{f_e} b_w (\cot\theta \sin\beta + \cos\beta) \frac{w_f}{s_f} \quad (7.14)$$

The comparison between the experimental and predicted V_f values using the ultimate stress, f_{fu} defined from tensile tests on TRM coupons is presented in Table 7.8. Table 7.8 also includes the average stress in the strengthening jacket, f_{fed} (that is the stress value in case of failure due to debonding of the jacket) calculated using the two modified versions of Chen and Teng 2003 model presented in the previous section (Chen and Teng – *Modified 1* and Chen and Teng – *Modified 2*) and the effective strength of anchors, $f_{fe,anc}$ (the minimum $f_{fe,anc}$ value was 903 MPa, based on Table 5.5) used in this study. For both non-anchored specimens G1 and B1, the ultimate stress value, f_{fu} was lower than the $f_{fed,max}$ value (calculated either by Chen and Teng – *Modified 1* model or Chen and Teng – *Modified 2* model), interpreting the failure of these beams due to fracture of the jacket instead of debonding of the TRM jacket. In addition, for the anchored G7_A100 specimen, the ultimate stress value, f_{fu} was lower than the effective strength of anchors, $f_{fe,anc}$ verifying the failure of this specimen due to fracture of the TRM jacket before the failure of the anchorage system. For the test conducted from Baggio et al. 2014 (Beam 4 in Table 7.8), the f_{fu} value was lower than the $f_{fed,max}$ value obtained from Chen and Teng – *Modified 2* model, as expected due to rupture of the TRM jacket in this specimen, but higher than this calculated using Chen and Teng – *Modified 1* model. This is one more indication that Chen and Teng – *Modified 2* model is more accurate than Chen and Teng – *Modified 1* model for predicting the contribution of non-carbon TRM (or FRP) jackets to the total shear resistance.

Table 7.7. Experimental data on shear strengthening of RC beams with TRM jacketing that failed due to fracture of the jacket.

Specimen	(1) b_w (mm)	(2) h_{fe} (mm)	(3) f_c (MPa)	(4) ρ_w (%)	(5) Jacketing properties[1]	(6) f_{fu} (MPa)	(7) t_f (mm)	(8) ρ_f (‰)	(9) E_f (GPa)	(10) $V_{f,exp}$ (kN)
Data of this study										
G1	102	159.3	20.0	0	G, UW	794.1	0.044	0.86	74	12.2
B1	102	159.3	23.1	0	B, UW	1206	0.037	0.72	89	14.4
G7_A100[2, 3]	200	238.5	14.5	0	G, UW	794.1	0.308	3.08	74	106.0
Baggio et al. 2014										
Beam 4	150	295	50	0.21	G, UW	1430[4]	0.054[4]	0.52	80[4]	35.5

[1] G for glass fibre textile, B for basalt fibre textile and UW for U-wrapped jackets, [2] T-beam section, [3] TRM jacket anchored by 100%, [4] according to manufacturer datasheet.

The average ratio of predicted to experimental V_f value is $V_{f,pre}$ /$V_{f,exp}$ = 0.96, whereas the coefficient of variation, *CoV* (%) value is equal to 11.77%. Thus, V_f values can be accurately predicted using the results of (successful) tensile tests on TRM coupons (or just using the results of tensile tests on samples of bare textile mesh materials) when failure is attributed to the fracture of the TRM jacketing.

Table 7.8. Comparison between experimental and predicted V_f values in case of failure due to fracture of the jacket.

Specimen	$V_{f,\,exp}$ **(kN)**	f_{fu} **(MPa)**	f_{fed} **(MPa) Chen and Teng *Modified 1***	f_{fed} **(MPa) Chen and Teng *Modified 2***	$f_{fe,anc}$ **(MPa)**	$V_{f,\,pre}$ **(kN)**	$V_{f,\,pre}$ /$V_{f,\,exp}$
Data of this study							
G1	12.2	794.1	1053.55	1812.91	-	11.13	0.909
B1	14.4	1206.0	1306.88	1995.36	-	14.26	0.991
G7_A100	106.0	794.1	-	-	903	116.67	1.101
Baggio et al. 2014							
Beam 4	35.5	1430	1282.65	2095.34	-	29.74	0.838
						Average	0.96
						Standard Deviation	0.113
						CoV (%)	11.77

7.4 Failure of strengthened specimens due to local damage of the TRM jacket

It is well known that the high (tensile) strength of epoxy resins usually used in FRP applications prevents the slippage of the fibres through the epoxy resin. However, in case of TRM jacketing, local damage of the jacket including slippage of the vertical fibres through the mortar constitutes a recurring failure mode. Based on the results of this study, TRM is less effective than equivalent FRP system in terms of ρ_f when failure is attributed to local damage of the jacket instead of debonding. In this case, a reduction factor should be introduced taking into account the characteristics of the TRM system. In this section, the failure mode associated with the local damage of the TRM jacket is in detail investigated and the characteristics of TRM systems that are prone to slippage of the fibre rovings through the mortar are specified.

To begin with, based on the results presented in Sections 4.2 and 4.3, one of the parameters affect the bond between the textile and the mortar and therefore the effectiveness of TRM jacket is the textile geometry. In particular, in textiles with small roving area (A_{rov}), the degree of impregnation of fibres with cement paste is higher, resulting in improved bond characteristics. On the other hand, textiles with bigger roving size are more prone to slippage of the fibre rovings through the mortar.

Furthermore, local damage of the jacket is prevented when the textile fibre materials are coated (i.e. Raoof et al. 2016).

The remaining parameters (apart from the roving area of the textile) that affect the failure mode associated with the local damage of the TRM jacket consisting of dry/uncoated textile fibre materials should be also defined. As also mentioned before, local damage of the jacket includes slippage of the fibres through the mortar and therefore this failure could be satisfactorily interpreted though bond behaviour mechanism. In particular, equilibrium of forces in a single roving of the textile fibre material and the surrounding mortar (Fig. 7.6) gives:

$$A_{rov}\sigma = f_{bm}P_{rov}l \tag{7.15}$$

where A_{rov} is the roving area, σ is the stress that the TRM jacket should have when local damage of the jacket is prevented, namely σ=min(f_{fed}, f_{fu}), f_{bm} is the bond strength of mortar, P_{rov} is the perimeter of a single roving and l is the length required to achieve stress value equal to σ. The cross-section shape of a single roving is approximately rectangular and as a result A_{rov} is equal to w_{rov}*t_{rov}, where w_{rov} and t_{rov} is the width and the thickness of a single roving, respectively and P_{rov} is equal to 2(w_{rov}+t_{rov}). Thus, for a specific TRM system the values of A_{rov}, σ, f_{bm} and P_{rov} are known and therefore the l can be defined by the following equation.

$$l = \frac{A_{rov}\sigma}{f_{bm}P_{rov}} \tag{7.16}$$

The term l takes into consideration the characteristics of a TRM system and therefore it is possibly related to the reduction factor, k that can be used in case of slippage of the fibres through the mortar. The parameters included in Eq. (7.16) should be also combined with the available bond length, L_{max}, of the TRM jacket to take into account the geometry of the beam. It should be mentioned that the bond strength is related to the tensile strength. This relationship is linear for concrete and it was also considered linear for mortar. Thus, the tensile strength of mortar (f_{tm}) was finally used, as this strength value of mortar was experimentally defined in many studies that investigated the bond behavior of TRM and the shear strengthening of beams with TRM. Therefore, the ratio λ_s is introduced here that is actually equal to:

$$\lambda_s = L_{\max}{}^{0.6}\,\frac{f_{tm}P_{rov}}{A_{rov}\sigma} \tag{7.17}$$

More details on how λ_s ratio was defined are given in the Appendix A. The L_{max} value is defined from Eq. (7.11) for UW and SB jackets, whereas in case of FW jackets L_{max} is equal to the height of the beam. The reduction factor, k is defined as:

$$k = \frac{\sigma_{\exp}}{\min(f_{fed}, f_{fu})} \tag{7.18}$$

where f_{fed} was calculated using Chen and Teng – *Modified 2* model that was the most accurate for the prediction of V_f values based on the results presented in sections 7.2 and 7.3, whereas f_{fu} is the ultimate stress defined from tensile tests on TRM coupons (or just from tensile tests on bare textiles). It should be mentioned that the maximum value of the reduction factor, k was limited to 1 indicating that if k values are greater than 1, there is no reason to apply a reduction factor as full composite action in the TRM system has been achieved.

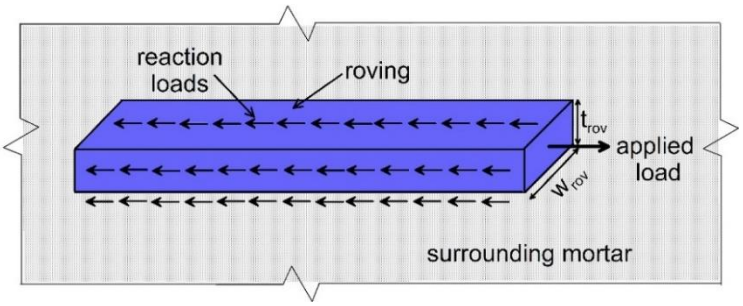


Figure 7.6. Local bond response between a single roving and the surrounding mortar.

Table 7.9 includes all the well reported available experimental data on shear strengthening of RC beams with TRM jackets consisting of dry/uncoated textile fibre materials (most data of Table 7.1 and 7.8 are also included in Table 7.9). Unfortunately, the data of Table 7.9 are quite limited and most of them were conducted in this study. There are data in the literature that they cannot be used for the following reasons: (a) failure of specimens is attributed to shear-compression instead of shear tension; (b) the textile fibre materials are coated and as a result their failure is not associated with slippage of the fibre rovings through the mortar that is studied in this section; (c) lack of information related to the TRM system (weight of textile fibre material, width and thickness of fibre roving, mortar strength or ultimate stress of the textile fibre material) or the RC beam (shear resistance of unretrofitted beam or concrete strength); (d) TRM jacketing was applied just at a part of the shear span and the failure occurred at the non-strengthened part of the shear span of the beam (most

specimens presented in Escrig et al. 2015) and (e) completely different concrete strength at the beams of the same study, resulting in strengthened beams with lower total shear resistance that the unretrofitted beam (V_f=0, i.e. some specimens presented in Ombres 2015).

In particular, Table 7.9 includes: (1) The width of the beam, b_w. (2) The effective height of the bonded reinforcement, h_{fe}. (3) The concrete compressive stength, f_c. (4) The jacketing properties, namely the material of textile fibres and the strengthening configuration. (5) The nominal thickness of the textile, t_f. (6) The average stress, f_{fed} in case of debinding predicted from Chen and Teng – *Modified 2* model. (7) The ultimate tensile stress of TRM jacket, f_{fu} defined from coupon tests (see Chapter 3). (8) The tensile strength of mortar, f_{tm}. (9) The λ_s value defined from Eq. (7.16) and (7.17). (10) The reduction factor, k obtained from Eq. (7.18).

To begin with, in Fig. 7.7a the reduction factor, k is plotted with λ_s values for all the medium-scale beams of this study strengthened with TRM jacketing comprising of dry/uncoated fibre textiles and tested at ambient temperature. It is evident that beams strengthened in shear with TRM jackets that have low λ_s values failed due to slippage of the fibre rovings through the mortar. It is clear that as λ_s increases, local damage of the jacket including slippage of the fibre rovings through the mortar is prevented. Failure of beams that received TRM jackets with λ_s values at the range of 0.5 and 0.8 is attributed to debonding of the TRM jacket at a large area of the shear span. Beams that received TRM jackets with λ_s values greater than 0.8, failed due to debonding of the jacket at the whole area of the shear span or rupture of the TRM jacket (it depends on which is the minimum stress, f_{fed} or f_{fu}) and they had k values very close to 1, indicating that full composite action has been developed.

Figure 7.7b presents the same data with Fig. 7.6a but now the results are grouped based on the number of layers instead of the failure mode observed. Increasing the number of layers in a specific TRM system, the stress value σ is decreased (σ value remains fixed only if the failure of specimens is attributed to fracture of the TRM jacket as the number of TRM layers increases, that was not the case for the results presented in Fig. 7.7a-d) and as a result the λ_s value is increased, leading to higher k values.

Table 7.9. Well reported available experimental data on shear strengthening of RC beams with TRM jacketing consisting of dry textile fibre materials.

Specimen	(1) b_w (mm)	(2) h_{fe} (mm)	(3) f_c (MPa)	(4) Jacketing[1] properties	(5) t_f (mm)	(6) f_{fed} (MPa)	(7) f_{fu} (MPa)	(8) f_{tm} (MPa)	(9) λ_s	(10) k
Data of this study										
CH1_SB	102	79.65	22.6	C, SB	0.095	895	1418	3.40	0.35	0.09
CH2_SB	102	79.65	22.6	C, SB	0.190	519	1418	3.40	0.63	0.67
CH3_SB	102	79.65	22.6	C, UW	0.285	3634	1418	3.40	0.85	0.93
CH1	102	159.3	23.8	C, UW	0.095	1109	1418	3.40	0.42	0.42
CH2	102	159.3	23.8	C, UW	0.190	727	1418	3.40	0.68	0.89
CH3	102	159.3	22.6	C, UW	0.285	547	1418	3.40	0.86	0.86
CL1	102	159.3	23.0	C, UW	0.062	1406	1545	3.40	0.83	1.00
CH1_CL1	102	159.3	20.0	C, UW	0.157	776	1481	3.40	0.88	0.97
CH2_CL1	102	159.3	20.0	C, UW	0.252	571	1460	3.40	1.01	0.91
CH3_CL1	102	159.3	20.0	C, UW	0.347	457	1450	3.40	1.18	0.90
CL1_strips	102	159.3	20.0	C, UW	0.098	1035	1545	3.40	1.14	1.00
G1	102	159.3	23.0	G, UW	0.044	1706	794	3.40	1.08	1.00
G3	102	159.3	20.0	G, UW	0.132	864	794	3.40	1.08	1.00
G7	102	159.3	20.0	G, UW	0.308	498	794	3.40	1.62	1.00
CL3	102	159.3	20.1	C, UW	0.186	706	1545	3.40	1.58	0.85
F10x20_1	102	159.3	23.8	C, UW	0.095	1109	1405	3.40	0.41	0.40
F10x20_3	102	159.3	22.0	C, UW	0.291	535	1405	3.40	0.86	0.88
F10x40_1	102	159.3	23.8	C, UW	0.095	1109	1524	3.40	0.41	0.36
F10x40_3	102	159.3	22.0	C, UW	0.291	535	1524	3.40	0.86	0.93
F20x20_1	102	159.3	23.8	C, UW	0.095	1109	1565	3.40	0.28	0.28
F20x20_3	102	159.3	22.0	C, UW	0.291	535	1565	3.40	0.59	0.78
F20x40_1	102	159.3	23.8	C, SB	0.095	1109	1611	3.40	0.28	0.32
F20x40_3	102	159.3	22.0	C, SB	0.291	535	1611	3.40	0.59	0.73
CL1_3.6	102	159.3	20.2	C, UW	0.062	1355	1545	3.40	0.87	1.00
CL3_3.6	102	159.3	20.2	C, UW	0.186	699	1545	3.40	1.60	0.90
CL1_1.6	102	159.3	20.2	C, UW	0.062	1355	1545	3.40	0.87	0.97
CL3_1.6	102	159.3	20.2	C, UW	0.186	699	1545	3.40	1.60	0.91
CH1_FW	102	203	23.8	C, FW	0.095	-	1418	3.40	0.41	0.79
CH2[2]	200	238.5	15.0	C, UW	0.095	709	1418	3.40	0.89	0.72
CH4[2]	200	238.5	14.1	C, UW	0.380	441	1418	3.40	1.35	1.00
CL3[2]	200	238.5	14.0	C, UW	0.186	686	1545	3.40	2.07	0.88
G7[2]	200	238.5	13.8	G, UW	0.308	502	794	3.40	2.05	1.00
G7_A100[2]	200	238.5	13.8	G, UW	0.308	-	794	3.40	1.38	1.00
Escrig et al. [53]										
V-CXM25[3]	300	228.6	34.1	C, UW	0.047	1895	1031	3.47[4]	1.5	1.00
Ombres [54]										
TRA2	150	186.3	30.8	PBO, UW	0.045	2493	1664	2.92[4]	0.90	0.61
TRB1	150	186.3	45.0	PBO, UW	0.045	2058	1664	2.92[4]	0.90	1.00
Tzoura and Triantafillou [30]										
L1	150	198.9	20.9	C, UW	0.048	1621	1800	2.34[4]	0.43	0.32
H1	150	198.9	23.4	C, UW	0.096	1136	1800	2.34[4]	0.32	0.52
L2	150	198.9	21.6	C, UW	0.096	1111	1800	2.34[4]	0.63	0.30
H2	150	198.9	23.4	C, UW	0.192	757	1800	2.34[4]	0.48	0.60
Loreto et al. [32]										
L_1_Ave	152	223.2	29.1	PBO, UW	0.046	1834	1664	3.14[4]	1.07	0.53
H_1_Ave	152	223.2	42.9	PBO, UW	0.046	2035	1664	3.14[4]	1.07	0.70

[1] C for carbon fibre textile, G for glass fibre textile, PBO for Polyparaphenylene Benzobis Oxazole fibre textile, SB for side-bonded jackets, UW for U-wrapped jackets and FW for fully-wrapped jackets, [2] T-beam section. [3]Average of specimens V-CXM25-1 and V-CXM25-2, [4] Tensile strength of mortar was calculated using Eq. (7.19).

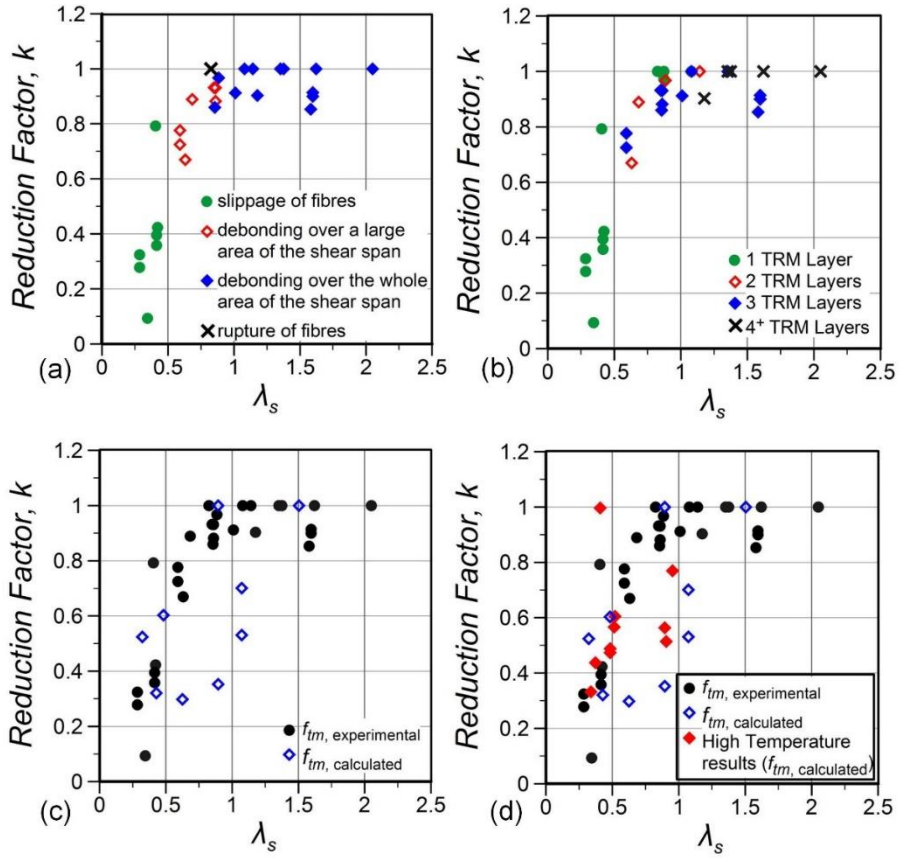


Figure 7.7. Reduction factor k versus λs values for: (a) all half-scale beams of this study grouped based on their failure mode; (b) all half-scale beams of this study grouped based on the number of layers; (c) for all beams strengthened in shear with TRM presented in Table 9 and (d) for all beams strengthened in shear with TRM tested either at ambient (Table 7.9) or at high temperature (Table 7.10).

Figure 7.7c presents the k versus λ_s values for all specimens of Table 7.9 that tested at ambient temperature. In most specimens, the tensile mortar strength was experimentally obtained, whereas in some data available in the literature, the tensile strength of mortar was not given and it was calculated according to the formula of EC2:

$$f_{tm}=0.3f_{cm}^{2/3} \quad (7.19)$$

where f_{cm} is the compressive strength of mortar.

Based on the results of Fig. 7.7c the λ_s versus k values of specimens in which the tensile strength of mortar was experimentally obtained are very consistent and fit very well each other. Regarding the specimens in which the mortar strength was not known and was obtained using Eq. (7.19), some data are in very good agreement with the data of specimens in which the tensile strength of mortar was experimentally obtained but

some data are quite scattered with the rest data, possible due to the inaccuracy in predicting the tensile strength of mortar.

Finally, in Fig. 7.7d the k versus λ_s values are plotted for all the data of Table 7.9 including also the specimens of this study that tested at high temperature (Table 7.10). Despite the fact that the tensile strength of the mortar at high temperature was not experimentally obtained but was calculated using Eq. (7.19), the k versus λ_s values of the high temperature results are in good agreement with the results of specimens tested at ambient temperature.

Table 7.10. Experimental data on shear strengthening of RC beams with TRM jacketing tested at high temperature.

Specimen	(1) b_w (mm)	(2) h_{fe} (mm)	(3) f_c (MPa)	(4) Jacketing[1] properties	(5) t_f (mm)	(6) Temperature (°C)	(7) λ_s[3]	(8) k
Data of this study								
SB_MCH2_150	102	79.65	22.2	C, SB	0.190	150	0.34	0.33
SB_MCH3_150	102	79.65	22.2	C, SB	0.285	150	0.48	0.48
UW_MCH2_150	102	159.3	22.2	C, UW	0.190	150	0.37	0.43
UW_MCH3_150	102	159.3	22.6	C, UW	0.285	150	0.48	0.47
UW_MCH3_100	102	159.3	20.7	C, UW	0.285	100	0.52	0.60
UW_MCH3_250	102	159.3	20.7	C, UW	0.285	250	0.51	0.56
UW_MCL3_150	102	159.3	20.7	C, UW	0.186	150	0.89	0.56
UW_MG7_150	102	159.3	20.7	G, UW	0.308	150	0.91	0.51
FW_CH2_150	102	203.0	21.8	C, FW	0.190	150	0.41	0.99
CH4_150[2]	200	238.5	14.5	C, UW	0.380	150	0.95	0.76

[1] C for carbon fibre textile, G for glass fibre textile, SB for side-bonded jackets, UW for U-wrapped jackets and FW for fully-wrapped jackets, [2] T-beam section, [3] Tensile strength of mortar was calculated using Eq. (7.20).

To sum up, based on the results presented at Fig. 7.7a-d, the ratio λ_s constitutes a very important parameter for distinguishing TRM systems that are prone to slippage of the fibre rovings through the mortar and TRM systems in which this failure mode is prevented. As mentioned before, the λ_s versus k values of specimens with experimentally obtained tensile strength of mortar are very consistent contrary to specimens in which the mortar strength was obtained using Eq. (7.19) that were quite scattered.

In order to complete this section, a formula for defining the reduction factor, k as a function of the term λ_s is required. Except from the results of specimens strengthened in shear with (dry/uncoated) TRM jackets, the results of (both single-lap and double-lap) direct shear tests carried out to investigate the bond between TRM and concrete substrates could be also used for extending the database. In particular, Table 7.11 includes all the well reported available data from direct shear tests on

prisms that received TRM strips (some of them had been already presented in Table 7.5), whereas in Fig. 7.8a the λ_s versus k values of data presented in Table 7.11 are plotted in combination with the data obtained from tests on RC beams strengthened in shear with TRM jacketing that already presented in Fig. 7.7d.

Table 7.11. Experimental data on direct shear tests that received TRM strips consisting of dry textile fibre materials.

Specimen	(1) b (mm)	(2) L (mm)	(3) f_c (MPa)	(4) Textile fibre material [1]	(5) t_f (mm)	(6) σ (MPa)	(7) λ_s	(8) k
Raoof et al. 2016								
L50-1	80	50	31.2	C	0.095	1335.3	0.18	0.38
L50-2	80	50	31.2	C	0.190	773.1	0.30	0.78
L50_3	80	50	31.2	C	0.285	540.1	0.43	0.92
L50_4	80	50	31.2	C	0.380	414.6	0.56	1.00
L100-1	80	100	30.4	C	0.095	1389.2	0.27	0.55
L100-2	80	100	30.4	C	0.190	982.3	0.36	0.79
L100_3	80	100	30.4	C	0.285	796.8	0.44	0.86
L100_4	80	100	30.4	C	0.380	661.6	0.54	0.87
L150-1	80	150	31.2	C	0.095	1398.2	0.34	0.57
L150-2	80	150	31.2	C	0.190	988.7	0.46	0.84
L150_3	80	150	31.2	C	0.285	807.3	0.56	0.95
L150_4	80	150	31.2	C	0.380	699.1	0.65	0.89
L200-1	80	200	32.8	C	0.095	1415.8	0.40	0.65
L200-2	80	200	32.8	C	0.190	1001.1	0.54	0.92
L200_3	80	200	32.8	C	0.285	817.4	0.80	0.97
L200_4	80	200	32.8	C	0.380	707.9	0.93	0.96
L250-1	80	250	32.5	C	0.095	1412.6	0.46	0.75
L250-2	80	250	32.5	C	0.190	998.8	0.61	0.97
L250_3	80	250	32.5	C	0.285	815.5	0.75	1.00
L250_4	80	250	32.5	C	0.380	706.3	0.87	0.97
L450-1	80	450	29.5	C	0.095	1378.8	0.65	0.83
L450-2	80	450	29.5	C	0.190	974.9	0.90	1.00
L100_3	80	100	14.7	C	0.285	626.8	0.56	1.00
L100_4	80	100	14.7	C	0.380	503.0	0.70	1.00
L150_3	80	150	14.7	C	0.285	668.8	0.68	1.00
L150_4	80	150	14.7	C	0.380	579.2	0.78	1.00
L200_3	80	200	14.7	C	0.285	668.8	0.80	1.00
L200_4	80	200	14.7	C	0.380	579.2	0.93	1.00
L100_3	80	100	29.3	C	0.285	788.2	0.45	0.87
L100_4	80	100	29.3	C	0.380	653.1	0.54	0.91
L150_3	80	150	29.3	C	0.285	794.7	0.57	0.94
L150_4	80	150	29.3	C	0.380	688.2	0.66	0.89
L200_3	80	200	29.3	C	0.285	794.7	0.68	1.00
L200_4	80	200	29.3	C	0.380	688.2	0.78	1.00
D'Antino et al. 2013								
100_34	34	100	42.5	PBO	0.045	2182.7	0.54	0.44
150_34	34	150	42.5	PBO	0.045	2182.7	0.69	0.66
150_60	60	150	42.5	PBO	0.045	2182.7	0.69	0.75
200_34	34	200	42.5	PBO	0.045	2182.7	0.83	0.89
250_34	34	250	42.5	PBO	0.045	2182.7	0.94	0.74
330_34	34	330	42.5	PBO	0.045	2182.7	1.12	1.00
330_43	43	330	42.5	PBO	0.045	2182.7	1.12	1.00
330_60	60	330	42.5	PBO	0.045	2182.7	1.12	1.00
330_43_L	43	330	42.5	PBO	0.045	2182.7	0.57	0.95
330_60_L	60	330	42.5	PBO	0.045	2182.7	0.57	1.00

[1] C for carbon fibre textile and PBO for PBO fibre textile

Specimen	(1) b (mm)	(2) L (mm)	(3) f_c (MPa)	(4) Textile fibre material [1]	(5) t_f (mm)	(6) σ (MPa)	(7) λ_s	(8) k
Sneed et al. 2015								
100_60	60	100	33.5	PBO	0.045	2056.6	0.56	0.75
200_60	60	200	33.5	PBO	0.045	2056.6	0.85	0.97
250_60	60	250	33.5	PBO	0.045	2056.6	0.97	1.00
330_34	34	330	33.5	PBO	0.045	2056.6	1.15	1.00
330_60	60	330	33.5	PBO	0.045	2056.6	1.15	1.00
330_80	80	330	33.5	PBO	0.045	2056.6	1.15	1.00
330_100	100	330	33.5	PBO	0.045	2056.6	1.15	1.00
D'Antino et al 2015								
330_60_W	60	330	26.9	PBO	0.045	1946.8	1.22	1.00
330_80	80	330	42.5	PBO	0.045	2182.7	1.08	1.00
450_60	60	450	33.5	PBO	0.045	2056.6	1.39	1.00
450_80	80	450	33.5	PBO	0.045	2056.6	1.39	1.00
330_60_U	60	330	33.5	PBO	0.045	2056.6	1.15	0.76
330_80_U	80	330	33.5	PBO	0.045	2056.6	1.15	1.00
450_60_U	60	450	33.5	PBO	0.045	2056.6	1.39	1.00
450_80_U	80	450	33.5	PBO	0.045	2056.6	1.39	1.00
Tran et al. 2014								
250	100	250	41.0	PBO	0.045	2163.2	0.67	1.00
300	100	300	41.0	PBO	0.045	2163.2	0.75	1.00
350	100	350	41.0	PBO	0.045	2163.2	0.83	1.00
400	100	400	41.0	PBO	0.045	2163.2	0.89	1.00
400	100	400	31.0	PBO	0.045	2017.1	0.96	1.00
400	100	400	41.0	PBO	0.045	2163.2	0.89	1.00
400	100	400	39.0	PBO	0.045	2136.3	0.91	1.00
D'Antino et al. 2014								
100_60	60	100	42.5	PBO	0.045	2182.7	0.53	0.63
200_60	60	200	42.5	PBO	0.045	2182.7	0.80	0.99
250_60	60	250	42.5	PBO	0.045	2182.7	0.92	1.00
450_34	34	450	33.5	PBO	0.045	2056.6	1.39	1.00
Ambrissi et al. 2012								
S1L50	100	50	35.0	PBO	0.045	2079.3	0.27	0.58
S1L100	100	100	35.0	PBO	0.045	2079.3	0.41	0.81
S1L150	100	150	35.0	PBO	0.045	2079.3	0.52	0.95
S1L200	100	200	35.0	PBO	0.045	2079.3	0.61	1.00
S1L250	100	250	35.0	PBO	0.045	2079.3	0.70	1.00
S2L100	100	100	35.0	PBO	0.091	1470.3	0.57	0.94
S2L200	100	200	35.0	PBO	0.091	1470.3	0.87	1.00
Ombres 2014								
1-150	70	150	30.0	PBO	0.045	2000.7	0.62	0.38
1-200	70	200	30.0	PBO	0.045	2000.7	0.73	0.56
1-250	70	250	30.0	PBO	0.045	2000.7	0.84	0.52
2-150	70	150	30.0	PBO	0.091	1414.7	0.87	0.79
2-200	70	200	30.0	PBO	0.091	1414.7	1.03	0.90
2-250	70	250	30.0	PBO	0.091	1414.7	1.18	0.80
1-250	50	250	30.0	PBO	0.045	2000.7	0.84	0.79
2-250	50	250	30.0	PBO	0.091	1414.7	1.18	0.96

[1] C for carbon fibre textile and PBO for Polyparaphenylene Benzobis Oxazole fibre textile, [2] Tensile strength of mortar was calculated using Eq. (7.17).

As also mentioned before for data presented in Fig. 7.7d, the data of specimens in which the tensile strength of mortar was calculated using Eq. (7.19) are quite scattered and they do not fit always very well with the rest data. Thus, only the data of TRM-strengthened specimens in which the tensile strength was experimentally

obtained (which are plotted in Fig. 7.8b) will be used for defining a formula to calculate the reduction factor, k as a function of the ratio λ_s. In total, 110 data were used for the definition of the reduction factor, k.

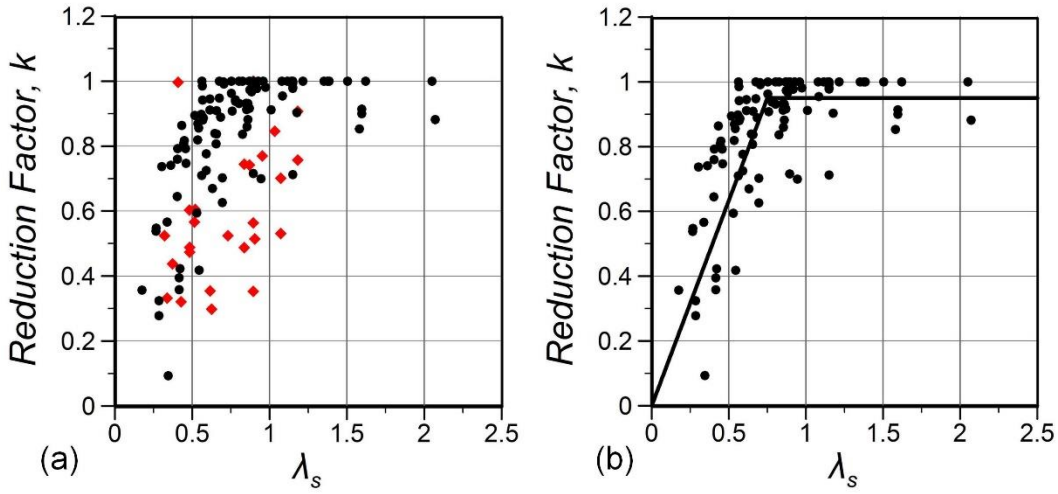


Figure 7.8. Reduction factor, k versus λ_s values for: (a) all available data obtained from tests on RC beams strengthened in shear with TRM and direct shear tests on concrete prisms received TRM strips; (b) all available data obtained from tests on RC beams strengthened in shear with TRM and direct shear tests on concrete prisms received TRM strips in which the tensile strength of mortar was experimentally obtained.

In general, from Fig. 7.8b, it seems that the reduction factor, k increases with the λ_s value and after a critical value of λ_s ($\lambda_{s,crit} \approx 0.75$), TRM jackets develop full-composite action resulting in k values close to 1. A bi-linear type expression was selected to be applied in the data of Fig. 7.8b as this is a very simple approach that agrees very well with the trend of data presented in Fig. 7.8a-b. When λ_s is 0, namely when TRM strengthening is not applied at all, k factor should be equal to 0. Therefore, the following bi-linear type expression is recommended:

$$k = \begin{cases} 1.2667\lambda_s & \lambda_s \le 0.75 \\ 0.95 & \lambda_s > 0.75 \end{cases} \tag{7.20}$$

7.5 Summary of design approach for the calculation of the contribution of TRM jacketing, V_f to the total shear resistance of RC beams

In this section, the design approach for the calculation of the contribution of TRM jacketing, V_f to the total shear resistance of RC beams is summarized based on the

results presented in paragraphs 7.2-7.4. In particular, the average stress, f_{fed} is first calculated using the following equations:

$$L_e = 15\sqrt{\frac{1000 t_f}{\sqrt{f_c}}} \quad (7.11), \quad \lambda = L_{\max} / L_e \quad (7.6), \quad D_f = \begin{cases} \frac{2}{\pi\lambda}\left(\frac{1-\cos\left(\frac{\pi\lambda}{2}\right)}{\sin\left(\frac{\pi\lambda}{2}\right)}\right), \lambda \le 1 \\ 1-\frac{\pi-2}{\pi\lambda}, \lambda > 1 \end{cases} \quad (7.5),$$

$$\beta_l = \begin{cases} 1, \lambda \ge 1 \\ \sin\left(\frac{\pi\lambda}{2}\right), \lambda < 1 \end{cases} \quad (7.3), \quad \beta_w = \sqrt{\frac{2 - w_f/(s_f \sin\beta)}{1 + w_f/(s_f \sin\beta)}} \quad (7.4),$$

$$f_{fed,\max} = 8.665 \beta_w \beta_l \sqrt{\frac{1000\sqrt{f_c}}{t}} \quad (7.14) \text{ and} \qquad f_{fed} = D_f f_{fed,\max} \quad (7.21)$$

After that, the stress σ that is actually the minimum of the average stress, f_{fed} and the ultimate tensile stress, f_{fu} is defined as:

$$\sigma = \min(f_{fed}, \ f_{fu}) \qquad (7.22)$$

The final stress value, of a TRM system is equal to $k\,\sigma$, where k is the reduction factor that is used to define the reduced stress of the TRM jackets in case of failure due to slippage of the fibres through the mortar.

For TRM systems consisting of coated textile fibre materials, the reduction factor, k is equal to 1, whereas for TRM systems consisting of uncoated/dry textile fibre materials k is defined as:

$$k = \begin{cases} 1.2667\lambda_s & \lambda_s \le 0.75 \\ 0.95 & \lambda_s > 0.75 \end{cases} \qquad (7.20),$$

where $\lambda_s = L_{max}/l$ (7.17) and $l = \frac{A_{rov}\sigma}{f_{tm} P_{rov}}$ (7.16)

Finally, the contribution of the TRM jacket to the total shear resistance is given by the following equation:

$$V_f = 2\ k\ \sigma\ t_f h_{f_e} b_w (\cot\theta \sin\beta + \cos\beta)\frac{w_f}{s_f} \qquad (7.23)$$

The peak load of direct shear tests is given by: $P_u = k\ min\ (f_{fed,max}, f_{fu})\ t_f\ b$ for single-lap shear tests and $P_u = 2\ k\ min\ (f_{fed,max}, f_{fu})\ t_f\ b$ for double-lap shear tests, respectively.

Table 7.12. Comparison between experimental and predicted stress values for all available data obtained from tests on either RC beams strengthened in shear with TRM jacketing or direct shear tests with TRM strips.

Specimen	(1) Textile fibres [1]	(2) σ_{exp} (MPa)	(3) σ (MPa)	(4) $k_{,pre}$	(5) σ_{pre} (MPa)	(6) $\sigma_{exp}/\sigma_{pre}$
Data from tests on RC beams strengthened in shear with TRM						
Data of this study						
CH1_SB*	D	89.2	951.2	0.44	415.7	4.66
CH2_SB	D	348.6	520.5	0.80	415.7	1.19
CH3_SB	D	360.1	386.5	0.95	367.2	1.02
CH1	D	498.9	1178.6	0.53	630.1	1.26
CH2	D	647.6	728.4	0.87	630.1	0.97
CH3	D	500.0	581.6	0.95	552.5	1.11
CL1	D	1463.1	1435.7	0.95	1363.9	0.93
CH1_CL1	D	752.3	777.7	0.95	738.8	0.98
CH2_CL1	D	553.0	606.5	0.95	576.2	1.04
CH3_CL1	D	438.7	485.9	0.95	461.6	1.05
CL1_strips	D	1080.4	1037.2	0.95	985.3	0.88
G1	D	873.3	794.1	0.95	754.4	0.86
G3	D	879.8	794.1	0.95	754.4	0.86
G7	D	540.1	528.6	0.95	502.1	0.93
CL3	D	639.6	749.7	0.95	712.2	1.11
F10x20_1	D	465.9	1178.6	0.53	619.0	1.33
F10x20_3	D	501.0	568.1	0.95	539.7	1.08
F10x40_1	D	422.6	1178.6	0.53	619.0	1.46
F10x40_3	D	528.7	568.1	0.95	539.7	1.02
F20x20_1	D	328.1	1178.6	0.36	425.1	1.30
F20x20_3	D	441.1	568.1	0.75	425.1	0.96
F20x40_1	D	382.3	1178.6	0.36	425.1	1.11
F20x40_3	D	412.0	568.1	0.75	425.1	1.03
CL1_3.6	D	1488.4	1358.4	0.95	1290.5	0.87
CL3_3.6	D	668.2	742.7	0.95	705.5	1.06
CL1_1.6	D	1321.3	1358.4	0.95	1290.5	0.98
CL3_1.6	D	678.4	742.7	0.95	705.5	1.04
CH1_FW	D	1123.3	1417.9	0.51	728.8	0.65
CH2[2]	D	507.6	709.0	0.95	673.6	1.33
CH4[2]	D	524.1	468.5	0.95	445.1	0.85
CL3[2]	D	642.5	728.9	0.95	692.4	1.08
G7[2]	D	633.0	532.8	0.95	506.1	0.80
B1	C	1217.0	1206.1	1.00	1206.1	0.99
B3	C	1018.0	1063.4	1.00	1063.4	1.04
B7	C	578.9	623.8	1.00	623.8	1.08
G7_A100	D	721.5	794.1	0.95	754.4	1.05
Awani et al. 2016						
S0-FRCM-1	C	1026.6	953.7	1.00	953.7	0.93
S0-FRCM-2	C	673.0	587.4	1.00	587.4	0.87
S1-FRCM-1	C	1055.6	953.7	1.00	953.7	0.90
S1-FRCM-2	C	556.1	587.4	1.00	587.4	1.06
S2-FRCM-1	C	1044.0	953.7	1.00	953.7	0.91
S2-FRCM-2	C	567.7	587.4	1.00	587.4	1.03
Baggio et al. 2014						
Beam 4	C	1707.2	1430.0	1.00	1430.0	0.84

Data from direct shear tests						
Specimen	**(1) Textile fibres [1]**	**(2) σ_{exp} (MPa)**	**(3) σ (MPa)**	**(4) $k_{,pre}$**	**(5) σ_{pre} (MPa)**	**(6) $\sigma_{exp}/\sigma_{pre}$**
Raoof et al. 2016						
L50-1	D	506.6	1417.9	0.22	1417.9	2.80
L50-2	D	605.3	821.3	0.38	821.3	1.36
L50_3	D	495.6	573.9	0.55	314.4	0.63
L50_4	D	458.9	440.5	0.71	314.4	0.69
L100-1	D	763.2	1417.9	0.34	1417.9	1.86
L100-2	D	773.0	1043.6	0.46	1043.6	1.35
L100_3	D	684.2	846.5	0.56	476.5	0.70
L100_4	D	575.7	702.9	0.68	476.5	0.83
L150-1	D	802.6	1417.9	0.43	1417.9	1.77
L150-2	D	832.2	1050.4	0.58	1050.4	1.26
L150_3	D	769.7	857.6	0.71	607.8	0.79
L150_4	D	623.4	742.7	0.82	607.8	0.98
L200-1	D	914.5	1417.9	0.51	1417.9	1.55
L200-2	D	924.3	1063.6	0.68	1063.6	1.15
L200_3	D	765.4	710.6	0.95	675.0	0.88
L200_4	D	620.1	615.4	0.95	584.6	0.94
L250-1	D	1059.2	1417.9	0.58	1417.9	1.34
L250-2	D	967.1	1061.2	0.78	1061.2	1.10
L250_3	D	834.0	866.4	0.95	823.1	0.99
L250_4	D	687.5	750.4	0.95	712.8	1.04
L450-1	D	1144.7	1417.9	0.83	1417.9	1.24
L450-2	D	1039.5	1035.8	0.95	1035.8	1.00
L100_3	D	655.7	666.0	0.72	476.5	0.73
L100_4	D	529.6	534.3	0.89	476.5	0.90
L150_3	D	673.2	710.6	0.86	607.8	0.90
L150_4	D	577.3	615.4	0.95	584.6	1.01
L200_3	D	765.4	710.6	0.95	675.0	0.88
L200_4	D	620.1	615.4	0.95	584.6	0.94
L100_3	D	684.2	837.4	0.57	476.5	0.70
L100_4	D	593.8	693.8	0.69	476.5	0.80
L150_3	D	743.4	844.3	0.72	607.8	0.82
L150_4	D	611.8	731.2	0.83	607.8	0.99
L200_3	D	886.0	844.3	0.86	722.3	0.82
L200_4	D	689.1	731.2	0.95	694.6	1.01
L150_1_C	C	1440.8	1417.9	1.00	1475.9	1.02
L200_1_C	C	1572.4	1417.9	1.00	1475.9	0.94
L150_2_C	C	970.4	1043.6	1.00	1043.6	1.08
L200_2_C	C	1049.3	1043.6	1.00	1043.6	0.99
D'Antino et al. 2015						
330_60_W	D	2310.3	2068.3	0.95	1964.9	0.85
330_80	D	2212.9	2318.9	0.95	2202.9	1.00
450_60	D	2428.6	2185.0	0.95	2075.7	0.85
450_80	D	2429.9	2185.0	0.95	2075.7	0.85
330_60_U	D	1556.8	2185.0	0.95	2075.7	1.33
330_80_U	D	2170.3	2185.0	0.95	2075.7	0.96
450_60_U	D	2559.5	2185.0	0.95	2075.7	0.81
450_80_U	D	2432.7	2185.0	0.95	2075.7	0.85
Sneed et al. 2015						
100_60	D	1550.4	2185.0	0.71	1555.6	0.77
200_60	D	1993.6	2185.0	0.95	2075.7	1.04
250_60	D	2143.8	2185.0	0.95	2075.7	0.97
330_34	D	2175.2	2185.0	0.95	2075.7	0.95
330_60	D	2136.1	2185.0	0.95	2075.7	0.97
330_80	D	2144.2	2185.0	0.95	2075.7	0.97
330_100	D	2309.3	2185.0	0.95	2075.7	0.90

Data from direct shear tests						
Specimen	**(1) Textile fibres [1]**	**(2) σ_{exp} (MPa)**	**(3) σ (MPa)**	**(4) $k_{,pre}$**	**(5) σ_{pre} (MPa)**	**(6) $\sigma_{exp}/\sigma_{pre}$**
Tran et al. 2014						
250	D	2406.6	2298.1	0.95	2183.2	0.91
300	D	2404.4	2298.1	0.95	2183.2	0.91
350	D	2298.9	2298.1	0.95	2183.2	0.95
400_41a	D	2369.2	2298.1	0.95	2183.2	0.92
400_31	D	2156.0	2143.0	0.95	2035.9	0.94
400_41b	D	2351.6	2298.1	0.95	2183.2	0.93
400_39	D	2226.4	2269.6	0.95	2156.1	0.97
D'Antino et al. 2014						
100_60	D	1377.3	2318.9	0.67	1555.6	1.13
200_60	D	2158.6	2318.9	0.95	2202.9	1.02
250_60	D	2264.8	2318.9	0.95	2202.9	0.97
450_34	D	2497.1	2185.0	0.95	2075.7	0.83
D'Antino et al. 2013						
100_34	D	969.6	2318.9	0.69	1600.0	1.65
150_34	D	1451.2	2318.9	0.88	2040.7	1.41
150_60	D	1628.8	2318.9	0.88	2040.7	1.25
200_34	D	1939.2	2318.9	0.95	2202.9	1.14
250_34	D	1622.5	2318.9	0.95	2202.9	1.36
330_34	D	2332.3	2318.9	0.95	2202.9	0.94
330_43	D	2356.2	2318.9	0.95	2202.9	0.93
330_60	D	2431.5	2318.9	0.95	2202.9	0.91
330_43_L	D	2063.7	2318.9	0.95	2148.7	1.04
330_60_L	D	2184.2	2318.9	0.95	2148.7	0.98
Ambrissi et al. 2012						
S1L50	D	1209.9	2209.0	0.34	747.7	0.62
S1L100	D	1679.1	2209.0	0.51	1133.3	0.67
S1L150	D	1975.8	2209.0	0.65	1445.5	0.73
S1L200	D	2086.8	2209.0	0.78	1717.8	0.82
S1L250	D	2203.3	2209.0	0.89	1963.9	0.89
S2L100	D	1384.6	1562.0	0.73	1133.3	0.82
S2L200	D	1718.7	1562.0	0.95	1483.9	0.86
		Average				1.04 (1.02[2])
		Standard Deviation				0.2 (0.27[2])
		CoV (%)				40.47 (26.47[2])

[1] D for dry (uncoated) textile fibre materials and C for coated textile fibre materials, [2] Calculated excluding CH1_SB specimen*

To conclude, the experimental and predicted stress values using the above described design model for all the well reported available data obtained either from tests on RC beams strengthened in shear with TRM (in this case σ_{pre} is equal to $k\,\sigma$) or direct shear tests on TRM strips [in this case σ_{pre} is equal to $k\ min\ (f_{fed,max,}\ f_{fu})$] are summarised and compared in Table 7.12 that is supported from Fig. 7.9. In total, 124 data were presented in Table 7.12 and in Fig. 7.9. The average ratio of predicted to experimental stress is $\sigma_{pre}/\sigma_{exp}$ = 1.04, the standard deviation is 0.42 and the coefficient of variation, *CoV* (%) value is equal to 40.47%. Based on the results presented in Table 7.12, the first data of this table (CH1_SB) has a quite large deviation ($\sigma_{pre}/\sigma_{exp}$ = 4.66) compared to the rest data and can be considered as statistical error. Thus, excluding this data, the results are significantly improved, namely the average ratio of predicted

to experimental stress is $\sigma_{pre}/\sigma_{exp}$ = 1.02, the standard deviation is 0.27 and the coefficient of variation, *CoV* (%) value is equal to 26.47%.

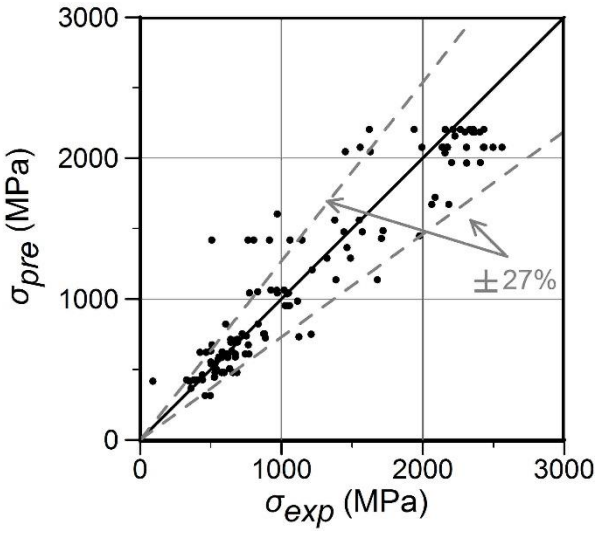


Figure 7.9. Experimental versus predicted stress values for all available data obtained from tests on either RC beams strengthened in shear with TRM jacketing or direct shear tests on TRM strips.

7.6 Prediction of shear resistance of un-retrofitted (control) specimens

The formulas suggested from EC2 could be used to calculate the contribution of concrete to shear capacity of RC beams ($V_{R,c}$) in all control specimens tested in this study. In particular, three medium-scale rectangular un-retrofitted specimens were tested in Chapter 4 with *a/d* equal to 1.6, 2.6 and 3.6, respectively and a control T-beam specimen tested at Chapter 5. The formulas of EC2 for the calculation of the shear resistance are in details presented in Appendix B.

The predicted versus experimental values for the rectangular control specimens of this study are presented in Table 7.13. Specimens CON and CON_3.6 failed due to shear – tension. The contribution of concrete to the shear resistance of the beams, $V_{R,c}$ is equal to 23.64 kN and 23.23 kN for CON and CON_3.6 specimens, respectively lower than the $V_{R,max}$ values (Table 7.13), verifying the failure of beams due to shear – tension (instead of shear compression). Generally, the predicted $V_{R,c}$ values using the formulas of EC2 are in very good agreement with the experimental values, namely the ratio of predicted to experimental shear resistance, $V_{R,pre}/V_{R,exp}$ is equal to 0.80 (=23.64/29.7) and 0.91 (=23.23/25.5) for CON and CON_3.6 specimens, respectively.

Specimen CON_1.6 failed due to shear-compression that is not predicted from the shear resistance values obtained from the EC2 formulas as $V_{R,c}$ value is lower than $V_{R,max}$ value for this specimen (Table 7.13). That means that the favorable contribution of arch mechanism (that is taken into account through the term β, see Appendix B) is considerably underestimated. Finally, the $V_{R,max}$ value predicted from EC2 formulas is in very good agreement with the experimental shear resistance of specimen CON_1.6, namely $V_{R,max}/V_{R,exp}$ is equal to 0.97 (=63.72/65.4).

Table 7.13. Comparison between experimental and predicted values for the shear resistance of the rectangular medium-scale beams.

	f_{ck} (MPa)	a_v/d	*Failure mode*	$V_{R,c}$ (kN)	$V_{R,max}$ (kN)	$V_{R,exp}$ (kN)
CON	21.6	2.03	Shear Tension	23.64	66.82	29.7
CON_1.6	20.5	1.02	Shear Compression	45.69	63.72	65.4
CON_3.6	20.5	3.02	Shear Tension	23.23	63.72	25.5

The shear resistance of the full-scale un-retrofitted beam (CON, presented in Chapter 5) can be calculated multiplying the value obtained from Eq. B.1 with the ratio $(b_f/b_w)^{0.5}$ (that is equal to $(400/200)^{0.5}$=1.4142) to take into account the contribution of the flanges to the shear resistance of the beams as described from Tureyen et al. 2006 (see also Appendix B). The $V_{R,c}$ value [obtained from Eq. (B.1) of Appendix B] is equal to 85.26 kN, whereas the $V_{R,max}$ value obtained from Eq. (B.2) is equal to 258.19 kN. The total shear resistance of the T-beam taking into account the contribution of the flanges (Tureyen et al. 2006) is equal to 85.26x1.4142=120.57 kN that is in perfect agreement with the experimental value that was equal to 124 kN (see Table 5.2). Specifically, the predicted to experimental shear resistance of the control T-beam is equal to $V_{R,pre}/V_{R,exp}$=120.57/124=0.97.

7.7 Summary

This Chapter presents a simple design approach for the calculation of the contribution of TRM jacketing to the total shear resistance of concrete beams (V_f). Firstly, all the well reported data available in the literature were collected and grouped based on their failure mode. In case of failure due to debonding, TRM jackets are as effective as FRP jackets. Therefore, Chen and Teng model developed for the calculation of the

contribution of the FRP jacketing was also used for TRM jackets, giving very accurate results after two modifications that were suggested. The accuracy of modified Chen and Teng model when failure is attributed to debonding of the jacket was also verified with results of bond tests (direct shear tests on concrete prisms connected with TRM strips). In case of failure due to rupture of the TRM jackets, V_f value can be accurately predicted using the ultimate stress (f_{fu}) obtained from (successful) tensile tests on TRM coupons (or alternatively on bare textile coupons).

Failure of TRM jackets associated with slippage of the fibre rovings through the mortar was also studied. Based on the available data this failure was observed when dry/uncoated textile materials were used, whereas it was prevented in case of coated TRM jackets. The term, λ_s which connects the geometrical characteristic of fibre rovings of TRM jackets, the tensile strength of mortar, the stress expected in the specific system when slippage of the fibres though the mortar is prevented and the available bond length was introduced to define TRM systems that are prone to slippage of fibre rovings through the mortar. Specifically, taking into account the results of beams strengthened in shear with TRM and results of direct shear tests on concrete prisms connected with TRM strips, TRM systems with low λ_s value (λ_s<0.75) are prone to slippage of fibre rovings through the mortar and therefore a reduction factor, k should be used in this case for the prediction of V_f values.

The above described design approach that was derived from 124 data, is quite simple and predicts the failure mode that is possible to be experienced in each TRM system based on the characteristics of its textile reinforcement and its mortar properties. Finally, the shear resistance of the un-retrofiited (control) specimens of rectangular cross-section can be satisfactory predicted using the EC2 formulas. The shear capacity of the un-retrofitted T-beam can be accuratrely predicted using the EC2 formulas combined with the approach suggested from Tureyen et al. (2006) to take into account the contribution of flanges to the shear resistance of the T-beam.

Chapter 8

SUMMARY, CONCLUSIONS AND RECOMMENDATIONS FOR FUTURE RESEARCH

8.1 Summary

The issue of upgrading existing structures is of great importance due to their deterioration (ageing, environmental induced degradation, lack of maintenance, need to meet the current design requirements). Recently, an innovative structural material, the so-called Textile-Reinforced Mortar (TRM), was successfully developed for structural retrofitting of deficient masonry and concrete structures. TRM is an advanced sustainable material which offers well-established advantages (good behaviour at high temperature, compatibility to concrete or masonry substrates material high strength to weight ratio, corrosion resistance, ease and speed of application, minimal change of cross section dimensions) at a low-cost and over the last decade it has been reported in the literature that TRM is a very promising alternative to the FRP (Fibre Reinforced Polymers) retrofitting solution. This study evaluates the use of TRM jacketing for shear strengthening of Reinforced Concrete (RC) beams.

First of all, the materials used for strengthening are described and the tensile and shear behaviour of textiles was characterised through tensile tests and picture-frame tests, respectively. Moreover, the tensile properties of TRM composite material are experimentally obtained through bell-shaped TRM coupons. Shear strengthening of RC beams was extensively studied carrying out 55 medium-scale rectangular beams and 14 full-scale T-beam ends.

The key investigated parameters on medium-scale rectangular beams comprise: (a) the strengthening system (TRM versus FRP), the (b) strengthening configuration, (c) the number of layers, (d) the external reinforcement ratio, (e) the textile material

mesh characteristics, (f) the shear-span-to depth ratio and (g) the optimisation of the textile geometry.

Experimental work was conducted also on full-scale T-beams focused on the use of a novel end-anchorage system comprising textile-based anchors to delay or prevent the debonding of TRM jacket. In particular, the anchorage percentage of the U-jacket, the number of layers, the textile material, the textile geometry, and the strengthening system (TRM versus FRP jackets) were the main investigated parameters.

The behaviour of TRM at high temperature used for shear strengthening of both medium-scale and full-scale beams was studied for the first time through demanding tests in which loading and high temperature were simultaneously applied. In particular, key parameters investigated on the medium-scale rectangular RC beams include: (a) the matrix used to impregnate the fibres, namely resin or mortar, resulting in two strengthening systems (TRM or FRP), (b) the level of high temperature to which the specimens are exposed (20 ^{o}C, 100 ^{o}C, 150 ^{o}C, 250 ^{o}C), (c) the strengthening configuration (side-bonding, U-wrapping and full-wrapping), (d) the number of jacketing layers (2 and 3) and (e) the textile properties (geometry, material). The effectiveness of both non-anchored and anchored TRM jackets in shear strengthening of full-scale T-beams at high temperature was also studied.

Finally, design models for the prediction of the contribution of the TRM jacket to the total shear resistance were proposed for each failure mode and verified with the available experimental data.

8.2 Conclusions

The general conclusion derived from this thesis is that TRM jacketing constitutes a very effective solution for the shear strengthening of concrete members and its use is progressively becoming more attractive for the shear strengthening of existing concrete members than the widely used fiber-reinforced polymers (FRPs). The specific conclusions derived from the experimental and analytical work of this study are reported in the following paragraphs grouped based on the chapters of this thesis.

8.2.1 Shear strengthening of medium-scale rectangular RC beams using TRM

8.2.1.1 TRM vs FRP in shear strengthening of RC beams

The main conclusions drawn from this part of study are summarized as follows:

- TRM is generally less effective in increasing the shear capacity of RC beams than FRP jacketing, but the effectiveness depends on both the strengthening configuration and the number of layers. The TRM versus FRP effectiveness factor varies from 0.09, which correspond to one layer of side-bonded jacket, to 0.91, which correspond to two layers of U-wrapped jacket.
- TRM jackets are more effective in increasing the beams deformation capacity (expressed as the average shear strain of the shear-critical span) than FRP jackets.
- U-wrapping (UW) strengthening configuration is much more effective than side-bonding (SB) in case of TRM jackets. On the contrary, in case of FRP jackets the UW configuration was found only slightly more effective than the SB configuration. Full-wrapping (FW) is the most effective strengthening configuration for both strengthening systems.
- A major difference between TRM and FRP strengthening systems is observed by increasing the number of layers from 1 to 2. In particular, the effectiveness of FRP jackets increases by 1.35 and 1.2 times for SB and UW configurations, respectively, whereas the effectiveness of TRM jackets increases by 7.8 and 2.6 times, respectively.
- The considerably higher effectiveness of TRM jackets when two instead of one textile layers are applied is linked to the change in the failure mode. The local damage the TRM jackets experience when one layer is applied (partial fibres rupture and slippage of fibre filaments through the mortar), is being shifted to the concrete substrate when two layers are applied (debonding of the jacket with peeling-off of the concrete). This is attributed to the better mechanical interlock conditions created by the overlapping of at least two textile layers.

8.2.1.2 Effect of amount of external reinforcement ratio, textile material and geometry and shear span-to-depth ratio on RC beams strengthening in shear with TRM

The main conclusions drawn from this part of study are summarized as follows:

- Carbon TRM U-jackets are as effective as carbon FRP U-jackets in increasing the shear capacity of RC beams, when failure is due to debonding of the jacket from the concrete substrate including peeling off of the concrete cover.
- The trend of the experimental effective strain values, ε_{eff}, for carbon, glass or basalt TRM jackets is descending for increasing ρ_f values, when failure is associated with debonding of the jacket, which is in agreement with the typical behaviour of FRP jackets.
- In case of low external reinforcement ratio, different carbon fibre textile geometries with the same reinforcement ratio result in different load increase and failure mode. The effect of the different textile geometry is drastically mitigated by increasing the external reinforcement ratio.
- The textile roving geometry affects the performance of TRM jackets in case of low external reinforcement ratio. In particular, textiles with smaller roving area arranged in a denser pattern result in better bond characteristics between the textile and the mortar, and hence improved efficiency.
- The shear span-to-depth ratio has no effect on both the failure mode and the contribution of the jacket to the total shear resistance of the beams.

8.2.1.3 Effect of textile mesh material characteristics (mesh size, amount and material of fibres in the horizontal direction)

This section studied the potential of optimising the geometry of textile materials used in TRM jackets for shear strengthening of RC beams. The main conclusions drawn from this part of study are summarized as follows:

- Shear capacity increase and failure mode of U-wrapped TRM jackets having the same amount of carbon fibres and roving geometry in the longitudinal direction (direction of loading) are not affected from the material or spacing (amount) of fibre rovings in the transverse direction.
- The effectiveness of the TRM jacket is being improved as the roving area of the textile in the longitudinal direction (loading direction) decreases (for both low and high external reinforcement ratios).
- The number of layers affects the failure mode of TRM U-wrapped jackets. When number of layers increases, local damage of the TRM jacket is limited (in case of large roving area) or totally prevented (in case of small roving area).

Taking into account the aforementioned conclusions, textile mesh materials having the following characteristics can be both performance and cost effective when used for shear strengthening of RC members: (a) distribution of fibres mainly in the longitudinal direction (principal direction of loading) and not in the transverse direction of textile material and (b) as much as possible small area of rovings in the longitudinal direction resulted in a dense-mesh pattern of fibres.

8.2.2 Shear strengthening of full-scale RC T-beams using TRM and textile-based anchors

The main conclusions drawn from the experimental work carried out on full-scale T-beams are summarized as follows:

- The use of textile–based anchors dramatically increases the effectiveness of carbon TRM U-jackets. Full anchorage of the carbon TRM layers improved the effectiveness of the jackets by 98% to 148%, depending on the number of TRM layers and the textile geometry.
- High effective strains, ε_{eff} can be achieved when the TRM jacket is anchored. Values ranging from 3.24‰ to 5.21‰ (depending on the number of TRM layers and the amount of anchors) were achieved in this study. Contrary, the effective strain in the TRM jackets without anchors ranged between 2.03‰ and 2.58‰.
- Anchoring the 2 (heavy) carbon layers TRM jacket is almost equivalent to the application of 4 (heavy) carbon TRM layers without anchorage, yielding significant cost benefits.
- The number of layers affects the failure mode of non-anchored TRM U-jackets. When number of layers increases, local damage of the TRM jacket (partial fibres rupture and slippage of fibre filaments through the mortar) is prevented and damage is shifted to the concrete substrate.
- In non-anchored jackets, different textile geometries with the same reinforcement ratio result in practically the same load increase but different failure modes develop. In anchored jackets the effect of the different textile geometry is eliminated as the failure is governed by the anchors behaviour.
- The effect of different textile material (glass versus carbon) is more pronounced in non-anchored jackets, where seven glass textile layers had approximately the same shear capacity with four heavy carbon textile layers, despite

the fact that seven glass textile layers were equivalent to just one heavy-carbon textile layer (in terms of axial stiffness).

- TRM U-jackets are as effective as FRP U-jackets in increasing the shear capacity of full-scale RC T-beams.
- A simple analytical model which calculates the contribution of anchored TRM jackets to the shear capacity of RC T-beams can be used for design purposes.

8.2.3 TRM versus FRP jacketing in shear strengthening of RC members subjected to high temperature

The main conclusions drawn from the experimental work carried out on medium-scale rectangular beams strengthened in shear with both TRM and FRP jackets when subjected to high temperature (100 ^{o}C, 150 ^{o}C, 250 ^{o}C) are summarized as follows:

- TRM is much more effective in increasing the shear capacity of RC beams subjected to high temperature than FRP jacketing.
- The strengthening configuration affects considerably the shear capacity increase for both TRM and FRP jackets at high temperature. In specific, fully-wrapping (FW) is the most effective strengthening configuration, following by U-wrapping (UW), whereas side-bonding (SB) is the less effective strengthening configuration, for both TRM and FRP jackets.
- The failure mode of SB and UW TRM jacketed specimens tested at high temperature is altered for different number of layers. Increasing them from 2 to 3, prevented the local damage of the TRM jacket and shifted it to the concrete surface. On the other hand, the increase in number of layers has no effect on the shear capacity increase nor the failure mode of SB and UW FRP jackets.
- The exposure of specimens strengthened with 3 layers of TRM or FRP to high temperatures (100 ^{o}C, 150 ^{o}C, 250 ^{o}C) had no effect on their failure mode. The effectiveness of FRP jackets dropped dramatically by increasing the temperature from 100 ^{o}C to 150 ^{o}C. On the other hand, the effectiveness of TRM jackets is marginally affected from their exposure to high temperatures, namely from 100 ^{o}C to 150 ^{o}C and 250 ^{o}C, respectively.
- For TRM strengthened members tested at high temperature, the denser geometry in the carbon textile is more effective in shear strengthening of concrete members.

- Both non-anchored and anchored U-wrapped TRM jackets applied at full-scale T-beams remained very effective at high temperature. The shear capacity increase of non-anchored TRM jacket decreased by 30.5% due to its exposure at 150 ^{o}C, whereas the failure mode was not affected. The use of anchors increased the effectiveness of the TRM jacket by 80% despite the pull-out of anchors due to adhesive bond failure caused from the high temperature.

8.2.4 Design models for the calculation of the contribution of the TRM jacketing to the total shear resistance (V_f) of RC beams

A simple design approach (derived from 124 data) was suggested in this study for the calculation of the contribution of TRM jacketing to the total shear resistance of concrete beams. Specifically, TRM jackets are as effective as FRP jackets in case of failure due to debonding of the jacket with peeling off of the concrete cover. Therefore, Chen and Teng model developed for the calculation of the contribution of the FRP jacketing was also used for TRM jackets, giving very accurate results after two modifications that were suggested. The accuracy of modified Chen and Teng model when failure is attributed to debonding of the jacket was also verified with results of bond tests. In case of failure due to rupture of the TRM jackets, V_f value can be accurately predicted using the ultimate stress obtained from (successful) tensile tests on TRM coupons (or alternatively on bare textile coupons).

Failure of TRM jackets associated with slippage of the fibre rovings through the mortar was observed when dry/uncoated textile materials were used, whereas it was prevented in case of coated TRM jackets. A term, λ_s which connects the geometrical characteristic of fibre rovings of TRM jackets, the tensile strength of mortar, the stress expected in the specific system when slippage of the fibres though the mortar is prevented and the available bond length was introduced to define TRM systems that are prone to slippage of fibre rovings through the mortar. Specifically, taking into account the results of beams strengthened in shear with TRM and results of direct shear tests on concrete prisms connected with TRM strips, TRM systems with low λ_s value (λ_s<0.75) are prone to slippage of fibre rovings through the mortar and therefore a reduction factor, k should be used in this case for the prediction of V_f values.

8.2.5 Future Research

TRM jacketing was found to be a very effective solution for shear strengthening of RC beams and therefore TRM is progressively becoming a very promising alternative to the FRP retrofitting solution. Future research should be directed towards the following fields:

- The textile-based anchors used in this study were very effective and significantly delayed or even prevented the debonding of TRM jackets. Thus, a variety of parameters including the anchors geometry, the anchors material or the embedment length could be studied in an attempt to optimize the textile-based anchors. Moreover, high-strength and fire-resistant cementitious grouts could be also investigated for anchor fixing replacing the chemical bond agent (epoxy resin) used in this study.
- Investigation of the performance of TRM at temperatures above 250 ^{o}C or fire and development of fire-resistant cement-based mortars for further improving the effectiveness of TRM jacketing at high temperatures or fire.
- Understanding of the long-term behavior of elements strengthend with TRM and investigation of the durability performance of TRM.
- Use of TRM for structural and energy retrofitting of existing concrete or masonry buildings and investigation of the performance of TRM for strengthening existing structures againgt exreme evnets (i.e. progressive collapse of a building).

REFERENCES

ACI 549.4R-13. Guide to Design and Construction of Externally Bonded Fabric-Reinforced Cementitious Matrix (FRCM) Systems for Repair and Strengthening Concrete and Masonry Structures.

ACI Committee 440, "Guide Test Methods for Fibre-Reinforced Polymers (FRPs) for Reinforcing or Strengthening Concrete Structures (ACI 440.3R-04)," American Concrete Institute, Farmington Hills, MI 2004, 40 pp.

Adhikary B B, Mutsuyoshi H and Ashraf M. Shear strengthening of reinforced concrete beams using fiber-reinforced polymer sheets with bonded anchorage. ACI Structural Journal, 2004;101(5).

Al-Salloum YA, Almusallam TH, Elsanadedy HM and Iqbal RA. Effect of elevated temperature environments on the residual axial capacity of RC columns strengthened with different techniques. Construction and Building Materials 2016;115:345-361.

Al-Salloum YA, Elsanadedy HM, Alsayed SH and Iqbal RA. Experimental and Numerical Study for the Shear Strengthening of Reinforced Concrete Beams Using Textile-Reinforced Mortar. Journal of Composites for Construction, 2012; 16(1), 74-90.

Al-Salloum YA, Siddiqui NA, Elsanadedy HM, Abadel AA, Aqel MA. Textile-reinforced mortar versus FRP as strengthening material for seismically deficient RC beam-column joints. J Comp Constr 2011;15(6):920-933.

Al-Sulaimani GJ, Sharif A, Basunbul IA, Baluch M. H. and Ghaleb B. N. Shear repair for reinforced concrete by fiberglass plate bonding. ACI Struct. J., 1994; 91(3), 458–464.

Altmeyer F, Weigl J, Scharf A. Safety analysis and rehabilitation of the natural draft cooling tower Block E at the power plant of Niederaußem. Beton Stahlbetonbau 2012;107 (5):318–327 (in German).

Anil Ö. Improving shear capacity of RC T-beams using CFRP composites subjected to cyclic load. Cement and Concrete Composites, 2006;28(7), 638-649.

Awani O, El-Maaddawy T, El Refai A. Numerical Simulation and Experimental Testing of Concrete Beams Strengthened in Shear with Fabric-Reinforced Cementitious Matrix. J Comp Constr 2016; doi: 10.1061/;(ASCE)CC.1943-5614.0000711.

Azam R, Soudki K. FRCM strengthening of shear-critical RC beams. J Comp Constr 2014;18(5), 04014012. doi: 10.1061/(ASCE)CC.1943-5614.0000464.

Babaeidarabad S, Caso F and Nanni A. Out-of-Plane Behavior of URM Walls Strengthened with Fabric-Reinforced Cementitious Matrix Composite. J Compos Constr 2014; 18(4), 04013057.

Baggio D, Soudki K. and Noel M, 2014. Strengthening of shear critical RC beams with various FRP systems. Construction and Building Materials, 2014; 66, 634-644.

Barros JA, Dias SJ and Lima JL. Efficacy of CFRP-based techniques for the flexural and shear strengthening of concrete beams. Cement and Concrete Composites, 2007;29(3), 203-217.

Berset J.D. Strengthening of reinforced concrete beams for shear using FRP composites. MSc thesis, Dept. of Civ. and Envir. Engrg. 1992, Massachusetts Institute of Technology, Cambridge, Mass.

Bisby L, Stratford T, Hart C, Farren S. Fire Performance of Well-Anchored TRM, FRCM, and FRP Flexural Strengthening Systems. Advanced Composites in Construction 2013.

Blanksvärd T, Täljsten B and Carolin A. Shear strengthening of concrete structures with the use of mineral-based composites. Journal of Composites for Construction, 2009; 13(1), 25-34.

Bournas DA, Lontou PV, Papanicolaou CG, Triantafillou TC. Textile-reinforced mortar versus fiber-reinforced polymer confinement in reinforced concrete columns. ACI Struct J, 2007;104(6).

Bournas DA, Pavese A, Tizani W. Tensile capacity of FRP anchors in connecting FRP and TRM sheets to concrete. Engin Struct 2015; 82(1):72-81.

Bournas DA, Triantafillou TC, Zygouris K, Stavropoulos F. Textile-reinforced mortar versus FRP Jacketing in seismic retrofitting of RC columns with continuous or Lap-spliced deformed bars. J Comp Constr 2009;13(5):360-371.

Bournas DA, Triantafillou TC. Bar buckling in RC columns confined with composite materials. J Comp Constr 2011; 15(3): 393-403.

Bournas DA, Triantafillou TC. Bond strength of lap-spliced bars in concrete confined with composite jackets. J Comp Constr 2011;15(2):156-167.

Bournas DA. Strengthening of existing structures: Selected case studies. In Textile fibre composites in civil engineering, (Ch. 17), Edited by T.C. Triantafillou, 2016;389-411, Elsevier, Woodhead Publishing Limited, http://dx.doi.org/10.1016/B978-1-78242-446-8.00018-5.

Bousselham A and Chaallal O. Effect of transverse steel and shear span on the performance of RC beams strengthened in shear with CFRP. Composites Part B: Engineering, 2006;37(1), 37-46.

Bousselham A and Chaallal O. Mechanisms of shear resistance of concrete beams strengthened in shear with externally bonded FRP. Journal of Composites for Construction, 2008;12(5), 499-512.

Bousselham A, Chaallal O. Behavior of reinforced concrete T-beams strengthened in shear with carbon fiber-reinforced polymer-an experimental study. ACI Struct J, 2006;103(3):339.

Bousselham A, Chaallal O. Behavior of reinforced concrete T-beams strengthened in shear with carbon fiber-reinforced polymer-an experimental study. ACI Struct J 2006;103(3):339.

Brameshuber W, Brockmann J, Roessler G (2001). Textile reinforced concrete for formwork elements—investigations of structural behaviour. In: Burgoyne, C.J. (Ed.), FRPRCS-5 Fiber Reinforced Plastics for Reinforced Concrete Structures, vol. 2. Thomas Telford, London, pp. 1019–1026.

Brückner A, Ortlepp R, Curbach M. Anchoring of shear strengthening for T-beams made of textile reinforced concrete (TRC). Mater Struct 2008;41(2):407-418.

Cao J, Akkerman R, Boissse P, Chen J, et al. Characterization of mechanical behavior of woven fabric: experimental methods and benchmark results. Composites: Part A 2008;39(6):1037–53.

Carloni C, Bournas DA, Carozzi FG, D'Antino T, Fava G, Focacci F, Giacomin G, Mantegazza G, Pellegrino C, Perinelli C and Poggi C. Fiber reinforced composites with cementitious (inorganic) matrix. Chapter 9 in: Design procedures for the use of composites in strengthening of reinforced concrete structures – State of the art report of the RILEM TC 234-DUC, (Eds: C. Pellegrino and J. Sena-Cruz); 2015; 349-391, Springer, RILEM STAR Book Series.

Carolin A and Täljsten B. Theoretical study of strengthening for increased shear bearing capacity. Journal of Composites for Construction, 2005;9(6), 497-506.

Cerniauskas G, Tetta Z, Bournas D and Bisby LA. Textile Reinforced Mortar versus FRP for confined concrete: behavior at elevated temperatures, 8t^{h} International Conference on Fibre-Reinforced Polymer (FRP) Composites in Civil Engineering, Hong Kong, China, December 2016.

Chen JF, Teng, JG. Shear capacity of FRP-strengthened RC beams: FRP debonding. Constr and Build Mat, 2003b;17(1):27-41.

CIDAR (2006) – "Design Guideline for RC Structures Retrofitted with FRP and Metal Plates: Beams and Slabs", Draft 3 – Submitted to Standards Australia, University of Adelaide.

CNR-DT 200 (2004), Guide for the Design and Construction of Externally Bonded FRP Systems for Strengthening Existing Structures, National Research Council, Italy.

Colombo I, Colombo M, Magri A, Zani G, di Prisco M. Textile Reinforced Mortar at High Temperatures. In Applied Mechanics and Materials 2011; 82:202-207.

Contamine R, Si Larbi A and Hamelin P. Identifying the contributing mechanisms of textile reinforced concrete (TRC) in the case of shear repairing damaged and reinforced concrete beams. Engineering Structures, 2013;46, 447-458.

Curbach M, Jesse F. High-performance textile-reinforced concrete. Struct. Eng. Int. 1999;4:289–291.

D' Ambrisi A and Focacci F. Flexural strengthening of RC beams with cement based composites. J Comp Constr 2011;10.1061/(ASCE)CC.1943-5614.0000218, 707-720.

D'Ambrisi A, Feo L, Focacci F. Experimental analysis on bond between PBO-FRCM strengthening materials and concrete. Compos Part B 2013;44(1):524-532.

D'Antino T, Sneed LH, Carloni C, Pellegrino C. Influence of the substrate characteristics on the bond behavior of PBO FRCM-concrete joints. Constr and Build Mat 2015;30;101:838-850.

D'Antino, T., Carloni, C., Sneed, L. H., and Pellegrino, C. Matrix–fiber bond behavior in PBO FRCM composites: A fracture mechanics approach. Eng. Fract. Mech., 2014;117:94–111.

D'Antino T, Sneed L, Carloni C and Pellegrino C. Bond behavior of the FRCM-concrete interface, Proceedings of the 11th International Symposium on Fiber Reinforced Polymers for Reinforced Concrete Structures, 2013, Guimarães, Portugal.

Deniaud C and Cheng JJR. Shear behaviour of reinforced concrete T-beams with externally bonded fibre-reinforced polymer sheets. ACI Struct. J., 2001;98(3), 386–394.

Deniaud C and Roger Cheng JJ. Reinforced concrete T-beams strengthened in shear with fiber reinforced polymer sheets. Journal of Composites for Construction, 2003;7(4), 302-310.

Dirar S H, Morley C and Lees J (2007). Effect of effective depth and longitudinal steel ratio on the behaviour of precracked reinforced concrete T-beams strengthened in shear with CFRP fabrics Proc 8th int symp FRP reinforcement for concrete structures. Patras, Greece.

Ehlig D and Hothan S. Reinforced concrete slabs strengthened with textile reinforced concrete subjected to fire. In E.A.B. Koenders and F. Dehn eds., 2011, 2nd international RILEM workshop on concrete spalling due to fire exposure (pp. 419-426). RILEM Publications SARL.

Elsanadedy HM, Almusallam TH, Alsayed SH, Al-Salloum YA. Flexural strengthening of RC beams using textile reinforced mortar–Experimental and numerical study. J Comp Struct 2013;97:40-45.

EN 1015-11. Methods of test for mortar for masonry – Part 11: Determination of flexural and compressive strength of hardened mortar, Brussels: Comité Européen de Normalisation; 1993.

Escrig C, Gil L, Bernat-Maso E and Puigvert F. Experimental and analytical study of reinforced concrete beams shear strengthened with different types of textile-reinforced mortar. Construction and Building Materials, 2015; 83, 248-260.

Eurocode 2: Design of concrete structures - Part 1-1: General rules and rules for buildings, EN 1992-1-1: 2004.

Fédération Internationale du Béton (fib) (2001), Bulletin 14 – Externally Bonded FRP Reinforcement for RC Structures, TaskGroup 9.3 Technical Report.

Firmo JP, Correia JR, Bisby LA. Fire behaviour of FRP-strengthened reinforced concrete structural elements: A state-of-the-art review. J Compos Part B: Eng, 2015;80, 198-216.

Galal K. and Mofidi A. Shear strengthening of RC T-beams using mechanically anchored unbonded dry carbon fiber sheets. J of Performance of Constructed Facilities, 2009;24(1), 31-39.

Harajli M, ElKhatib H and San-Jose J. Static and cyclic out-of-plane response of masonry walls strengthened using textile-mortar system. J. Mater. Civ. Eng., 2010; 22(11), 1171-1180.

Jesse F, Weiland S and Curbach M. Flexural strengthening of RC structures with textile-reinforced concrete. American Concrete Institute, Special Publication 2008;250, 49-521 58.

Khalifa A, Gold WJ, Nanni A, MI AA. Contribution of externally bonded FRP to shear capacity of RC flexural members. J Comp Constr 1998;2(4):195-202.

Kodur VKR, Bisby LA, Green M F. FRP retrofitted concrete under fire conditions. J Concrete International, 2006;28(12), 37-44.

Kodur VKR, Bisby LA, Green M. Experimental evaluation of the fire behaviour of insulated fibre-reinforced-polymer-strengthened reinforced concrete columns. Fire safety journal, 2006;41(7), 547-557.

Koutas L, Bournas DA. Flexural strengthening of two-way RC slabs with textile-reinforced mortar: experimental investigation and design equations. J Compos Constr. 2016;doi:10.1061/(ASCE)CC.1943-5614.0000713.

Koutas L, Bousias SN, Triantafillou TC. Seismic strengthening of masonry-infilled RC frames with TRM: Experimental study. J Comp Constr 2014; 04014048. doi: 10.1061/(ASCE)CC.1943-5614.0000507.

Koutas LN, Bousias SN, Triantafillou TC. Seismic strengthening of masonry-infilled RC frames with TRM: Experimental study. J Comp Constr 2015;19(2):04014048. doi: 10.1061/(ASCE)CC.1943-5614.0000507.

Koutas LN, Pitytzogia A, Triantafillou TC, Bousias SN. Strengthening of infilled reinforced concrete frames with TRM: Study on the development and testing of

textile-based anchors. J Compos Constr 2014;18(3).doi:10.1061/(ASCE)CC.1943-5614.0000390.

Koutas LN, Triantafillou TC. Use of anchors in shear strengthening of reinforced concrete T-beams with FRP. J Comp Constr 2013;17(1):101-107.

Lima JL and Barros JA. Design models for shear strengthening of reinforced concrete beams with externally bonded FRP composites: a statistical vs. reliability approach. Proceedings of the 8th International Symposium on Fiber Reinforced Polymer Reinforcement for Concrete Structures. Patras, Greece: University of Patras, 2007.

Loreto G, Babaeidarabad S, Leardini L, Nanni A. RC beams shear-strengthened with fabric-reinforced-cementitious-matrix (FRCM) composite. Int J Adv Struct Eng (IJASE) 2015;1-12.

Loreto G, Leardini L, Arboleda D and Nanni A. Performance of RC slab-type elements strengthened with fabric-reinforced cementitious-matrix composites. J. Compos. Constr., 2014; 10.1061/(ASCE)CC.1943-5614.0000415, A4013003.

Majumder M, Gangopadhyay TK, Chakraborty AK, Dasgupta K and Bhattacharya DK. Fibre Bragg gratings in structural health monitoring—Present status and applications. Sensors and Actuators A: Physical, 2008;147(1):150-164.

Micelli F, Annaiah RH and Nanni A. Strengthening of Short Shear Span Reinforced Concrete T Joists with Fiber-Reinforced Plasic Composites. Journal of Composites for Construction, 2002;6(4), 264-271.

Monti G and Liotta MA. Tests and design equations for FRP-strengthening in shear. Construction and Building Materials,2007;*21*(4), 799-809.

Nanni A. A new tool in the concrete and masonry repair. Concr. Int. Des. Constr, 2012;34:43-49.

Ombres L. Analysis of the bond between Fabric Reinforced Cementitious Mortar (FRCM) strengthening systems and concrete. Compos Part B 2015;28;69:418-26.

Ombres L. Confinement effectiveness in eccentrically loaded masonry columns strengthened by fiber reinforced cementitious matrix (FRCM) jackets. Key Eng. Mater. 2015; 624, 551-558.

Ombres L. Structural performances of reinforced concrete beams strengthened in shear with a cement based fiber composite material. Comp Struct 2015;122, 316-329.

Ortlepp R, Lorenz A, Curbach M. Column strengthening with TRC: Influences of the column geometry onto the confinement effect. Advances in Materials Science and Engineering 2009; Article ID 493097.

Ozbakkaloglu T, Saatcioglu M. Tensile behavior of FRP anchors in concrete. Journal of J Comp Constr 2009;13:2(82), 82-92.

Panda KC, Bhattacharyya SK and Barai SV. Shear strengthening of RC T-beams with externally side bonded GFRP sheet. Journal of Reinforced Plastics and composites, 2011;0731684411417202.

Papanicolaou C, Triantafillou T, Papantoniou I and Balioukos, C. Strengthening of two-way reinforced concrete slabs with textile reinforced mortars (TRM). Proc. 4th Colloquium on textile reinforced structures (CTRS4), Curbach, M. and Jesse, F. (eds.), Dresden, Germany, 2009; 409-420.

Papanicolaou CG, Triantafillou TC and Lekka M. Externally bonded grids as strengthening and seismic retrofitting materials of masonry panels. Constr Build Mater 2011; 25(2), 504-514.

Papanicolaou CG, Triantafillou TC, Karlos K and Papathanasiou M. Textile reinforced mortar (TRM) versus FRP as strengthening material of URM walls: in-plane cyclic loading. Mater Struct 2007; 40(10), 1081-1097.

Papanicolaou CG, Triantafillou TC, Papathanasiou M and Karlos K. Textile reinforced mortar (TRM) versus FRP as strengthening material of URM walls: out-of-plane cyclic loading. Mater Struct 2008; 41(1), 143-157.

Peled A. Confinement of damaged and nondamaged structural concrete with FRP and TRC sleeves. Journal of Composites for Construction, 2007; 11(5), 514-522.

Pellegrino C, Vasic M. Assessment of design procedures for the use of externally bonded FRP composites in shear strengthening of reinforced concrete beams. Compos Part B 2013;45(1), 727-741.

Raoof SM, Koutas LN, Bournas DA, Bond between textile-reinforced mortar (TRM) and concrete substrates: Experimental investigation, Composites Part B 2016; 98:350-361, doi: 10.1016/j.compositesb.2016.05.041.

Rousakis T, Saridaki M, Mavrothalassitou S, Hui D. Utilization of hybrid approach towards advanced database of concrete beams strengthened in shear with FRPs. Compos Part B 2016;85, 315-335.

Schladitz F, Frenzel M, Ehlig D and Curbach M. Bending load capacity of reinforced concrete slabs strengthened with textile reinforced concrete. Eng. Struct. 2012; 40, 317-326.

Si Larbi A, Contamine R, Ferrier E and Hamelin P. Shear strengthening of RC beams with textile reinforced concrete (TRC) plate. Construction and Building Materials, 2010; 24(10), 1928-1936.

Sneed LH, D' Antino T, Carloni C and Pellegrino C. A comparison of the bond behavior of PBO-FRCM composites determined by double-lap and single-lap shear tests. Cem and Conc Compos 2015;64:37-48.

Tetta Z, Bournas DA. Effectiveness of TRM versus FRP jacketing at high temperature on shear strengthening of RC beams, IFireSS 2017 – 2nd International Fire Safety Symposium, Naples, Italy, June 7-9, 2017.

Tetta Z, Koutas L, and Bournas DA, Salihi B. Shear Strengthening of RC Beams using Textile Reinforcement in Cement or Epoxy Based Matrices, 3rd International Conference on Textile-Reinforced Concrete (3rd ICTRC), Aachen, Germany, June 2015.

Tetta ZC and Bournas DA. TRM versus FRP Jacketing in Shear Strengthening of Concrete members subjected to High Temperature. Compos Part B 2016; 106:190-205, doi:org/10.1016/j.compositesb.2016.09.026.

Tetta ZC, Koutas LN, Bournas DA. Shear strengthening of full-scale RC T-beams using textile-reinforced mortar and textile-based anchors. Compos Part B 2016;95:225-239, doi:10.1016/j.compositesb.2016.03.076.

Tetta ZC, Koutas LN, Bournas DA. Textile-reinforced mortar (TRM) versus fibre-reinforced polymers (FRP) in shear strengthening of concrete beams. Compos Part B 2015;77:338-348, doi:10.1016/j.compositesb.2015.03.055.

Tran CT, Stitmannaithum B, Ueda T. Investigation of the bond behaviour between PBO-FRCM strengthening material and concrete. J Adva Conc Tech 2014;12(12):545-57.

Trapko T, Urbańska D, Kamiński M. Shear strengthening of reinforced concrete beams with PBO-FRCM composites. Compos Part B 2015; 80: 63-72.

Trapko T. The effect of high temperature on the performance of CFRP and FRCM confined concrete elements. Compos Part B: Eng 2013;54:138-145.

Triantafillou TC and Papanicolaou CG. Shear strengthening of reinforced concrete members with textile reinforced mortar (TRM) jackets. Mater Struct 2006;39(1):93-103.

Triantafillou TC, Antonopoulos CP. Design of concrete flexural members strengthened in shear with FRP. J Comp Constr 2000;4(4):198-205.

Triantafillou TC, Papanicolaou CG, Zissimopoulos P, Laourdekis T. Concrete confinement with textile-reinforced mortar jackets. ACI Struct J 2006;103(1):28-37.

Triantafillou TC, Papanicolaou CG. Shear strengthening of reinforced concrete members with textile reinforced mortar (TRM) jackets. Mater Struct 2006;39(1):93-103.

Triantafillou TC. Shear strengthening of reinforced concrete beams using epoxy-bonded FRP composites. ACI Struct J 1998;95(2):107-115.

Tsamasphyros GJ, Kanderakis GN, Fournarakis NK, Marioli-Riga ZP. Detection of patch debonding in composite repaired cracked metallic specimens, using optical fibers and sensors. SPIE Optical Metrology Conference, 2003 Munich, Germany.

Tureyen K, Wolf T and Frosch R. Shear Strength of Reinforced Concrete TBeams without Transverse Reinforcement, ACI Struct J 2006;103(5), 656-663.

Tzoura E, Triantafillou TC. Shear strengthening of reinforced concrete T-beams under cyclic loading with TRM or FRP jackets. Mater Struct 2016;49(1):17-28. doi: 10.1617/s11527-014-0470-9.

APPENDIX A – DEFINITION OF λ_s

In this Appendix, the procedure for the definition of λ_s ratio is described in details. The ratio $L_{max}/[A_{rov}\ \sigma/(f_{tm}\ P_{rov})]$was initially introduced as a parameter that could be used for the definition of the reduction factor, k. In Fig. A.1a the reduction factor, k is plotted with $L_{max}/[A_{rov}\ \sigma/(f_{tm}\ P_{rov})]$ values for the data of Tables 7.9 and 7.11 for specimens in which the tensile strength of mortar was experimentally obtained. Based on Fig. A.1a, the trend of k factor is increasing for increasing λ_s values up to a critical $L_{max}/[A_{rov}\ \sigma/(f_{tm}\ P_{rov})]$ value ($L_{max}/[A_{rov}\ \sigma/(f_{tm}\ P_{rov})] \approx 6$) and after that point, k values are very close to 1 for the majority of data. However, the data of Fig. A.1a having $L_{max}/[A_{rov}\ \sigma/(f_{tm}\ P_{rov})]$ value lower than 6 are quite scattered (i.e. for $L_{max}/[A_{rov}\ \sigma/(f_{tm}\ P_{rov})] \approx 2$ k varies from 0.1 to almost 1). In particular, the best fit power-type expression for all data of Fig. A.1a (expression a) has coefficient of determination, R^2 value equal to 0.4459 (Fig. A.1b). The R^2 value for the best fit power-type expression just for the data of Fig. A.1a having $L_{max}/[A_{rov}\ \sigma/(f_{tm}\ P_{rov})]$ values lower than 6 (expression b) is equal to 0.3643 (Fig. A.1b).

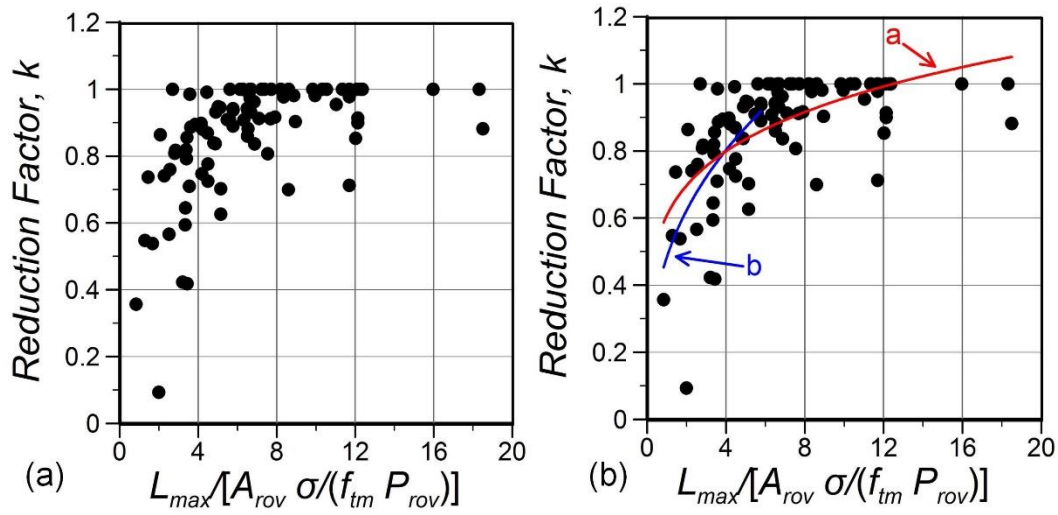


Figure A.1. Reduction factor, k versus λ_s values.

In an attempt to reduce this scatter, k values were plotted with $L_{max}/[A_{rov}\ \sigma/(f_{tm}\ P_{rov})]$ ratios trying different powers in L_{max} values, namely $L_{max}^{a}/[A_{rov}\ \sigma/(f_{tm}\ P_{rov})]$, where a varied from 0 to1. To check if the results are improved (the scatter is reduced)

as a value in $L_{max}^{a}/[A_{rov}\ \sigma/(f_{tm}\ P_{rov})]$ ratio varies from 0 to 1, power-type expressions were applied to best fit all the data of Fig. A.1 (expression a) or fit the data of Fig. A.1 that have $L_{max}/[A_{rov}\ \sigma/(f_{tm}\ P_{rov})]$ values lower than 6 (expression b). The R^2 values for the aforementioned power-type expressions (a and b) are plotted in Fig. A.2 with values of a. It is clear from Fig. A.2 that the highest R^2 values where achieved for a value equal to 0.6. Therefore, λ_s ratio was defined as $\lambda_s = L_{max}^{0.6}/[A_{rov}\ \sigma/(f_{tm}\ P_{rov})]$.

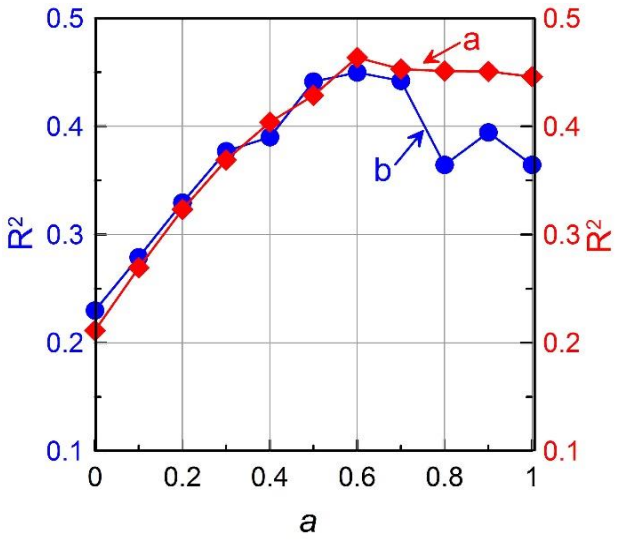


Figure A.2. Coefficient of determination, R^2 values versus a values.

APPENDIX B – DESIGN OF BEAMS

For the design of beams, standard calculations were conducted and basic formulas were used. The aim of the experimental work conducted in this thesis is the evaluation of the contribution of TRM jackets to shear strengthening of RC beams. Thus, the critical spans of both un-strengthened and strengthened beams are deficient in shear in order to fail in shear prior the yielding of tensile reinforcement. In other words, the shear failure load (P_{shear}) should be considerably lower than the flexural failure load ($P_{flexure}$). Through the proper design of beams, a high value of the ratio $P_{flexure}/P_{shear}$ in un-strengthened specimens is aimed. As the ratio $P_{flexure}/P_{shear}$ in control beams increases, the margin between shear failure and flexural failure is extended. Therefore, a high ratio $P_{flexure}/P_{shear}$ is desirable in un-strengthened specimens in order to ensure the shear failure of both un-strengthened and strengthened specimens. Tables presented in following paragraphs include:

- P_{shear} → shear failure load
- $P_{flexure}$ → flexural failure load
- $P_{flexure}/P_{shear}$ → ratio of flexural failure load over shear failure load
- V_{R1} → Shear resistance of critical shear span
- M_R → Moment Resistance of beam
- $M_{failure}$ → Moment at the failure
- V_{Rmax} → Maximum shear force that the specific cross-section resists, limited by crushing of the compression struts
- x → neutral axis of cross-section

To begin with, moment resistance of beam is simply calculated based on cross-section analysis, assuming simplified rectangular distribution of compressive stress in compression zone (Fig. B.1).

Shear capacity of beams was calculated according to EC2 codes without using safety factors. In particular, shear resistance of the member without shear reinforcement is given by equation (B.1):

$$V_{R,c} = [c_{R,c} \cdot k \cdot (100 \cdot \rho_l \cdot f_c)^{1/3} + k_1 \cdot \sigma_{cp}] \cdot b_w \cdot d \quad \text{(B.1)}$$

where b_w and d is the width and the effective depth of cross-section, respectively, ρ_l is the tensile reinforcement ratio ($A_{s1}/(b_w\ d)$), f_{ck} is the characteristic compressive strength of concrete and σ_{cp} is the axial stress that in our case is equal to zero as no axial force is applied to the beams. The constant $c_{R,c}$ is equal to 0.18, k_1 is equal to 0.15, while k is given by the following equation: $k = 1 + \sqrt{\frac{200}{d}} \le 2$ (d in mm) (B.2)

A minimum of $V_{R,c}$ is given by the following expression:

$$V_{R,c,\min} = (v_{\min} + k_1 \cdot \sigma_{cp}) \cdot b_w \cdot d$$
$$v_{\min} = 0.035 \cdot k^{3/2} \cdot f_c^{1/2} \quad \text{(B.3)}$$

For members with loads applied on the upper side within a distance $0.5d \le a_v \le 2d$ (a_v is the clear shear span) from the edge of a support, the shear resistance $V_{R,c}$ can be multiplied by $\beta = 2d/a_v$ to take into account the favorable contribution of arch mechanism.

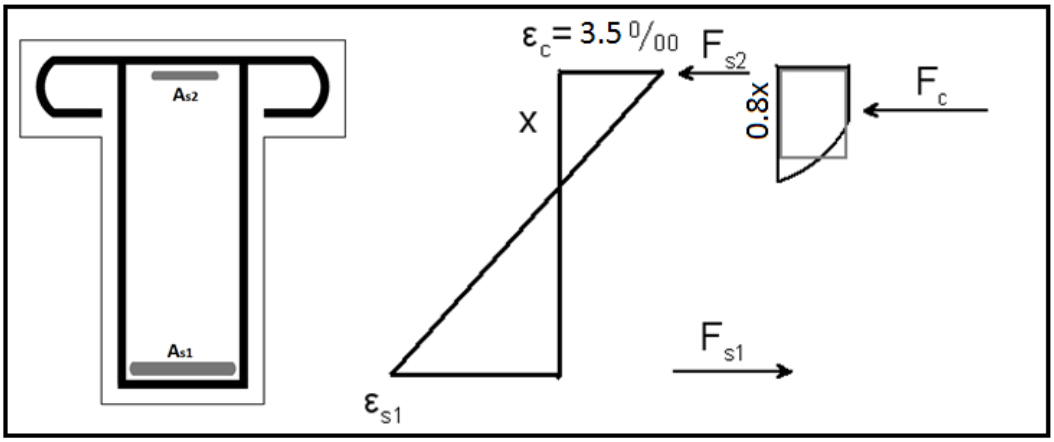


Figure B.1. Cross-section analysis.

Maximum shear force that the specific cross-section resists, limited by crushing of the compression struts, V_{Rmax} is given by:

$$V_{R,max} = \frac{a_{cw} \cdot b_w \cdot z \cdot \nu_1 \cdot f_c}{\cot\theta + \tan\theta} \text{, where } a_{cw} = 1 \quad \text{(B.4)}$$

$$\nu_1 = 0.6 \cdot \left[1 - \frac{f_c}{250}\right] \quad \text{(B.5)}$$

$$\text{and } z = 0.9 \cdot d \quad \text{(B.6)}$$

In $V_{R,max}$ calculation, a cracking angle, θ=22° was considered as a conservative estimation. Finally, the shear force that can be sustained by the yielding shear reinforcement in non-critical shear span is given by:

$$V_{R,s} = \frac{A_{sw}}{s} \cdot z \cdot f_{yw} \quad \left(A_{sw} = 2 \cdot \frac{\pi \cdot \Phi_w^{\,2}}{4}\right) \tag{B.7}$$

Moment and Shear diagrams – Failure loads

Figure B.2 includes moment and shear diagrams of the simply supported beam. Based on the values of maximum moment and maximum shear in combination with the moment and shear resistance, the flexural and shear failure load can be calculated making use of the following formulas:

$$P_{flex} = \frac{(l_1 + l_2) \cdot M_R}{l_1 \cdot l_2} \tag{B.8}$$

and $$P_{shear} = V_{R,c} \cdot \frac{l_1 + l_2}{l_2} \tag{B.9}$$

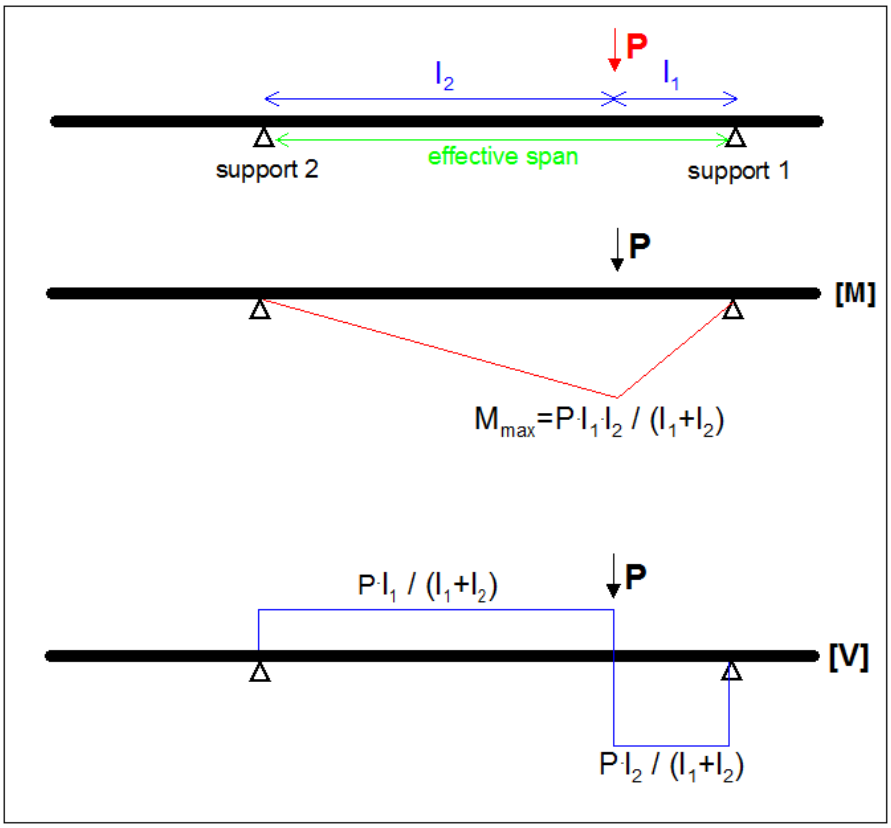


Figure B.2. Moment and shear diagrams.

Contribution of flanges to Shear Resistance of T-beams

In the above calculations for the shear capacity of RC beams, the contribution of T-beam flanges to shear capacity of RC members is not taken into account in case of T-beam specimens. For design purposes, this is a conservative and over safety approach. However, in the framework of experimental work of this project, an as much as accurate estimation of the shear resistance of T-beam is required in order to ensure a successful design of specimens. The presence of flanges increases the shear capacity of a RC beam. The shear failure load (P_{shear}) is defined based on the shear resistance of the RC beam. In particular, shear failure load increases as the RC member resistance increases. Thus, a more accurate estimation of shear capacity of T-beams comparing with this obtained from EC2 is of major importance in order to ensure that the actuator capacity is sufficient to induce failure to both un-strengthened and strengthened beams. According to Tureyen et al. (2006), the multiplier $\sqrt{b_f / b_w}$ can be used in shear capacity calculations to take into account the contribution of flanges to the shear resistance of T-beams without internal shear reinforcement. However, this approach to estimate the shear capacity of T-beams has not been verified with experimental data. Thus, at this point a verification of the above approach is attempted. Experimental data of T-beams that failed in shear were collected. Table B.1 includes the experimental and predicted failure loads values using Tureyen et al. (2006) approach in combination with EC2 calculations.

In particular, Fig. B.3 compares the experimental and predicted failure load values calculated according to EC2 formulas (without Tureyen approach) for specimens without (B.3a) or with (B.3b) stirrups in the critical shear span. Figure B.4 compares the predicted values of failure load calculated using Tureyen approach with the corresponding experimental values for specimens without (B.4a) or with (B.4b) stirrups in the critical span. It is obvious that Tureyen et al. (2006) approach can accurately predict the failure load of T-beams without transverse reinforcement when its failure is attributed to shear-tension. However, shear capacity of T-beams with stirrups in the critical span is underestimated (especially for T-beams with a/d>2.5) by applying Tureyen et al. (2006) approach. It should be mentioned that the suggestion of an approach to accurately calculate the shear capacity of T-beams is far from the

aim of this project. Tureyen et al. (2006) approach was used in this study for the design of T-beams, as it gives much more accurate results comparing with the EC2 formulas.

Table B.1. Comparison of predicted failure loads calculated using Tureyen et al. (2006) approach in combination with EC2 formulas for calculating shear capacity with experimental failure loads for T-beams that failed in shear-tension.

	NO STIRRUPS		STIRRUPS	
	PREDICTED FAILURE LOAD (kN)	EXPERIMENTAL FAILURE LOAD (kN)	PREDICTED FAILURE LOAD (kN)	EXPERIMENTAL FAILURE LOAD (kN)
Deniaud and Cheng (2001)	184	220	219	375
			254	714
Micelli at al. (2002)	291	318		
Deniaud and Cheng (2003)	267	231	337	314
			404	403
Bousselham and Chaallal (2005)	209	214	344	389
			349	399
	205	123	375	397
Bousselham and Chaallal (2005)	68	176	96	180
Dirar et al. (2007)			185	214
Anil (2006)	69	37		
Bousselham and Chaallal (2008)	139	123	256	397
			375	446
	43	54	80	140
Panda et al. (2011)	77	100	85	141
			92	160
Koutas et al. (2012)	94	105		
Bruckner et al. (2008)			406	548

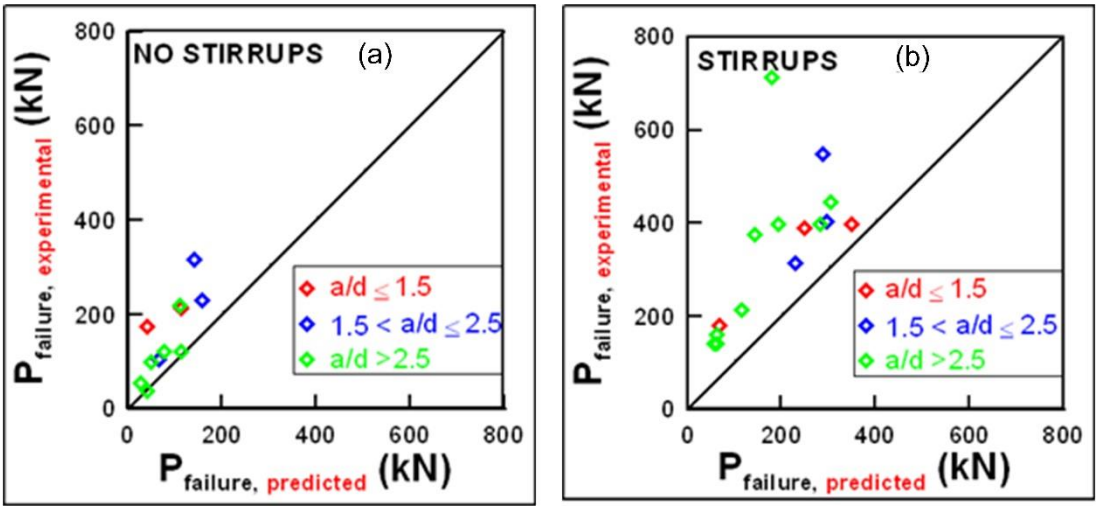


Figure B.3. Comparison between predicted failure loads calculated according to EC2 formulas and experimental failure loads for T-beams wihout (a) or with (b) stirrups in critical shear span that failed in shear-tension.

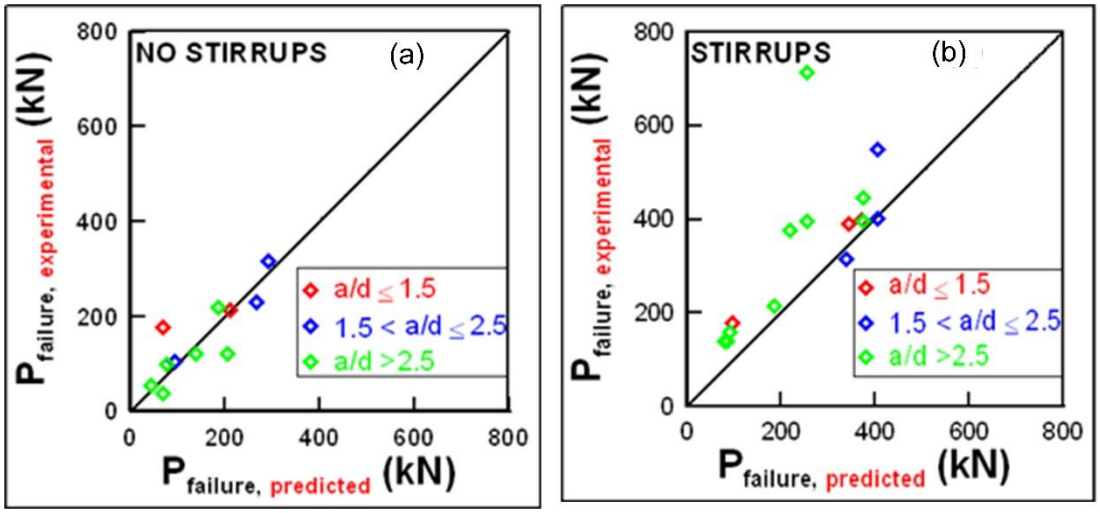


Figure B.4. Comparison between predicted failure loads obtained using Tureyen (2006) approach combined with EC2 formulas and experimental failure loads for T-beams wihout (a) or with (b) stirrups in critical shear span that failed in shear-tension.

The basic calculations for both rectangular and T-beam specimens are summarized in Table B.2. The concrete compressive strength considered in these calculations are 20 MPa and 14 MPa for rectangular and T-beam specimens, respectively. It is clear from the results presented in Table B.2 that the flexural capacity of both rectangular and T-beam specimens is significantly higher than the shear capacity. Finally, the neutral axis of T-beam specimens was at the web of the T-beam.

Table B.2. Summary of basic calculations for both rectangular and T-beams.

	T-beams	**Rectangular beams**		
		***a/d*=1.6**	***a/d*=2.6**	***a/d*=3.6**
P_{shear} (kN)	158.21	61.23	40.22	56.14
$P_{flexure}$ (kN)	549.06	144.95	113.97	115.25
$P_{flexure}/P_{shear}$	3.47	2.37	2.83	2.05
V_{R1} (kN)	120.58	45.31	23.04	23.04
M_R (kNm)	368.26	30.04	30.04	30.04
$M_{failure}$ (kNm)	106.11	12.69	10.60	14.63
V_{Rmax} (kN)	258.19	62.31	62.31	62.31
x (mm)	270.6	76.2	76.2	76.2

APPENDIX C – READINGS OF STRAIN GAUGES IN T-BEAMS

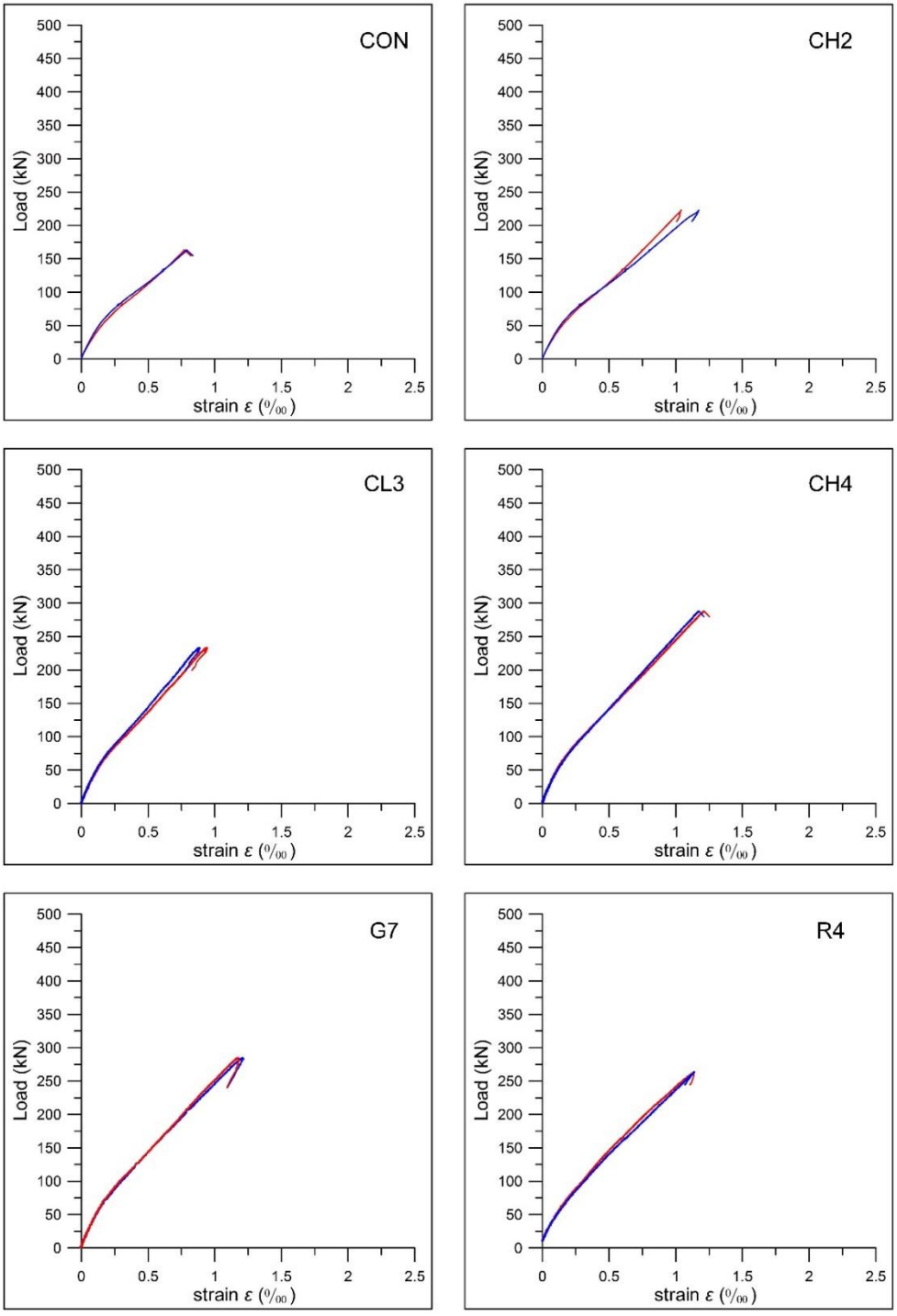


Figure C.1. Strain versus load curves using readings of strain gauges that were bonded to the (bottom) tensile steel bars for control and non-anchored T-beams.

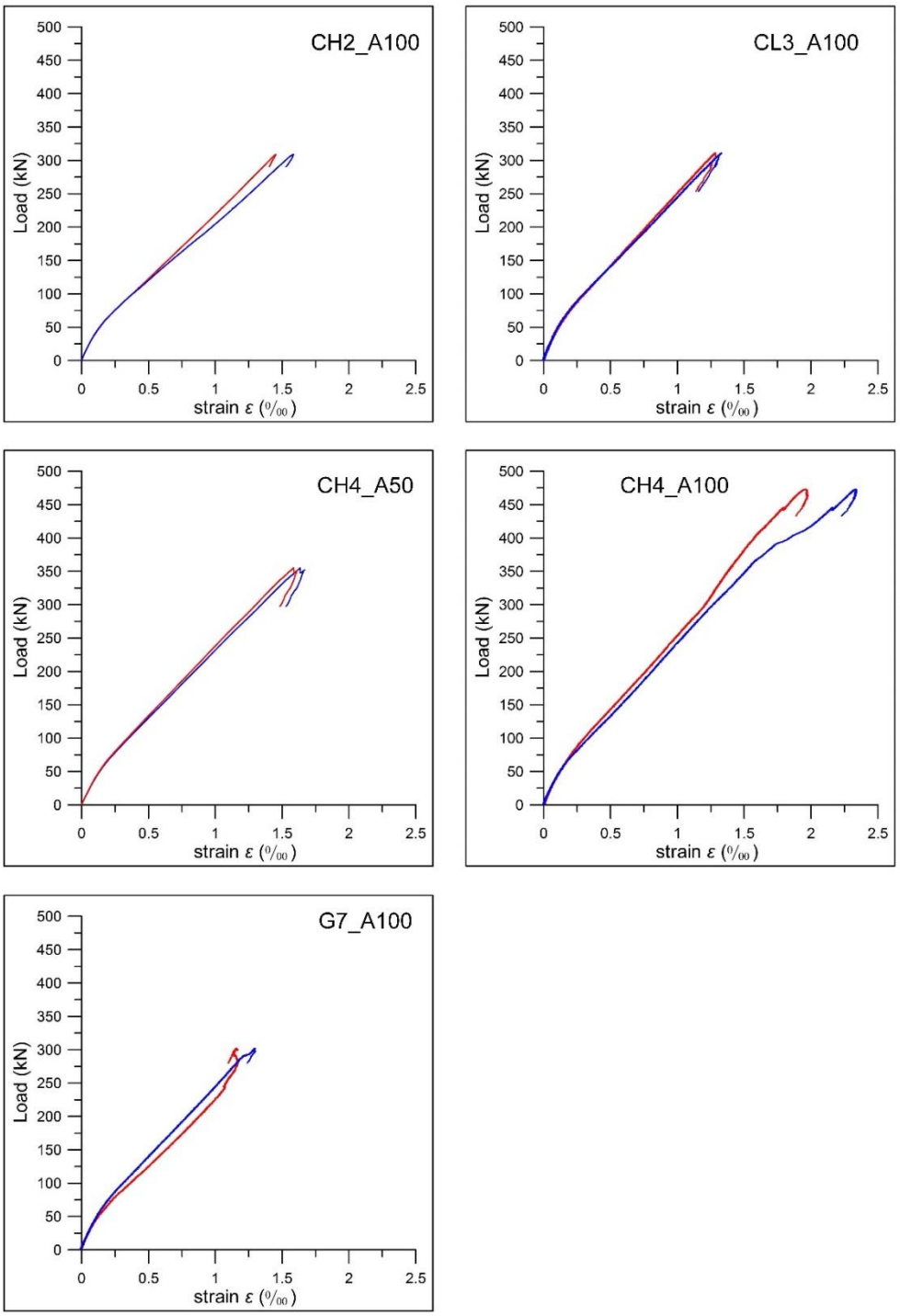


Figure C.2. Strain versus load curves using readings of strain gauges that were bonded to the (bottom) tensile steel bars for anchored T-beams.

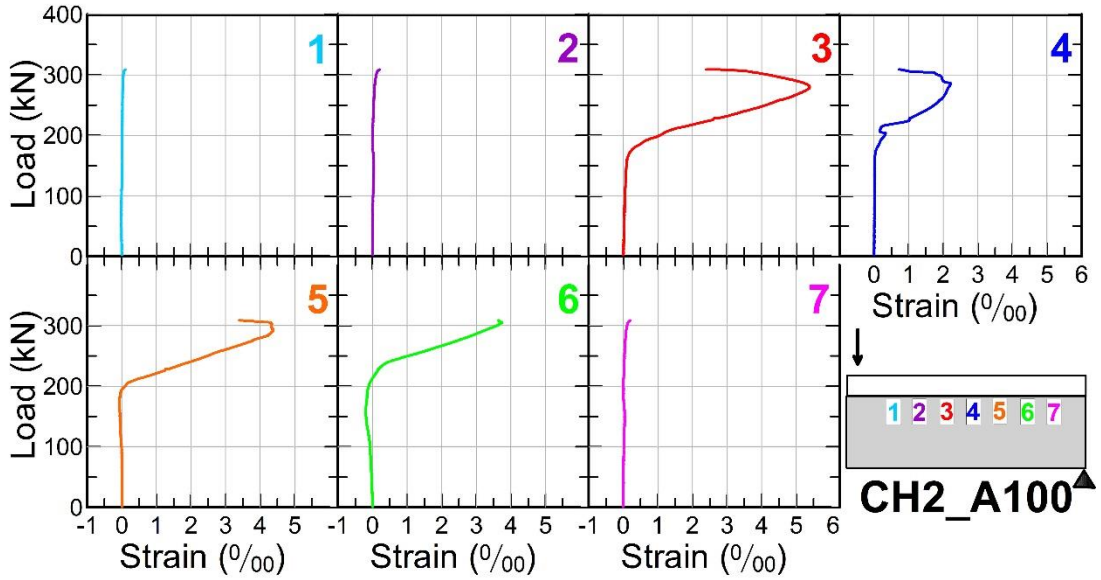


Figure C.3. Strain versus load curves using strain gauges readings that were bonded to the face of the TRM jacket at the position of anchors for CH2_A100 specimen.

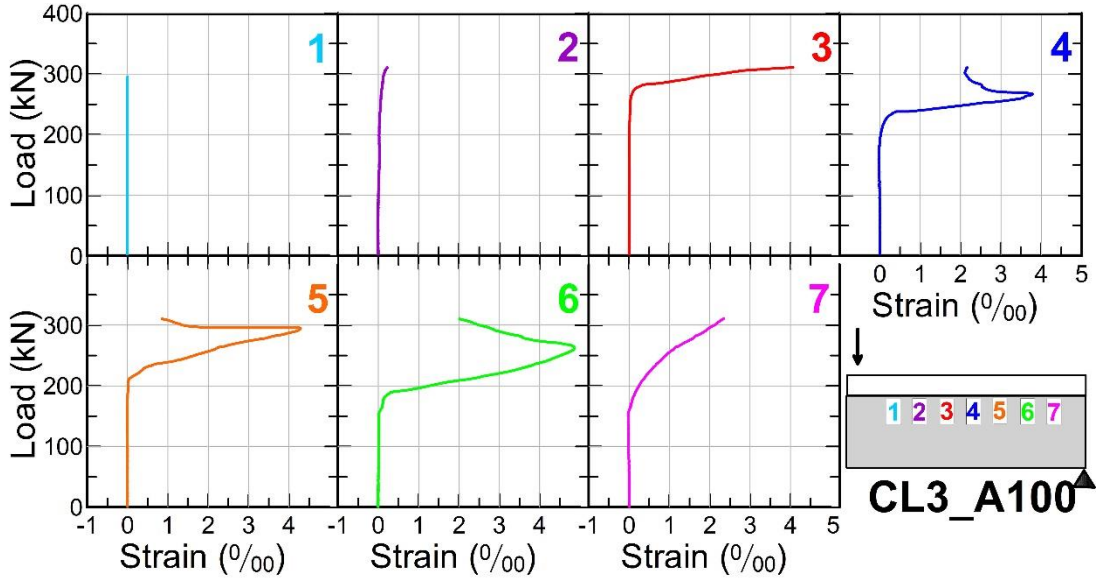


Figure C.4. Strain versus load curves using strain gauges readings that were bonded to the face of the TRM jacket at the position of anchors for CL3_A100 specimen.

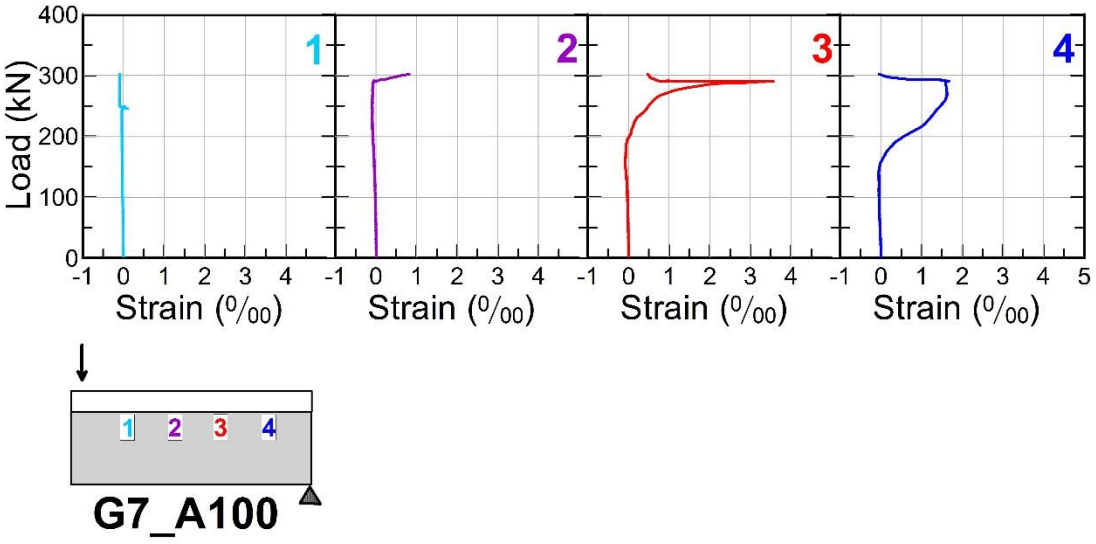


Figure C.5. Strain versus load curves using strain gauges readings that were bonded to the face of the TRM jacket at the position of anchors for G7_A100 specimen.

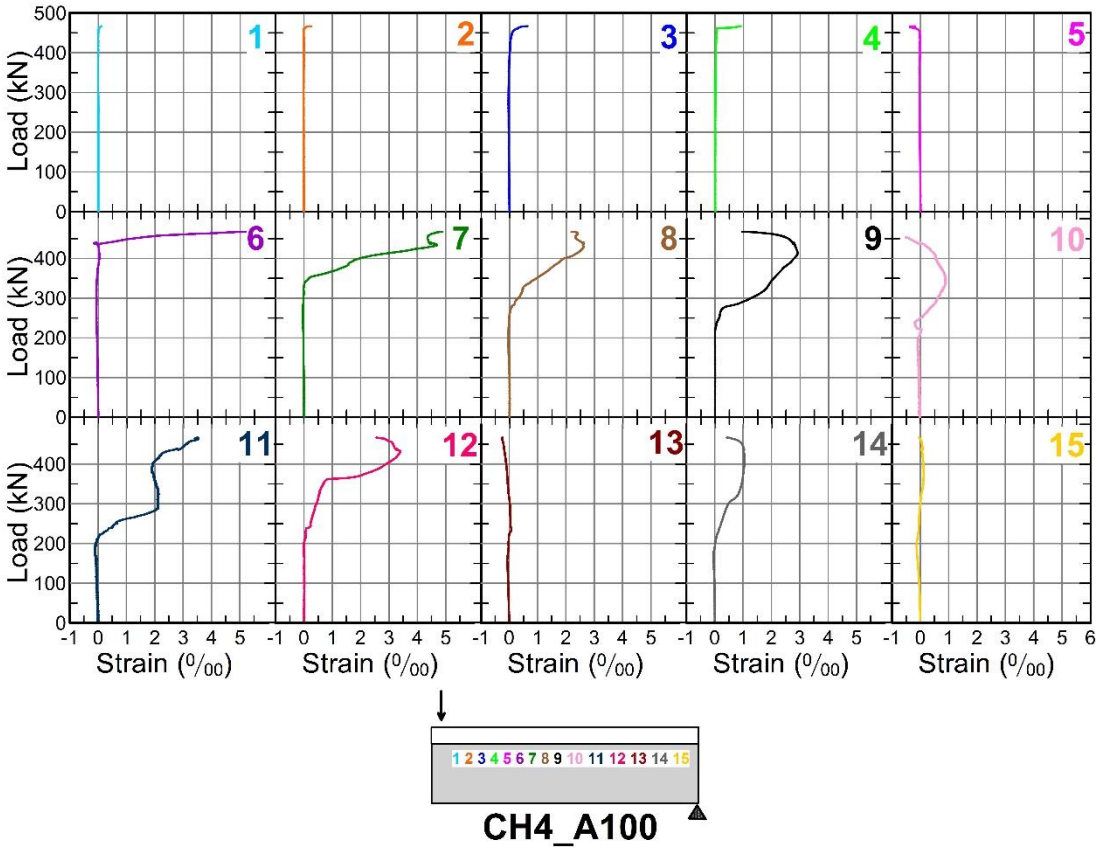


Figure C.6. Strain versus load curves using strain gauges readings that were bonded to the face of the TRM jacket at the position of anchors for CH4_A100 specimen.

APPENDIX D – ADDITIONAL INFORMATION

Table D.1. Calculation of all terms included in Cheng and Teng model for data on shear strengthening of RC beams with TRM (or equivalent FRP) jacketing that failed due to debonding of the jacket.

Specimen	L_e (mm)	h_{fe} (mm)	λ	D_f	β_l	f_{fed} (MPa)	σ_{exp} (mm)
Data of this study							
CH2_SB	94.83	79.65	0.84	0.59	0.97	552.058	348.6
CH3_SB	116.14	79.65	0.69	0.55	0.88	386.740	360.1
CH2	93.61	159.3	1.70	0.79	1.00	772.476	647.6
CH3	116.14	159.3	1.37	0.74	1.00	581.931	500.0
CL1	53.93	159.3	2.95	0.88	1.00	1495.06	1463.1
CH1_CL1	88.88	159.3	1.79	0.80	1.00	824.800	752.3
CH2_CL1	112.60	159.3	1.41	0.74	1.00	606.837	553.0
CH3_CL1	132.13	159.3	1.21	0.70	1.00	486.137	438.7
CL1_strips	70.20	159.3	2.27	0.84	1.00	1099.96	1080.4
G3	81.49	159.3	1.95	0.81	1.00	918.522	879.8
G7	124.48	159.3	1.28	0.72	1.00	528.882	540.1
B3	72.18	159.3	2.21	0.84	1.00	1064.04	1018.0
B7	110.26	159.3	1.44	0.75	1.00	624.146	578.9
CL3	95.79	159.3	1.66	0.78	1.00	750.100	639.6
F10x20_3	118.15	159.3	1.35	0.73	1.00	568.474	501.0
F10x40_3	118.15	159.3	1.35	0.73	1.00	568.474	528.7
F20x20_3	118.15	159.3	1.35	0.73	1.00	568.474	441.1
F20x40_3	118.15	159.3	1.35	0.73	1.00	568.474	412.0
CL1_3.6	55.71	159.3	2.86	0.87	1.00	1440.63	1488.4
CL3_3.6	96.50	159.3	1.65	0.78	1.00	743.102	668.2
CL1_1.6	55.71	159.3	2.86	0.87	1.00	1440.63	1321.3
CL3_1.6	96.50	159.3	1.65	0.78	1.00	743.102	678.4
CH1_R_SB[1]	67.82	79.65	1.17	0.69	1.00	936.308	1007.7
CH2_R_SB[1]	95.91	79.65	0.83	0.59	0.96	541.513	687.2
CH1_R[1]	66.19	159.3	2.41	0.85	1.00	1179.32	1166.3
CH2_R[1]	93.61	159.3	1.70	0.79	1.00	772.476	703.7
CH3_R[1]	118.58	159.3	1.34	0.73	1.00	565.673	550.7
CH4[3]	151.00	238.5	1.58	0.77	1.00	468.807	524.1
CL3[3]	105.76	238.5	2.26	0.84	1.00	729.300	642.5
G7[3]	136.58	238.5	1.75	0.79	1.00	533.094	633.0
CH4_R[1, 3]	149.33	238.5	1.60	0.77	1.00	475.621	424.8
Awani et al. 2016							
S0-FRCM-1	73.48	112.5	1.53	0.76	1.00	954.23	1026.6
S0-FRCM-2	103.92	112.5	1.08	0.66	1.00	587.756	673.0
S0-FRP-1[1]	73.48	112.5	1.53	0.76	1.00	954.23	1200.2
S1-FRCM-1	73.48	112.5	1.53	0.76	1.00	954.23	1055.6
S1-FRCM-2	103.92	112.5	1.08	0.66	1.00	587.756	556.1
S1-FRP-1[1]	73.48	112.5	1.53	0.76	1.00	954.23	1114.6
S2-FRCM-1	73.48	112.5	1.53	0.76	1.00	954.23	1044.0
S2-FRCM-2	103.92	112.5	1.08	0.66	1.00	587.756	567.7
S2-FRP-1[1]	73.48	112.5	1.53	0.76	1.00	954.23	1200.2
Tzoura and Triantafillou 2014							
RL2[1 3]	68.93	144.5	2.10	0.83	1.00	1102.46	664.1

[1] FRP jackets, [2] C for carbon fibre textile, G for glass fibre textile, B for basalt fibre textile, SB for side-bonded jackets and UW for U-wrapped jackets, [3] T-beam section.

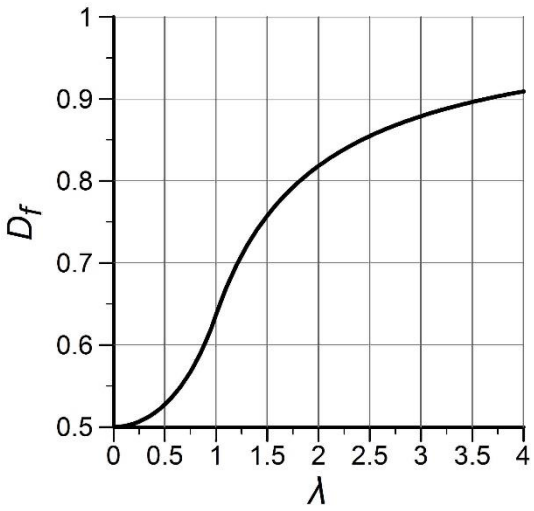


Figure D.1. λ versus D_f values obtained from Chen and Teng model.

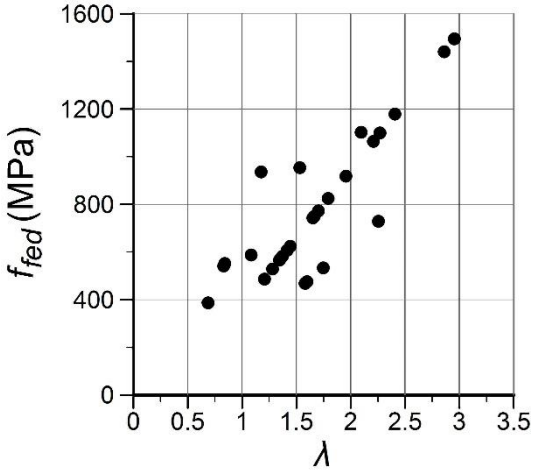


Figure D.2. λ versus average stress values (f_{fed}) obtained from Chen and Teng model.

PERSONAL DEVELOPMENT

Papers in Journals

Tetta Z, Koutas L, and Bournas DA (2017). "Shear Strengthening of Concrete Members with TRM jackets: Effect of Shear Span-to-Depth Ratio, Material and Amount of External Reinforcement", submitted to *Composites Part B: Engineering*.

Tetta Z and Bournas DA (2016). "TRM versus FRP Jacketing in Shear Strengthening of Concrete members subjected to High Temperature". *Composites Part B: Engineering*; Vol. 106, pp. 190-205.

Tetta Z, Koutas L, and Bournas DA (2016). "Shear Strengthening of Full-Scale RC T-beams using Textile-Reinforced Mortar and Textile-based Anchors", *Composites Part B: Engineering*, Vol. 95, pp. 225-239.

Tetta Z, Koutas L, and Bournas DA, (2015). "Textile-Reinforced Mortar (TRM) versus Fiber-Reinforced Polymers (FRP) in Shear Strengthening of Concrete Beams", *Composites Part B: Engineering*, Vol. 77, pp. 338-348.

Papers in Conference proceedings

Tetta Z, Bournas DA (2017). "Effectiveness of TRM versus FRP jacketing at high temperature on shear strengthening of RC beams", *IFireSS 2017 – 2nd International Fire Safety Symposium*, Naples, Italy, June 7-9, 2017.

Cerniauskas G, Tetta Z, Bournas D and Bisby LA, (2016). "Textile Reinforced Mortar versus FRP for confined concrete: behavior at elevated temperatures", *8th International Conference on Fibre-Reinforced Polymer (FRP) Composites in Civil Engineering*, Hong Kong, China, December 2016.

Tetta Z, Koutas L, and Bournas DA, Salihi B, (2015). "Shear Strengthening of RC Beams using Textile Reinforcement in Cement or Epoxy Based Matrices", *3rd International Conference on Textile-Reinforced Concrete (3rd ICTRC)*, Aachen, Germany, June 2015.

Papers in Workshop proceedings

Tetta Z and Bournas DA (2016). "Performance of Textile-Reinforced Mortar (TRM) at High Temperature for Shear Strengthening of RC members", *3rd Year Plenary Meeting of Cost Action TU1207 – Next Generation Design Guidelines for Composites in Construction*, November 2016, Prague, Czech Republic.

Tetta Z, Koutas L, and Bournas DA, (2016). "Novel TRM Systems for Shear strengthening of full-scale RC T-beams", *3rd Year Plenary Meeting of Cost Action TU1207 – Next Generation Design Guidelines for Composites in Construction*, April 2016, Lodz, Poland.

Best Poster Award

"Novel TRM Systems for Shear strengthening of full-scale RC T-beams", Tetta Z, Koutas L, and Bournas DA, (2016), *3rd Year Plenary Meeting of Cost Action TU1207 – Next Generation Design Guidelines for Composites in Construction*, April 2016, Lodz, Poland.

Summer School

Attendance in Dresden International Summer School (DISS) 'HIGH-PERFORMANCE FIBRE-REINFORCED CEMENT-BASED COMPOSITES (HPFRCC) FOR FUTURE', 26-31 July, 2015 (30 international PhD students and Post-Docs had been selected to join the DISS).

Presentations

Tetta Z and Bournas DA (2016). "Performance of Textile-Reinforced Mortar (TRM) at High Temperature for Shear Strengthening of RC members", *3rd Year Plenary Meeting of Cost Action TU1207 – Next Generation Design Guidelines for Composites in Construction*, November 2016, Prague, Czech Republic.

Tetta Z. (2016) "Innovative Shear Strengthening of existing concrete members with Textile-Based Composite Materials", *CSEI seminar*, January 2016, Nottingham, UK.

Tetta Z, Koutas L, and Bournas DA (2016). "Novel TRM Systems for Shear strengthening of full-scale RC T-beams", *3rd Year Plenary Meeting of Cost Action TU1207 – Next Generation Design Guidelines for Composites in Construction*, April

2016, Lodz, Poland.

Shear Strengthening of RC Beams using Textile Reinforcement in Cement or Epoxy Based Matrices", *3rd International Conference on Textile-Reinforced Concrete (3rd ICTRC)*, Aachen, Germany, June 2015.

Tetta Z, Koutas L, and Bournas DA, (2015). "Textile-Reinforced Mortar (TRM) versus Fiber-Reinforced Polymers (FRP) in Shear Strengthening of Concrete Beams", *2nd Year Plenary Meeting of Cost Action TU1207 – Next Generation Design Guidelines for Composites in Construction*, May 2015, Lecce, Italy.